THE
PHYSICAL REVIEW

A journal of experimental and theoretical physics established by E. L. Nichols in 1893

SECOND SERIES, VOL. 72, NO. 6 SEPTEMBER 15, 1947

Total Cross Section of Aluminum for Fast Neutrons

L. W. SEAGONDOLLAR* AND H. H. BARSCHALL
University of Wisconsin, Madison, Wisconsin

(Received June 12, 1947)

The total neutron cross section of aluminum was measured as a function of neutron energy in the range from 10 to 1000 kev. Neutrons of known mean energy and small energy spread were produced by the Li(p,n) reaction. The cross section was found to be a rapidly varying function of energy indicating the presence of at least ten resonances in the range of energies investigated. The extreme values of the cross section were found to be 0.9×10^{-24} cm^2 and 11.5×10^{-24} cm^2.

INTRODUCTION

ALTHOUGH the total cross section of most elements for fast neutrons is known for some neutron energies, information about the variation of the cross section over a wide, continuous range of energy is still limited. The neutron energy region between 2 and 3 Mev has been explored by MacPhail and by Aoki.[1] Both authors found an anomalous behavior of the cross sections for several elements in this region. More recently, studies of the total neutron cross sections of some of the light elements have been carried out over a wider range of neutron energies.[2] Resonances were found in these investigations in helium, beryllium, carbon, oxygen, and aluminum.

In the energy region below 1 Mev, photoneutron sources have been used by Good and Scharff-Goldhaber,[3] Leipunsky,[4] and Fields *et al.*[5] The work of the last authors shows that the total neutron cross sections of several elements do not vary monotonically with neutron energy, even for the heavier elements. In many cases the variation of the cross section does not follow the trend predicted by Feshbach, Peaslee, and Weisskopf.[6] The present measurements were undertaken to obtain more information about the variation of cross section with energy. Aluminum was selected for the first measurements because the results of Fields *et al.* showed a particularly anomalous behavior for this element. In addition, it has the advantage of having only one isotope.

APPARATUS

Neutrons were obtained from the Li(p,n) reaction. The protons were accelerated by an

* Now at the University of Kansas, Lawrence, Kansas.

[1] M. R. MacPhail, Phys. Rev. **57**, 669 (1940); H. Aoki, Proc. Phys. Math. Soc. Jap. **21**, 232 (1939).

[2] Bailey, Bennett, Bergstrahl, Nuckolls, Richards, and Williams, Phys. Rev. **70**, 583 (1946); D. H. Frisch, Phys. Rev. **70**, 589 (1946); Nuckolls, Bailey, Bennett, Bergstrahl, Richards, and Williams, Phys. Rev. **70**, 805 (1946); H. Staub and H. Tatel, Phys. Rev. **58**, 820 (1940); P. G. Koontz and T. A. Hall, Los Alamos Report LADC No. 16; Allen, Burcham, and Wilkinson, Nature **159**, 473 (1947).

[3] W. E. Good and G. Scharff-Goldhaber, Phys. Rev. **59** 917 (1941).

[4] A. I. Leipunsky, J. Phys. USSR **3**, 231 (1940).

[5] Fields, Russell, Sachs, and Wattenberg, Phys. Rev. **71**, 508 (1947).

[6] Feshbach, Peaslee, and Weisskopf, Phys. Rev. **71**, 145 (1947).

electrostatic generator[7] which gives a proton beam of 3 to 5μa with an energy definition of about ±3 kev. It is possible to get much higher energy resolution by electrostatic analysis of the proton beam,[8] but the resultant analyzed proton current would be too small for the present experiments. The protons impinged upon a lithium film evaporated onto a 0.010-in. thick tantalum disk. In order to prevent deterioration of this target, the proton beam was focused near the periphery of the tantalum disk which was rotated at slow speed, and a jet of compressed air cooled the outer surface of the disk.

The neutrons were detected by a proportional counter (see Fig. 1) which was filled with normal boron trifluoride to a pressure of 35 cm of Hg. To increase the sensitivity of the counter for fast neutrons, it was surrounded by a cylindrical shell of paraffin, $\frac{1}{2}$-in. thick. In order to reduce the sensitivity of the counter to slow neutrons, the paraffin shell was surrounded by a cylindrical layer, $\frac{1}{4}$-in. thick, containing a mixture of paraffin and boron carbide, and then the whole assembly was covered with cadmium. The center wire of the counter was held at 2100 volts positive with respect to the grounded outer cylinder. To avoid spurious pulses which often originate in condensers placed at such voltage,[9] the counter was coupled to the preamplifier by two condensers in series, with the point between the two condensers maintained at 1000 volts. Pulses from the counter were passed through a preamplifier, a linear amplifier[10] and a pulse height discriminator to a scale-of-64 counter,[11] and a mechanical recorder. The proportional counter did not have a plateau, but tests using a Ra-Be source showed that for a given discriminator setting, the counting rate remained constant from day to day. At the discriminator setting used for the present experiments, the counter was not sensitive to gamma-rays.

Two cylindrical disks of aluminum were used as scatterers. The purity of the aluminum was higher than 99 percent. Both disks were $1\frac{1}{2}$ in. in diameter and one was $\frac{1}{2}$-in. thick, containing 0.0766×10^{24} atoms/cm², while the other was 1-in. thick and contained 0.153×10^{24} atoms/cm².

The center of the active volume of the counter was placed 10 in. from the lithium target. The scatterers were located midway between the front of the counter and the target. Reproducibility of the location of the scatterer was obtained by placing it on a V-shaped support which was held rigidly in place by a $\frac{1}{8}$-in. iron rod and guy wires. In the geometry used, the maximum angle through which a neutron could be scattered and reach the center of the front surface of the counter was 20°.

The primary neutron intensity was monitored by measuring the number of protons incident upon the lithium target by a current integrator.

PROCEDURE

Since the distribution in angle of the neutron yield from the Li(p,n) reaction has a maximum in the forward direction, this direction was chosen for most of the experiment in order to obtain highest intensity. Also, the spread of energy of the neutrons for a given angle subtended by the counter is smallest in the forward direction. For neutrons of energy below 120 kev, however, a

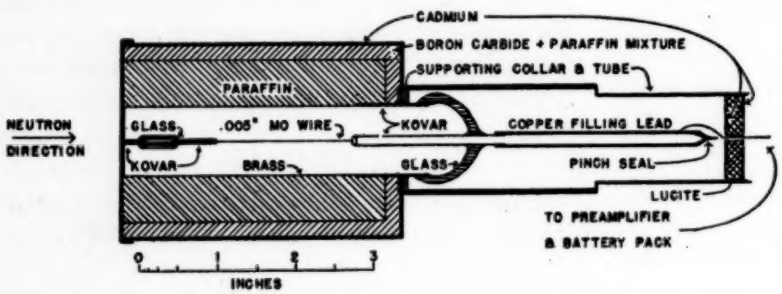

FIG. 1. BF_3-filled proportional counter for neutron detection.

[7] Herb, Turner, Hudson, and Warren, Phys. Rev. **58**, 579 (1940).
[8] Warren, Powell, and Herb, Rev. Sci. Inst. (to be published).
[9] J. H. Coon and R. A. Nobles, Rev. Sci. Inst. **18**, 44 (1947).
[10] Model 100 amplifier designed by M. Sands.
[11] Designed by W. A. Higginbotham.

second group of neutrons of lower energy is present in the forward direction, and these would be detected with a counter sensitive to slow neutrons. To avoid this double energy region, the energy range below 120 kev was covered by using neutrons emitted at an angle of 115° with respect to the proton beam.

The measurements consisted of counting alternately the number of neutrons incident on the counter with and without the scatterer in place. Cross sections were calculated under the assumption that the neutron intensity decreases exponentially in the scatterer.

Since both the lithium target and the neutron detector were only 4 ft. from the concrete floor of the laboratory, an appreciable number of the counts were due to neutrons which did not come directly from the target, in spite of the shielding surrounding the counter. This background was measured by placing a shadow cone of paraffin and boron carbide between the target and the detector. Such measurements were carried out for two different positions of the counter; first with the counter at the position at which the scattering data were taken, and then using a longer shadow cone, with the counter 22 in. from the target. The background count per current integrator count was approximately the same at both positions, indicating that the shadow cones absorbed practically all the direct neutrons. Measurements of background as a function of neutron energy were made both at 0° and at 115° with respect to the proton beam. The background varied from 3 to 10 percent of the direct neutron count for the distance at which the scattering measurements were performed.

In the geometry used, the cross section measured is approximately that for scattering through angles greater than 20°. The total cross section was obtained under the assumption that the average differential scattering cross section in the angular interval between 0° and 20° is the same as the average for angles greater than 20°. Since the solid angle between 0° and 20° is 3 percent of 4π steradians, 3 percent of the difference in count with and without the scatterer was subtracted from the count observed in the presence of the scatterer. No correction was made for multiple scattering.

Lithium targets of 5-kev and 10-kev stopping power were used. The stopping power was determined by observing the neutron counting rate as a function of proton energy near the threshold of the Li(p,n) reaction. The counting rate rises rapidly above threshold to a maximum. The difference in proton energy between threshold and the energy corresponding to this maximum yield was taken as the target thickness. The determination of target thickness has an accuracy of ± 3 kev.

The proton energies were measured by an electrostatic analyzer,[12] using the threshold energy of the Li(p,n) reaction (1.86 Mev[13]) as a reference point. To obtain the effective average proton energy, one-half of the target thickness was subtracted from the proton energy so obtained. When the neutron detector is placed at an angle of 115° with respect to the proton beam, the average energy of the neutrons incident on the face of the detector is very nearly the same as the energy of neutrons emitted at 115°. When the detector is placed in the forward position, however, the neutrons of highest energy are those emitted at 0°, and the average neutron energy is somewhat lower. Therefore, the average neutron energy for this position of the detector was taken as that of neutrons emitted at 5°.

RESULTS

The results of the measurements are shown in Fig. 2, where the total neutron cross section is plotted as a function of neutron energy for a target of 10-kev thickness and for the 1-in. thick scatterer. Each point is the average of two successive runs. The upper and lower part of the figure shows measurements taken several days apart. Some energy intervals were covered more than twice, but only two representative runs are shown in Fig. 2. Change of symbol representing experimental points indicates a lapse of more than a day between runs. All measurements were taken in the forward direction except the points marked as circles, which were taken at an angle of 115° with respect to the proton beam.

The statistical standard error in the cross section for all points plotted in Fig. 2 is less than 0.25×10^{-24} cm². In drawing a curve through the

[12] A. O. Hanson, Rev. Sci. Inst. **15**, 57 (1944).
[13] Haxby, Shoupp, Stephens, and Wells, Phys. Rev. **58**, 1035 (1940).

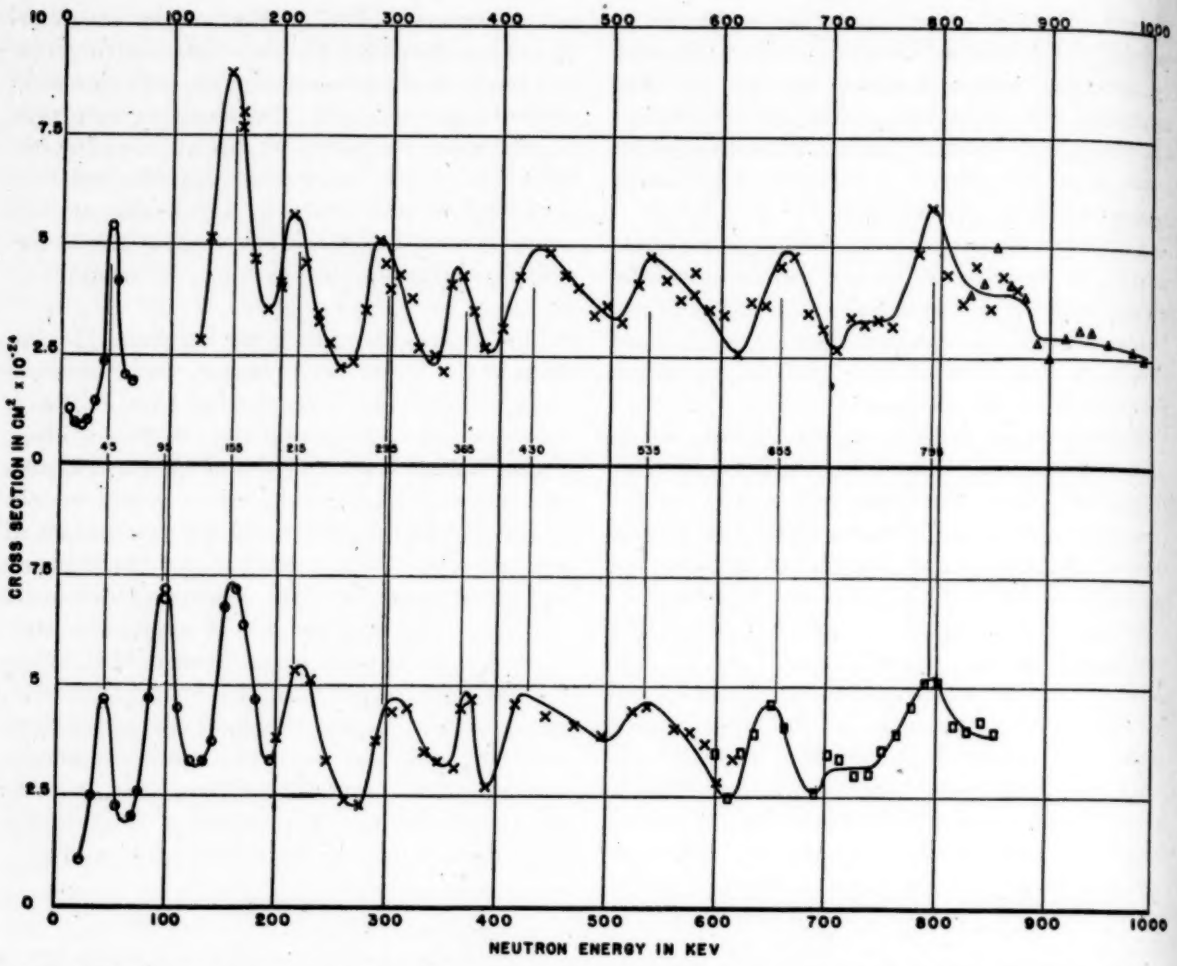

FIG. 2. The total neutron cross section of aluminum as a function of neutron energy. The neutrons were obtained by proton bombardment of a lithium film of 10-kev stopping power. The upper and lower curves represent measurements taken several days apart. Circles indicate measurements taken at 115° with respect to the proton beam, while all other symbols give results for neutrons emitted in the forward direction.

experimental points, peaks were indicated only when at least two successive points were clearly outside the statistical error from a smooth curve in at least two separate runs. Using this criterion, there appeared to be ten peaks in the energy interval covered, i.e., at 45, 95, 155, 215, 295, 365, 430, 535, 655, and 795 kev. In addition, there are indications of unresolved peaks, especially at higher energies. The neutron energies corresponding to the peaks are given to the nearest 5 kev because the separation of the experimental points by approximately 10 kev, combined with their statistical uncertainty, make the drawing of the curve through such points somewhat arbitrary and result in an uncertainty of the energy of the peaks of about 10 kev. In addition, there is an uncertainty in neutron energy of approximately 5 kev, which is primarily caused by the limit of reproducibility of the proton energy determined by the electrostatic analyzer.

The value of the cross section is strongly dependent on the spread in neutron energy as determined by target thickness, proton-energy spread, and geometry. For example, the peak appearing in Fig. 2, at a neutron energy of 155 kev, was measured with the detector in the forward direction for the upper curve and with the detector at 115° for the lower curve. Since the spread in energy of the neutrons emitted at 115° with a mean energy of 155 kev, is greater than the spread in energy of neutrons emitted in

the forward direction with the same mean energy, the peak value of the cross section in the lower curve appears to be smaller. This effect is still more evident in Fig. 3 which shows the results of an investigation of this same peak using a lithium target of 5-kev stopping power and a scatterer, 1-in. thick. Figure 3 is plotted on the same scale as Fig. 2. The peak appears to be higher and narrower than the corresponding peaks in Fig. 2.

In measurements using a 10-kev target, the most important cause of spread in neutron energy is the target thickness. The magnitude of this spread varies with proton energy for a given target. For 150-kev neutrons in the forward direction, a 10-kev target causes a spread in neutron energy of 14 kev. Another limitation of resolving power is the spread of neutron energy over the face of the detector, since the energy depends upon the direction of neutron emission. In the geometry used, this spread amounts to 4 kev at a neutron energy of 150 kev in the forward direction. In addition, the spread in energy of the protons incident upon the lithium target of approximately ± 3 kev results in a neutron energy spread of approximately ± 4 kev. In view of the other limitations of the resolving power, it was felt that a target of less than 5-kev thickness would not give a sufficient improvement to warrant measurements at the resultant low neutron intensity.

In the upper part of Fig. 2, the peak shown at 155 kev has a width at half-maximum of about 35 kev, while according to Fig. 3, it has a width of about 16 kev. A width of 35 kev is somewhat more than one would expect from the above causes of neutron energy spread, although the relatively few experimental points through which the curve is drawn make the determination of the width uncertain. The considerable reduction in width, observed when a thinner target and a thinner scatterer were used, precludes any conclusion regarding the natural width of the resonance peak other than that the width of this peak is less than 16 kev.

The widths of the other peaks shown in Fig. 2 vary from 10 kev to 55 kev, the narrowest peak being at 45 kev where the resolving power is relatively high. Wider maxima appear at higher neutron energies and may well represent two or more unresolved peaks.

In Table I a summary of the results of other authors is given for measurements of the total cross section of aluminum in the range covered by the present measurements, and a comparison is made with cross sections obtained in the present experiment as read from the curves in Fig. 2. While the agreement appears rather poor, an inspection of Fig. 2 shows that small shifts in neutron energy would bring the values into good agreement. It is possible that the energy of the photo-neutron sources is slightly in error or that the different distribution in energy of the photo-neutrons from that of the Li+p neutrons might yield a different value of cross section.

The absorption cross section of aluminum at thermal energies[14] is only 0.2×10^{-24} cm^2, and it would be expected to be smaller at higher energies. One might assume, therefore, that the measured cross sections represent scattering cross sections.

The resonance curves for scattering should show a small decrease in cross section at energies just below the energy of each peak.[6] The complicated resonance structure, which is observed in the present experiment, makes it difficult to

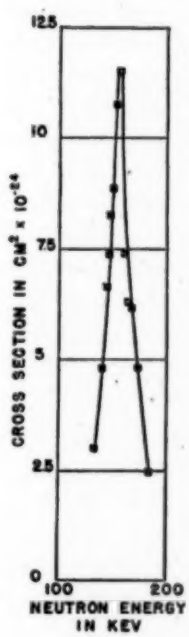

FIG. 3. The 155-kev peak of Fig. 2 measured using neutrons from a lithium target of 5-kev stopping power.

[14] R. D. O'Neal and M. Goldhaber, Phys. Rev. 59, 102 (1941).

TABLE I. Comparison of total neutron cross section of aluminum obtained in present measurements with the results of other authors.

Neutron energy (Mev)	Reference	Cross section (10^{-24} cm^2)	Cross section at same energy according to present data
0.024	a	0.80	1.0
0.13	b	4.0	3.7
0.13	a	5.3	3.7
0.20	c	5.8	4.0
0.22	a	3.2	5.2
0.22	b	3.8	5.2
0.60	c	3.6	3.0
0.62	a	4.1	2.7
0.83	a	3.5	4.1
0.88	b	3.1	3.9
0.88	d	3.4	3.9

a See reference 5.
b See reference 4.
c Barschall, Battat, Bright, Graves, Jorgensen, and Manley, Phys. Rev. (to be published).
d See reference 3.

recognize the expected minima. There may be an indication of such a decrease at 20 kev, however, provided that there are no further resonances below that energy. The total neutron cross section of aluminum at thermal energy[15] and at 1.4 ev[16] is 1.5×10^{-24} cm^2. The lack of variation in this energy range may indicate that there is no resonance in aluminum for slow neutrons. On the other hand, Lichtenberger[17] *et al.* report a resonance for capture in aluminum at 9.1 kev. In the present measurements, no resonance for the total cross section appears in this region.

The theoretical predictions[6] regarding the variations of total cross section with neutron energy are based on the assumption that the measurements represent averages over many resonances. The present measurements indicate that in aluminum the most prominent resonances are spaced at energy intervals of 50 to 100 kev. Thus, neither the present measurements nor measurements on aluminum using photo-neutron sources will give averages over several resonances. It is planned to extend the present measurements to heavier elements in which one would expect the energy-level density to be sufficiently great for the theory to be applicable.

ACKNOWLEDGMENTS

We wish to thank Professor R. G. Herb for making the electrostatic generator available to us and for his interest in this work. We are indebted to Mr. B. Petree for his assistance in the measurements and to the Wisconsin Alumni Research Foundation for financial support.

[15] Dunning, Pegram, Fink, and Mitchell, Phys. Rev. **48**, 265 (1935).
[16] H. B. Hanstein, Phys. Rev. **59**, 489 (1941).
[17] Lichtenberger, Nobles, Monk, Kubitschek, and Dancoff, Bull. Am. Phys. Soc. **22**, 18 (1947).

An Upper Limit for the Cross Section for Scattering of Neutrinos by Hydrogen

E. O. WOLLAN
Clinton Laboratories, Oak Ridge, Tennessee

(Received May 10, 1947)

An upper limit of about 2.0×10^{-30} cm² for the cross section for scattering of neutrinos by hydrogen has been determined. The experiment consisted in an attempt to measure the ionization in hydrogen in the vicinity of the Clinton pile under as nearly ideal shielding conditions as possible. The fact that the ion current in the hydrogen-filled chamber could not be measured and the known sensitivity of the instrument were used to deduce the above-mentioned upper limit to the cross section. One reason for making this determination was to rule out the possibility of neutrinos constituting a health hazard in the vicinity of a high flux pile.

SINCE chain reacting piles constitute very powerful sources of radioactivity, they are presumably also very strong sources of neutrinos. This fact made it logical to consider in the early days of the Plutonium Project whether or not neutrinos could constitute a radiation hazard problem. Wigner considered this problem in a Project Report "On the Available Information Concerning the Interaction of Neutrinos with Matter," June 2, 1943. He pointed out that the only type of interaction of neutrinos with matter for which a cross section can be even approximately calculated is that of the inverse beta-decay. This is the process by which a stable nucleus (A, Z) is converted into one of the nuclei $(A, Z+1)$ or $(A, Z-1)$. Both these processes require energy, and this energy must be furnished by the neutrino. The cross section calculated for this process is in the neighborhood of 10^{-42} cm².

In addition to the inverse beta-decay process there is, however, also the process of elastic scattering of neutrinos by electrons or by heavy particles. It is possible at present only to set a theoretical upper limit to the cross section for the scattering process, and the actual cross section may differ from this by a large amount. Wigner showed that from neutrinos of a few Mev one can expect ionization to occur only in the case of hydrogen, because for heavier nuclei (even helium) the velocity imparted to the recoiling nucleus is insufficient to separate it from its electrons. Nahmias[1] tried to observe the ionization in air produced by the neutrinos emitted by a source of radium heavily shielded against gamma-rays. The negative results from these experiments made it possible to set an upper limit of 10^{-31} cm² to the interaction of neutrinos with electrons. So fas as the cross section for interaction of neutrinos with nuclei is concerned, no conclusions can be drawn from Nahmias' results.

It became possible in connection with some measurements made at the time of the start-up of the Clinton pile (October, 1943) to set an upper limit of about 2.0×10^{-30} cm² for the neutrino-hydrogen scattering cross section. The experiment from which these results were obtained had to do with determining the efficiency for neutron absorption of the shield material to be used in the Hanford piles.* A pair of balanced ionization chambers was used in these measurements. One of these chambers was filled with CH_4 at about 11 atmosphere pressure and the other with argon at a pressure just sufficient to give an equal response to gamma-rays. When these chambers have opposite collecting potentials applied to them and are connected together to an electrometer, the apparatus measures the difference in ionization produced in them. Although the apparatus was built for measuring neutrons it will measure any radiation for which the ratio of ionization in CH_4 and argon is different from that for gamma-rays.

Since the scattering of neutrinos by hydrogen should produce ionization in that gas, the

[1] M. E. Nahmias, Proc. Camb. Phil. Soc. **31**, 99 (1935).

* This experiment was carried out by K. Z. Morgan, H. M. Parker, and E. O. Wollan.

measurements at Clinton permit one to set an upper limit to the cross section for neutrino-hydrogen scattering. One would expect the cross section for the scattering of neutrinos by other nuclei to be of the same order of magnitude although it would not lead equally readily to ionization.

The sensitivity of the above apparatus for neutrons was determined with a Ra-Be source (at a voltage sensitivity of the electrometer of 160 div/volt) to be 1 neutron per cm^2 sec. $=0.032$ div/sec., or making use of the voltage sensitivity one has that 1 neutron per cm^2 sec. $=2\times10^{-4}$ volt/sec. The electrical capacity of the system being about 4×10^{-11} farad, this gives the current response of the instrument for 1 neutron per cm^2 sec. $=8\times10^{-15}$ ampere or 5×10^4 ion pairs per second formed in the chamber.

For the measurements of the neutron activity through the shield the pile was operated at constant power for several minutes. The electrometer showed no measurable deflection during this time but wandered very slightly some of the time in one direction and some of the time in the opposite direction. An analysis of the readings showed a maximum rate of drift corresponding to that which would be produced by about ±0.25 neutron per cm^2 sec. If the rate of drift had been four times this amount (i.e., corresponding to 1, neutron per cm^2 sec. or 5×10^4 ion pairs per sec. in the chamber) the deflection rate would certainly have been measurable. On this basis then if the neutrino-hydrogen scattering cross section were of such magnitude that the ionization by neutrinos reached a value of 5×10^4 ion pairs per sec. in the chamber, a measurable current would have been observed.

An upper limit to the neutrino-hydrogen cross section can be calculated from these results, on the assumption that about two pile neutrinos per fission will have sufficient energy to produce on the average about $\frac{1}{4}$ ion pair per neutrino-hydrogen scattering event.

If F = number of fissions per sec. at operation power, d = distance from center of pile to chamber, n = number of atoms of hydrogen in the chamber, and σ = neutrino-hydrogen scattering cross section, then the ionization, I, produced in the chamber will be

$$I=\tfrac{1}{4}(2Fn\sigma/4\pi d^2)$$

or

$$\sigma_{\text{upper limit}}=(8\pi d^2/Fn)\times I_{\text{upper limit}}.$$

The ion chambers had a volume of about 2000 cm^3, and one of them was filled with CH_4 at a pressure of 11 atmospheres. F and d are not given for security reasons..

On the basis of $I_{\text{upper limit}}=5\times10^4$ ion pairs per sec. the following value of the upper limit for neutron-hydrogen scattering cross section was obtained.

$$\sigma_{\text{upper limit}}\cong2\times10^{-30}\ \text{cm}^2.$$

This document is based on work performed under Contract No. W-35-058-eng-71 for the Manhattan Project, and the information covered therein will appear in Division IV of the MPTS as part of the contribution of the Clinton Laboratories.

Alpha-Particles Associated with Fission*

E. O. WOLLAN, CHARLES D. MOAK, AND R. B. SAWYER**
Clinton Laboratories, Oak Ridge, Tennessee

(Received June 2, 1947)

The photographic emulsion technique has been applied to the study of the long range particles associated with the fission of uranium. Twenty such long range tracks were observed and studied. From the grain spacing along the tracks it was possible to show that the particles are not protons but are most likely alpha-particles. The maximum range observed for the long range alphas is about 40 cm of normal air. From the distribution in angle with respect to the fission tracks, it is shown that the alphas are not emitted from the fission fragments but are released as a part of the fission process.

IN this work the photographic emulsion technique has been applied to the study of the long range particles associated with the fission of uranium.

Alvarez first observed these particles and Segrè, *et al.* have made a study of them with ion chambers arranged to give coincidences between the particles and the fission fragments. They have identified the particles as alpha-particles from measurements of the density of ionization near the ends of their range. Hughes has observed some of these alpha-particles in the cloud chamber, but his set-up did not permit him to observe the associated fission tracks.

The cloud chamber or photographic emulsion technique permits information to be obtained about the alpha-particles and their association with the fission process that cannot be easily obtained by the ion chamber method.

The photographic emulsion technique has been

TABLE I.

No.	Fission fragment tracks: One fragment Length microns	One fragment No. of grains	Other fragment Length microns	Other fragment No. of grains	Alpha-tracks Length microns	Alpha-tracks No. of grains	Angle of α with fission $\theta°$	Deviation of fission tracks from 180° $\Delta°$	Range of α in cm air*	Energy of α Mev
1	10.0	11	10.2	14	282	138	130	—	39.4	22.1
2	17.0	10	16.0	10	154	66	72	—	21.6	15.2
3	14.5	10	17.5	8	160	82	80	—	22.4	15.6
4	13.8	10	12.8	8	284	140	51	—	39.7	22.2
5	13.5	9	12.7	7	154	65	75	12	21.6	15.2
6	8.5	10	9.5	9	208	97	17	—	29.0	18.2
7	9.9	11	9.45	14	207	94	84	10	28.9	18.1
8	10.35	12	14.2	14	244	129	62	4	34.2	20.2
9	9.5	6	11.5	11	64.5	27	88	2	9.0	9.2
10	14.5	9	10.2	8	97	48	72	6	13.7	11.6
11	12.2	8	11.5	8	161	94	83	2	22.4	15.6
12	11.5	9	10.0	9	108	66	72	0	15.1	12.2
13	10.6	9	13.1	11	160	71	57	23	22.4	15.6
14	11.1	9	7.8	8	105	49	73	2	14.7	12.0
15	15.8	10	14.0	10	251	115	82	0	35.2	20.3
16	9.3	6	11.3	8	256	122	90	8	35.8	20.8
17	13.9	10	10.5	11	186	97	87	2.5	26.0	17.0
18	14.3	11	14.0	9	111	60	86	5	15.6	12.6
19	10.7	9	10.7	9	171	74	90	8	23.9	16.1
20	9.4	10	10.5	5	151	80	89	0	21.2	15.0

* The stopping power of the emulsion is taken as 1400 times that of air.

* This paper appeared as a report on the Manhattan Project in July 1944. The report is maintained in essentially the same form as originally written, without regard to more recent work which has been done on the project and to work which has now been published in this Journal; i.e., Pierre Demers, Phys. Rev. 70, 974 (1946); G. Farwell, E. Segrè, and C. Wiegand, Phys. Rev. 71, 327 (1947); Tsien San-Tsiang, Ho Zah-Wei, R. Chastel, and L. Vigneron, Phys. Rev. 71, 382 (1947). D. L. Hill has made a rather extensive study of the range of these particles with a coincidence chamber arrangement.

** Now at Lehigh University, Bethlehem, Pennsylvania.

used in this case because it lends itself very well to a study of rare events of this type.

EXPOSURE OF PLATES

Eastman alpha-particle plates with an emulsion thickness of about 50μ were used. It was desirable to obtain as large a number of fission events in the emulsion as possible without too high a background. It was found that the plates could be soaked in a saturated water solution of uranyl acetate without damaging the emulsion. Plates soaked in this solution for 30 minutes were dried and then exposed near the edge of the reflector of the Clinton Pile for 1 or 2 sec. This gave of the order of 10^6 fission tracks on a $3'' \times 1''$ plate. Control plates (a) irradiated but unsoaked, and (b) soaked but not irradiated, were made as a check on natural alpha-particle tracks and recoil protons from the small percent of fast neutrons from this place in the pile. A single good plate which can be made in a few hours after the conditions of exposure have been determined furnishes material for a long and tedious examination under the microscope.

TRACK DATA

A plate area of about 10 cm^2 has been searched for long range alphas. In all cases to date in which both ends of the alpha-track are observed to lie in the emulsion, it has been found that the alpha-particle originates near the center of a fission track. So far twenty such tracks have been observed and measured. The data on these tracks are given in Table I. The lengths and number of grains are listed for each fission particle track and for the alpha-particles. The true angle between one fission fragment and the alpha-track is given as θ. This angle was determined from the horizontal projection angle and the depths of the track ends in the emulsion. The angular deviation of the fission track from a straight line is listed as $\Delta°$. Natural curvatures in the tracks make it impossible to expect any accuracy in these values. Most of the angles are, however, positive, as is to be expected for conservation of momentum.

In order to get a good microphotograph of a track, it should lie nearly in a plane perpendicular to the axis of the microscope. So far no track has fulfilled this condition for both the fission and alpha-particle. A few cases have, however, been photographed and are shown in Figs. 1 and 2. All these photographs have been made by piecing together sections of the track for which the grains were in approximate focus at one setting of the microscope. In Fig. 1b the track has been retouched in a few places where the grains were not in sharp focus.

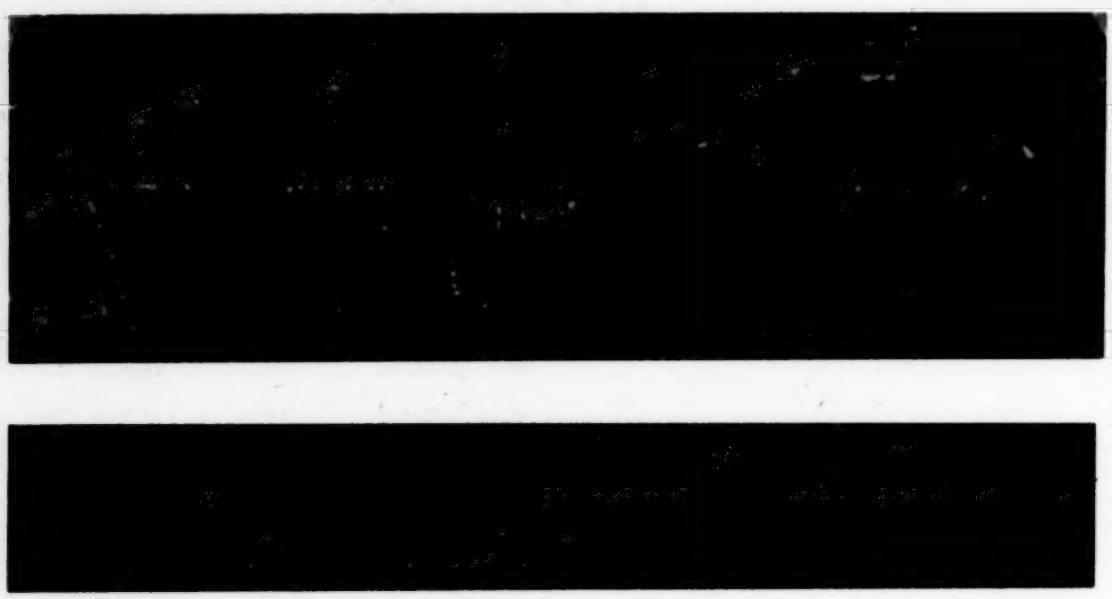

FIG. 1. Examples of long range alpha-tracks associated with fission.

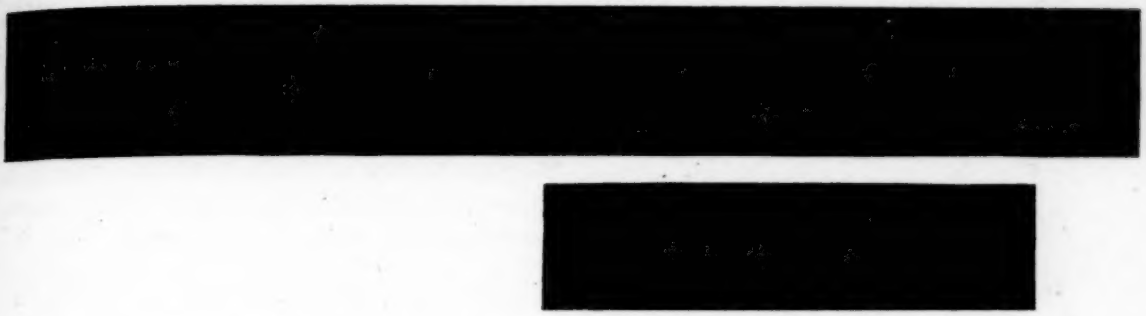

FIG. 2. Long alpha-track associated with fission (upper picture) as compared with a recoil proton track (lower picture). The difference between the two tracks can be seen by comparing their average grain spacings. The pictures are so placed that the ends of the tracks fall at the same distance from the left side of the page.

In Fig. 2 a short proton track has been included for comparison of grain spacing with the alpha-track. This point is discussed in the next paragraph.

EVIDENCE THAT PARTICLES ARE ALPHAS

Alpha-particle tracks can be distinguished from proton tracks by the relative grain spacings along the tracks. To check this, a plate was exposed to fast neutrons from the cyclotron and the grain spacings for long recoil proton tracks were measured. In Table II comparison is made of the grain spacing for two (α_1 and α_2) of our so-called long range alpha-tracks with the average spacing for 6 long proton tracks. Figure 3 shows the data of Table II in graphical form. It is evident that these long range particles are not protons, and hence it seems logical to assume that they are alpha-particles, although the evidence presented here does not exclude the possibility of their being identified with other light nucleii.

EVIDENCE FOR ALPHA-PARTICLES BEING EMITTED IN FISSION PROCESS

The fact that the alpha-particles originate near the center of the fission track does not in itself show that these alphas are liberated in the fission act; they may be ejected from one of the fission fragments left in a highly excited state.

The time scale given by the velocity and range of the fission particles is very short in a photographic emulsion. The time for a fission particle to travel 10 microns in the film is in the neighborhood of 10^{-12} sec. The alpha must then be coincident with fission within less than 10^{-13} sec. For alpha-particles of the high energy encountered here, however, even this short a time is long compared to the average lifetime before emission of the alpha-particle, and hence this gives no information regarding the nature of the process.

If the alpha-particles were emitted from the fission fragments after fission has occurred, one should expect in the center of gravity system a random angular distribution of the alphas with respect to the fission tracks. This would mean an angular distribution function $N(\alpha)d\alpha = \sin\alpha d\alpha$ in the center of gravity system from which the angular distribution function in the laboratory system can be calculated for a given energy and

TABLE II. Grain spacing of long range alphas compared to spacing of proton tracks.

Tracks	Grains per 20 microns as a function of distance from end of tracks in microns						
	0–20	20–40	40–60	60–80	80–100	100–150	150–200
α_1	14	14	13	13	11	10.2	8.8
α_2	10	14	13	11	13	8.4	8.8
Average of 6 proton tracks	10	9	6	6	5.5	3.4	3.4

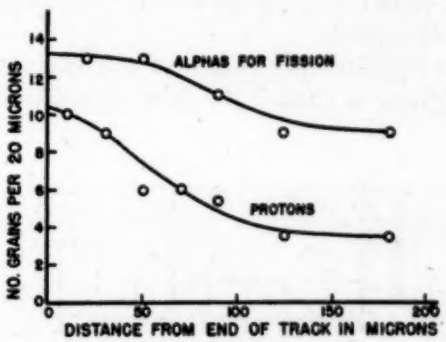

FIG. 3. Comparison of grain spacings for α-particles and protons.

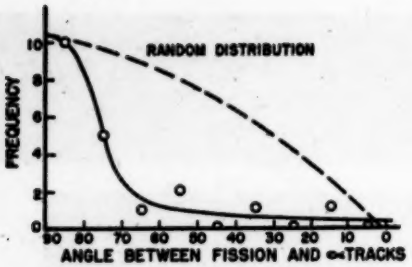

FIG. 4. Angular distribution of α-tracks.

mass of the alphas and the fission fragments. This was done by an approximate method for the more or less average case for which $E_f/E_\alpha=6$ and $m_f/m_\alpha=24$. It is found on this basis that in the laboratory system there is a preponderance of alphas emitted near 45° with its fission track, but when the emission for the two fission fragments is averaged, the distribution function is not very different from that in the center of gravity system, being slightly higher than the sine function at small angles.

If, instead of being emitted by a fission fragment, the alpha-particle is more or less pinched off between the two heavier fragments in the fission act, then it is to be expected that the angular distribution of the alphas will favor the direction normal to the fission track. This is readily seen when one considers the forces on the alpha-particle located in the region between two positively charged particles. The path which the alpha-particle will travel will be determined by the magnitude and direction of its initial velocity and on the magnitude of the charges carried by the fission fragments. If the initial velocity is small, the alpha will move down the potential valley of the two charged particles, in which case the alpha will make a large angle with the fission track. With a large initial velocity, however, any angle is possible.

The angular distribution of the twenty particles given in Table I is plotted as the solid line and points of Fig. 4. The dashed line is for random distribution. The observed distribution is sufficiently different from the random case to indicate quite definitely that many of the alphas at least are ejected in the fission act. This might be taken as the first evidence of the existence of three-particle fission, although this is certainly a very special case of such a process.

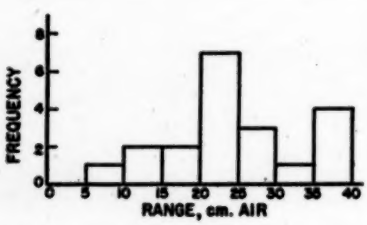

FIG. 5. Energy distribution of the α-particles.

RANGE AND ENERGY OF ALPHA-PARTICLES

We have not yet been able to make accurate stopping power determinations for the alpha-particle plates which we have been using, but this has been done previously for these plates. From the literature it seems that the stopping power of the plates relative to air is about 1400. Using this value and Bethe's energy-loss formula, the energy of the particles has been calculated. The range in air and the calculated energy are tabulated in the last two columns of Table I. An energy distribution for the twenty measured alphas is also shown in the block diagram of Fig. 5. The highest energy alphas (~22 Mev) which we find are higher than any of those reported so far by Alvarez, Segrè, or Hughes, and are much higher than any alphas previously observed to accompany any natural process.

RANGE DISTRIBUTION OF FISSION FRAGMENTS

The distribution in length of the normal fission tracks (total track) is plotted in the upper curve of Fig. 6. The range distribution for the fission tracks which are accompanied by alpha-emission is plotted in the lower curve of the same figure. It is seen that the average range of the latter is about 20 percent less than for normal tracks. This is to be expected if the

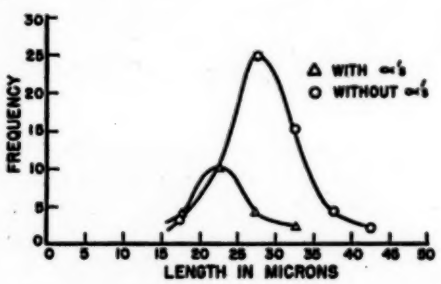

FIG. 6. Distribution in length of fission tracks (upper curve). Range distribution of fission tracks which are accompanied by α-emission (lower curve).

available energy is about the same in the two cases, and in one case the alpha takes off from 10 percent to 15 percent of the energy.

For the fission tracks listed in Table I, a distribution in range can be plotted for individual fragments, since the alphas mark the point of origin. Such a distribution curve is shown in Fig. 7. With only 40 tracks, the accuracy of the curve is necessarily low, but it is felt that the two groups are within the accuracy of the data to resolve. Two groups might be expected from the two energy groups associated with the light and heavy fragments as shown by Jentsche[1] and Flammersfeld, Jensen, and Gentner.[2]

[1] W. Jentsche, Zeits. f. Physik **120**, 165 (1943).
[2] A. Flammersfeld, P. Jensen, and W. Gentner, Zeits. f. Physik **120**, 450 (1943).

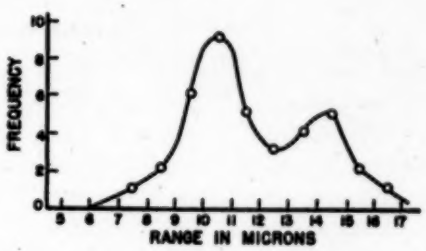

FIG. 7. Distribution in range of individual fragments in fission.

This document is based on work performed under Contract No. W-7405-eng-39 for the Manhattan Project, and the information covered therein will appear in Division IV of the MPTS as part of the contribution of the Argonne National Laboratory.

PHYSICAL REVIEW VOLUME 72, NUMBER 6 SEPTEMBER 15, 1947

Hyperfine Structure and Nuclear Moments of Columbium[93]

WILKISON W. MEEKS* AND RUSSELL A. FISHER
Department of Physics, Northwestern University, Evanston, Illinois

(Received May 31, 1947)

Measurements have been made on the hyperfine structure of 32 lines in the spectrum of CbI. Analysis of these structures supports the previously reported spin value of $4\frac{1}{2}$ units for the Cb^{93} nucleus and yields 32 hyperfine interval factors. These data, when used in conjunction with semi-empirical formulas for the coupling between the nucleus and an s electron in the configuration $4d^4\,5s$, lead to values for the nuclear g-factor and nuclear magnetic moment of 1.18 and 5.3 nuclear magnetons, respectively, for stable Cb^{93}. No nuclear electric quadrupole moment is detected.

INTRODUCTION

THE first published measurements and analysis of columbium hyperfine structure were by Ballard[1] who examined the intervals and intensities in ten visible lines. On a basis of this study he reported the nuclear spin as $4\frac{1}{2}$ units and the nuclear magnetic moment as 3.7 nuclear magnetons. Ballard's analysis was handicapped by a lack of information concerning the term structure of CbI, which was at that time very incompletely known. Subsequently, Meggers and Scribner[2] and Humphreys and Meggers[3] published very extensive classifications of the CbI lines and energy states, thus greatly facilitating a more detailed investigation of the hyperfine structure. We have measured the structure of 32 lines in the visible and by analysis of these data determined 32 hyperfine interval factors. Our analysis is in agreement with Ballard's value of $4\frac{1}{2}$ for the nuclear spin, but indicates a nuclear magnetic moment 43 percent larger than reported by him.

* Now at Western Maryland College, Westminster, Maryland.
[1] S. S. Ballard, Phys. Rev. **46**, 806 (1934).
[2] W. F. Meggers and B. F. Scribner, J. Research Nat. Bur. Stand. **14**, 629 (1935).
[3] C. J. Humphreys and W. F. Meggers, J. Research Nat. Bur. Stand. **34**, 477 (1945).

TABLE I. Hyperfine structure of CbI lines.

Wave-length (A.U.)	Intensity (estimated)	Component separations (cm^{-1})	Wave-length (A.U.)	Intensity (estimated)	Component separations (cm^{-1})
		0.000	4287.0	3	0.000
		−0.305		2	0.158
6660.8*		−0.567			
		−0.800	4262.1	2	0.000
	e	−1.416		1	0.168
	4	0.000		5	0.000
	2	0.122	4205	4	0.108
5664.7	2	0.245		e	0.430
	2	0.365		5	0.000
	2	0.445	4195.1	4	0.163
	5	0.000		6	0.000
	4	−0.109		5	0.146
5350.7	3	−0.199	4192.1	4	0.283
	e	−0.344		e	0.667
	7	0.000		6	0.000
	6	−0.152		5	0.149
	5	−0.282	4190.9	4	0.292
5344.1*	4	−0.397		3	0.398
	3	−0.490		e	0.733
	e	−0.607		1	0.000
	4	0.000	4168.1	1	0.258
	2	0.126		1	0.551
5271.5	2	0.247			
	2	0.371		5	0.000
	2	0.448	4163.7	2	0.169
				3	0.273
	5	0.000		7	0.000
5180.3	2	0.120		6	0.141
	3	0.000	4152.6	5	0.269
5160.3	2	0.131		4	0.382
				e	0.624
	2	−0.116		8	0.000
5134.7	10	0.000		7	0.171
	6	0.143		6	0.321
	1	0.298	4139.7	5	0.455
	3	0.000		4	0.573
5120.3	2	−0.143		e	?
	5	0.000		6	0.000
5100.2	3	−0.174	4137.1	5	0.222
	3	0.000		5	0.000
5095.2	2	−0.176		3	0.117
	5	0.000	4123.8	2	0.216
5079.0	2	−0.154		7	0.000
	1	−0.323	4116.9	6	0.287
	6	−0.148		6	0.000
5058.0	10	0.000		5	0.125
	2	0.132	4100.9	4	0.233
				e	0.433
	10	0.000		8	0.000
5039.0	7	−0.178		7	0.145
	3	0.000		6	0.275
4989.0	2	−0.215	4079.7	5	0.384
	6	0.000		4	0.481
	5	−0.099		e	0.618
4606.8	e	−0.446			
				10	0.000
	5	0.000		9	0.191
4546.8	2	−0.119		8	0.359
	6	0.000	4058.9	7	0.510
	5	0.133		6	0.638
4523	4	0.245		5	0.747
	3	0.326		e	0.862

* As reported by Ballard.

EXPERIMENTAL DATA

In our observations the columbium spectrum was excited in helium in a water-cooled hollow cathode-discharge tube, thin sheets of metallic columbium being used to line the cathode cavity. Dispersion was provided by a Fabry-Perot interferometer with silvered mirrors, combined with a Littrow type prism spectrograph having glass optics.

Table I gives the results of our measurements on 32 line patterns and includes two additional lines of interest from Ballard's data. Component separations in each pattern are expressed in cm^{-1} with respect to the strongest line of the pattern. Since many of the structures are only partially resolved, the measured positions may refer only to points of maximum intensity in the pattern. The e's appearing in the intensity column indicate the estimated end of an incompletely resolved pattern. All lines here reported with the exception of λ4205 were measured on at least three photographic plates.

ANALYSIS

All evidence based on measured component intervals is in agreement with Ballard's assigned value of $I=4\frac{1}{2}$ for the nuclear spin of Cb^{93}. Because of the large indicated spin and the possibility of pattern distortion by a nuclear electric quadrupole, other spin values could not immediately be excluded on the ground of the observed intervals alone. In particular, careful consideration had to be given to the possibility of a spin of $3\frac{1}{2}$, which was also found to be consistent with observed interval ratios in resolved "flag" type patterns such as λ4059. Over-all consistency in the analysis of the numerous patterns favors overwhelmingly the spin of $4\frac{1}{2}$ units, however. No other assumed spin value permits a consistent interpretation of all the observed patterns. Accepting the spin as $4\frac{1}{2}$ units, it may be said that no nuclear electric quadrupole moment is detectible in Cb^{93} within the limit of accuracy of the present observations.

The classification and electron configurations

TABLE II. Classification of Cb lines.

		$4d^4(^5D)5s\ ^6D$					$4d^35s^2\ ^4F$			
	J	$\frac{1}{2}$	$1\frac{1}{2}$	$2\frac{1}{2}$	$3\frac{1}{2}$	$4\frac{1}{2}$	$1\frac{1}{2}$	$2\frac{1}{2}$	$3\frac{1}{2}$	$4\frac{1}{2}$
$4d^35s(^5F)5p\ ^6D^\circ$	$\frac{1}{2}$		5134.7							
	$1\frac{1}{2}$	5058.0		5160.3						
	$2\frac{1}{2}$		5039.0	5100.2	5180.3					
	$3\frac{1}{2}$				5095.3					
	$4\frac{1}{2}$				4989.0	5079.0				
$4d^4(^5D)5p\ ^6F^\circ$	$\frac{1}{2}$	4168.1	4195.1							
	$1\frac{1}{2}$	4137.1	4163.7	4205.3						
	$2\frac{1}{2}$		4123.8							
	$3\frac{1}{2}$			4100.9	4152.6					
	$4\frac{1}{2}$				4079.7	4139.7				
	$5\frac{1}{2}$					4058.9				
$4d^4(^5D)5p\ ^6P^\circ$	$1\frac{1}{2}$	4116.9								
	$2\frac{1}{2}$				4192.1					
	$3\frac{1}{2}$					4190.9				
$4d^35s(^5F)5p\ ^6F^\circ$	$\frac{1}{2}$						5664.7			
	$1\frac{1}{2}$									
	$2\frac{1}{2}$									
	$3\frac{1}{2}$			5120.5						
	$4\frac{1}{2}$									
	$5\frac{1}{2}$									
$4d^35s(^3F)5p\ ^4D^\circ$	$\frac{1}{2}$						5271.5			
	$1\frac{1}{2}$									
	$2\frac{1}{2}$								5350.7	
	$3\frac{1}{2}$									5344.2
$4d^35s(^3F)5p\ ^4F^\circ$	$1\frac{1}{2}$						4523.4			
	$2\frac{1}{2}$							4546.8		
	$3\frac{1}{2}$				4287.0					
	$4\frac{1}{2}$					4262.1				4606.8

reported by Meggers and Scribner[2] and Humphreys and Meggers[3] for the lines here of interest are given in Table II. The wave-lengths of the lines appear within the rectangles and the terms from which they originate along the margins, even terms above and odd terms to the left.

Graphical analysis procedures described elsewhere[4, 5] were applied to the observed line patterns and lead to the hyperfine interval factors for thirty-two terms given in Table III. Because some of the patterns are more completely resolved and hence permit more positive interpretation than others, the interval factors cannot be given equal weight regardless of the indicated numerical accuracy. They have, therefore, been rated *A*, *B*, and *C* to indicate the degree of confidence with which they may be regarded, *A* indicating that we consider both the interpretation and the measurement reliable, *C* that the interpretation is somewhat doubtful.

TABLE III. Hyperfine interval factors for CbI.

State	*J*	Interval factor (cm^{-1})		
$4d^4(^5D)5s\ ^6D$	$\frac{1}{2}$	0.060		
	$1\frac{1}{2}$	0.028		
	$2\frac{1}{2}$	0.024	±0.001	*A*
	$3\frac{1}{2}$	0.022		
	$4\frac{1}{2}$	0.021		
$4d^35s^2\ ^4F$	$1\frac{1}{2}$	0.021	±0.001	*A*
	$2\frac{1}{2}$	0.013	±0.001	
	$3\frac{1}{2}$	0.004		*C*
	$4\frac{1}{2}$	0.005		
$4d^35s(^5F)5p\ ^6D^\circ$	$\frac{1}{2}$	0.057		
	$1\frac{1}{2}$	0.029		
	$2\frac{1}{2}$	0.028	±0.001	*A*
	$3\frac{1}{2}$	0.026		
	$4\frac{1}{2}$	0.024		
$4d^4(^5D)5p\ ^6F^\circ$	$\frac{1}{2}$	0.049	±0.001	*A*
	$1\frac{1}{2}$	0.010		
	$2\frac{1}{2}$	0.005		
	$3\frac{1}{2}$	0.004		*C*
	$4\frac{1}{2}$	0.002		
	$5\frac{1}{2}$	0.000		
$4d^4(^5D)5p\ ^6P^\circ$	$1\frac{1}{2}$	0.001		
	$2\frac{1}{2}$	0.004		*C*
	$3\frac{1}{2}$	0.004		
$4d^35s(^5F)5p\ ^6F^\circ$	$\frac{1}{2}$	−0.026	±0.001	*A*
	$1\frac{1}{2}$	?		
	$2\frac{1}{2}$	?		
	$3\frac{1}{2}$	0.021	±0.001	*B*
	$4\frac{1}{2}$	?		
	$5\frac{1}{2}$	?		
$4d^35s(^3F)5p\ ^4D^\circ$	$\frac{1}{2}$	−0.025	±0.001	*A*
	$1\frac{1}{2}$	?		
	$2\frac{1}{2}$	0.020	±0.003	*C*
	$3\frac{1}{2}$	0.025	±0.001	*B*
$4d^35s(^3F)5p\ ^4F^\circ$	$1\frac{1}{2}$	0.000	±0.001	*B*
	$2\frac{1}{2}$	0.016	±0.001	*C*
	$3\frac{1}{2}$	0.018	±0.001	*B*
	$4\frac{1}{2}$	0.017	±0.001	*B*

NUCLEAR MAGNETIC MOMENT

An approximate calculation of the nuclear *g*-factor of Cb^{93} may be made by means of certain semi-empirical relations suggested by Goudsmit.[6] These relations connect the nuclear *g*-factor to the observed hyperfine coupling factors and other experimentally determinable parameters which depend upon the coupling between a single optical electron and the nucleus. Most favorable for this purpose are the five hyper-multiplets occurring in the ^6D states arising from the $4d^4(^5D)5s$ electron configuration. These five hyperfine interval factors are rather accurately known from our analysis and are theoretically favorable because the contribution of the 5*s* electron to the splittings is separable to a good approximation from that of the $4d^4$ group.

Goudsmit's relations expressing the nuclear *g*-factor in terms of the coupling between an *s* electron and the nucleus can be written in a single formula as follows:

$$g(I)=a(s)\frac{R^{\frac{1}{2}}Z_0 1840(3-4\alpha^2Z^2)(1-\alpha^2Z^2)^{\frac{1}{2}}}{8\alpha^2ZW^{\frac{1}{2}}}.$$

Here W is the energy in cm^{-1} necessary to remove the *s* electron from the atom in that stage of ionization in which it is the only outer electron, and the other symbols have their usual conventional meaning. The coupling coefficient $a(s)$ for an *s* electron in a given configuration and state can be obtained from hyperfine structure data, provided there are available interaction relations expressing the observed interval factors in terms of the nuclear coupling factors for individual electrons of the configuration. A set of formulas directly applicable to the $4d^45s\ ^6D$ states has been derived by Fisher and Peck[5] for

[4] R. A. Fisher and S. Goudsmit, Phys. Rev. **37**, 1057 (1931).
[5] R. A. Fisher and E. R. Peck, Phys. Rev. **55**, 270 (1939).
[6] S. Goudsmit, Phys. Rev. **43**, 636 (1933).

d^4s ^6D states.** These formulas may be written:

$$A(\tfrac{1}{2}) = \frac{7}{15}a(s) - \frac{4}{3}a(d^4) - \frac{4}{3}b(d^4),$$

$$A(1\tfrac{1}{2}) = \frac{13}{75}a(s) + \frac{2}{15}a(d^4) + \frac{74}{105}b(d^4),$$

$$A(2\tfrac{1}{2}) = \frac{23}{175}a(s) + \frac{12}{35}a(d^4) + \frac{164}{245}b(d^4),$$

$$A(3\tfrac{1}{2}) = \frac{37}{315}a(s) + \frac{26}{63}a(d^4) + \frac{222}{441}b(d^4),$$

$$A(4\tfrac{1}{2}) = \frac{1}{9}a(s) + \frac{4}{9}a(d^4) - \frac{20}{63}b(d^4),$$

$$\Sigma A = a(s).$$

Here $A(\frac{1}{2}) - A(4\frac{1}{2})$ are the hyperfine interval factors for the different states of the ^6D multiplet, the inner quantum number of the state being indicated in the parenthesis, $a(s)$ the coupling coefficient of the s electron, and $a(d^4)$ and $b(d^4)$ the orbital and spin parts, respectively, of the coupling coefficient for the d^4 electron group. Values of $a(s)$, $a(d^4)$, and $b(d^4)$ are determined by inserting in these formulas the experimental values of the A's from Table III. Since there are more equations than unknowns, consistency provides some check upon the accuracy of the formulas. Values of the coupling constants found to give best consistency are:

$$a(s) = 0.155 \text{ cm}^{-1},$$
$$a(d^4) = 0.0089 \text{ cm}^{-1},$$
$$b(d^4) = 0.0004 \text{ cm}^{-1}.$$

Substitution of these values into the formulas gives for the interval factors $A(\frac{1}{2}) - A(4\frac{1}{2})$ respective values of 0.060, 0.028, 0.023, 0.022, and 0.021 cm^{-1}. These are to be compared with the values in Table III and seem to speak well for the validity of the formulas in this case.

An experimental value of $a(s)$ is now available for substitution into the formula for $g(I)$ given above. The value for W required by the formula is found by using the data of Humphreys and Meggers[3] to determine the energy change in going from the center of gravity of the ^6D and ^4D terms of the $3d^4 4s$ configuration in CbI to the center of gravity of the $3d^4$ ^5D in CbII. For this we use the value 51,200 cm^{-1}. Using for the other parameters the values $R = 1.097 \times 10^5$ cm^{-1}, $\alpha = 1/137$, $Z_0 = 1$, $Z = 41$, we obtain for $g(I)$, the nuclear *g-factor* of the Cb^{93} nucleus, the numerical value 1.18. Multiplying this by the nuclear spin of $4\frac{1}{2}$ units gives a nuclear magnetic moment of 5.3 nuclear magnetons.

The value 1.18 here obtained for $g(I)$ is 43 percent larger than that reported by Ballard. While admittedly both results are approximations, we believe that somewhat more confidence may be placed in the larger value since it is based upon more complete hyperfine structure data, a knowledge of the ionization potential of the atom, and computations which take into account the coupling between the s electron and the nucleus in a more detailed way. The significance of the third figure in our g-value is, of course, doubtful.

** It is to be recognized that the assumption of a coupling factor like $a(s)$, which is constant for all states of a multiplet, is valid only within limits.

The Relative Abundance of Some Light Nuclear Species as Determined from the Composition of Stony Meteorites

HARRISON BROWN AND CLAIRE PATTERSON
Institute for Nuclear Studies, University of Chicago, Chicago, Illinois

(Received June 9, 1947)

A statistical study has been made of the relative abundances of the major constituents of the silicate phase of stony meteorites. The results of that study, for the case of lithophile elements, have been combined with data on isotopic abundances, thus giving figures for the abundances, relative to one another, of several nuclear species. The abundance ratios of three isobaric pairs: $K^{40}-Ca^{40}$, $Ca^{46}-Ti^{46}$, and $Ca^{48}-Ti^{48}$, are given.

I. INTRODUCTION

IN recent years increasing thought has been given by physicists to such questions as the relationships between nuclear stability and relative abundance, and in particular to the question of the origin of the elements. To date the only reasonably adequate compilation of relative abundances of nuclear species available, for comparing theory with experiment, is that of V. M. Goldschmidt,[1] compiled in 1938 after much painstaking work on the part of both himself and his colleagues.

The major portion of Goldschmidt's compilation of abundance data depends upon the observed chemical composition of meteoritic matter. Necessarily, one must make certain important, and as yet unproved assumptions concerning the nature and origin of meteors and meteorites,[2] before one is able to apply data on their composition to a compilation of the relative abundance of nuclear species. Nevertheless, if one is willing to assume the validity of those assumptions, until they are either proved or disproved, it is important to evaluate the accuracy with which relative abundances can be determined.

TABLE I. Average composition of the silicate phase of stony meteorites by elements.

Element	Atomic percent	Atoms per 100 atoms of Si
*oxygen	58.09 ±1.36	350 ±11
*silicon	16.60 ±0.15	100
*magnesium	14.73 ±0.28	88.7 ± 2.5
iron	5.11 ±0.16	30.8 ± 1.3
*calcium	1.11 ±0.11	6.70 ± 0.74
*aluminum	1.46 ±0.12	8.82 ± 0.81
*sodium	0.76_8 ±0.05_2	4.62 ± 0.36
nickel	0.14_5 ±0.02_5	0.87 ± 0.16
chromium	0.15_0 ±0.02_5	0.90 ± 0.16
manganese	0.12_2 ±0.02_5	0.74 ± 0.16
*potassium	0.11_5 ±0.01_1	0.69_3 ± 0.07_5
*titanium	0.04_3 ±0.01_4	0.26_0 ± 0.09_0
phosphorus	0.11_6 ±0.01_0	0.69_3 ± 0.06_5
hydrogen	1.40 ±0.35	8.4 ± 2.2
cobalt	0.0079±0.0033	0.048± 0.020

* Denotes that element is markedly lithopile in character, i.e., the concentrations of the element in the iron and sulfide phases are completely negligible.

II. THE SILICATE PHASE OF STONY METEORITES

For the light elements sodium, magnesium, aluminum, silicon, potassium, calcium, and titanium, Goldschmidt used the average composition of stony meteorites as reported in 1916 by G. P. Merrill.[3] Merrill determined his averages from the selected analyses of 59 stony meteorites. Since his work was done, a sufficient number of additional analyses of stony falls have become available to warrant a re-evaluation.

The authors have recently completed a statistical study of the analyses of 107 separate stony meteorites.[4] From the study, averages for each of the major constituents in the silicate phase were obtained, together with standard deviations and the precisions of the averages. The results, expressed in terms of elements, are shown in Table I.

Stony meteorites are commonly broken down

[1] V. M. Goldschmidt, "Geochemische Verteilungsgesetze der Elemente, IX. Die Mengenverhältnisse der Elemente und der Atom-Arten," Norske Videnskaps-Akademi i Oslo; 1. Mat.-Naturv. Klasse. 1937, No. 4 (1938).

[2] See for example, V. M. Goldschmidt, reference 1, and G. Hevesy, *Chemical Analysis by X-Rays and Its Applications* (McGraw-Hill Book Company, Inc., New York, 1932), pp. 255–315.

[3] G. P. Merrill, Nat. Acad. Sci. Mem. **14**, 1 (1916).

[4] H. Brown and C. Patterson, J. Geology (in press).

TABLE II. Relative abundances of individual nuclear species (atoms per 10,000 atoms of silicon).

Species	Abundance	Species	Abundance
Na^{23}	462 ± 36	Ca^{40}	650 ±72
Mg^{24}	6870 ±240	Ca^{42}	4.29 ± 0.49
Mg^{25}	1020 ±110	Ca^{43}	1.01 ± 0.12
Mg^{26}	985 ±101	Ca^{44}	13.8 ± 1.6
Al^{27}	882 ± 81	Ca^{46}	0.0221 ± 0.0042
Si^{28}	9228 ± 3	Ca^{48}	1.27 ± 0.15
Si^{29}	467 ± 1	Ti^{46}	2.07 ± 0.72
Si^{30}	305 ± 3	Ti^{47}	2.02 ± 0.70
K^{39}	64.7 ± 7.0	Ti^{48}	19.1 ± 6.6
K^{40}	0.00832 ± 0.00011	Ti^{49}	1.43 ± 0.50
K^{41}	4.58 ± 0.50	Ti^{50}	1.39 ± 0.48

into three major components: the silicate phase, composed primarily of silicon, magnesium, and iron as oxides; the metallic phase, composed primarily of iron and nickel; and troilite, composed primarily of iron sulfide. Elements distribute themselves among these phases according to rules as yet incompletely understood. Many elements are found in two or three phases, thus greatly complicating an evaluation of relative abundances. Although the concentration of a given element in a given phase can be measured fairly accurately, the relative weights of the three phases are but poorly known.

However, a class of elements, generally known as *lithophile elements*, exists, the components of which are found primarily in the silicate phase and fortunately in completely negligible concentration in the metallic and sulfide phases. It is possible, then, to compare the abundances of those elements with one another without limiting the accuracy by assumptions as to the relative proportions of the phases themselves.

In view of the above, we have combined the relative abundance data for those lithophile elements shown in Table I, with the most recent isotopic abundance data available, thus obtaining the abundances for those individual species shown in Table II. The errors calculated in our evaluation of elemental abundances have been combined with the estimated errors in the isotopic ratio determinations. We have used Dempster's value for magnesium,[5] Inghram's value for silicon,[6] Nier's values for calcium and titanium,[7] and Nier's[8] and Cook's[9] values for potassium. It is interesting that the data enables one to calculate the abundance ratios of three sets of isobars: $K^{40}-Ca^{40}$, $Ca^{46}-Ti^{46}$, and $Ca^{48}-Ti^{48}$. Values for those ratios are given in Table III.

TABLE III. Abundance ratios of isobaric pairs.

Pair	Abundance ratio
K^{40}/Ca^{40}	$(1.28\pm0.23)\times10^{-5}$
Ca^{46}/Ti^{46}	$(1.06\pm0.39)\times10^{-3}$
Ca^{48}/Ti^{48}	$(6.65\pm2.44)\times10^{-3}$

[5] F. W. Aston, *Mass Spectra and Isotopes* (E. Arnold and Company, London, 1942).
[6] M. G. Inghram, Phys. Rev. **70**, 653 (1946).
[7] A. O. Nier, Phys. Rev. **53**, 282 (1938).
[8] A. O. Nier, Phys. Rev. **50**, 1041 (1936).
[9] K. L. Cook, Phys. Rev. **64**, 278 (1943).

The Vector Meson Field and Projective Relativity

BANESH HOFFMANN
The Institute for Advanced Study, Princeton, New Jersey[1]
(Received May 26, 1947)

In the projective theory of relativity, if, instead of the projective metric $G_{\alpha\beta}$ of index $2N$, one uses the restricted metric $\gamma_{\alpha\beta}(\equiv G_{\alpha\beta}/G_{00})$ of index zero, one is led to a formal unification of the gravitational and electromagnetic fields of the general theory of relativity. The present paper discusses the case of the general metric $G_{\alpha\beta}$. It is shown that a natural four-dimensional, gauge invariant variational principle, involving the curvature scalar of $G_{\alpha\beta}$, yields field equations unifying the gravitational and vector meson fields, the range of the meson force being determined by the inverse length $(12)^{\frac{1}{2}}N$. Reasons are given for supposing that an extension to conformal geometry could prove of interest.

I. INTRODUCTION

THE projective theory of relativity[2] was proposed in order to give a four-dimensional significance to the five-dimensional theory, initiated by Kaluza[3] and developed by Klein,[4] which led to a formal unification of the gravitational and electromagnetic fields of the general theory of relativity. The projective formalism developed by Veblen,[5] was used by Veblen and Hoffmann in P. R. in 1930. In 1932 an equivalent formalism in terms of homogeneous coordinates in space-time was given by van Danzig.[6] The use of homogeneous coordinates was further discussed by Pauli,[7] whose formulation of the projective theory brought out similarities between it and the 1931 theory of Einstein and Mayer.[8] The relationship between the Einstein-Mayer theory and the projective theory had also been discussed by other writers.[9]

In the present paper, the original formalism of the projective theory is adhered to. Though less symmetric, it seems to the writer more direct than the formalism used by van Danzig, Schouten, and Pauli, especially in regard to the question of the index (called the excess in the van Danzig treatment), which is fundamental for the present discussion. Indeed, the reciprocal of the index has here the significance that, to within a numerical factor, it is the range of the meson force.

Since the ideas and basic formulas of the projective theory of relativity have been fully described in the literature,[10] they will not be repeated in detail here. It is convenient, however, to list the following items:

Latin indices have the range 1, 2, 3, 4, and Greek indices the range 0, 1, 2, 3, 4.

In four dimensions, a projective tensor $T_{\beta\ldots}{}^{\alpha\cdots}$ has 5^λ components of the form $\exp(Nx^0)\bar{T}_{\beta\ldots}{}^{\alpha\cdots}(x^\alpha)$, where N is a constant called the index, and x^0 is a gauge variable which undergoes transformations of the type

$$x'^0=x^0+\log[\rho(x^\alpha)]. \tag{1}$$

Under a transformation of coordinates and gauge variable, $T_{\beta\ldots}{}^{\alpha\cdots}$ transforms as

$$T'_{\beta\ldots}{}^{\alpha\cdots}(x')=\frac{\partial x'^\alpha}{\partial x^\gamma}\cdots\frac{\partial x^\delta}{\partial x'^\beta}\cdots T_{\delta\ldots}{}^{\gamma\cdots}(x(x')). \tag{2}$$

The fundamental symmetric projective tensor

[1] On leave from Queens College, Flushing, New York.

[2] O. Veblen and B. Hoffmann, Phys. Rev. **36**, 810 (1930); we shall refer to this paper as P. R.

[3] Th. Kaluza, Sitz. Preuss. Akad. Wiss. **54**, 966 (1921).

[4] O. Klein, Zeits. f. Physik **37**, 895 (1926); *ibid.* **46**, 188 (1927).

[5] O. Veblen, J. Lond. Math. Soc. **42**, 140 (1929); Quart. J. Math. (Oxford) **1**, 60 (1930).

[6] D. van Danzig, Math. Ann. **106**, 400 (1932); J. A. Schouten and D. van Danzig, Zeits. f. Physik **78**, 639 (1932). Van Danzig pointed out that his homogeneous coordinates X^α were related to the variables x^α of Veblen's formalism by the transformation

$$x^0\to X^0=e^{x^0},\quad x^\alpha\to X^\alpha=e^{x^0}x^\alpha,\quad (\alpha=1,2,3,4).$$

This amounted to a transition from an affine representation in which portions of space-time are pictured as cross sections of systems of parallel lines in a five-dimensional space to an affine representation in which the lines meet in a point.

[7] W. Pauli, Ann. d. Physik **18**, 305 (1933).

[8] A. Einstein and W. Mayer, Sitz. Preuss. Akad. Wiss. **25**, 541 (1931).

[9] J. A. Schouten and D. van Danzig, Proc. Amsterdam **34**, 1398 (1931); O. Veblen, *Projektive Relativitätstheorie* (Julius Springer, Berlin, 1933), Chap. VIII; B. Hoffmann, Phys. Rev. **43**, 615 (1933).

[10] See for instance P. R., or the book "*Projektive Relativitätstheorie*" by O. Veblen, cited in reference 9, where the geometrical implications are developed in considerable detail.

$G_{\alpha\beta}$ is of index $2N$. Because

$$\partial x^0/\partial x'^a = 0, \tag{3}$$

the component G_{00} is a projective scalar. It is denoted by Φ^2, so that Φ is a projective scalar of index N.

The zero index projective tensor, $\gamma_{\alpha\beta}$, is defined by

$$\gamma_{\alpha\beta} = G_{\alpha\beta}/G_{00} = G_{\alpha\beta}/\Phi^2. \tag{4}$$

Because of (3), the components $\gamma_{\alpha 0}$ of $\gamma_{\alpha\beta}$ form a projective vector. It is denoted by φ_α. The components φ_a of φ_α acquire an added gradient under a change of the gauge variable (1) and are identified in P. R. with the electromagnetic four-potential. We may remark here that they do not have this significance in the present paper.

The zero index projective tensor, $g_{\alpha\beta}$, defined by

$$g_{\alpha\beta} = \gamma_{\alpha\beta} - \varphi_\alpha \varphi_\beta \tag{5}$$

has

$$g_{\alpha 0} = 0. \tag{6}$$

It follows from (3) that g_{ab} is an affine tensor. It is identified with the Riemannian metric of Einstein's general theory of relativity. The antisymmetric tensor φ_{ab} (which turns out to be affine) is defined by

$$\varphi_{ba} = -\frac{1}{2}\left(\frac{\partial \varphi_a}{\partial x^b} - \frac{\partial \varphi_b}{\partial x^a}\right), \tag{7}$$

with

$$\varphi^a{}_b = g^{ac}\varphi_{cb} \quad \text{and} \quad \varphi^{ab} = g^{ac}g^{bd}\varphi_{cd}. \tag{8}$$

The curvature tensor formed from $\gamma_{\alpha\beta}$ is denoted by $B_{\beta\gamma\delta}{}^\alpha$. Also $B_{\beta\delta} = B_{\beta\alpha\delta}{}^\alpha$ and $B = \gamma^{\beta\delta}B_{\beta\delta}$. The corresponding tensors formed from g_{ab} are denoted by $R_{bcd}{}^a$, R_{bd}, R.

In P. R. the field equations based on the projective tensor of zero index are obtained from the variational principle.

$$\delta \int B(\gamma)^{\frac{1}{2}} dx^1 dx^2 dx^3 dx^4 = 0, \tag{9}$$

by variation of $\gamma_{\alpha\beta}$, the variations $\delta\gamma_{\alpha\beta}$ vanishing at the boundary of the region of integration. Since B is of zero index, and $\gamma = g$ (see P. R. p. 815), the variational integral in (9) is an affine scalar.

The field equations resulting from (9) may be expressed in the form

$$T_{\alpha\beta} \equiv \Gamma_{\alpha\beta} - \varphi_\alpha \varphi_\beta \Gamma = 0, \tag{10}$$

where

$$\Gamma_{\alpha\beta} \equiv B_{\alpha\beta} - \tfrac{1}{2}\gamma_{\alpha\beta}B, \quad \Gamma \equiv \gamma^{\alpha\beta}\Gamma_{\alpha\beta}. \tag{11}$$

Since $T_{\alpha\beta}$ is a projective tensor of index zero, T^{ab}, $T_0{}^a$, and T_{00} are affine tensors. Thus the fifteen equations (10) separate naturally into the affine sets

$$T^{ab} \equiv (R^{ab} - \tfrac{1}{2}g^{ab}R) + 2(g^{cd}\varphi^a{}_c\varphi^b{}_d + \tfrac{1}{4}g^{ab}\varphi^e{}_d\varphi^d{}_c) = 0, \tag{12}$$

$$T_0{}^a \equiv \varphi^{ab}{}_{,b} = 0, \tag{13}$$

$$T_{00} \equiv R = 0. \tag{14}$$

Here the comma denotes the affine covariant derivative with respect to g_{ab}. Equation (14) is an algebraic consequence of (12); it is obtained by multiplying (12) by g_{ab} and summing over a and b. Thus there are only fourteen algebraically independent field equations. This is important, because with $\gamma_{00} = 1$ there are only fourteen independent quantities $\gamma_{\alpha\beta}$, and fifteen independent field equations would give an overdetermination of the field.

The field equations (12) and (13) are precisely those of the general theory of relativity for the case of a field of gravitation and electromagnetism in the absence of matter. Equation (12) equates the gravitational stress-energy-momentum tensor to that of the electromagnetic part of the field, while Eq. (13), together with the definition of φ_{ab}, gives the Maxwell equations in their general relativity form.

In this way the projective theory of relativity provided a unification of the gravitational and electromagnetic fields in the general theory of relativity.

II. VARIATIONAL PRINCIPLE BASED ON $G_{\alpha\beta}$

An attempt was made in P. R. to use field equations based on the general projective metric $G_{\alpha\beta}$ of index $2N$. The field equations there discussed were of the type (10), with the curvature tensor formed from $G_{\alpha\beta}$ instead of $\gamma_{\alpha\beta}$. Like their prototype, these equations were related by one algebraic identity, but they were not derived from a variational principle. Their form was complicated and though a relativistic Schrödinger

equation for the quantity $\Phi^{5/3}$ could be found in the field equations, the possible physical significance of the field equations was obscure.

Let $P_{\beta\gamma\delta}{}^{\alpha}$ be the projective curvature tensor formed from $G_{\alpha\beta}$, and let its contractions be $P_{\beta\delta}$ and $\bar{P}$, where

$$\bar{P}=G^{\beta\delta}P_{\beta\delta}. \tag{15}$$

Using the five-dimensional representation, it would be natural to consider field equations resulting from the variational principle

$$\delta\int\bar{P}(G)^{\frac{1}{2}}dx^0dx^1dx^2dx^3dx^4=0, \tag{16}$$

under variations of the $G_{\alpha\beta}$. Because of the integration over x^0, the integral in (16) is gauge invariant. When the field equations are separated into their affine sets, fourteen are identical with those given explicitly in P. R. on page 820, while the fifteenth can be expressed in the form of a relativistic Schrödinger equation for the quantity Φ, with an addition to the usual mass term. This fifteenth equation cannot be regarded as giving a scalar field in addition to the gravitational and electromagnetic fields, however, since, as in P. R., the quantity Φ enters the field equations only in the combination $\theta_a\equiv(\varphi_a-N^{-1}\partial\log\Phi/\partial x^a)$. The physical significance of the equations remains obscure.

Now the projective theory of relativity is a four-dimensional theory. It is therefore of interest to consider a variational principle based on a quadruple integral over space and time. In this case there will be no integration with respect to the gauge variable x^0, so that if we wish the variational integral to be gauge invariant we must have it a scalar of zero index, and thus affine.

Since $G_{\alpha\beta}$ is of index $2N$, $G^{\alpha\beta}$ is of index $(-2N)$. The Christoffel symbols formed from $G_{\alpha\beta}$ are of index zero. So is the projective curvature tensor, $P_{\beta\gamma\delta}{}^{\alpha}$, formed from them, and also the generalized Ricci tensor, $P_{\beta\delta}$, obtained by contraction. This means that the projective curvature scalar $\bar{P}$ is of index $(-2N)$. Also, because $G_{\alpha\beta}$ is of index $2N$, its determinant, G, is of index $10N$.

Hence the integrand, $\bar{P}(G)^{\frac{1}{2}}$, in (16) is of index $3N$.

The simplest way to convert it into a quantity of zero index is to use the projective scalar Φ of index N which is contained in $G_{\alpha\beta}$. By using Φ we do not bring into the variational integral any quantities other than components of $G_{\alpha\beta}$ and their first and second derivatives.

Therefore, we propose to consider the following gauge invariant, four-dimensional variational principle:

$$\delta\int\{\bar{P}(G)^{\frac{1}{2}}/\Phi^3\}dx^1dx^2dx^3dx^4=0. \tag{17}$$

We shall show that, whether we vary $G_{\alpha\beta}$ or $\gamma_{\alpha\beta}$, the resulting field equations, though not identical, are physically equivalent.

If, following the usage of Veblen, we write

$$P=\gamma^{\alpha\beta}P_{\alpha\beta} \tag{18}$$

so that P is of zero index, we have, by (15),

$$\bar{P}=\Phi^{-2}P. \tag{19}$$

Also, by (4),

$$G=\Phi^{10}\gamma=\Phi^{10}g. \tag{20}$$

Hence the variational principle (17) can be written in the alternative form

$$\delta\int P(g)^{\frac{1}{2}}dx^1dx^2dx^3dx^4=0. \tag{21}$$

Later a slight modification of (17) and (21) will be introduced.

III. LEMMAS CONCERNED WITH THE VARIATION

Because of the Φ^{-3} factor in (17), the method of Palatini[11] is not applicable to the present variation. Obtaining the field equations in their general, projective tensor form is thus difficult. But since we are interested mainly in the affine subsets of the projective field equations, the problem may be avoided by using the following lemmas:

Lemma I

After making the usual Green's theorem transformations of the calculus of variations and discarding terms because the variations of $G_{\alpha\beta}$ vanish at the boundary, let

$$\delta\int Kdx^1dx^2dx^3dx^4=\int T^{\alpha\beta}\delta G_{\alpha\beta}dx^1dx^2dx^3dx^4, \tag{22}$$

[11] A. Palatini, Rend. del Circolo Matematico di Palermo XLIII, 205 (1919).

under variations of $G_{\alpha\beta}$, so that the field equations resulting from

$$\delta \int K dx^1 dx^2 dx^3 dx^4 = 0 \tag{23}$$

are, on multiplying by G_{00} to make them of zero index,

$$G_{00} T^{\alpha\beta} = 0. \tag{24}$$

Let indices of $T^{\alpha\beta}$ be lowered by $\gamma_{\alpha\beta}$. Then the affine equations

$$G_{00} T^{ab} = 0, \tag{25}$$

$$G_{00} T_0{}^a = 0, \tag{26}$$

$$G_{00}\gamma_{\alpha\beta} T^{\alpha\beta} \equiv G_{00} T = 0,^{12} \tag{27}$$

are the Euler conditions for (22) under variations of g_{ab}, φ_a, and $\log G_{00}$, respectively.

Proof of Lemma I

By (4) and (5), we have

$$G_{\alpha\beta} = G_{00}\gamma_{\alpha\beta} = G_{00}(g_{\alpha\beta} + \varphi_\alpha \varphi_\beta). \tag{28}$$

So

$$\delta G_{\alpha\beta} = G_{00}(\delta g_{\alpha\beta} + \varphi_\alpha \delta\varphi_\beta + \varphi_\beta \delta\varphi_\alpha) + \gamma_{\alpha\beta}\delta G_{00}. \tag{29}$$

Also, by (6) and the fact that $\varphi_0 = \gamma_{00} = 1$, we have

$$\delta g_{a0} = 0, \quad \delta\varphi_0 = 0. \tag{30}$$

Therefore, by (22), and using the fact that $T^{\alpha\beta}$ must be symmetric,

$$\delta \int K dx^1 dx^2 dx^3 dx^4 = \int T^{\alpha\beta}\delta G_{\alpha\beta} dx^1 dx^2 dx^3 dx^4$$

$$= \int T^{\alpha\beta}\{G_{00}(\delta g_{\alpha\beta} + 2\varphi_\alpha \delta\varphi_\beta) + \gamma_{\alpha\beta}\delta G_{00}\} dx^1 dx^2 dx^3 dx^4$$

$$= \int (G_{00} T^{ab}\delta g_{ab} + 2G_{00} T^{ab}\varphi_a \delta\varphi_b + G_{00} T^{\alpha\beta}\gamma_{\alpha\beta}\delta \log G_{00}) dx^1 dx^2 dx^3 dx^4$$

$$= \int (G_{00} T^{ab}\delta g_{ab} + 2G_{00} T_0{}^b \delta\varphi_b + G_{00} T\delta \log G_{00}) dx^1 dx^2 dx^3 dx^4,$$

since

$$T^{ab}\varphi_\alpha = T^{ab}\gamma_{a0} = T_0{}^b.$$

Thus variation of g_{ab} alone yields (25), variation of φ_b alone yields (26), and variation of $\log G_{00}$ alone yields (27).

[12] Note that this equation involves T, rather than T_{00}.

Lemma II

After making the usual Green's theorem transformations of the calculus of variations and discarding terms because the variations of $\gamma_{\alpha\beta}$ vanish at the boundary, let

$$\delta \int K dx^1 dx^2 dx^3 dx^4 = \int \bar{T}^{\alpha\beta}\delta\gamma_{\alpha\beta} dx^1 dx^2 dx^3 dx^4, \tag{31}$$

under variations of $\gamma_{\alpha\beta}$. Then the field equations resulting from

$$\delta \int K dx^1 dx^2 dx^3 dx^4 = 0 \tag{32}$$

will be

$$\bar{T}^{\alpha\beta} - \delta_0{}^\alpha \delta_0{}^\beta \bar{T} = 0. \tag{33}$$

where

$$\bar{T} \equiv \bar{T}^{\alpha\beta}\gamma_{\alpha\beta}. \tag{34}$$

Also, the affine equations

$$\bar{T}^{ab} = 0, \tag{35}$$

$$\bar{T}_0{}^a = 0, \tag{36}$$

will be the Euler conditions for (32) under variations of g_{ab}, φ_a, respectively, while the fifteenth affine equation,

$$\bar{T}_{00} - \bar{T} = 0, \tag{37}$$

of the set (33) will be an algebraic consequence of (35).

Proof of Lemma II

That the field equations are (33) rather than just $\bar{T}^{\alpha\beta} = 0$, is due to the fact that $\gamma_{00} = 1$ always. For, since $\delta\gamma_{00} = 0$, we may infer from (32) and (31) only that[13]

$$\bar{T}^{\alpha\beta} = \delta_0{}^\alpha \delta_0{}^\beta W,$$

where W is some function of x^a; and contraction by means of $\gamma_{\alpha\beta}$ shows that $W = \bar{T}$.

The proof that (35), (36) result from variation of g_{ab}, φ_a, respectively, is so similar to the proof in Lemma I it need not be given in detail.

That (37) is an algebraic consequence of (35) follows from P. R. page 820, footnote 7. Thus, in the present notation,

$$\bar{T} = \gamma_{\alpha\beta}\bar{T}^{\alpha\beta} = (g_{\alpha\beta} + \varphi_\alpha\varphi_\beta)\bar{T}^{\alpha\beta}$$

$$= (g_{\alpha\beta} + \gamma_{\alpha0}\gamma_{\beta0})\bar{T}^{\alpha\beta} = g_{ab}\bar{T}^{ab} + \gamma_{\alpha0}\gamma_{\beta0}\bar{T}^{\alpha\beta}$$

$$= g_{ab}\bar{T}^{ab} + \bar{T}_{00}.$$

[13] See P. R., p. 818.

Therefore,

$$\bar{T}_{00}-\bar{T}\equiv g_{ab}\bar{T}^{ab}. \tag{38}$$

From (38), we see incidentally that (27) can be reduced to $G_{00}T_{00}=0$ by algebraic manipulation of it and (25).

Lemma III

The field equations (25) are identical with the field equations (35), and the field equations (26) are identical with the field equations (36).

Proof of Lemma III

Equations (25) and (35) are each the result of varying g_{ab} in (22) (which is the same as (32)). Equations (26) and (36) are each the result of varying φ_a.

IV. THE AFFINE FIELD EQUATIONS

By Lemmas I, II, and III, we see that varying $G_{\alpha\beta}$ yields fifteen field equations without an algebraic identity between them, while varying $\gamma_{\alpha\beta}$ yields fifteen equations, of which only fourteen are algebraically independent. Further, we see that, so far as these fourteen equations are concerned, it does not matter whether we vary $G_{\alpha\beta}$ or $\gamma_{\alpha\beta}$. It will appear in the course of the work that, though there is no algebraic relation between the fifteen field equations obtained by varying $G_{\alpha\beta}$, there is a simple differential relation which in effect reduces them to fourteen independent equations equivalent to those obtained by varying $\gamma_{\alpha\beta}$.

To perform the variations, we use the value of P as calculated by Veblen,[14] namely,

$$P=B-8N\theta^{\alpha}{}_{,\alpha}+12N^2(1+\theta^{\alpha}\theta_{\alpha}), \tag{39}$$

where the comma denotes the covariant derivative with respect to g_{ab}, and

$$\theta_{\alpha}\equiv\varphi_{\alpha}-\Phi_{\alpha}, \tag{40}$$

$$\Phi_{\alpha}\equiv N^{-1}\partial\log\Phi/\partial x^{\alpha}. \tag{41}$$

Since $\Phi_0=1$ and $\varphi_0=1$, we have $\theta_0=0$. Therefore, because of (3), θ_a is an affine vector. It will be recalled that φ_a is not affine, being altered by an additive gradient under a change of the gauge variable. This added gradient is just cancelled by the alteration induced in Φ_a by the change of gauge, with the result that θ_a is left unaffected.

Because of (39), the variational principle (17), in the form (21), becomes

$$\delta\int\{B-8N\theta^{\alpha}{}_{,\alpha}+12N^2(1+\theta^{\alpha}\theta_{\alpha})\}(g)^{\frac{1}{2}}\times dx^1dx^2dx^3dx^4=0. \tag{42}$$

By the familiar formula for the contracted covariant derivative of a contravariant vector, we have

$$\theta^{\alpha}{}_{,\alpha}(g)^{\frac{1}{2}}=\frac{\partial}{\partial x^{\alpha}}\{g^{\frac{1}{2}}\theta^{\alpha}\}.$$

Therefore, since variations vanish at the boundary, Green's theorem shows that the second term of the integrand in (42) will contribute nothing to the field equations.

The part $B(g)^{\frac{1}{2}}$ of the integrand is the same as the integrand of (9), the result of varying which is already known. This leaves only the term $12N^2(1+\theta^{\alpha}\theta_{\alpha})(g)^{\frac{1}{2}}$ needing special attention.

We shall use the following well-known formulas:

Since $g^{ab}g_{bc}=\delta_c{}^a$

$$g_{bc}\delta g^{ab}=-g^{ab}\delta g_{bc},$$

or

$$\delta g^{cd}=-g^{ac}g^{bd}\delta g_{ab}. \tag{43}$$

Also

$$\delta g=(\delta g_{ab})(gg^{ab}),$$

so that

$$\delta(g)^{\frac{1}{2}}=\tfrac{1}{2}(g)^{\frac{1}{2}}g^{ab}\delta g_{ab}. \tag{44}$$

Performing the needed variations, we have in turn:

$$\delta_{(g_{ab})}\int(g)^{\frac{1}{2}}dx^1dx^2dx^3dx^4=\int(\tfrac{1}{2}g^{ab})(g)^{\frac{1}{2}}\delta g_{ab}dx^1dx^2dx^3dx^4. \tag{45}$$

[14] Quart. J. Math. (Oxford) 1, 60 (1930), Eq. (5.17) for the case $n=4$, and Eqs. (5.6), (5.3).

Also

$$\delta_{(g^{ab})}\int \theta^a\theta_a(g)^{\frac{1}{2}}dx^1dx^2dx^3dx^4=\delta_{(g^{ab})}\int(\theta_a\theta_b g^{ab}(g)^{\frac{1}{2}})dx^1dx^2dx^3dx^4$$

$$=\int(\theta_a\theta_b)(\delta g^{ab}+\tfrac{1}{2}g^{ab}g^{cd}\delta g_{cd})(g)^{\frac{1}{2}}dx^1dx^2dx^3dx^4$$

$$=\int(\theta_a\theta_b)(-g^{ac}g^{bd}+\tfrac{1}{2}g^{ab}g^{cd})(g)^{\frac{1}{2}}\delta g_{cd}dx^1dx^2dx^3dx^4$$

$$=\int(-\theta^c\theta^d+\tfrac{1}{2}g^{cd}\theta^a\theta_a)(g)^{\frac{1}{2}}\delta g_{cd}dx^1dx^2dx^3dx^4. \tag{46}$$

Again,

$$\delta_{(\varphi_a)}\int\theta^a\theta_a(g)^{\frac{1}{2}}dx^1dx^2dx^3dx^4=\delta_{(\varphi_a)}\int g^{ab}(\varphi_a-\Phi_a)(\varphi_b-\Phi_b)(g)^{\frac{1}{2}}dx^1dx^2dx^3dx^4$$

$$=\int 2g^{ab}(\varphi_b-\Phi_b)\delta\varphi_a(g)^{\frac{1}{2}}dx^1dx^2dx^3dx^4$$

$$=\int 2\theta^a(g)^{\frac{1}{2}}\delta\varphi_a dx^1dx^2dx^3dx^4, \tag{47}$$

and finally, by (40) and (41),

$$\delta_{(\log G_{00})}\int\theta^a\theta_a(g)^{\frac{1}{2}}dx^1dx^2dx^3dx^4=\delta_{(\log G_{00})}\int g^{ab}\left(\varphi_a-\frac{1}{2N}\frac{\partial\log G_{00}}{\partial x^a}\right)\left(\varphi_b-\frac{1}{2N}\frac{\partial\log G}{\partial x^b}\right)(g)^{\frac{1}{2}}dx^1dx^2dx^3dx^4$$

$$=\int 2g^{ab}\left(\varphi_a-\frac{1}{2N}\frac{\partial\log G_{00}}{\partial x^a}\right)\left(-\frac{1}{2N}\frac{\partial(\delta\log G_{00})}{\partial x^b}\right)(g)^{\frac{1}{2}}dx^1dx^2dx^3dx^4$$

$$=\int\left(-\frac{1}{N}g^{ab}\theta_a(g)^{\frac{1}{2}}\right)\frac{\partial(\delta\log G_{00})}{\partial x^b}dx^1dx^2dx^3dx^4$$

$$=\int\frac{1}{(g)^{\frac{1}{2}}}\left(\frac{\partial}{\partial x^b}\left\{\frac{1}{N}g^{ab}\theta_a(g)^{\frac{1}{2}}\right\}\right)(g)^{\frac{1}{2}}\delta\log G_{00}dx^1dx^2dx^3dx^4$$

$$=\int\left(\frac{1}{N}\theta^a{}_{,a}\right)(g)^{\frac{1}{2}}\delta\log G_{00}dx^1dx^2dx^3dx^4. \tag{48}$$

In combining the results (45), (46), (47), and (48) with the known results for the part $B(g)^{\frac{1}{2}}$ in (42), we must allow for a minus sign that occurs in the latter:

$$\delta\int B(g)^{\frac{1}{2}}dx^1dx^2dx^3dx^4=\int\Gamma_{\alpha\beta}(g)^{\frac{1}{2}}\delta\gamma^{\alpha\beta}dx^1dx^2dx^3dx^4=-\int\Gamma^{\alpha\beta}(g)^{\frac{1}{2}}\delta\gamma_{\alpha\beta}dx^1dx^2dx^3dx^4,\ \text{by (43)}.$$

Thus the fifteen field equations arising from variation of $G_{\alpha\beta}$ have the affine form

$$(R^{ab}-\tfrac{1}{2}g^{ab}R)-6N^2g^{ab}+2(g^{cd}\varphi^a{}_c\varphi^b{}_d+\tfrac{1}{4}g^{ab}\varphi^c{}_d\varphi^d{}_c)-12N^2(\theta^a\theta^b-\tfrac{1}{2}g^{ab}\theta^c\theta_c)=0, \tag{49}$$

$$\varphi^{ab}{}_{,b}+24N^2\theta^a=0, \tag{50}$$

$$\theta^a{}_{,a}=0. \tag{51}$$

The field equations arising from variation of $\gamma_{\alpha\beta}$ are, as we have seen, equivalent to the affine sets (49), (50). The fifteenth equation, (51), is, however, a direct consequence of (50). For, taking

the divergence of Eq. (64) we have

$$\varphi^{ab}{}_{,ba}+24N^2\theta^a{}_{,a}=0. \tag{52}$$

But, because φ^{ab} is antisymmetric, we have

$$\varphi^{ab}{}_{,b}=\frac{1}{(g)^{\frac{1}{2}}}\frac{\partial((g)^{\frac{1}{2}}\varphi^{ab})}{\partial x^b},$$

and so

$$\varphi^{ab}{}_{,ba}=\frac{1}{(g)^{\frac{1}{2}}}\frac{\partial}{\partial x^a}\left\{\frac{\partial(g)^{\frac{1}{2}}\varphi^{ab}}{\partial x^b}\right\}=\frac{1}{(g)^{\frac{1}{2}}}\frac{\partial^2((g)^{\frac{1}{2}}\varphi^{ab})}{\partial x^a\partial x^b},$$

and this vanishes because of the antisymmetry of φ^{ab}. Therefore (52) reduces to (51).

Thus the fifteen field equations arising from variation of $G_{\alpha\beta}$ place upon the field quantities g_{ab}, θ_a exactly the same restrictions as are imposed by the field equations arising from variation of $\gamma_{\alpha\beta}$.

Since φ_{ab} is defined with a $\frac{1}{2}$ factor, let us write

$$\theta_{ab}=2\varphi_{ab}=\frac{\partial\varphi_a}{\partial x^b}-\frac{\partial\varphi_b}{\partial x^a}=\frac{\partial\theta_a}{\partial x^b}-\frac{\partial\theta_b}{\partial x^a}. \tag{53}$$

Then the field equations (49), (50) become

$$(R^{ab}-\tfrac{1}{2}g^{ab}R)-6N^2g^{ab}+\tfrac{1}{2}(g^{cd}\theta^a{}_c\theta^b{}_d+\tfrac{1}{4}g^{ab}\theta^c{}_d\theta^d{}_c)-12N^2(\theta^a\theta^b-\tfrac{1}{2}g^{ab}\theta^c\theta_c)=0, \tag{54}$$

$$\theta^{ab}{}_{,b}+12N^2\theta^a=0. \tag{55}$$

Taking g_{ab} to be of signature $(---+)$, and N^2 to be positive, we see that, except for the term $(-6N^2g^{ab})$, these are the classical (i.e., unquantized) field equations for a vector meson and gravitational field in the general theory of relativity.

Though the term $(-6N^2g^{ab})$ has the appearance of a cosmological term, it is of quite the wrong order of magnitude for such a term. For if (55) is to represent a vector meson field in the galilean case, $12N^2$ must be of the order of magnitude 10^{25} cm^{-2}, while the usual cosmological constant, being of the order of magnitude of the reciprocal of the square of the radius of the universe, is more like 10^{-50} cm^{-2}. The presence of the term $(-6N^2g^{ab})$ would mean that, for the case $\theta_a=0$, there would be a solution for g_{ab} pertaining to a space-time of constant negative curvature, the radius of curvature being of the order of magnitude of the range of nuclear forces.

It is easy to remove the term $(-6N^2g^{ab})$ from the field equations. If one replaces the variational principle (21) by

$$\delta\int(P-12N^2)(g)^{\frac{1}{2}}dx^1dx^2dx^3dx^4=0, \tag{56}$$

the resulting field equations are identical with those obtained from (21), except that the term $(-6N^2g^{ab})$ no longer appears in (54).[15] Despite the presence of the projective scalar Φ in the fundamental projective tensor $G_{\alpha\beta}$, there is no rigorous scalar meson field equation in the field equations of the present paper; the scalar Φ enters only in the combination denoted by θ_a.

[15] If one retains the $(-6N^2g_{ab})$ term and makes the usual approximation for weak gravitational fields of assuming that only g_{44} differs significantly from its galilean value, one finds, for the case $\theta_a=0$, that g_{44} satisfies the scalar meson equation. This result is of dubious significance, however, since the rigorous solution for the static spherically symmetric case is known and g_{44} does not there have the form of a meson potential, nor is the weak field approximation there justified for small values of the radial coordinate. Thus though g_{44} might appear as a scalar meson outside the nucleus the indications are that it would not so appear inside.

I have tried to find a rigorous solution for the static, spherically symmetric case, with $\theta_a\neq0$, with or without the $(-6N^2g_{ab})$ term, but the field equations, after promising manipulation, became too complicated to solve. In an endeavor to assess the effect of the gravitational field on the singularities of the meson field, I arbitrarily replaced the vector meson field by a scalar meson field in the hope that this would yield a rigorous solution. Surprisingly, the field equations proved more recalcitrant than those pertaining to the case of the vector meson, and no rigorous solution was forthcoming.

This is especially curious in view of the discovery by many writers[16] that in terms of a five-dimensional, or of a homogeneous four-dimensional formalism, in the galilean case, the vector and scalar (or pseudo-scalar) meson fields fit naturally together as a single unit. The electromagnetic field, too, is absent from the present field equations, unless we set $N=0$, in which case the whole character of the field equations is changed, there being fifteen independent equations for fifteen field quantities which have the significance of gravitational and electromagnetic fields and a new scalar field. There is, however, no longer a fundamental length in the theory.[17]

It may be that a broader geometrical base is needed than the projective geometry affords. It has long been known, for instance, that the Maxwell equations may be regarded as belonging to conformal geometry.[18] An indication of the possibilities residing in the conformal geometry may be seen in the following brief calculation, which is expressed in galilean terms:

Let φ_α be a projective vector of index N, and write

$$\varphi_{\alpha\beta}=\partial\varphi_\alpha/\partial x^\beta-\partial\varphi_\beta/\partial x^\alpha. \tag{57}$$

Consider the equation

$$\varphi_{\alpha\beta,\,\beta}=0. \tag{58}$$

This combines the two equations

$$\varphi_{ab,\,b}+\varphi_{a0,\,0}=0, \tag{59}$$

$$\varphi_{0b,\,b}=0. \tag{60}$$

The second of these is a consequence of the first, for $\varphi_{ab,\,ba}\equiv 0$, and so $\varphi_{a0,\,0a}=0$, which implies (60). The first equation, (59), can be written

$$\varphi_{ab,\,b}+N^2(\varphi_a-N^{-1}\varphi_{0,\,a})=0, \tag{61}$$

which is a vector meson equation for the vector $(\varphi_a-N^{-1}\varphi_{0,\,a})$. It will be noted that this closely parallels the situation in the present paper, the scalar meson being absent, and the scalar φ_0 being absorbed in the vector meson part.

Now let us go over to a restricted form of the general conformal geometry developed by E. Cartan, H. Weyl, J. M. Thomas, T. Y. Thomas, O. Veblen, and others,[19] namely, the case in which $U_0{}^0$ is independent of the space-time coordinates. In this case $\partial\log U_0{}^0/\partial x^\sigma$ vanishes, and it is possible to express the transformation matrix $U_\tau{}^\sigma$ ($\sigma, \tau=0, 1, 2, 3, 4, 5$) in the form of a constant multiple of a Jacobian matrix for a transformation involving six variables x^σ.

Let φ_σ be a conformal vector, having an index N, but not containing the variable x^5, and write

$$\varphi_{\sigma\tau}=\partial\varphi_\sigma/\partial x^\tau-\partial\varphi_\tau/\partial x^\sigma. \tag{62}$$

Then the equation

$$\varphi_{\sigma\tau,\,\tau}=0 \tag{63}$$

yields Eqs. (59), (60) above, and in addition the equation

$$\varphi_{5\alpha,\,\alpha}=0, \tag{64}$$

or

$$\varphi_{5,\,bb}+N^2\varphi_5=0,$$

which is a meson equation for the scalar φ_5, the N in this equation being the same inverse length as in the vector meson equation (61) above.

Since a second-rank symmetric conformal tensor contains not only a symmetric projective tensor of the second rank, but also a projective vector and a scalar, it is possible that the gravitational, electromagnetic, vector meson, and scalar meson fields (and perhaps a further scalar field[20]) may together form a single geometric object belonging to the general conformal geometry, and that the field equations governing them may find unitary expression within that geometry.

I wish to thank Professor O. Veblen, and Dr. A. Pais for many stimulating discussions and suggestions.

[16] See, for example, C. Møller, Proc. Copenhagen **18** (1941). J. K. Lubański and L. Rosenfeld, Physica **9**, 117 (1942). A. Pais, Physica **9**, 267 (1942). K. C. Wang and K. C. Cheng, Phys. Rev. **70**, 516 (1946).

[17] Setting $N=0$ does not bring us back to the field equations of P.R., formed from $\gamma_{\alpha\beta}$ because $\gamma_{00}=1$ while, when $N=0$, G_{00} is a scalar function of x^α.

[18] E. Cunningham, Proc. Lond. Math. Soc. **8**, 77 (1910). H. Bateman, Proc. Lond. Math. Soc. **8**, 223, 469 (1910); **21**, 256 (1920). H. Weyl, Sitz. Preuss. Akad. Wiss. 465 (1918). J. A. Schouten and J. Haantjes, Physica **1**, 869 (1934). Compare also, D. van Danzig, Proc. Camb. Phil. Soc. **30**, 421 (1934).

[19] See, for example, Chapter IV of the book *Differential Invariants of Generalised Spaces* (Cambridge, 1934), by T. Y. Thomas. I use here the formalism of O. Veblen, Proc. Nat. Acad. Sci. **21**, 168 (1935).

[20] Compare, for instance, E. C. G. Stueckelberg, Helv. Phys. Acta **14**, 51 (1941).

PHYSICAL REVIEW VOLUME 72, NUMBER 6 SEPTEMBER 15, 1947

On the Heitler Theory of Radiation Damping*

JOHN M. BLATT
Laboratory for Nuclear Science and Engineering, Massachusetts Institute of Technology, Cambridge, Massachusetts
(Received April 26, 1947)

Heitler has developed a method of including radiation damping in scattering problems. It involves an integral equation for the scattered field amplitude far from the scatterer. We have derived this integral equation classically for a special group of problems. Our derivation allows a comparison between the Heitler method and the Wentzel-Dirac λ-process. Two simple problems are discussed, involving the interaction of an oscillator with scalar and vector meson fields, respectively. Both problems have exact solutions, which we compare with approximate solutions by the Heitler method. The Heitler method preserves the shape of the resonance but neglects the shift in resonance frequency caused by the additional mass of the oscillator coming from the coupling to the meson field. The strong radiation damping encountered in vector meson theory appears in the second example, although we assumed no spin interaction. The damping can be traced to the Lorentz condition

$$\sum_{i=1}^{4} \partial U_i/\partial x_i = 0$$

on the 4-vector field quantity U_i.

1. INTRODUCTION

HEITLER and his collaborators[1] have published a series of papers during the last few years in which they have developed a theory of radiation damping. The aim of this theory is twofold. It tries to improve on the usual perturbation methods of calculating cross sections for processes involving elementary particles. It also aims at avoiding the divergence difficulties which have plagued all field theories to this day.

It is obvious that the perturbation method of calculating cross sections needs improvement quite badly. One need only recall the fact that a perturbation calculation of the scattering of vector mesons by heavy particles leads to cross sections which increase indefinitely with the energy of the incident mesons. This is in clear contradiction to the law of conservation of matter. This law expresses itself mathematically as a limit on the size of the scattering cross sections. The Born scattering cross section, to which perturbation calculations lead, is not limited in this way. Therefore, the Born scattering calculations can be trusted only where the cross sections so calculated stay well below this limit. When they exceed this limit, as they do for vector mesons, then one has to look for a better method of calculating cross sections.

It is difficult, however, to find such a better method. The trouble comes from the divergence difficulties which beset all our theories of elementary particles. The mathematical problem is not well-defined. Therefore, any "approximation" scheme is really first of all a prescription for dropping out divergent terms and only afterwards a method of treating the mutilated equations. The usual perturbation theory provides one such scheme, but we have seen that perturbation theory is not good enough.

The Heitler theory of radiation damping is an attempt to provide an alternative scheme for calculations. It includes a clear-cut prescription for leaving out divergent terms. Moreover, it can be shown[2] that scattering cross sections calculated by means of this theory can never exceed the natural limit imposed by the law of conservation of matter.

The usual derivation of the Heitler integral equation starts with notions taken from perturbation theory. Nevertheless, the method is essentially *not* a perturbation method. It does not lead to power-series in the coupling constant, in the same way that a perturbation scheme would. In fact, it turns out that the Heitler

* The research described in this article was supported in part by Contract N5ori-78, U. S. Navy Department.

[1] W. Heitler, Proc. Camb. Phil. Soc. **37**, 291 (1941); A. H. Wilson, Proc. Camb. Phil. Soc. **37**, 301 (1941); S. T. Ma, Proc. Camb. Phil. Soc. **39**, 168 (1943). S. T; Ma and C. F. Hsüeh, Proc. Camb. Phil. Soc. **40**, 167 (1944).

[2] J. Schwinger, unpublished.

method differs from the λ-process[3] precisely because it is not a perturbation scheme.

In this paper the Heitler equation is first derived for an especially simple case. This enables us to point out some interesting features of the method and to relate it to other schemes for avoiding divergencies (in particular, the Wentzel-Dirac λ-process). Then we apply the Heitler method to the solution of a few simple problems for which exact solutions are possible. The exact solution, the Heitler solution, and the perturbation solution are compared and the differences are discussed. No great physical interest is claimed for any of these simple examples. However, the examples show many of the features of problems which do possess great physical interest.

2. A CLASSICAL DERIVATION OF THE HEITLER EQUATION FOR A SPECIAL GROUP OF PROBLEMS

Consider a classical scalar field $\varphi(\mathbf{x})$ which satisfies the linear homogeneous equation:

$$(\nabla^2+k^2)\varphi(\mathbf{x})=L\varphi(\mathbf{x}), \tag{2.1}$$

where L is some linear operator, which need not be specified further. We shall require that the solution of this equation be of the form

$$\varphi(\mathbf{x})=\varphi_0(\mathbf{x})+\varphi_{sc}(\mathbf{x}). \tag{2.2}$$

Here $\varphi_0(\mathbf{x})$ is an incident plane wave which satisfies the wave equation

$$(\nabla^2+k^2)\varphi_0(\mathbf{x})=0. \tag{2.3}$$

$\varphi_{sc}(\mathbf{x})$ is the scattered wave associated with the incident wave $\varphi_0(\mathbf{x})$. This implies that for large $r=|\mathbf{x}|$, $\varphi_{sc}(\mathbf{x})$ behave like

$$\varphi_{sc}(\mathbf{x})\sim f(\omega\leftarrow\omega_0)(e^{ikr}/r). \tag{2.4}$$

Here ω_0 and ω stand for directions in space; ω_0 denotes the direction of the incoming wave, ω the direction in which the scattered wave is observed. The differential scattering cross section for elastic scattering from ω_0 into ω is then given by

$$d\sigma=|f(\omega\leftarrow\omega_0)|^2d\omega, \tag{2.5}$$

provided that $\varphi_0(\mathbf{x})$ is normalized to unit amplitude, i.e. $\varphi_0(\mathbf{x})=\exp(i\mathbf{k}_0\cdot\mathbf{x})$, $\mathbf{k}_0$=a vector of magnitude k and direction ω_0.

It is clear from (2.1) and (2.2) that

$$\varphi_{sc}(\mathbf{x})=-\frac{1}{4\pi}\int\frac{\exp(ik|\mathbf{x}-\mathbf{x}'|)}{|\mathbf{x}-\mathbf{x}'|}L\varphi(\mathbf{x}')d^3\mathbf{x}'. \tag{2.6}$$

We substitute (2.2) on the right-hand side to get

$$\varphi_{sc}(\mathbf{x})=\varphi_B(\mathbf{x})-\frac{1}{4\pi}\int\frac{\exp(ik|\mathbf{x}-\mathbf{x}'|)}{|\mathbf{x}-\mathbf{x}'|}\times L\varphi_{sc}(\mathbf{x}')d^3\mathbf{x}', \tag{2.7}$$

$\varphi_B(\mathbf{x})$ is the scattered wave in the Born approximation. It is obtained by putting $\varphi(\mathbf{x}')=\varphi_0(\mathbf{x}')$ on the right-hand side of (2.6). Equation (2.7) is *exact*. We now investigate the behavior of $\varphi_{sc}(\mathbf{x})$ at large distances from the scattering center. From (2.4) and (2.7) we obtain

$$f(\omega\leftarrow\omega_0)=f_B(\omega\leftarrow\omega_0)-(4\pi)^{-1}\int\exp(-i\mathbf{k}\cdot\mathbf{x}')L\varphi_{sc}(\mathbf{x}')d^3\mathbf{x}', \tag{2.8}$$

where

$$f_B(\omega\leftarrow\omega_0)=-(4\pi)^{-1}\int\exp(-i\mathbf{k}\cdot\mathbf{x}')\times L\varphi_0(\mathbf{x}')d^3\mathbf{x}'. \tag{2.9}$$

Now we substitute a particular function, φ_{rad}, instead of $\varphi_{sc}(\mathbf{x}')$ in (2.8). φ_{rad} is defined as

$$\varphi_{rad}(\mathbf{x})=(ik/2\pi)\int d\omega'\exp(i\mathbf{k}'\cdot\mathbf{x})f(\omega'\leftarrow\omega_0), \tag{2.10}$$

where $\mathbf{k}'$ is a vector of magnitude k and direction ω'. The choice of this function will be explained in the next section.

We then obtain from (2.8) the *Heitler integral equation:*

$$f(\omega\leftarrow\omega_0)=f_B(\omega\leftarrow\omega_0)+i\pi(k/4\pi^2)\times\int d\omega' f_B(\omega\leftarrow\omega')f(\omega'\leftarrow\omega_0). \tag{2.11}$$

The integrals in (2.10) and (2.11) are over directions only.

[3] G. Wentzel, Zeits. f. Physik **86**, 479, 635 (1933); **87**, 726 (1934); P. A. M. Dirac, Ann. de l'Inst. Poincaré **9**, 13 (1939), Proc. Roy. Soc. **A180**, 1 (1942); W. Pauli, Rev. Mod. Phys. **15**, 175 (1943).

3. INTERPRETATION OF THE DEVIATION. RELATIONSHIP OF THE HEITLER EQUATION TO THE λ-PROCESS

Equation (2.8) is exact. It is, however, not equivalent to (2.7), since it is only the asymptotic form of (2.7). In order to derive the Heitler equation from (2.8), we had to make the *ad hoc* assumption (2.10). It is interesting to look at (2.10) more closely. Clearly $\varphi_{\text{rad}}(\mathbf{x})$ is square integrable over every finite region of space and is a solution of (2.3). Outgoing waves which satisfy (2.3) are not square integrable over regions containing the origin of the coordinate system. Therefore $\varphi_{\text{rad}}(\mathbf{x})$ cannot correspond to outgoing waves only.

If one investigates the asymptotic behavior of $\varphi_{\text{rad}}(\mathbf{x})$ for large values of $r=|\mathbf{x}|$ one finds

$$\varphi_{\text{rad}}(\mathbf{x})\sim\tfrac{1}{2}[f(\omega\leftarrow\omega_0)(e^{ikr}/r) - f(-\omega\leftarrow\omega_0)(e^{-ikr}/r)]. \quad (3.1)$$

The first term in the square bracket represents an outgoing wave in the direction ω. The second term, however, is an incoming wave of the same amplitude as the outgoing wave in the direction diametrically opposed to ω. Therefore (3.1) can be understood as half the difference of a retarded and an advanced potential.

Equation (2.7) can be interpreted as follows. Two terms contribute to the scattered field. One of them is φ_B. It represents the effect of the incident field φ_0 which creates a scattered wave when it strikes the source. The other term is a reaction term. It corrects for the fact that φ_0 is *not* the field present at the source. That field is actually $\varphi_0+\varphi_{sc}$. *The assumption (2.10) therefore means that we take one-half the difference between a retarded and an advanced potential as that part of the scattered wave which reacts back upon the source.*

Now this term $\frac{1}{2}(\varphi_{\text{ret}}-\varphi_{\text{adv}})$ is a familiar expression. It was treated by Wentzel and Dirac.[3] Indeed, it is just the essence of the λ-limiting process that one substitutes $\varphi_{\text{rad}}=\frac{1}{2}(\varphi_{\text{ret}}-\varphi_{\text{adv}})$ instead of φ_{ret} for the field which reacts back on the particle. One would be tempted to think, therefore, that the Heitler formalism is equivalent to the λ-limiting process of Wentzel and Dirac.

This, however, is incorrect. The distinction is due to the fact that Dirac uses a Hamiltonian formalism whereas Heitler does not. It may be recalled that Dirac introduces a Hamiltonian which depends upon a parameter λ. One is supposed to solve the Hamiltonian problem for small values of λ and to proceed *afterwards* to the limit $\lambda\rightarrow 0$. This order of procedure is the essence of the method.

The Lorentz[4] equation of motion (which is the ultimate result of the λ-process) is of third order. Thus one has to specify the initial acceleration of the particle, in addition to its initial velocity and initial position, in order to define its subsequent motion. It turns out that for the vast majority of choices of the initial acceleration the particle will speed up to the velocity of light at some future time. In order to pick the *particular* value of the initial acceleration which will make the motion convergent, one has to know all the forces which are going to act on the particle throughout its *future* course.

Since the Lorentz equation is of third order, it is not possible to write it in Hamiltonian form in a simple manner. The λ-process Hamiltonian leads to the Lorentz equation only in the limit $\lambda\rightarrow 0$. The fact that the particle can speed up to the velocity of light is reflected in the λ-process Hamiltonian in the following way. The Hamiltonian is not positive definite even for a free particle. Thus, it introduces *artificial* potential holes into which the particle can fall, thereby acquiring infinite kinetic energy.

Exact solutions of this Hamiltonian problem are therefore meaningless. One is *restricted to perturbation methods in using the λ-process*. This means that in the examples worked out later on in this paper, the λ-process would yield the same result as the ordinary perturbation calculation. This is true since the λ-process is a *regular* limiting process. The result of any calculation which is already convergent is not changed by application of the λ-process. Only in certain divergent problems does the λ-process eliminate the divergent terms.

On the other hand, the Heitler formalism leads to a clearly defined problem which need *not* be treated by perturbation procedures at all. *The distinguishing characteristic of the Heitler method*

[4] H. A. Lorentz, *Theory of Electrons* (G. E. Stechert & Co., New York, 1923), Note 18, p. 252.

is precisely this point. If it were a perturbation method, its results would agree with results obtained by using perturbation methods with the λ-limiting process. One cannot tell what the λ-process would give *without* perturbation treatment, since that problem is not defined mathematically unless one *does* use perturbation methods.

We mentioned before that one has to know the forces which are going to act on the particle in the *future*, in order to determine its *initial* acceleration. This apparently paradoxical position has lately been elaborated upon by Feynman and Wheeler.[5] They maintain that the paradox is indeed only apparent and can be exploited to yield an electromagnetic field theory without electromagnetic fields. It is significant in this connection that Feynman and Wheeler have so far been unable to put their theory in a conventional Hamiltonian form. It seems that the Hamiltonian formalism is too narrow to encompass the theories of radiation damping.

It is interesting to note that Heisenberg[6] maintains that a consistent, future theory of elementary particles will not use the Hamiltonian formalism. He has suggested the scattering matrix treatment as an alternative. This treatment is equivalent to the Hamiltonian formalism where the latter is applicable; but it is more general, since it can be used in cases where the Hamiltonian treatment fails. The Heitler theory of radiation damping fits naturally into this scattering matrix scheme.[7] This must not be taken as proof of the correctness of the Heitler theory, of course. Practically any formalism other than the simplest perturbation approach can be written in scattering matrix terminology; however. it is interesting that the Heitler theory does *not* lend itself to a Hamiltonian treatment. So while all this proves nothing about the Heitler theory, it does provide a confirmation of Heisenberg's ideas.

The Heitler method will give *poor* results when applied to problems which are convergent. The linear operator L in (2.1) is usually big near the scattering center. The expression (2.10) is nowhere equal to $\varphi_{sc}(\mathbf{x})$, but least of all near the scattering center. So the reaction of the field back upon the source is certainly treated incorrectly. This will show up later on in the examples.

In (2.11) the integral is multiplied by i. This leads us to believe that the term which is neglected is essentially an *inductive* term, while the radiation *resistance* is included to a reasonable approximation. Indeed, the choice (2.10) of φ_{rad} was motivated by the desire to treat the radiation resistance alone, as if no inductive effect existed. In this approximation, it can be shown that the resistive term is treated rigorously.[7] Now the inductive term (the "electromagnetic mass") is by no means zero in general. For point particles it is infinite. It is just this neglect of the inductive term which makes the method convergent when applied to problems involving point particles.

One can see this also from the quantum-mechanical derivation of Ma and Hsüeh.[8] They arrive at an integral equation which involves the quantity

$$1/(W-E)-i\pi\delta(W-E)$$

as one of the factors under an integral sign. One is supposed to take the principal value of this expression in integrating across $E=W$. Dirac[9] has shown that the term $1/(W-E)$ leads to $\frac{1}{2}[\varphi_{out}+\varphi_{in}]$ at large distances, where φ_{out} stands for the Schrödinger wave function corresponding to outgoing waves, φ_{in} stands for the Schrödinger wave function corresponding to ingoing waves. The term $[-i\pi\delta(W-E)]$ leads to $\frac{1}{2}[\varphi_{out}-\varphi_{in}]$ at large distances from the scattering center. The sum of the two, therefore, is an outgoing wave and represents the wave function of the scattered wave correctly. The essential step in the Ma-Hsüeh derivation consists in dropping the $1/(W-E)$ term. This means that they replace the scattered wave by $\frac{1}{2}(\varphi_{out}-\varphi_{in})$. It is clear that this is closely analogous to our classical derivation of Section 2, where a classical field φ was replaced by $\frac{1}{2}(\varphi_{ret}-\varphi_{adv})$.

It is possible[7] to construct a general proof to show that the Heitler method treats all resistive terms rigorously, while the reactive terms are

[5] J. A. Wheeler and R. P. Feynman, Rev. Mod. Phys. **17**, 157 (1945).
[6] W. Heisenberg, Ann. d. Physik **32**, 20 (1938), Zeits. f. Physik **120**, 513, 673 (1943).
[7] J. Schwinger, unpublished.
[8] S. T. Ma and C. F. Hsüeh, Proc. Camb. Phil. Soc. **40**, 167 (1944).
[9] P. A. M. Dirac, *Quantum Mechanics* (Clarendon Press, Oxford, 1930), Chapter 9.

taken into account only insofar as they lead to finite results. In most cases the first non-zero term in a perturbation expansion of the kernel $1/(W-E)$ is also the last finite term; all the later ones diverge. As a rule, the Heitler method takes into account only the first non-zero term in a perturbation expansion of the inductive term. This is not a general rule, however. In example 2 we shall see a case where two terms in the expansion are used jointly.

4. EXAMPLE 1

Consider a scalar meson field coupled to a source according to the Hamiltonian:

$$H=\tfrac{1}{2}\int[\pi^2(\mathbf{x})+(\nabla\varphi(\mathbf{x}))^2+\mu^2\varphi^2(\mathbf{x})]d^3x + \tfrac{1}{2}g(\bar{\varphi})^2. \quad (4.1)$$

$$\bar{\varphi}=\int\varphi(\mathbf{x})\,U(\mathbf{x})d^3x. \quad (4.2)$$

Here φ is the quantized meson field quantity, π its canonical conjugate, μ is the rest mass of the meson, and g is the coupling constant. We use units in which lengths are measured in centimeters, while the velocity of light and $\hbar=h/2\pi$ are unity. $U(\mathbf{x})$ is a source function which depends only upon $|\mathbf{x}|=r$. In the limit $U(\mathbf{x})\to\delta(\mathbf{x})$, $\bar{\varphi}\to\varphi(0)$ and we get a point interaction.

The commutation rules are the standard ones

$$i[\pi(\mathbf{x}),\,\varphi(\mathbf{x}')]=\delta(\mathbf{x}-\mathbf{x}'). \quad (4.3)$$

We shall first solve this problem exactly by a reduction to normal coordinates. This is possible since (4.1) leads to a linear problem, that is, a problem for which the equations of motion are linear in π and φ. The method used for the reduction to normal coordinates is given in the appendix to this paper. Equations (A.6) and (A.7) in the appendix can be combined into

$$(\nabla^2+k^2)\Phi(\mathbf{x})=g\bar{\Phi}U(\mathbf{x}), \quad (4.4)$$

where $\Phi(\mathbf{x})$ corresponds to Q_i of the appendix in the same way that $\varphi(\mathbf{x})$ corresponds to q, and $k^2=E^2-\mu^2$. Equation (4.4) is of the form (2.1). The linear operator L is an integral operator with the kernel $gU(\mathbf{x})\,U(\mathbf{x}')$. We define the function

$$V(k,\mathbf{x})=-\frac{1}{4\pi}\int\frac{\exp(ik|\mathbf{x}-\mathbf{x}'|)}{|\mathbf{x}-\mathbf{x}'|}U(\mathbf{x}')d^3\mathbf{x}'. \quad (4.5)$$

We introduce $V(k,\mathbf{x})$ because its satisfies (4.4) with $g\bar{\Phi}$ replaced by 1. It is square integrable over every finite volume, and it behaves at large distances like

$$V(k,\mathbf{x})\sim-\frac{v(k)}{4\pi}\cdot\frac{e^{ikr}}{r}, \quad (4.6)$$

where

$$v(k)=\int\exp(-i\mathbf{k}\cdot\mathbf{x}')\,U(\mathbf{x}')d^3\mathbf{x}'. \quad (4.7)$$

The solutions of (4.4) which are of the form (2.2) are clearly

$$\Phi(\mathbf{x})=\Phi_0(\mathbf{x})+g\bar{\Phi}V(k,\mathbf{x}). \quad (4.8)$$

This is only consistent if $\bar{\Phi}$ comes out correctly when calculated from (4.8). Multiply (4.8) by $U(\mathbf{x})$ and integrate to get

$$\bar{\Phi}=\bar{\Phi}_0+g\bar{\Phi}\bar{V}(k).$$

(The bar will be used throughout this paper to denote this operation.) This leads to

$$\bar{\Phi}=\Phi_0[1-g\bar{V}(k)]^{-1}. \quad (4.9)$$

We pick plane waves for $\Phi_0(\mathbf{x})$, i.e.,

$$\Phi_0(\mathbf{k},\mathbf{x})=(2\pi)^{-\frac{1}{2}}(2E)^{-\frac{1}{2}}\exp(i\mathbf{k}\cdot\mathbf{x}). \quad (4.10)$$

The normalization condition (A.5) of the appendix is satisfied. We then have the normal mode decomposition of the Hamiltonian (4.1)

$$\Phi(\mathbf{k},\mathbf{x})=(2\pi)^{-\frac{1}{2}}(2E)^{-\frac{1}{2}} \times\left[\exp(i\mathbf{k}\cdot\mathbf{x})+\frac{gv(-k)}{1-g\bar{V}(k)}V(\mathbf{k},\mathbf{x})\right], \quad (4.11)$$

$$\varphi(\mathbf{x})=\int d^3k[\Phi(\mathbf{k},\mathbf{x})a(k) +\Phi^*(\mathbf{k},\mathbf{x})a^+(k)], \quad (4.12)$$

$$\pi(\mathbf{x})=\int d^3k[(-iE)\Phi(\mathbf{k},\mathbf{x})a(\mathbf{k}) +(iE)\Phi^*(\mathbf{k},\mathbf{x})a^+(\mathbf{k})], \quad (4.13)$$

$$H=\tfrac{1}{2}\int d^3\mathbf{k}\cdot E\cdot[a^+(\mathbf{k})a(\mathbf{k}) +a(\mathbf{k})a^+(\mathbf{k})], \quad (4.14)$$

$$E=+(k^2+\mu^2)^{\frac{1}{2}}. \quad (4.15)$$

In order to find the scattering cross section, we notice that (4.11) represents an incident plus

a scattered wave. Using (4.6) and (2.4) we get

$$f(\omega\leftarrow\omega_0)=-\frac{G(k)}{4\pi}\frac{g}{1-g\bar{V}(k)}, \qquad (4.16)$$

where $G(k)\equiv v(k)v(-k)$ is approximately unity for all wave-lengths longer than the dimensions of the source.

The differential scattering cross section is

$$d\sigma=|f(\omega\leftarrow\omega_0)|^2 d\omega.$$

The quantity

$$\bar{V}(k)=\int V(\mathbf{k},\mathbf{x})\,U(\mathbf{x})d^3\mathbf{x}$$

is clearly of interest here. From (4.5) we have

$$\bar{V}(k)=-\frac{1}{4\pi}\int\int U(\mathbf{x})\,U(\mathbf{x}')\times\frac{\exp(ik|\mathbf{x}-\mathbf{x}'|)}{|\mathbf{x}-\mathbf{x}'|}d^3\mathbf{x}d^3\mathbf{x}'.$$

Here we use the expansion attributable to Lorentz, i.e., we expand the exponential in a power series to get

$$\bar{V}(k)=-\frac{1}{4\pi}\left(\frac{1}{a}+ik+\text{higher terms}\right), \qquad (4.17)$$

$$\frac{1}{a}=\int\int\frac{U(\mathbf{x})\,U(\mathbf{x}')}{|\mathbf{x}-\mathbf{x}'|}d^3\mathbf{x}d^3\mathbf{x}'. \qquad (4.18)$$

a is the "radius of the source," and it is clear that $1/a$ diverges as $U(\mathbf{x})\rightarrow\delta(\mathbf{x})$.

We now turn to the *approximate methods*. Clearly the normal-mode-expansion of the Hamiltonian for the free meson field is obtained by setting $g=0$ in (4.11) to (4.15). Then it is easy to determine the matrix element of $V=\frac{1}{2}g(\bar{\varphi})^2$ connecting two states of equal energy

$$E=+(k^2+\mu^2)^{\frac{1}{2}}.$$

It is

$$\langle E,\omega|\,V\,|E,\omega_0\rangle=gG(k)/2(2\pi)^3E. \qquad (4.19)$$

The perturbation $f(\omega\leftarrow\omega_0)$ corresponding to this is

$$f_B(\omega\leftarrow\omega_0)=-gG(k)/4\pi. \qquad (4.20)$$

This has to be so, of course, since (4.20) is the first term of (4.16) in an expansion in increasing powers of g.

We now use (4.20) to write down the *Heitler integral equation*, (2.11). We then obtain the *Heitler solution*

$$f_H(\omega\leftarrow\omega_0)=-gG(k)/4\pi(1-gB) \qquad (4.21)$$

with

$$B=-G(k)(ik)/4\pi. \qquad (4.22)$$

When we compare this with (4.16), we see that the only change is the replacement of $\bar{V}(k)$ by B. Comparing (4.17) and (4.22), we see two differences. $G(k)$ appears in (4.22), while it did not in (4.17). This is not significant, since $G(k)\cong 1$ for all wave-lengths of interest. The other change is the *omission of* $1/a$. This is the essential point. It must be noticed that $k\ll 1/a$ for all wave-lengths of interest (i.e., for which the expansion (4.17) is at all valid). So this omission is *not justified* at all in this problem. It is only in divergent problems, in which $1/a$ is infinite, that we can debate about the wisdom of subtracting it out. For the convergent problem discussed here, the Heitler method offers no significant improvement over the simple perturbation result (4.20). This is a special feature of the problem, however. In the next section, we will discuss a problem which is also convergent and in which the Heitler method leads to a much better result than the simple perturbation approach.

5. EXAMPLE 2

Consider a simple harmonic oscillator with coordinate q, momentum p, and frequency Ω. It has a "mesonic charge" ϵ by means of which it is coupled to a scalar meson field. The coupling we shall postulate to be a point interaction; i.e., the meson field $\varphi(x)$ must be evaluated at the instantaneous position of the oscillator $x=q$; the form of the coupling term we postulate to be similar to the coupling in electrodynamics. It must be emphasized that we are *constructing* an imaginary problem with the intention of testing various approximation schemes against an exact solution. The problem will admit an exact solution because we shall make it up in such a way that an exact solution is possible. The

Hamiltonian of the problem becomes:

$$H=\tfrac{1}{2}[(p-\epsilon\varphi(q))^2+\Omega^2q^2]+H_f, \quad (5.1)$$

$$H_f=\tfrac{1}{2}\int[\pi^2+(\nabla\varphi)^2+\mu^2\varphi^2]d^3\mathbf{x}. \quad (5.2)$$

This cannot be solved exactly. We shall, however, neglect the retardation; i.e., we replace $\varphi(q)$ in (5.1) by $\varphi(0)$, the meson field evaluated at the equilibrium position of the oscillator. Now the problem can be solved exactly by reduction to normal coordinates, but the solution diverges. We therefore replace $\varphi(0)$ by an average $\bar{\varphi}$ (see 4.2). Finally, we want to get rid of the cross term $p\bar{\varphi}$ which corresponds to $B_{ij}\neq 0$ in the notation of the appendix (A.1). To do this, we make the canonical transformation $p\rightarrow\Omega q$, $q\rightarrow -p/\Omega$. This preserves the commutation rules and brings the Hamiltonian into the form

$$H=\tfrac{1}{2}[p^2+(\Omega q-\epsilon\bar{\varphi})^2]+H_f. \quad (5.3)$$

It is this problem which we propose to solve, first exactly and afterwards by approximation methods.

We solve this again by a reduction to normal coordinates. The equations analogous to (A.6) and (A.7) are

$$-iE\Phi(\mathbf{x})=\Pi(\mathbf{x}), \quad -iEQ=P. \quad (5.4)$$

$$\left.\begin{aligned} iE\Pi(\mathbf{x})&=(\mu^2-\nabla^2)\Phi(\mathbf{x})-\epsilon(\Omega Q-\epsilon\Phi)U(\mathbf{x})\\ iEP&=\Omega(\Omega Q-\epsilon\Phi)\end{aligned}\right\}. \quad (5.5)$$

Here $\Phi(\mathbf{x})$ and Q are analogous to Q_i; $\Pi(\mathbf{x})$ and P are analogous to P_i of the appendix. We can eliminate Q, P, $\Pi(\mathbf{x})$ from these equations, to get an equation for $\Phi(\mathbf{x})$ alone:

$$(\nabla^2+k^2)\Phi(\mathbf{x})=\epsilon^2\frac{E^2}{E^2-\Omega^2}\bar{\Phi}U(\mathbf{x}). \quad (5.6)$$

This is clearly of the same form as (4.4), where again $k^2=E^2-\mu^2$, but g is replaced by $\epsilon^2E^2/(E^2-\Omega^2)$. We can, therefore, use the results for the scattering cross section from the previous example, provided that we remember the changed meaning of g.

If $\Omega<\mu$ there will exist a bound mode also, with a frequency slightly less than Ω. In that bound mode the oscillator vibrates with appreciable amplitude, while the meson field is strong only near the oscillator. This mode does not lead to scattering of free mesons.

If $\Omega>\mu$, the method we have used to eliminate Q, P from (5.4) and (5.5) will fail when $E=\Omega$. The result for the scattering cross section will not be changed, however, since the scattering cross section is a continuous function of the energy E.

Therefore, the short-cut method used here to find the scattering cross section is justified.

The scattering cross section is plotted against energy in Fig. 1 for an extreme case. The scattering cross sections found by perturbation theory and by the Heitler method are also shown in this figure.

The quantity $f(\omega\leftarrow\omega_0)$ is given by (4.16). Its absolute square has a strong maximum at the resonance point, $E=\Omega(1+m)^{-\frac{1}{2}}$, where $m=\epsilon^2/4\pi a$ is the ratio of the electromagnetic mass of the oscillator (in the Lorentz approximation) to its mechanical mass ($m=\frac{1}{2}$ in Fig. 1).

The perturbation expression for the cross section (4.20) agrees with the Heitler expression except around the *undisplaced* resonance point $E=\Omega$, where it diverges.

The Heitler expression (4.21) shows the same general behavior as the exact cross section. The line-shape and the maximum cross section are essentially unchanged. However, the resonance is at the point $E=\Omega$, because of the fact that the $1/a$ term has been neglected. This means that the *electromagnetic mass of the oscillator has been set equal to zero.*

The Heitler method leads to a significant im-

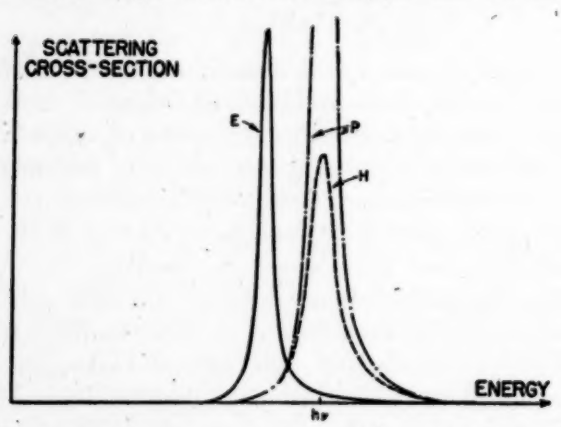

FIG. 1. Scattering cross section of an oscillator (example 2) *vs.* energy of incident mesons. E is the exact solution, H the Heitler solution, and P the perturbation (Born) solution. $h\nu$ is the resonance energy of the *free* oscillator (without electromagnetic mass).

provement over the simple perturbation expression in this problem. The cross section is everywhere finite, and its value is always less than or equal to k^{-2} (the equality holds only at the peak of the resonance curve). This must be so since the scattering is purely s-scattering.

While the shape of the line is given correctly, the resonance point is not displaced as it should be. Whether the electromagnetic mass *should* be set zero or not for *divergent* problems cannot be decided on purely mathematical grounds.

It may be of interest to point out that the perturbation here is of a mixed type. The Hamiltonian (5.3) can be written

$$H=H_0+V_1+V_2, \tag{5.7}$$

where H_0 is the Hamiltonian of the free field plus the free oscillator,

$$V_1=\tfrac{1}{2}\epsilon^2\bar{\varphi}^2, \tag{5.8}$$

$$V_2=-\epsilon\Omega q\bar{\varphi}. \tag{5.9}$$

V_1 induces one-step transitions, with matrix elements of order ϵ^2. V_2 induces two-step transitions only. The perturbation is calculated from the transitions of order ϵ^2, i.e., both V_1 and V_2 enter. It is *this* expression which is then used to write down the Heitler integral equation. If we had kept to the letter of the usual Heitler prescription, we would have taken only V_1 but not V_2, because V_1 gives the lowest order (direct) matrix-element different from zero.

6. EXAMPLE 3

Consider an oscillator which can vibrate in the direction indicated by the unit vector $\mathbf{e}_1$. It interacts with a vector meson field. In analogy with electrodynamics, we write for the Hamiltonian of the problem:

$$H=\tfrac{1}{2}\{[(p-\epsilon\mathbf{e}_1\cdot\boldsymbol{\phi}(q)]^2+\Omega^2q^2\}+H_f, \tag{6.1}$$

$$H_f=\tfrac{1}{2}\int d^3x[\boldsymbol{\pi}^2+\mu^{-2}(\mathrm{div}\boldsymbol{\pi})^2+(\mathrm{curl}\boldsymbol{\phi})^2+\mu^2\boldsymbol{\phi}^2]. \tag{6.2}$$

We again neglect retardation $\boldsymbol{\phi}(q)\to\boldsymbol{\phi}(0)$, make the problem convergent $\boldsymbol{\phi}(0)\to\bar{\boldsymbol{\phi}}$, and use the substitution

$$q\to -p/\Omega, \quad p\to\Omega q.$$

This gives

$$H=\tfrac{1}{2}[p^2+(\Omega q-\epsilon\mathbf{e}_1\cdot\boldsymbol{\phi})^2]+H_f. \tag{6.3}$$

We again solve this problem by a reduction to normal coordinates. The equations analogous to (A.6) and (A.7) of the appendix are

$$-iEQ=P, \quad -iE\boldsymbol{\Phi}(\mathbf{x})=(1-\mu^{-2}\,\mathrm{grad\,div})\boldsymbol{\Pi}(\mathbf{x}), \tag{6.4}$$

$$iEP=\Omega^2Q-\Omega\epsilon(\mathbf{e}_1\cdot\bar{\boldsymbol{\Phi}}), \quad iE\boldsymbol{\Pi}(\mathbf{x})=(\mu^2+\mathrm{curl\,curl})\boldsymbol{\Phi}(\mathbf{x})-\epsilon(\Omega Q-\epsilon(\mathbf{e}_1\cdot\bar{\boldsymbol{\Phi}}))\mathbf{e}_1U(\mathbf{x}). \tag{6.5}$$

We can eliminate Q, P, $\boldsymbol{\Pi}(\mathbf{x})$ from these equations to get one equation for $\boldsymbol{\Phi}(\mathbf{x})$:

$$(\nabla^2+k^2)\boldsymbol{\Phi}(\mathbf{x})=g(\mathbf{e}_1\cdot\bar{\boldsymbol{\Phi}})(1-\mu^{-2}\,\mathrm{grad\,div})\mathbf{e}_1U(\mathbf{x}), \tag{6.6}$$

where

$$g=\epsilon^2\cdot E^2/(E^2-\Omega^2). \tag{6.7}$$

(6.6) can be derived from the simpler Hamiltonian

$$H=H_f+\tfrac{1}{2}g(\mathbf{e}_1\cdot\boldsymbol{\phi})^2. \tag{6.8}$$

We shall therefore use this as our Hamiltonian. The scattering cross sections so obtained can then be used directly for the more complicated problem (6.3), provided we replace the constant g by the variable (6.7). The justification of this for scattering calculations is the same as in the previous example.

In the reduction to normal modes, we must remember that (6.8) is of the form (A.1) in the appendix with $B_{ij}=0$ but with $C_{ij}\neq\delta_{ij}$. If we keep this in mind, we can easily find the normal mode decom-

position of H in Eq. (6.8). The results are as follows: We first define three vectors $\mathbf{b}_s(\mathbf{k})$ associated with each wave-vector $\mathbf{k}$. $\mathbf{b}_1(\mathbf{k})$ and $\mathbf{b}_2(\mathbf{k})$ are two unit vectors orthogonal to each other and orthogonal to $\mathbf{k}$, while

$$\mathbf{b}_3(\mathbf{k}) = (E/\mu)(\mathbf{k}/k). \tag{6.9}$$

Then we define

$$\mathbf{\Phi}^{(0)}(\mathbf{k}, s; \mathbf{x}) = (2E)^{-\frac{1}{2}}(2\pi)^{-\frac{3}{2}}\mathbf{b}_s(\mathbf{k}) \exp(i\mathbf{k}\cdot\mathbf{x}), \tag{6.10}$$

$$\mathbf{\Phi}(\mathbf{k}, s; \mathbf{x}) = \mathbf{\Phi}^{(0)} + (\mathbf{e}_1\cdot\bar{\mathbf{\Phi}}^{0})g(1-gA)^{-1}(1-\mu^{-2}\,\text{grad div})\mathbf{e}_1 V(\mathbf{k}, \mathbf{x}). \tag{6.11}$$

Here $V(\mathbf{k}, \mathbf{x})$ is the function defined in (4.5), and

$$A = [1+\tfrac{1}{3}(k/\mu)^2]\bar{V}(k) - (3\mu^2)^{-1}\cdot\bar{U}. \tag{6.12}$$

$\bar{U}$, in accordance with our convention, is the integral of $U^2(x)$ over all of space, and is of order $1/a^3$. We also define

$$\mathbf{\Pi}(\mathbf{k}, s; \mathbf{x}) = (iE)^{-1}\{(\mu^2+\text{curl curl})\mathbf{\Phi}(\mathbf{k}, s; \mathbf{x}) + g(\mathbf{e}_1\cdot\bar{\mathbf{\Phi}}(\mathbf{k}, s))\mathbf{e}_1 U(x)\}. \tag{6.13}$$

With all these definitions, the conditions of the appendix are satisfied; in particular this is true of the normalization condition (A.8)

$$\int d^3\mathbf{x}[\mathbf{\Phi}(\mathbf{k}, s; \mathbf{x})\cdot\mathbf{\Pi}^*(\mathbf{k}', s'; \mathbf{x}) - \mathbf{\Phi}^*(\mathbf{k}', s'; \mathbf{x})\cdot\mathbf{\Pi}(\mathbf{k}, s; \mathbf{x})] = i\delta_{ss'}\delta(\mathbf{k}-\mathbf{k}'). \tag{6.14}$$

The normal mode decomposition is then given by

$$\boldsymbol{\phi}(\mathbf{x}) = \sum_s \int d^3\mathbf{k}[\mathbf{\Phi}(\mathbf{k}, s; \mathbf{x})a(\mathbf{k}, s) + \mathbf{\Phi}^*(\mathbf{k}, s; \mathbf{x})a^+(\mathbf{k}, s)], \tag{6.15}$$

$$\boldsymbol{\pi}(\mathbf{x}) = \sum_s \int d^3\mathbf{k}[\mathbf{\Pi}(\mathbf{k}, s; \mathbf{x})a(\mathbf{k}, s) + \mathbf{\Pi}^*(\mathbf{k}, s; \mathbf{x})a^+(\mathbf{k}, s)], \tag{6.16}$$

$$H = \tfrac{1}{2}\sum_s \int d^3\mathbf{k}E[a^+(\mathbf{k}, s)a(\mathbf{k}, s) + a(\mathbf{k}, s)a^+(\mathbf{k}, s)], \tag{6.17}$$

$$[a(\mathbf{k}, s), a^+(\mathbf{k}', s')] = \delta_{ss'}\delta(\mathbf{k}-\mathbf{k}'). \tag{6.18}$$

We can determine the scattering cross section by an investigation of the behavior of (6.11) for large $\mathbf{x}$. It is clear that we must specify the polarizations of the incident wave and of the particular scattered wave we intend to observe. The differential scattering cross section from an incident wave specified by the direction ω_0 and the polarization s_0 into a direction ω and a polarization s is given by

$$d\sigma = |f(\omega, s\leftarrow\omega_0, s_0)|^2 d\omega, \tag{6.19}$$

where

$$f(\omega, s\leftarrow\omega_0, s_0) = -(4\pi)^{-1}G(k)g(1-gA)^{-1}\cdot(\mathbf{e}_1\cdot\mathbf{b}_{s_0}(\mathbf{k}_0))(\mathbf{e}_1\cdot\mathbf{b}_s(\mathbf{k})). \tag{6.20}$$

$G(k)$ is again essentially unity for all wave-lengths less than the radius of the source.

In order to do *perturbation theory*, we notice that the normal mode decomposition of the free-field Hamiltonian (6.2) is obtained from (6.15)–(6.18) by letting g go to zero. The perturbation matrix element is then

$$\langle E, \omega, s|\, V\,|E, \omega_0, s_0\rangle = [gG(k)/2(2\pi)^3E](\mathbf{e}_1\cdot\mathbf{b}_{s_0}(\mathbf{k}_0))(\mathbf{e}_1\cdot\mathbf{b}_s(\mathbf{k})), \tag{6.21}$$

whence

$$f_B(\omega, s\leftarrow\omega_0, s_0) = -(4\pi)^{-1}gG(k)(\mathbf{e}_1\cdot\mathbf{b}_{s_0}(\mathbf{k}_0))(\mathbf{e}_1\cdot\mathbf{b}_s(\mathbf{k})). \tag{6.22}$$

This must be so, of course, since (6.22) is the first term in an expansion of (6.20) in increasing powers of g.

The *Heitler integral equation* can be written down with the help of (6.22). Its solution gives

$$f_H(\omega, s \leftarrow \omega_0, s_0) = -(4\pi)^{-1}G(k)g(1-gB)^{-1}(\mathbf{e}_1\cdot\mathbf{b}_{s_0}(\mathbf{k}_0))(\mathbf{e}_1\cdot\mathbf{b}_s(\mathbf{k})), \tag{6.23}$$

where

$$B = -(4\pi)^{-1}G(k)[1+\tfrac{1}{3}(k/\mu)^2](ik). \tag{6.24}$$

We now proceed to discuss these results. Clearly (6.22) and (6.23) can be obtained from (6.20) by replacing A by 0 and B, respectively. (6.22) is not an acceptable cross section. Consider the scattering of a longitudinal meson. s_0 is then equal to three, and the vector $\mathbf{b}_{s_0}(\mathbf{k}_0)$ is proportional to the energy, by (6.9). There is no inverse dependence on E in (6.22) to cancel this. Therefore, the *Born scattering cross section increases indefinitely as the energy increases.*

Now consider the exact cross section (6.20). Here the $(1-gA)^{-1}$ gives the needed inverse dependence upon the energy. Combining (6.12) and (4.17), we see that this term goes as E^{-3} for large energies. So the cross section not only stays finite, but it goes down as E^{-2} with increasing energy.

It is worth while to trace back the reason for this extremely strong damping. The crucial term is the $(k/\mu)^2$ in (6.12). This comes from the average

$$\langle \partial^2 V(\mathbf{k}, \mathbf{x})/\partial x_i \partial x_j\rangle_{\text{Av}} = -\tfrac{1}{3}\delta_{ij}[(k/\mu)^2\bar{V} - \bar{U}].$$

This term in turn is due to the

$$(1/\mu^2)\ \text{grad div}(\mathbf{e}_1 U(x))$$

in (6.6); but that can be traced to the

$$(1/\mu^2)\ \text{grad div}\boldsymbol{\pi}$$

in the second part of equation (6.4), and we finally come back to the $(1/\mu^2)(\text{div}\boldsymbol{\pi})^2$ term in the free-field Hamiltonian (6.2).

The Hamiltonian (6.2) is derived by Wentzel[10] in the following way. He starts from the relativistically invariant formalism given by Pauli.[11] The Lorentz condition

$$\sum_{r=1}^{4} \frac{\partial U_r}{\partial x_r} = 0, \tag{6.25}$$

which Pauli imposes, is used to eliminate the component U_0. The result of this elimination is a formalism in which only the space-like components of U_r appear. These form the 3-vector $\boldsymbol{\phi}$. The term $(1/\mu^2)(\text{div}\boldsymbol{\pi})^2$ comes from this elimination. Since this term leads to the strong damping encountered in the vector meson theory, we see that *the Lorentz condition (6.25) is responsible for the strong damping.* This strong damping is therefore an *intrinsic property of the vector meson field.*

The Heitler cross section (6.23) differs from the exact cross section in that A is replaced by B. Comparing (6.12) and (6.24), we see that this amounts to replacing

$$\bar{V}(k) \quad \text{by} \quad -(4\pi)^{-1}G(k)(ik),$$
$$\bar{U} \quad \text{by} \quad 0.$$

The first of these we have already encountered in the scalar theory. The term omitted is the $1/a$ in (4.17). The second change is an even more radical one, since $\bar{U}$ is of the order $1/a^3$. Thus, $\bar{U}/\mu^2$ is of order $a^{-1}(\mu a)^{-2}$. Now $\mu a \ll 1$ is the condition that the source model has any meaning at all. (The condition merely states that the radius of the source is much less than the range of the nuclear forces, $1/a$.) Therefore, the neglect here is numerically much worse than the neglect of $1/a$ alone.

It is natural that the $1/a^3$ term should disappear. The divergent terms which are omitted are the same ones that are eliminated by the λ-process. The λ-process is known to annihilate all terms in odd powers of $1/a$.

Because of the fact that such big terms are thrown away, it is not true that the Heitler procedure gives a good approximation to the exact result for this problem. Whether these same terms *should* be set equal to zero in problems which would otherwise be divergent, is a physical question which cannot be settled by a mathematical discussion.

[10] G. Wentzel, *Quantentheorie der Wellenfelder* (Franz Deuticke Press, Vienna, 1943), Chapter 3.
[11] W. Pauli, Rev. Mod. Phys. **13**, 203 (1941).

Bethe and Oppenheimer[12] have shown that it is *not* permissible to set these divergent terms equal to zero in a problem involving long wave-length radiation. This proves that the Heitler method is certainly not *universally* valid. One might still have thought that the neglect of the self-energy terms *is* permissible for very *short* wave-lengths, as an approximation to a future, consistent theory. *However, the examples worked out in this paper* (especially example 3) *show that if one believes in the finite source-model at all, then the Heitler method cannot even be used for short wave-lengths.*

One is, of course, not required to believe in the finite source-model for an elementary particle. So far, however, the only reason advanced for setting the inductive terms equal to zero is that they would otherwise be infinite. This argument does not seem entirely convincing.

In conclusion, the author wishes to express his thanks to Professor V. F. Weisskopf and to Professor Julian Schwinger for many interesting and helpful discussions.

APPENDIX

Reduction to Normal Coordinates

Consider a Hamiltonian of the form

$$H=\tfrac{1}{2}\sum_{i,j=1}^{N}(A_{ij}q_iq_j+2B_{ij}q_ip_j+C_{ij}p_ip_j), \quad \text{(A.1)}$$

where the q, p are operators which satisfy the commutation relations $i[p_i, q_j]=\delta_{ij}$. This operator is more general than the one usually considered in small vibration problems. Usually $B_{ij}=0$ and $C_{ij}=\delta_{ij}$. We needed this generality for example 3 of the paper, where $C_{ij}\neq\delta_{ij}$.

We shall reduce this to the normal form

$$H=\tfrac{1}{2}\sum_{r=1}^{N}E_r(a_r^+a_r+a_ra_r^+) \quad \text{(A.2)}$$

by means of the substitutions

$$q_i=\sum_{r=1}^{N}(Q_i^{(r)}a_r+Q_i^{(r)*}a_r^+), \quad \text{(A.3)}$$

$$p_i=\sum_{r=1}^{N}(P_i^{(r)}a_r+P_i^{(r)*}a_r^+). \quad \text{(A.4)}$$

Here a, a^+ are operators; Q and P are c-numbers. The operators a, a^+ will satisfy the commutation rules

$$[a_r, a_s^+]=\delta_{rs}. \quad \text{(A.5)}$$

This implies that the operator $a_r^+a_r$ assumes only non-negative integral eigenvalues and can be interpreted as the number of quanta in the normal mode number r. The "shape" of the mode r is specified by $Q_i^{(r)}$ and $P_i^{(r)}$.

The method used to find $Q_i^{(r)}$, $P_i^{(r)}$ is a slight modification of the one given in Whittaker, *Analytical Dynamics*.[13] The equations of motion which follow from the Hamiltonian (A.1) are

$$\dot{q}_i=B_{ji}q_j+C_{ij}p_j, \quad -\dot{p}_i=A_{ij}q_j+B_{ij}p_j,$$

provided that $A_{ij}=A_{ji}$, $C_{ij}=C_{ji}$. B need not be symmetric. Summation over repeated indices is understood.

Now consider the c-number equations

$$-iEQ_i=B_{ji}Q_j+C_{ij}P_j, \quad \text{(A.6)}$$

$$+iEP_i=A_{ij}Q_j+B_{ij}P_j. \quad \text{(A.7)}$$

These are $2N$ linear homogeneous equations in the $2N$ variables $Q_1Q_2\cdots Q_N$, $P_1P_2\cdots P_N$. They will have solutions only for certain discrete values of E. There will be $2N$ different values for E, but only N of them will be essentially distinct, since any solution of (A.6) (A.7) with $E=E_r$ will go over into a solution with $E=-E_r$ when we let $Q\rightarrow Q^*$, $P\rightarrow P^*$. From now on we shall denote the N positive values of E by E_r, where the index r goes from 1 to N. The corresponding values of P_i, Q_i we shall denote by $P_i^{(r)}Q_i^{(r)}$.

It is proved in Whittaker that

$$\sum_{i=1}^{N}(Q_i^{(r)}P_i^{(k)}-Q_i^{(k)}P_i^{(r)})=0,$$

$$\sum_{i=1}^{N}(Q_i^{(r)*}P_i^{(k)*}-Q_i^{(k)*}P_i^{(r)*})=0,$$

$$\sum_{i=1}^{N}(Q_i^{(r)}P_i^{(k)*}-Q_i^{(k)*}P_i^{(r)})=0 \text{ unless } k=r.$$

We shall normalize the Q_iP_i so that

$$\sum_{i=1}^{N}(Q_i^{(r)}P_i^{(r)*}-Q_i^{(r)*}P_i^{(r)})=i. \quad \text{(A.8)}$$

[12] H. Bethe and J. R. Oppenheimer, Phys. Rev. **70**, 451 (1946).

[13] E. T. Whittaker, *Analytical Dynamics* (Cambridge University Press, Teddington, England, 1937), Chapter 16.

This normalization differs from the one in Whittaker. *Equations (A.6), (A.7), (A.8) define the quantities* E_r, $Q_i^{(r)}$, $P_i^{(r)}$ *uniquely*, except for (immaterial) factors of absolute value 1 in front of $Q_i^{(r)}$ and $P_i^{(r)}$.

When we substitute *these* $Q_i^{(r)}$ and $P_i^{(r)}$ into (A.3) and (A.4), we find that the Hamiltonian reduces to (A.2). To check on the commutation rules (A.5) we use the inversion formulae

$$a_r = i\sum_{i=1}^{N}(Q_i^{(r)*}p_i - P_i^{(r)*}q_i), \qquad (A.9)$$

$$a_r^+ = -i\sum_{i=1}^{N}(Q_i^{(r)}p_i - P_i^{(r)}q_i). \qquad (A.10)$$

The identities in the $P_i^{(r)}$ and $Q_i^{(r)}$ given ahead of Eq. (A.8), together with Eq. (A.8) itself, then suffice to establish that (A.5) follows from the commutation rules for the p, q.

PHYSICAL REVIEW VOLUME 72, NUMBER 6 SEPTEMBER 15, 1947

On the Rise of the Wire-Potential in Counters

S. A. KORFF
New York University, University Heights, New York 53, New York

(Received June 9, 1947)

The rate at which the potential of the central wire in a counter changes when a count takes place is considered. The electron collection-time is found to be between 1 and 3×10^{-8} second. The subsequent variations in potential are controlled by the motion of the positive ions. Some experiments are reported, in which rises of 100 volts per microsecond were observed. The factors controlling fast counting are briefly discussed.

INTRODUCTION

FOR some time it has been well known that the potential of the central wire of a counter, either operating as a proportional or as a Geiger counter, rises quite rapidly to its maximum value. Various estimates of the rise-time have been made, the usual values being between one-half and four microseconds, some estimates falling outside either limit. The quantity in question is of great importance in determining the maximum speed with which counters can be operated. However, it is not immediately obvious how or whether it is connected with the much longer "dead time" or "recovery time," studied by Stever and others, nor with the much shorter electron travel time. It was, therefore, felt that it might be worth while to explore the factors involved and to see whether the rise time could be related to other already understood properties of counters and gas discharges.

MOTION OF THE ELECTRONS

It is evident that we have to discuss the motion of the electrons from the time of the formation of the first electron in the counter (the initial ionizing event) to the appearance of the electrons on the sensitive portions of our measuring device. Let us view the phenomenon in two steps. First we shall discuss the motion of the electron in the gas, including the avalanche formation. The second step will take the electron from the point on the central wire where it is collected to the measuring instrument.

Consider first an electron formed in the sensitive volume of a counter. We shall not discuss the process whereby the electron came to be separated from an originally neutral atom or molecule but shall assume that the electron came into being as a result of the initial ionizing event. The electron finds itself in the field produced by the applied voltage. Since almost all counters have cylindrical geometry, we can write for the field E, in volts per centimeter, the expression:

$$E = 2q/r = V/(r\log(b/a)), \qquad (1)$$

where q is the charge per unit length on the wire, r is the radius measured from the center of the wire, V is the applied potential in volts, b is the radius of the cylinder, and a is the radius of the

TABLE I. Field as function of radius inside typical counter.

Radius from wire center (cm)	Field (volts/cm)
5×10^{-3} (wire surface)	37,400
0.01	18,700
0.05	3,740
0.1	1,870
0.5	374
1.0 (at cylinder)	187

wire in centimeters. Let us assume that we have a counter in which the cylinder has a radius of 1 cm and a wire of 5×10^{-3} cm (approximately 4-mil wire). If the potential applied to the counter is assumed to be 1000 volts, we can compute the field in volts per cm at any point inside the counter. The results of such a computation are presented in Table I.

The electron, as it travels toward the central wire, impelled by the field, will make collisions with atoms or molecules present in the counter. The classical mean free path l of an electron in a gas, between collisions with gas molecules, will be given nearly enough by the relation:

$$l=4/N\pi R^2, \tag{2}$$

where l is the mean free path in cm, N is the number of atoms or molecules per cc, and R is the average collision radius of each. If we take N as 2.7×10^{18} per cc (corresponding to a gas pressure of 7.6-cm Hg in the counter) and R as 10^{-8} cm, then the mean free path in this counter is 4.8×10^{-3} cm. Although Eq. (2) will give only approximate values for l, we may consider the mean free path established nearly enough, since both R and N may be considerably varied in any practical case.

We shall now consider how much energy an electron will gain in one free path at any given point in the counter. Let us divide the counter volume into three sections with differing properties. The outermost region will be called the low field region. In this region, the electron will gain less than 2 volts per free path. The next region we shall call the medium field region. Here the electron gains between 2 and 15 volts per free path. The region next to the wire is the high field region, and in this region the electron will acquire 15 volts or more per free path. The reasons for the selection of these particular values will be discussed below. The energy gain dV, in electron-volts, will be related to the field through:

$$dV=-E(r)dr, \tag{3}$$

where $E(r)$ is the field at radius r, and dr is the radial distance traversed by the electron. We neglect the third derivative term produced by variations in the field over so small a distance as a free path. If we take dr as equal to a mean free path, then we find that dV becomes 2 volts at $r=0.4$ cm, and 15 volts where r is 0.06 cm. Hence the high field region occupies a space of only half a millimeter about the central wire.

A 2 volt electron making a collision with an atom or molecule will be able to transfer energy by inelastic collisions to the target atom in many cases. For example, the lowest level in sodium is at 2.01 volts. In molecules with bands in the red or infra-red it is lower, while only for hydrogen, helium, and argon is it substantially higher. If a polyatomic constituent is present, electrons will start making inelastic collisions at quite low energies. As soon as an electron makes inelastic collisions we may think of it as coming essentially to rest after each collision and starting from rest to travel its next free path. The energy transferred in this manner to the atom or molecule will be lost either by radiation or by de-excitation collisions. However, such radiation cannot produce new electrons, because there are no photoelectric work functions as low as 2 volts characteristic of any substances ordinarily used in counters. The energy will therefore eventually be dissipated thermally. As the electron gains more and more energy per free path nearer the wire, there will be more and more available energy levels of the atom or molecule to which it can transfer energy, and consequently all further collisions will also be inelastic.

The electron now enters the high field region. Here the electron is a fraction of a millimeter from the wire and will gain, per free path, the 15.6 volts needed to ionize argon. Here the familiar Townsend avalanche process will start. This process has been fully described elsewhere[1] and will not be considered here. The result of ionizing collisions will be as before, that the electron will lose almost all of its energy per

[1] S. A. Korff, *Electron and Nuclear Counters* (D. Van Nostrand and Company, Inc., New York, 1946).

collision and may be regarded as starting from rest after each encounter.

The total time required for the electron to move from the place where it is produced to the wire will now be discussed. To know this we must know the average velocity. It is evident that the total time will equal the sum of the times dt required to traverse each free path. Hence we may write, for T, the total time,

$$T=\sum dt=\sum l/v(r), \qquad (4)$$

where the sum is to be taken over all free paths. Again neglecting the third derivative over any one free path, the average velocity v in any free path is one half the final velocity, and this may be computed from the energy gained, since $\frac{1}{2}mv^2=eV$. Therefore, the average velocity v depends on the field, and since this varies inversely as the radius, $v(r)$ varies as the inverse square root of the radius. Since an electron starting at the cylinder gains about 0.2 volt between collisions, and since this energy rises only to 0.5 volt by the time the electron has traversed more than half the counter, it is obvious that the electron spends most of its time in the low field regions. Inserting actual values, we recall that a 1-volt electron has a speed of 5.93×10^7 cm/sec. Hence for an average energy of $\frac{1}{4}$ volt, the average velocity will be about 3×10^7 cm/sec., and it will require around 3×10^{-8} sec. for the electron to traverse the 1000 free paths between cylinder and wire.

The Townsend avalanche process, on this picture, will be characterized by an average electron velocity of perhaps 5 times the figure cited, and for a distance of 0.5 mm, and hence requires between 1 and 2×10^{-10} sec. to complete. It will be appreciated that the exact times involved will depend on the nature and amount of the gas used and on the voltage applied. However, if more gas is put in, the mean free path is shortened, but a higher voltage has to be applied. These two factors operate inversely to each other as far as the time is involved, so that 3×10^{-8} sec. will be the proper figure for many ordinary counters.

We are now ready to consider what happens after the electrons have arrived on the central wire. The central wire will generally be connected to the grid of the first tube in the detecting arrangement, and we shall assume that the wire, grid, and connecting leads have a distributed capacity of about 10^{-11} farad. We are interested in inquiring the rate at which the voltage of the grid will change.

When the Townsend avalanche is over, a sheath of positive ions will be left about the central wire. The role of this sheath in quenching the discharge and its influence on the rise-time has been thoroughly discussed by the Montgomerys.[2] The positive charges in the sheath will hold negative charges on the central wire. We may treat the problem by the familiar method of electrostatic images. It will be recalled that the image in a convex conductor of radius a, produced by a charge e at distance r from the center is $-ea/r$. This expression is exact for a sphere, and a good approximation for a cylinder. When the sheath is first formed and r is only a little greater than a, the image charge is roughly equal to the charge in the sheath, and almost all the electrons are held on the wire. However, as the sheath travels outward and r becomes large compared to a, the number of electrons held on the central wire lessens. The electrons are freed to travel to the grid of the tube and to cause its potential to vary.

We may estimate the speed of this process. The rise in potential of the grid will depend on the rate at which charge arrives, and this will depend on the rate at which charge is freed by the process we have just described. The freeing of charge depends on the time-rate of change of r, dr/dt. This in turn is in practice a function of the sheath position, or of the velocity of the positive ions. The velocity may be taken as varying with the field, and hence inversely as the radius.

Another way of viewing this problem is to consider the effect of the sheath as increasing the capacity of the central wire. As the sheath moves outward, the capacity decays down to the value determined by the counter geometry, and hence the potential of the system rises. The relation between charge q, potential V, and capacity C is the familiar equation $q=CV$. If we differentiate this with respect to time and

[2] C. G. and D. D. Montgomery, Phys. Rev. **57**, 1030 (1940).

recall that both C and V will vary, we obtain:

$$dq/dt = CdV/dt + VdC/dt. \quad (5)$$

We are interested in ascertaining dV/dt, and we can write down the factors on which dC/dt depends. Once the charge has been collected, dq becomes zero; the electrons are merely held and redistributed. The capacity of a cylindrical condenser is given by:

$$C = \tfrac{1}{2}\log(b/a) \quad (6)$$

per unit length, where b and a are the electrode diameters. In this case, we have to consider what happens when a, the wire diameter, remains constant, and b, the sheath, moves outward. The outward (radial) velocity of the sheath we shall assume to be proportional to the field. This assumption may be wrong in the high field region, but is nearly enough right in the region in which the sheath spends most of its time. The field varies inversely as the radius. The outward velocity, $d/dt(b)$, varies as $(1/r)$. Hence we have:

$$Kd/dt(\log b) = d/dt(1/C), \quad (7)$$

where K is a constant of proportionality involving $\log a$.

Inspection of this relation shows that the capacity will be large (and hence the potential of the grid will be small), while b is nearly equal to a and that after the sheath has moved out so that b is any substantial fraction of the size of the counter, the rate of change of the capacity will be small and the grid potential will approach a constant value. We may expect, therefore, that the rise of potential of the grid of the tube will give us a straight line on a semi-log plot and that the intercept on the time axis will give us a measure of the avalanche formation and electron collection time.

COMPARISON WITH EXPERIMENT

W. E. Ramsey[3] has made a careful series of measurements of the time-rate-of-change of the potential of the wire of a counter. Inspection of his curves will show at once that the predictions based on the above picture are admirably fulfilled. The predicted straight-line relationship suggested by Eq. (7) is found. The intercept noted by Ramsey is around 3×10^{-8} sec., which also agrees with the values computed above with the aid of Eq. (3) and the subsequent argument. He shows curves for argon-alcohol and for argon-oxygen counters. He finds that the argon-oxygen counter has a faster "breakdown" and shows an intercept of nearer 1.5×10^{-8} sec. This is also in accord with the point of view developed above, for in the polyatomic counters the electron will make inelastic collisions at a lower voltage because of the many available levels in the band-structure and so it will start to lose energy (radial velocity) at points further out in the counter.

In order to ascertain whether the above picture was also valid in the proportional region, a counter filled with BF_3 was used. It was connected to a P4 Synchroscope. A one megacycle timing wave gave a time calibration and a high resistance voltmeter gave the vertical pulse size scale. The counter wire was connected to ground through 100,000 ohms, and the distributed capacity of the wire and leads was estimated at about 30 mmf. Hence the pulses on the wire decayed with about a three-microsecond exponent. This quantity was made long compared to the rise of the pulse so that the exponential decay would not interfere with the rise-time measurements and so that the pulses would be large enough to be easily measured.

The wire was found to change in potential by about 25 volts in $\frac{1}{4}$ microsecond, i.e., at the rate of 100 volts per microsecond. It must be noted that the rate of rise is not uniform but is rapid at first and then becomes slower. Hence the rate is initially greater and afterwards less than 100 v/ms, and the figures refer to a particular magnitude and instant only. Further, in these tests it required the presence of about 2×10^{8} electrons on the wire to cause a change in potential of 1 volt, so that even for large initial ionizing events a considerable gas amplification in the Townsend avalanche took place. Fluctuations were observed, the magnitude of which corresponded to about ten percent in the times required to rise 25 volts. The rates of change observed in these tests were similar to those found by Ramsey for his counters. The experi-

[3] W. E. Ramsey, Phys. Rev. **57**, 1022 (1940).

ments, therefore, bear out the picture developed above. We expect to make some further measurements at smaller pulse sizes.

One may also expect that the rise-time of the pulse will be slowed down if the capacity of the wire-system is increased. This was tested and found to be the case. Increasing the capacity also has the effect of decreasing the pulse size. Similar effects were noted by Ramsey[3] and are found in his curves.

DISCUSSION

In conclusion a few words may be said about high counting rates. In the Geiger region the normal recovery time is determined by the mobility of the positive ion sheath. This may be shortened by collecting the positives on the center wire, using the Simpson[4] circuit. The effective speed of operation of this circuit is limited by the spread-time of the sheath.[5] In the proportional region, the sheath does not spread the whole length of the wire,[1] and the recovery times can be made much more rapid.[6] The greater the gas amplification, however, the larger the number of positive ions that produce space charge which will limit counting speeds. At low amplifications, recovery times can be considerably shortened, but the recovery time still is the limiting factor. Only a small benefit can be achieved by operating the counter at a higher voltage. The field is increased, and hence the electron velocity is higher, but many more positives are formed at varying distances from the wire. The use of grids[7] is beneficial, since the positives have a smaller distance to travel. However, grids present added constructional difficulty and in the proportional region pose collection problems. A pulse sufficient in size to be easy to measure can be obtained in 10^{-7} sec., as we have shown. Therefore, an application of the Simpson circuit to a proportional counter will permit counting at rates up to several million per second. The matter is under study and further tests will be reported in due course.

[4] J. A. Simpson, Phys. Rev. 66, 39 (1944).
[5] E. Wantuch, Phys. Rev. 71, 646 (1947).
[6] C. O. Muelhause and H. Friedman, Rev. Sci. Inst. 17 506 (1946).
[7] S. A. Korff, Phys. Rev. 68, 53 (1945).

The Absorption Spectrum of InCl

HAROLD M. FROSLIE AND J. G. WINANS
University of Wisconsin, Madison, Wisconsin
(Received June 6, 1947)

A study of the band spectrum of InCl has been carried out in absorption with a determination of vibrational, rotational, and electronic energy levels associated with the band system in the region 2650 to 3000 angstrom units. The B_v' and B_v'' values were found to be of the order of 0.11 wave numbers, from which can be calculated a nuclear separation of the order of 2.3×10^{-8} centimeter. Predissociation in the band system provided a value for the energy of dissociation of the ground state between 4.64 and 4.66 electron volts.

INTRODUCTION

WHILE studying the absorption of a mixture of Hg and In vapor, Winans, Davis, and Leitzke[1] observed a band system appearing in the region 2650 to 2800 angstrom units. The present study is the outgrowth of an attempt to verify the earlier observations and to study the bands under greater dispersion. By duplicating the conditions previously found necessary to produce the bands, it was possible to photograph them with sufficient dispersion to make an accurate measurement of the isotope shift. These measurements showed that the bands were due to InCl and not HgIn, as first supposed.

A survey of the literature showed that this same band system had been observed previously a number of times. Grotrian[2] obtained the

[1] J. G. Winans, Frances Davis, and Victor Leitzke, Phys. Rev. 57, 1079 (1940).
[2] W. Grotrian, Zeits. f. Physik 12, 229 (1923).

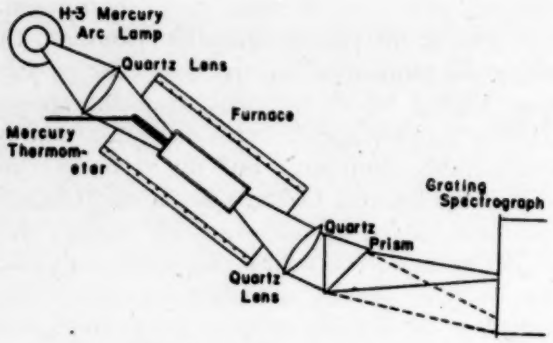

FIG. 1. Schematic diagram of apparatus.

stronger bands in a study of the absorption of In vapor. He interpreted the system as being due to a weakly bound In_2 molecule. Waring[3] obtained the same spectrum in the absorption of In and Cd vapor. He suggested that the spectrum was probably that of the InCd molecule. Barratt and Bonar[4] observed bands in absorption by Bi vapor whose wave-length agreed with those reported by Waring. They attributed these bands to the Bi_2 molecule. Miescher and Wehrli[5] were the first observers to obtain the bands under sufficient dispersion to positively identify the spectrum as due to InCl. They substantiated their assignment to InCl with measurements on the isotope shift due to Cl_{35} and Cl_{37}.

Since none of the previous investigators had studied the band system with sufficient dispersion to resolve the rotational structure or to make an accurate null-line vibrational analysis, it seemed desirable to make a rather detailed study of the band system.

The spectrum was photographed in the fourth order of a 21-foot grating spectrograph, which gave a dispersion of approximately 0.6 angstrom per millimeter and resolved lines as close as 0.03 angstrom unit. The grating was one ruled by R. W. Wood on an aluminum surface to give maximum intensity at 11,000 angstrom units in the first order.

EXPERIMENTAL PROCEDURE

After the band system was positively identified as due to the InCl molecule, a fused-quartz absorption cell, 10 centimeters in length and 2.5 centimeters in diameter, was prepared containing the sample. The quartz cell was evacuated by a two-stage mercury diffusion pump system equipped with a liquid air trap. As soon as a vacuum of the order of 10^{-4} millimeter of mercury was obtained, the absorption cell was baked at a temperature just below the softening point of the quartz until a "sticking vacuum" was obtained as indicated by a McLeod gauge. At this point the system was opened and a small pellet of high purity In was placed in a tube extending back from the absorption cell. On the other side of the absorption cell, toward the vacuum system proper, was placed at the same time a small amount of $InCl_3$. This was accomplished as rapidly as possible so that the quartz cell was open to the atmosphere only as long as absolutely necessary. After the system was sealed and a vacuum of the order of 10^{-6} millimeter of mercury was obtained, a furnace was placed over the cell in such a way that the tube with the In was at the hottest point in the furnace. In spite of the fact that the vapor pressure of In is extremely small even at 1000°C, it was possible,

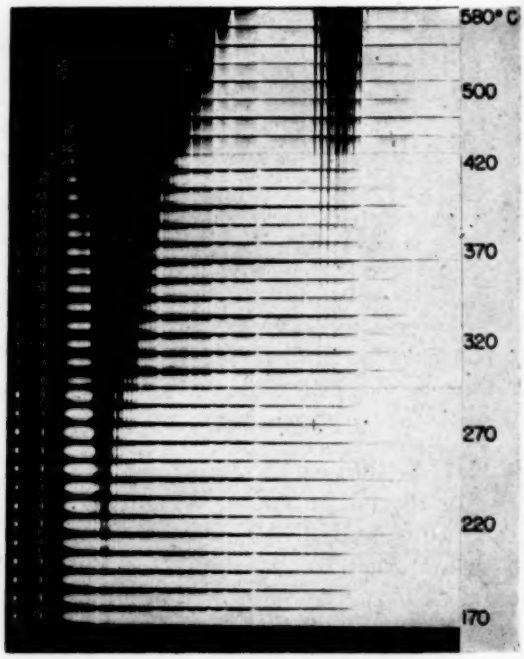

FIG. 2. The absorption of InCl vapor at pressures up to one atmosphere. Temperatures indicated were those measured at the coldest part of the cell.

[3] R. K. Waring, Phys. Rev. **32**, 441 (1928).
[4] S. Barratt and A. R. Bonar, Phil. Mag. **9**, 1519 (1930).
[5] E. Miescher and M. Wehrli, Helv. Phys. Acta **7**, 298 (1934).

with sufficient time, to distill the In from the extended tube into the absorption cell. When this had been achieved the furnace was removed, and the portion of the tube containing the undistilled In was sealed off from the system under vacuum. Then with a hand torch a quantity of the $InCl_3$ was distilled from the other side into the absorption cell. After the cell was sealed off, it then contained pure In metal and a small amount of $InCl_3$ under a vacuum of the order of 10^{-7} millimeter of mercury. When this was heated in a furnace to just above the melting point of the In, the $InCl_3$ was converted to InCl. Care was taken to assure that there should be an excess of In so that the conversion would be complete. Otherwise one might encounter troublesome absorption either caused by $InCl_2$ or $InCl_3$. The above described method of preparing the sample proved to be very satisfactory and yet simpler than that used for example by Miescher and Wehrli.[5]

To provide the continuous background for the absorption, a H-3 high pressure mercury lamp was used as described previously by Winans.[1] Since the continuum of the mercury discharge in this type of lamp is comparatively intense from 5000 angstrom units to 2536 angstrom units, it was possible to obtain good spectrograms even in the fourth order of the grating spectrograph with a maximum exposure time of only a few hours, using Eastman 40 or Eastman II-0 plates.

A number of preliminary plates were taken with a Bausch and Lomb medium quartz spectrograph. This was done to determine the proper conditions to obtain a particular band of the system and to explore the extent of the system or any other systems due to this molecule.

To eliminate the overlapping of orders in the grating spectrograph, the arrangement shown schematically in Fig. 1 was used. With this set-up it was possible to eliminate almost completely the third order without appreciable loss of intensity in the fourth order. All of the spectrograms of the system from 2650 to 3000 angstrom units were taken with this arrangement.

Two other band systems of this molecule which overlap occur in the range from 3300 to 3700 angstrom units. They could be conveniently photographed in the third order. To eliminate the overlapping from the fourth order here, the light was taken from the high pressure mercury lamp through the glass envelope which absorbed the radiation below 3000 angstrom units. In all cases, the overlapping caused by the second order gave no difficulty, since the plate emulsions used were insensitive in that wave-length region.

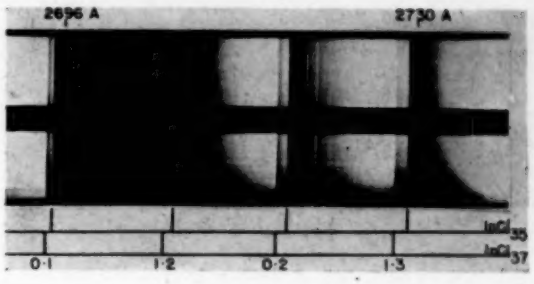

FIG. 3. Bands of the fundamental system taken in the fourth order of the 21 foot grating spectrograph.

DESCRIPTION OF THE SPECTRUM

Figure 2 is a photograph of the spectrum of the InCl molecule taken on the Bausch and Lomb medium quartz spectrograph. The exposures were taken at various pressures of the absorbing gas, which was controlled by varying the temperature of the furnace in which the absorption cell was placed. As indicated in the figure, the pressures were determined by the temperature as measured at the end of the protruding tube of the absorption cell where the excess liquid InCl collected. Temperatures were measured with a high temperature mercury thermometer.

From a spectrogram with the dispersion of Fig. 2 it is not possible to obtain more than a qualitative idea of the band system. At temperatures as low as 200°C a very intense absorption appears at about 2650 angstrom units. With increasing temperature and hence pressure of the absorbing vapor, this system broadens toward the red until at a temperature corresponding to about one atmosphere of the vapor it extends from 2650 to 3000 angstrom units. The individual bands of the system show a double head, and throughout the region all are shaded toward the red.

At about 300°C another system or systems in the region from 3300 to 3700 angstrom units appears. This group of bands broadens somewhat symmetrically with increasing pressure of the

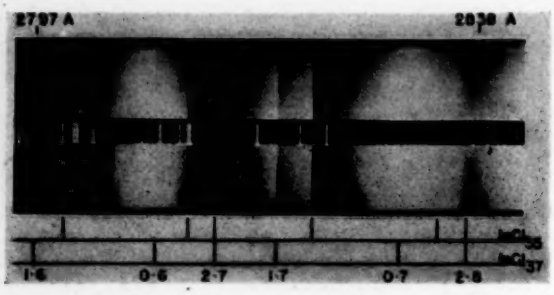

FIG. 4. Bands of the fundamental system taken in the fourth order of the 21 foot grating spectrograph. Two bands of the $(2,v'')$ progression can be detected superimposed on the (0,6) and (0,7) bands.

absorbing vapor. Although this group of bands has a much more complicated pattern than the 2650 angstrom group, it can be easily seen to consist of a series of overlapping bands with sharp heads, each band shaded toward the violet.

At the higher pressures two regions of continuous absorption also appear. One is at about 2610 angstrom units. With increasing pressure it broadens and merges into the absorption in the 2650 angstrom region. Another region of continuous absorption appears to set in at about 2100 angstrom units and broadens toward the red, finally joining with the absorption in the 2610 angstrom region.

Figures 3 and 4 are spectrograms of the fundamental system (the system in the region 2650–3000 angstrom units) taken in the fourth order of the 21 foot grating spectrograph. These spectrograms show that the system consists of a series of nearly equally spaced bands with alternate bands showing rotational structure and the others no rotational structure. All bands have sharp heads with the exception of some showing in Fig. 4. Superimposed on the (0,6) and (0,7) bands there is another series of bands overlapping the ones with rotational structure. For these bands not only is the rotational structure missing but also the heads are not sharp.

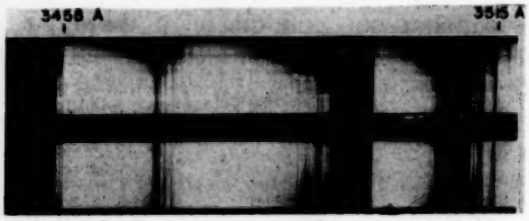

FIG. 5. Bands of the intercombination systems of InCl, taken in the third order of the 21 foot grating spectrograph.

Miescher and Wehrli[5] have identified the band at 2672.3 angstrom units as the $v'=0, v''=0$ band and have shown that all of these bands fit as members of the $(0,v'')$, $(1,v'')$, and $(2,v'')$ progressions. Bands in the $(0,v'')$ progression have rotational structure. Bands in the $(1,v'')$ progression have sharp heads but no rotational structure. Bands in the $(2,v'')$ progression not only have no rotational structure but also have diffuse heads. This spectrum is a striking example of predissociation in the upper electronic state. That this is actually the phenomenon of predissociation is verified by the fact that in emission only the $(0,v'')$ progression is obtained.

The absorption in the region 3300 to 3700 angstrom units, which hereafter will be referred to as the intercombination systems, is shown in Fig. 5. Under the larger dispersion, it is found from a study of the isotope shift that actually in this region there are two separate band systems which almost completely overlap each other.[5] Miescher and Wehrli showed that the lower vibrational levels for these bands are the same as those for the fundamental system. As can be seen from the plate, all of these bands have rotational structure. Since the intercombination systems and the fundamental system have the same lower electronic state, this is further evidence that the breaking off of fine structure in the fundamental system is actually a predissociation in the upper state.

ANALYSIS OF THE FUNDAMENTAL SYSTEM

a. Vibrational Analysis

A vibrational analysis of this spectrum and an assignment of quantum numbers has been made by Miescher and Wehrli[5] from spectrograms taken under low dispersion. Only the band heads were measured and these somewhat inaccurately. Since the bands arise from a $^1\Pi \leftrightarrow \Sigma_0^+$ transition (see later section), they consist of a P, Q, and R branch. Even with the high dispersion available in the present experiment in the fourth order of the grating spectrograph, the rotational lines in the neighborhood of the null line are not resolved. Nevertheless, the Q branch head is for practical purposes located at the null line. On the spectro-

grams taken in this experiment, the Q branch head could be measured in the $(0,v'')$ and $(1,v'')$ progressions. The Q branch heads can be detected for some bands in these progressions in Figs. 3 and 4. For the $(2,v'')$ progression, since the R heads are not even sharp, an attempt was made to locate the maximum of absorption in each band. The observed bands are arranged in Table I according to the Deslandres' scheme.[6] Since each band is double because the two Cl isotopes, both components are entered in the table. The upper numbers refer to the Cl_{35} component, and the lower numbers refer to the Cl_{37} component. Also listed are the wave numbers calculated from the formula

$$\nu_{cm^{-1}}=37483.6+\frac{177.3}{173.6}(v'+\tfrac{1}{2})-\frac{12.6}{12.1}(v'+\tfrac{1}{2})^2$$
$$-\frac{317.4}{310.8}(v''+\tfrac{1}{2})+\frac{1.01}{0.97}(v''+\tfrac{1}{2})^2.$$

It can be seen that in all cases the agreement between the observed and calculated values is less than one wave number.

By considering the coefficients in the formula for $InCl_{35}$ and $InCl_{37}$, it is verified that the two components are due to these isotopes. When ρ is calculated, using Cl_{35} and Cl_{37} and In_{115}, one obtains

$$\rho=0.9790.$$

The average value from the coefficients of the empirical equation gives

$$\rho=0.9796.$$

b. Rotational Analysis

As mentioned previously, each band of the fundamental system consists of a single P, Q, and R branch. Since the bands are shaded toward the red, it is the R branch that forms the head.[6] At a distance from the band head, where the rotational lines are resolved, the intensity of the R branch has practically dropped to zero. Thus, in the resolved region of a band, there remain only the P and Q branches which intersect each other, producing a kind of modulation noticeable in Fig. 3. Alternately, they are in phase, so to speak, and are not resolved, and then out of phase and then resolved. In the regions where the two series of lines are neither in phase or out of phase, a measurement gives a wave-length or wave number which does not truly represent either a Q line or a P line. Because of this inherent difficulty it was not possible to apply the combination relations[6] directly to a set of measurements on a band to determine the numbering in the two branches. In the $(0,v'')$ progression all bands have a common upper state, so that if the combination relations could be worked out, the relative numbering of the P and Q lines could be determined and then the absolute numbering. However, because of the above mentioned difficulty, the combination differences were too erratic to show when the correct relative numbering had been obtained, if these differences were computed from the values measured directly.

TABLE I. Deslandres table (scheme of origins) of the fundamental system of InCl.

v''	$v'=0$ Obs.	$v'=0$ Cal.	$v'=1$ Obs.	$v'=1$ Cal.	$v'=2$ Obs.	$v'=2$ Cal.
0	37410.6 37412.2	37410.6 37412.2	37562.9	37562.7 37561.6	37690	37689.6 37686.8
1	37095.0 37103.2	37095.2 37104.3	37247.3 37252.8	37247.3 37253.7		
2	36781.6 36796.2	36781.8 36796.5	36934.0 36946.2	36933.9 36945.9		
3	36470.5 36491.5	36470.5 36491.5	36622.5 36641.2	36622.6 36640.9		
4	36161.2 36188.6	36161.2 36188.5	36313.2 36338.2	36313.3 36337.9		
5	35854.2 35887.6	35853.9 35887.5	36006.0 36036.8	36006.0 36036.9		
6	35549.2 35588.9	35548.6 35588.3	35700.9 35738.2	35700.7 35737.7	35828	35827.6 35862.9
7			35397.4 35440.8	35397.4 35440.5	35524	35524.3 35565.7
8			35095.9 35145.3	35096.1 35145.3	35223	35223.0 35270.5
9			34796.8 34852.1	34796.9 34852.0	34924	34923.8 34977.2
10			34499.7	34499.7 34560.6	34627	34626.6 34685.8
11			34204.5	34204.5 34271.2	34331	34331.4 34396.4
12					34038	34038.2 34108.9

[6] Gerhard Herzberg, *Molecular Spectra and Molecular Structure* (Prentice-Hall Inc., New York, 1939). All theory necessary for the interpretation can be found there.

The analysis as it was finally obtained was made in essentially two independent ways. First an empirical formula of the type

$$\nu=\nu_0+am(m+1)+bm^2(m+1)^2$$

was obtained to represent the Q branch in the (0,0) and (0,2) bands. From quantum theory analysis the Q branch should be represented by[6]

$$\nu=\nu_0+(B_v'-B_v'')m(m+1)-(D_v'-D_v'')m^2(m+1)^2.$$

Thus when the empirical equation for the Q branch is known for any band, one has the value of $(B_v'-B_v'')$. Also since the R branch is represented theoretically by

$$\nu=\nu_0+(B_v'+B_v'')m+(B_v'-B_v'')m^2,$$

which is valid for small m, the quantity $(B_v'+B_v'')$ can be obtained from measurements on ν_0 and ν at the band head. The procedure is as follows:

$$d\nu/dm=(B_v'+A_v'')+2m(A_v'-B_v''),$$

and

$$d\nu/dm\,|_{\text{Head}}=0$$

so

$$m_{\text{Head}}=\frac{-(B_v'+B_v'')}{2(B_v'-B_v'')}.$$

Then

$$\nu_{\text{Head}}=\nu_0-\frac{(B_v'+B_v'')^2}{2(B_v'-B_v'')}+\frac{(B_v'+B_v'')^2}{4(B_v'-B_v'')}.$$

This gives

$$(B_v'+B_v'')^2=-4(B_v'-B_v'')(\nu_{\text{Head}}-\nu_0).$$

If the Q branch has been analyzed, $(B_v'-B_v'')$ is known and thus $(B_v'+B_v'')$ can be determined. Two simultaneous equations are then available to determine B_v' and B_v''.

The above method of analysis was carried out for the (0,0) and (0,2) bands. The difficulties are in measuring accurately the null line, ν_0, and determining the m value of Q branch lines. Since the lines are not resolved down to the null line, it is impossible to obtain the m value directly. To find it the following procedure was used. The wave number of two Q lines which could be measured accurately was selected. One of the lines was as close to the null line as possible and the other as far from the null line as possible. Even though the absolute m number for either line was not known, the difference Δm was known by merely counting the intervening lines. Then with the measured value of ν_0 and an assumed value for the m of the first of these lines, the a and b values in the empirical equation were computed. Since Δm was known, the m value of the second line was determined by the assumed value plus Δm. Using this scheme, the assumed m for the first line was systematically varied, each time obtaining different values of the constants a and b. From the table of a and b values thus obtained, the pair was chosen which gave an equation which not only passed through ν_0 and the two lines chosen, but also represented the intervening lines the best. With this method it was possible to obtain the absolute numbering to within possible ± 2. By this method the molecular constants

$$B_0'=0.1037\ \text{cm}^{-1},\quad B_0''=0.1107\ \text{cm}^{-1},$$

$$B_2''=0.1093\ \text{cm}^{-1}$$

were determined.[7] The empirical formulas arrived at for the Q branches of these bands were

$$(0,0);\quad \nu=37410.60-0.00696m(m+1)-1.39\times10^{-7}m^2(m+1)^2$$

$$(0,2);\quad \nu=36781.84-0.00609m(m+1)-1.40\times10^{-7}m^2(m+1)^2.$$

Since the values of the molecular constants obtained by the above method are subject to the errors in determining the true numbering in the band and the exact position of the null line, some method of using the combination relations seemed desirable.

As is evident from Fig. 3, the P and Q branches intersect each other several times throughout a band. There are regions where both branches are completely resolved and regions where both branches coincide. Thus, in these regions the true position of the lines of both branches could be determined. The procedure was as follows. An empirical formula was used to compute the wave numbers in a Q branch. Then the difference between the observed wave numbers and the calculated wave numbers was formed for both the P and Q branches. When these differences are plotted against a running number, the re-

[7] J. G. Winans and H. M. Foslie, Phys. Rev. **71**, 137 (1947).

sulting curve should be a smooth one. If the empirical formula was the true one, for example, for the Q branch, these differences should average zero. If the empirical formula was off either in the m number or the value of ν_0, at least the trend should be a continuous one. The plot of the differences between the observed lines in the (0,0) band and values calculated from

$$\nu = 37410.6 - 0.007m(m+1) - 1.35\times10^{-7}m^2(m+1)^2$$

is shown in Fig. 6. The solid circles are the values of the differences in the regions where the branches were completely resolved or completely on top of each other, as indicated by sharp spectral lines. These points were used to determine the course of the smooth curve which was drawn. The distribution of the points shows very strikingly the measurement errors when the two branches are not resolved and yet not coincident. With the use of the curve the correct differences between wave numbers of an actual line and those calculated from the equation were obtained and combined with the calculated wave numbers to give the true line-wave number. This gives the wave number which would have been obtained if the P and Q lines could have been resolved. With these corrected wave numbers for lines in the P and Q branches, it was possible to apply the combination relations

$$Q(J+1) - P(J+1) = \Delta_1F'(J),$$

where $\Delta_1F'(J)$ is the separation of successive rotational levels in the upper electronic state, and J is the number of any particular line referred to the rotational quantum number of the lower electronic state. This method of correcting the measurements was carried out for the (0,0), (0,1), and (0,2) bands of the fundamental system. Since all of these bands have a common upper state, the $\Delta_1F'(J)$ should agree within the experimental error when the correct relative numbering of the P and Q branches has been found. The wave numbers of the bands, after correction by the above method, are listed in Table II as well as the $\Delta_1F'(J)$ and the $\Delta_1F''(J)$.

To obtain the molecular constants from the values of the combination relations, the following graphical method was used. According to the theory we have[6]

$$\Delta_1F(J)/(J+1) = 2B - 4D(J+1)^2,$$

so that $\Delta_1F(J)/(J+1)$ plotted against $(J+1)^2$ should give a straight line with an intercept of $2B$ and a slope of $-4D$. The plots of the $\Delta_1F(J)/(J+1)$ values given in Table II *versus* $(J+1)^2$ are shown in Fig. 7, and the values of the

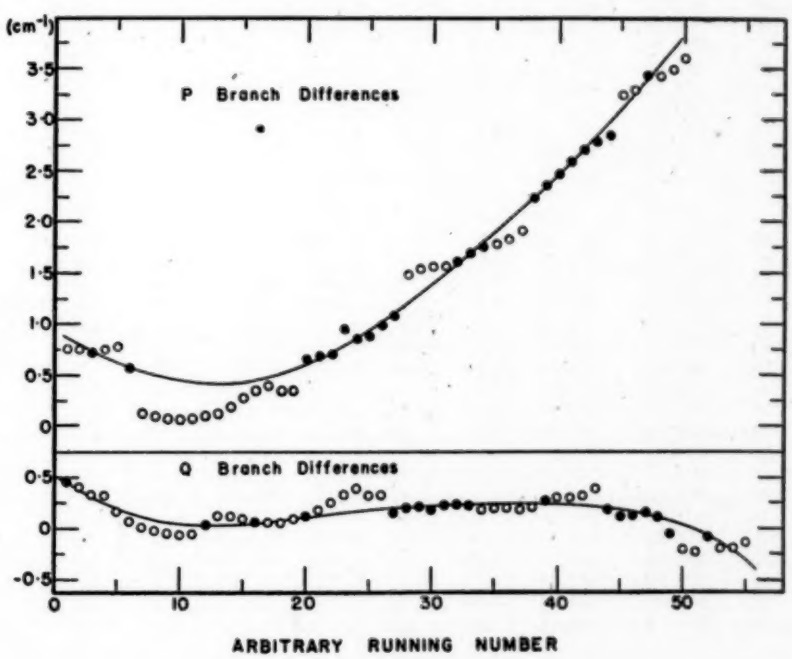

FIG. 6. Differences between wave numbers of an actual line in the P and Q branches of the (0,0) band and those calculated from an empirical equation.

TABLE II. Fine structure of the bands of the fundamental system of InCl.

Wave numbers of the lines of the (0,0), (0,1), and (0,2) bands and the combination differences for these bands.

J	$Q(J)$	$P(J)$	$\Delta_1F'(J)$	$\Delta_1F''(J)$	$\frac{\Delta_1F'(J)}{(J+1)}$	$\frac{\Delta_1F''(J)}{(J+1)}$
			(0,0) band			
43			9.69		0.2202	
44	37397.97	37388.28	9.89	10.61	0.2198	0.2358
45	397.25	387.36	10.06	10.81	0.2187	0.2350
46	396.50	386.44	10.25	10.99	0.2181	0.2338
47	395.76	385.51	10.46	11.20	0.2179	0.2333
48	395.02	384.56	10.67	11.43	0.2178	0.2333
49	394.26	383.59	10.87	11.64	0.2174	0.2328
50	393.49	382.62	11.09	11.87	0.2175	0.2327
51	392.71	381.62	11.31	12.10	0.2175	0.2327
52	391.92	380.61	11.55	12.34	0.2179	0.2328
53	391.13	379.58	11.75	12.56	0.2176	0.2325
54	390.32	378.57	11.97	12.79	0.2176	0.2325
55	389.50	377.53	12.18	13.03	0.2175	0.2327
56	388.65	376.47	12.40	13.25	0.2175	0.2325
57	387.80	375.40	12.62	13.48	0.2176	0.2324
58	386.92	374.32	12.86	13.72	0.2180	0.2325
59	386.03	373.20	13.05	13.96	0.2175	0.2327
60	385.12	372.07	13.25	14.18	0.2172	0.2325
61	384.19	370.94	13.46	14.40	0.2171	0.2323
62	383.25	369.79	13.70	14.65	0.2175	0.2325
63	382.30	368.60	13.90	14.88	0.2172	0.2325
64	381.32	367.42	14.12	15.11	0.2172	0.2325
65	380.33	366.21	14.33	15.36	0.2171	0.2327
66	379.30	364.97	14.55	15.58	0.2172	0.2325
67	378.27	363.72	14.74	15.82	0.2168	0.2326
68	377.19	362.45	14.95	16.04	0.2167	0.2325
69	376.10	361.15	15.16	16.27	0.2166	0.2324
70	374.99	359.83	15.35	16.49	0.2162	0.2323
71	373.85	358.50	15.56	16.71	0.2161	0.2321
72	372.70	357.14	15.77	16.96	0.2160	0.2323
73	371.51	355.74	15.97	17.17	0.2158	0.2320
74	370.31	354.34	16.18	17.41	0.2175	0.2321
75	369.08	352.90	16.37	17.63	0.2154	0.2320
76	367.82	351.45	16.59	17.86	0.2155	0.2319
77	366.55	349.96	16.80	18.09	0.2154	0.2319
78	365.26	348.46	17.00	18.33	0.2152	0.2320
79	363.93	346.93	17.20	18.55	0.2150	0.2319
80	362.58	345.38	17.40	18.77	0.2148	0.2317
81	361.21	343.81	17.60	19.00	0.2146	0.2317
82	359.81	342.21	17.79	19.23	0.2143	0.2317
83	358.37	340.58	17.99	19.43	0.2142	0.2313
84	356.93	338.94	18.19	19.67	0.2140	0.2314
85	355.45	337.26	18.37	19.89	0.2136	0.2313
86	353.93	335.56	18.58	20.11	0.2136	0.2311
87	352.40	333.82				
			(0,1) band			
40	...	...	8.97	...	0.2188	...
41	37084.78	37075.81	9.17	9.77	0.2183	0.2326
42	084.18	075.01	9.38	9.99	0.2181	0.2323
43	083.57	074.19	9.58	10.19	0.2177	0.2316
44	082.96	073.38	9.78	10.41	0.2173	0.2313
45	082.33	072.55	10.01	10.63	0.2176	0.2311
46	081.71	071.70	10.21	10.86	0.2172	0.2311
47	081.06	070.85	10.45	11.09	0.2177	0.2310
48	080.42	069.97	10.66	11.32	0.2175	0.2310
49	079.76	069.10	10.87	11.55	0.2174	0.2310
50	079.08	068.21	11.06	11.77	0.2169	0.2308
51	078.37	067.31	11.29	11.98	0.2171	0.2304
52	077.68	066.39	11.51	12.22	0.2172	0.2306
53	076.97	065.46	11.72	12.46	0.2170	0.2307
54	076.23	064.51	11.94	12.69	0.2171	0.2307
55	075.48	063.54	12.15	12.93	0.2170	0.2309
56	074.70	062.55	12.37	13.15	0.2170	0.2307
57	073.92	061.55	12.58	13.38	0.2169	0.2307
58	073.12	060.54	12.80	13.63	0.2169	0.2310
59	072.29	059.49	13.03	13.86	0.2172	0.2310
60	071.46	058.43	13.23	14.10	0.2169	0.2312
61	070.59	057.36	13.44	14.31	0.2168	0.2308
62	069.72	056.28	13.67	14.56	0.2170	0.2311
63	068.83	055.16	13.87	14.79	0.2167	0.2311
64	067.91	054.04	14.09	15.02	0.2168	0.2311
65	066.98	052.89	14.31	15.26	0.2168	0.2312
66	066.03	051.72	14.51	15.49	0.2165	0.2312
67	065.05	050.54	14.73	15.71	0.2166	0.2310
68	064.07	049.34	14.92	15.94	0.2162	0.2310
69	063.05	048.13	15.13	16.17	0.2161	0.2310
70	062.01	046.88	15.34	16.39	0.2160	0.2308
71	060.96	045.62	15.56	16.64	0.2161	0.2311
72	059.88	044.42	15.76	16.86	0.2159	0.2309
73	058.78	043.02	15.97	17.09	0.2158	0.2309
74	057.66	041.69	16.17	17.31	0.2156	0.2308
75	056.52	040.35	16.36	17.53	0.2152	0.2307
76	055.35	038.99	16.58	17.77	0.2153	0.2308
77	054.16	037.58	16.80	18.02	0.2153	0.2310
78	052.94	036.14	17.01	18.26	0.2153	0.2311
79	051.69	034.68	17.21	18.48	0.2151	0.2310
80	050.42	033.21	17.43	18.72	0.2152	0.2311
81	049.13	031.70	17.63	18.95	0.2150	0.2311
82	047.81	030.18				
			(0,2) band			
66	...	...	14.43	...	0.2154	...
67	36754.02	36739.59	14.67	15.60	0.2157	0.2294
68	753.09	738.42	14.89	15.84	0.2158	0.2296
69	752.14	737.25	15.10	16.08	0.2157	0.2297
70	751.16	736.06	15.32	16.31	0.2158	0.2297
71	750.17	734.85	15.53	16.55	0.2157	0.2299
72	749.15	733.62	15.74	16.77	0.2156	0.2297
73	748.12	732.38	15.94	16.99	0.2154	0.2296
74	747.07	731.13	16.13	17.21	0.2151	0.2295
75	745.99	729.86	16.34	17.44	0.2150	0.2295
76	744.89	728.55	16.54	17.66	0.2148	0.2294
77	743.77	727.23	16.73	17.88	0.2145	0.2292
78	742.62	725.89	16.95	18.11	0.2146	0.2292
79	741.46	724.51	17.12	18.32	0.2140	0.2290
80	740.26	723.14	17.34	18.55	0.2141	0.2290
81	739.05	721.71	17.62	18.75	0.2148	0.2287
82	737.92	720.30	17.76	19.13	0.2140	0.2305
83	736.55	718.79	17.97	19.26	0.2139	0.2292
84	735.26	717.29	18.16	19.48	0.2136	0.2292
85	733.94	715.78	18.37	19.71	0.2136	0.2292
86	732.60	714.23	18.60	19.95	0.2138	0.2293
87	731.25	712.65	18.82	20.21	0.2139	0.2297
88	729.86	711.04	19.03	20.46	0.2138	0.2299
89	728.43	709.40	19.25	20.69	0.2139	0.2299
90	726.99	707.74	19.45	20.94	0.2137	0.2301
91	725.50	706.05	19.69	21.18	0.2140	0.2302
92	724.01	704.32	19.90	21.44	0.2139	0.2305
93	722.47	702.57	20.11	21.68	0.2139	0.2306
94	720.90	700.79	20.32	21.92	0.2139	0.2307
95	719.30	698.98	20.50	22.15	0.2135	0.2307
96	717.65	697.15	20.71	22.39	0.2135	0.2308
97	715.97	695.26	20.88	22.61	0.2131	0.2307
98	714.24	693.36	21.05	22.81	0.2126	0.2304
99	712.48	691.43	21.22	23.03	0.2122	0.2303
100	710.67	689.45	21.37	23.21	0.2116	0.2298
101	708.83	687.46	21.53	23.41	0.2111	0.2295
102	706.95	685.42	21.65	23.58	0.2102	0.2289
103	705.02	683.37	21.77	23.75	0.2093	0.2284
104	703.04	681.27	22.21	23.91	0.2115	0.2277
105	701.34	679.13				

molecular constants obtained by this method are listed in Table III.

The accuracy obtained in the present experiment is not sufficient to detect a definite trend in the D_v'' values. Actually the D_1'' and D_2'' are less than the D_0''. It is not believed that this is significant, so that the D' and D'' values listed in Table III are the average values obtained from the three bands analyzed.

The above rotational analysis appears completely satisfactory with possibly one exception. In the bands observed, the R branch was not resolved and measurable, and hence the $P-R$ combination relations could not be used. Using only the $Q-P$ combination relations does not give an opportunity to ascertain whether "Λ doubling" in the $^1\Pi_1$ state is appreciable. Should it be significant, the rotational constants obtained would not be the true rotational constants for the states. However, the AlCl molecule does not appear to show an appreciable "Λ doubling."[8] Since InCl is even heavier, one would expect the doubling to be even less for InCl than for the AlCl molecule.

The values of the molecular constants, as obtained by the two essentially independent methods, differ by as much as six percent. Although it is difficult to estimate the percentage error for the two methods, one would expect the values obtained from the combination relations to be more reliable.

TABLE III. Molecular constants for the fundamental system of InCl.

$B_0'(cm^{-1})$	$B_0''(cm^{-1})$	$B_1''(cm^{-1})$	$B_2''(cm^{-1})$	$D'(cm^{-1})$	$D''(cm^{-1})$
0.1091	0.1166	0.1155	0.1149	1.2×10^{-7}	2×10^{-8}

$r_0'(cm)$	$r_0''(cm)$	ω_e''
2.39×10^{-8}	2.32×10^{-8}	0.0009

ELECTRONIC CONFIGURATION FOR InCl AND DISSOCIATION ENERGY

The Cl atom has 5 p-electrons and the In atom has $1p$-electron in their outer electron shells. Hence in the ground state of the molecule there is formed a closed shell of the type $\sigma^2\pi^4$. Thus the ground state is probably a $^1\Sigma_0^+$ state similar to the situation for atoms where a closed shell gives a ^1S state. According to the theory $In(^2P_{\frac{1}{2}})Cl(^2P_{\frac{1}{2}})$ should result in the following electronic states: $^3\Pi_{2,1,0}$; $^1\Pi_1$; $^1\Sigma_0^+$; $^1\Sigma_0^-$. Since the fundamental system is much more intense in absorption, it is reasonable to suppose that it is due to $^1\Pi_1 \leftrightarrow {}^1\Sigma_0^+$ transition. The intercombination system then must result from a transition from the $^1\Sigma_0^+$ ground state to the $^3\Pi$ terms and is thus less intense, because the transition probability between single and triplet terms is much less than the transition probability between two singlet terms. The fact that the intercombination system consists of two band systems further supports this. The selection rules forbid a transition from $^3\Pi_2$ to $^1\Sigma_0^+$. Also because of "Λ-type doubling," the $^3\Pi_0$ term splits into two

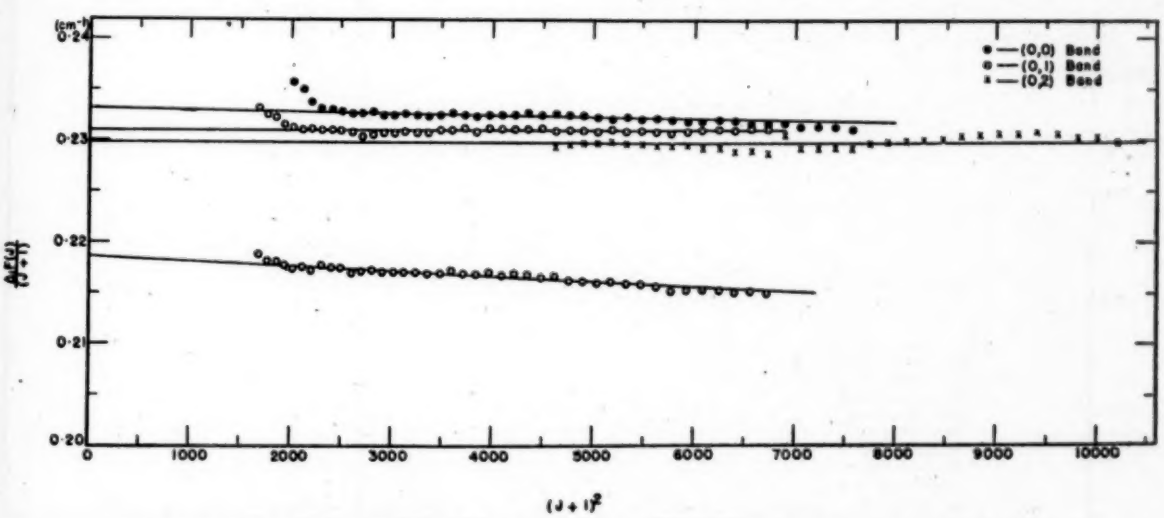

FIG. 7. Graphical determination of the molecular constants from the data given in Table II.

[8] W. Holst, Zeits. f. Physik **93**, 55 (1935).

components, namely, $^3\Pi_0^-$ and $^3\Pi_0^+$. Of these two only the transition $^3\Pi_0^+ \leftrightarrow {}^1\Sigma_0^+$ is permitted because of the selection rule that $+$ combines only with $+$. There remain only the two possible transitions, $^3\Pi_1 \leftrightarrow {}^1\Sigma_0^+$ and $^3\Pi_0^+ \leftrightarrow {}^1\Sigma_0^+$. Further considerations show that one of these systems should contain a P, Q, and R branch, and the other system only a P and R branch.[5] Close examination of the bands bears this out.

The predissociation that takes place in the fundamental system makes it possible to determine the dissociation energy of the ground state within rather small limits. The upper state is a $^1\Pi$ state and, according to Kronig's selection rules for predissociation ($\Delta J=0$, $\Delta S=0$, $\Delta\Omega=0$, ± 1, $+\leftrightarrow-$), the perturbing state must be a $^1\Pi$ or a $^1\Delta$ state. A $^1\Sigma$ state is ruled out, since if it were the perturbing state only one Λ component of the $^1\Pi$ state would be predissociated, because the selection rules

$$\Delta J=0 \quad \text{and} \quad +\leftrightarrow-$$

cannot be satisfied simultaneously for both Λ components. This type of predissociation would result in only the P and R branch or the Q

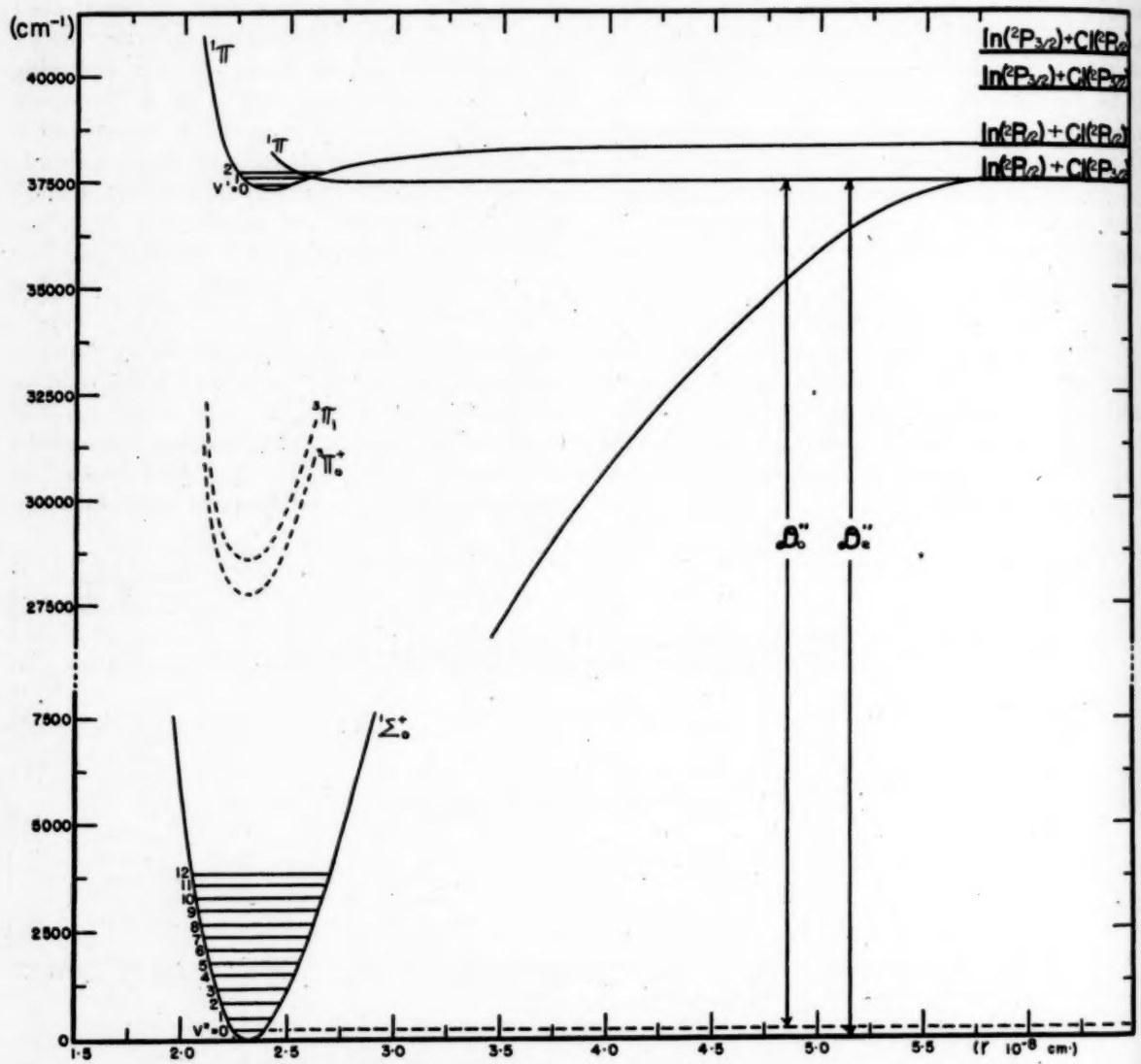

FIG. 8. Possible arrangement of the electronic states from which the fundamental and intercombination band systems of InCl arise. The perturbing state which causes predissociation in the fundamental system is also shown.

branch being predissociated. The observed bands show all branches predissociated.

Since the upper state potential curve and the perturbing potential curve intersect very close to the minimum of the upper state potential curve, it is reasonable that the upper state cannot have the same dissociation products as the perturbing state or the ground state. The next higher energy possibility for the dissociation products of the upper state is normal $\mathrm{In}(^2P_{\frac{1}{2}})$ plus excited $\mathrm{Cl}(^2P_{\frac{1}{2}})$. Now the dissociation energy of the upper state for the fundamental system must be small, as shown by the large $\omega_e'x_e'$ in the formula for the vibrational states. Calculating the dissociation energy D_e' from the formula

$$D_e' = \omega_e'^2/4\omega_e'x_e'$$

given by the theory, one obtains $D_e' = 600\ \mathrm{cm}^{-1}$. If the dissociation products for the upper electronic state for the fundamental system are as suggested above, then the potential curves must be of the type shown in Fig. 8. The perturbing state and the ground state for the fundamental system have the same dissociation products as indicated. That the $v'=0$ state lies below the asymptote for the perturbing state is indicated by the fact that the rotational lines in the $(0,v'')$ progression are sharp. If it actually was above the asymptote, one would expect the "barrier penetration" to make the lines in this progression somewhat diffuse. That the upper electronic state and the perturbing state intersect just above $v'=1$ is indicated by the fact that, even though the bands in the $(1,v'')$ progression show no rotational structure in the region where one would expect it to be resolved, the band heads are still sharp. Since both the Q and R heads in this progression appear as sharp as in the $(0,v'')$ progression, it seems that, for small values of the rotational quantum number, J, in the $v'=1$ state, there exists rotational quantitization, but for higher J values predissociation sets in, causing the lines to be diffuse in the region where they could be resolved. Therefore, for $J \cong 0$, the potential curves intersect just above $v'=1$. For higher J values the change in the potential curves are due to rotation, which causes them to intersect just below $v'=1$. The result is that any band in the $(1,v'')$ progression appears completely diffuse although actually, in the region of the null line, the lines must be sharp in order to produce the sharp band heads.

With the above observations, the electronic states for the fundamental system would appear to be determined to within the limits of one vibrational quantum of the upper state. It cannot be determined just where the asymptote for the perturbing state intersects between $v'=0$ and $v'=1$. The dissociation energy of the lower state must lie between

$$D_e'' = 37568\ \mathrm{cm}^{-1} = 4.66\ \mathrm{volts}$$

and

$$D_e'' = 37720\ \mathrm{cm}^{-1} = 4.68\ \mathrm{volts}.$$

Although this appears to be the most reasonable arrangement of the electronic states, the possibility of the upper state having $\mathrm{In}(^2P_{\frac{1}{2}})\mathrm{Cl}(^2P_{\frac{1}{2}})$ as its dissociation products cannot be completely ruled out. However, this possibility would seem to be unlikely because any electronic state resulting from this combination would almost certainly be completely predissociated by the large number of electronic states arising from the less energetic combinations. Nevertheless, admitting this possibility places the dissociation energy between

$$D_e'' = 37720\ \mathrm{cm}^{-1} = 4.68\ \mathrm{volts}$$

and

$$D_e'' = 35520\ \mathrm{cm}^{-1} = 4.40\ \mathrm{volts}.$$

Electromechanical Properties of Rochelle Salt at the Lower Curie Point*

ROLAND M. LICHTENSTEIN
*Physics Department, Massachusetts Institute of Technology, Cambridge, Massachusetts***

(Received May 23, 1947)

The electrical characteristics of a.c. excited rochelle salt crystals were measured at temperatures in the neighborhood of the lower Curie point. From the experimental data the coefficients describing the electromechanical (i.e., dielectric, elastic, piezoelectric) properties were calculated. The results can be coordinated by an empirical formula for the thermodynamic potential. The values of the numerical coefficients in this formula as determined from the measurements near the lower Curie point agree with those found from previous studies of the upper Curie point. The numerical agreement indicates that the two Curie points are an outcome of a single physical phenomenon: the reciprocal of the susceptibility is given by the difference of two terms. The first is an expression of the interatomic restoring forces; it is a slowly varying function of the temperature. The second term accounts for the electrostatic interaction between distant parts of the crystal; its numerical value is $4\pi/3$. In rochelle salt the first term happens to be approximately equal to $4\pi/3$, so that (small differences of large numbers!) the susceptibility is a rapidly varying function of the temperature. In this way a change of no more than 5 percent in the magnitude of the intrinsic physical properties of the crystal lattice over a temperature range of 80 degrees can produce all the remarkable electromechanical effects in rochelle salt.

INTRODUCTION

IN most ferroelectric crystals the dielectric constant in a certain crystallographic direction becomes abnormally large in the neighborhood of one single temperature, known as the Curie point. Rochelle salt, on the other hand, is distinguished by the fact that there are two such critical temperatures. At the higher of these temperatures, the so-called upper Curie point, the dielectric behavior of rochelle salt is similar to that of other ferroelectric substances in that the crystal becomes permanently polarized when it is cooled below this critical temperature. At the lower of the two critical temperatures, the so-called lower Curie point, the behavior is reversed in that the crystal is permanently polarized only above this temperature and neutral below it.

The phenomenon of the upper Curie point can be explained in terms of the Langevin-Debye theory, which applies to freely rotating dipoles in electrostatic interaction with each other. In order to explain the existence of the lower Curie point, more complicated mechanisms have been postulated, but nothing definite about the nature of a lower Curie point is known as yet.

In order to shed some light on the problem of the lower Curie point we felt it necessary first to collect a sufficient amount of experimental data. The first part of this paper deals with the theory and the experimental results of this investigation. In the remaining portion these results are coordinated into a theory. The numerical results of the experimental investigation cause us to advance the opinion that both the upper and the lower Curie point are the outcome of one and the same phenomenon, namely, the accidental fact that the interatomic "spring" forces are of such a strength that the susceptibility of a spherical sample, in which for geometrical reasons there is no electrostatic interaction between distant parts, happens to be in the neighborhood of $3/4\pi$.

THEORY

Rochelle salt is noted for its extraordinary electromechanical (i.e., elastic, dielectric, and piezoelectric) properties (cf. Mueller[1-6], and

* This communication is an abstract of a thesis submitted in 1947 to the Physics Department of Massachusetts Institute of Technology in partial fulfillment of the requirements for the degree of Doctor of Philosophy.

** Present address: Physics Department, University of Pennsylvania, Philadelphia, Pennsylvania.

[1] H. Mueller, Phys. Rev. **47**, 175 (1935).
[2] H. Mueller, Phys. Rev. **57**, 829 (1940).
[3] H. Mueller, Phys. Rev. **58**, 565 (1940).
[4] H. Mueller, Phys. Rev. **58**, 805 (1940).
[5] H. Mueller, Ann. N. Y. Acad. Sci. **40**, 321 (1940).
[6] H. Mueller, Phys. Rev. **57**, 842 (1940).

Cady[7]), which we shall summarize by means of a single thermodynamic formula as first suggested by Mueller.[2,3] The symmetry elements of rochelle salt crystals are three twofold rotation axes at right angles to each other. These axes are commonly referred to as the x, y, and z axes.

The electromechanical state of a rochelle salt crystal is uniquely determined by assigning definite values to the temperature T, the six stress components X_x, Y_y, Z_z, Y_z, Z_x, X_y, and the three components E_x, E_y, E_z of the electric field strength. Then also the six strain components x_x, y_y, z_z, y_z, z_x, x_y, and the three components P_x, P_y, P_z of the electric polarization will have definite values.

The electromechanical behavior of rochelle salt can be most concisely described by giving an expression for that thermodynamic potential A which has T, X_x, Y_y, Z_z, Z_x, X_y, E_y, E_z, y_z, and P_z as independent variables. A sufficiently accurate empirical expression, which takes the symmetry properties of rochelle salt into account, is

$$A=-\tfrac{1}{2}\{s_{11}X_x^2+s_{22}Y_y^2+s_{33}Z_z^2+2s_{23}Y_yZ_z+2s_{31}Z_zX_x+2s_{12}X_xY_y+s_{55}Z_x^2+2d_{25}Z_xE_y+\kappa_{22}E_y^2$$
$$+s_{66}X_y^2+2d_{36}X_yE_z+\kappa_{33}E_z^2\}+(B/4)P_x^4+\tfrac{1}{2}\cdot[(T-T_L)(T-T_U)/C(T_U-T_L)]P_x^2$$
$$+\tfrac{1}{2}\cdot(f_{14}^2/c_{44})(P_x+(c_{44}/f_{14})y_z)^2+f(T),$$

where s_{11}, s_{22}, s_{33}, s_{23}, s_{31}, s_{12}, s_{55}, s_{66}, d_{25}, d_{36}, κ_{22}, κ_{33}, B, C, T_L, T_U, f_{14}, c_{44} are constants, and $f(T)$ is a function of the temperature T alone. Our notation is the same as Mueller's. The quantities x_x, y_y, z_z, z_x, x_y, P_y, P_z, Y_z, E_x can then be determined by differentiation:

$$x_x=+\partial A/\partial X_x;\quad y_y=+\partial A/\partial Y_y;\quad z_z=+\partial A/\partial Z_z;\quad z_x=+\partial A/\partial Z_x;\quad x_y=+\partial A/\partial X_y;$$
$$P_y=-\partial A/\partial E_y;\quad P_z=-\partial A/\partial E_z;\quad Y_z=-\partial A/\partial y_z;\quad E_x=+\partial A/\partial P_x.$$

The range of our experiments extended to conditions for which the stress components X_x, Y_y, Z_z, Z_x, X_y, and the field components E_y, E_z vanish. Furthermore we were not interested in the values of the strain components x_x, y_y, z_z, z_x, x_y, and the polarization components P_y, P_z. We, therefore, need not make further use of the curled bracket in the expression for A; we write A simply as a function of the temperature T, the shearing strain y_z, and the polarization P_z.

$$A=(B/4)P_z^4+\tfrac{1}{2}[(T-T_L)(T-T_U)/C(T_U-T_L)]P_z^2+\tfrac{1}{2}(f_{14}^2/c_{44})(P_z+(c_{44}/f_{14})y_z)^2+f(T);\quad (1)$$
$$Y_z=-\partial A/\partial y_z;\quad E_z=+\partial A/\partial P_z.\quad (2)$$

An expression of this kind was first given by Mueller. Equation (1) is an obvious extension of Mueller's expression to a larger temperature range. It was the purpose of our experimental investigation to examine how well the expression (1) for A can describe the electromechanical properties of rochelle salt. The answer to this question will have much significance as to the molecular mechanism which is responsible for the strange electromechanical properties of rochelle salt.

Most of these properties can be deduced from Eqs. (1) and (2). For the stress component Y_z and the field component E_z we find

$$-Y_z\equiv+\partial A/\partial y_z=c_{44}y_z+f_{14}P_z;$$
$$E_z\equiv+\partial A/\partial P_z=f_{14}y_z+\{[(T-T_L)(T-T_U)/C(T_U-T_L)]+(f_{14}^2/c_{44})\}P_z+BP_z^3.\quad (3)$$

These equations show that for a stress-free and field-free crystal the strain y_z and the polarization P_z are zero, as long as $T\leq T_L$ or $T\geq T_U$. On the other hand, if the temperature lies between T_L and T_U, the crystal, even in a stress-free and field-free state, acquires a strain y_{z0} and a polarization P_{z0}

[7] W. G. Cady, *Piezoelectricity* (McGraw-Hill Book Company, Inc., New York, 1946).

given by

$$y_{x0}=\mp(f_{14}/c_{44})\{-[(T-T_L)(T-T_U)/B\cdot C\cdot(T_U-T_L)]\}^{\frac{1}{2}},$$
$$P_{x0}=\pm\{-[(T-T_L)(T-T_U)/B\cdot C\cdot(T_U-T_L)]\}^{\frac{1}{2}}. \tag{4}$$

The subscript 0 refers to the absence of stress and field. The two temperatures T_L and T_U have the values: lower Curie point $T_L=254.7°K$; upper Curie point $T_U=296.9°K$. We see that between the two Curie points rochelle salt crystals exhibit a permanent strain and a permanent polarization.

By differentiating Eqs. (3) we find the change of stress ΔY_x and the change of field ΔE_x which are required to change the strain by Δy_x and the polarization by ΔP_x. We have

$$\Delta(-Y_x)=c_{44}\Delta y_x+f_{14}\Delta P_x;$$
$$\Delta(E_x)=f_{14}\Delta y_x+\{[(T-T_L)(T-T_U)/C(T_U-T_L)]+(f_{14}^2/c_{44})+3BP_x^2\}\Delta P_x. \tag{5}$$

Solving these equations for Δy_x and ΔP_x we obtain

$$-\Delta y_x=s_{44}\Delta Y_x+d_{14}\Delta E_x;\quad \Delta P_x=d_{14}\Delta Y_x+\kappa_{11}\Delta E_x, \tag{6}$$

where the "electromechanical response coefficients" s_{44}, d_{14}, κ_{11} are given by:

$$\begin{aligned}&\text{elastic compliance} && s_{44}=1/c_{44}+(f_{14}/c_{44})^2\kappa_{11};\\ &\text{piezoelectric modulus} && d_{14}=(f_{14}/c_{44})\cdot\kappa_{11};\\ &\text{susceptibility} && \kappa_{11}=\{[(T-T_L)(T-T_U)/C(T_U-T_L)]+3BP_x^2\}^{-1}.\end{aligned} \tag{7}$$

In the stress-free and field-free state these coefficients have the values

$$s_{44_0}=1/c_{44}+(f_{14}/c_{44})^2[C(T_U-T_L)/(T-T_L)(T-T_U)],$$
$$d_{14_0}=(f_{14}/c_{44})\cdot[C(T_U-T_L)/(T-T_L)(T-T_U)], \tag{8}$$
$$\kappa_{11_0}=[C(T_U-T_L)/(T-T_L)(T-T_U)],$$

for $T\leq T_L$ and $T\geq T_U$. Furthermore,

$$s_{44_0}=1/c_{44}-(f_{14}/c_{44})^2\cdot\tfrac{1}{2}\cdot[C(T_U-T_L)/(T-T_L)(T-T_U)],$$
$$d_{14_0}=-(f_{14}/c_{44})\cdot\tfrac{1}{2}\cdot[C(T_U-T_L)/(T-T_L)(T-T_U)], \tag{9}$$
$$\kappa_{11_0}=-\tfrac{1}{2}\cdot[C(T_U-T_L)/(T-T_L)(T-T_U)],$$

for $T_L\leq T\leq T_U$. A plot of P_{x0} and κ_{11_0} *vs.* the temperature T is given in Fig. 1, which has been taken from Mueller.[5] With κ_{11} also the two other response coefficients become abnormally large at the two Curie points.

Equations (7) show that the response coefficients depend not only on the temperature T but also on the polarization P_x, which in its turn depends on the stress Y_x and the field E_x. Elimination of the strain y_x from Eqs. (3) gives us

$$[(T-T_L)(T-T_U)/C(T_U-T_L)]P_x+BP_x^3=E_x+(f_{14}/c_{44})Y_x. \tag{10}$$

Thus an electric field E_x or a stress Y_x changes P_x and, therefore, also the response coefficients. This saturation effect is of a rather complicated character when the temperature lies between the two Curie points. However, when $T\leq T_L$ or $T\geq T_U$, a stress Y_x, or a field E_x, increases P_x^2 from zero to a positive value according to (10). Then, according to (7), the values of the three response coefficients are reduced; i.e., we have

$$s_{44}<s_{44_0},\quad d_{14}<d_{14_0},\quad \kappa_{11}<\kappa_{11_0},\quad \text{for } T\leq T_L,\quad T\geq T_U. \tag{11}$$

The quantitative treatment of the saturation effect is particularly simple when the temperature coincides with either of the Curie points. Then from (10)

$$P_x^2=[(1/B)(E_x+(f_{14}/c_{44})Y_x)]^{\frac{1}{2}} \text{ for } T=T_L \text{ or } T=T_U; \tag{12}$$

and from (7)

$$s_{44}=1/c_{44}+(f_{14}/c_{44})^2\cdot\frac{1}{3B^{\frac{1}{2}}}\cdot\frac{1}{[E_x+(f_{14}/c_{44})Y_x]^{\frac{1}{2}}},$$

$$d_{14}=(f_{14}/c_{44})\frac{1}{3B^{\frac{1}{2}}}\cdot\frac{1}{[E_x+(f_{14}/c_{44})Y_x]^{\frac{1}{2}}}, \tag{13}$$

$$\kappa_{11}=\frac{1}{3B^{\frac{1}{2}}}\frac{1}{[E_x+(f_{14}/c_{44})Y_x]^{\frac{1}{2}}}, \quad \text{for } T=T_L, \text{ or } T=T_U.$$

These equations describe the following saturation effects:

1. Elastic saturation: A stress Y_x lowers the elastic compliance s_{44}.
2. Dielectric saturation: An electric field E_x lowers the susceptibility κ_{11}.
3. Crosswise dielectric saturation: A stress Y_x lowers the susceptibility κ_{11}.
4. Crosswise elastic saturation: An electric field E_x lowers the elastic compliance s_{44}.

The first two types of saturation have been known for many years. Mueller[3,6] was the first to predict the other types and to show that they existed. Crosswise elastic saturation is shown most conspicuously by the fact that the resonance frequency of a vibrating rochelle salt crystal, which is excited piezoelectrically, is increased by a biasing d.c. electric field. A field of 300 volts/cm was found to change the resonance frequency by as much as 75 percent. This indeed is a rather unusual effect.

Finally also the phenomenon of hysteresis is contained by the expression (1) for the thermodynamic potential A. Suppose the temperature T lies between the two Curie points and the stress Y_x is zero. Then suppose we vary the field E_x from a large negative value to a large positive value and back again. From (10) we can calculate the polarization P_x, and from the first Eq. (3) we can then find the strain y_x, so that the electromechanical state is completely known. Of the several roots of the cubic Eq. (10) stability considerations force us to select that for which $dE_x/dP_x>0$. Thus P_x changes with E_x according to the graph shown in Fig. 2. The numbers and the arrows indicate how the hysteresis loop is traversed.

EXPERIMENTAL RESULTS

In the experimental investigation the impedance of X cut 45° bars was measured with a Wien bridge. An X cut 45° bar is obtained in the following fashion: Out of a rochelle salt crystal a plate is cut whose plane is perpendicular to the x axis. Metallic foils, which will serve as electrodes, are attached to the two major surfaces. Out of this foiled plate a thin bar is cut whose longitudinal axis forms an angle of 45° with the positive portions of both the y and z axes. The result is an X cut 45° bar.

The capacity of these bars changes with the frequency of the applied voltage. The reason is that, because of the converse piezoelectric effect, an applied a.c. voltage excites vibrations, which in their turn influence the electrical characteristics because of the direct piezoelectric effect. The capacity C of a slender foiled X cut 45° bar

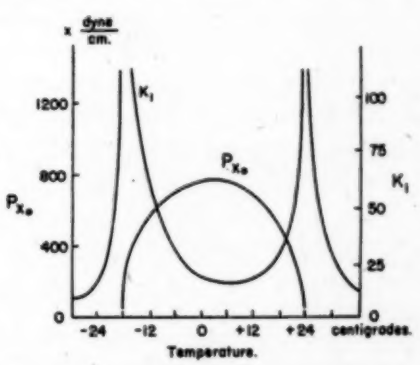

FIG. 1. Permanent polarization P_{x_0} and free susceptibility K_1 vs. temperature (From Mueller[5]).

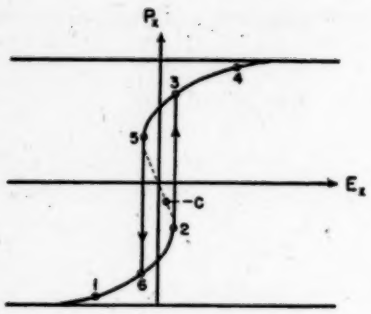

FIG. 2. Hysteresis loop.

of length l, width w, and thickness t (as measured from foil to foil) is given by (for a derivation see Mueller[2])

$$C=(w\cdot l/t)(1/4\pi+\kappa_{11_{eff}}), \tag{14}$$

where

$$\kappa_{11_{eff}}=\kappa_{11}-\frac{d_{14}^2}{s_{44}+s_{22}+2s_{23}+s_{33}}$$

$$\times\left[1-\frac{\tan\omega[\rho(s_{44}+s_{22}+2s_{23}+s_{33})]^{\frac{1}{2}}\cdot l/4}{\omega[\rho(s_{44}+s_{22}+2s_{23}+s_{33})]^{\frac{1}{2}}l/4}\right]. \tag{15}$$

Here ρ is the density, and ω is the circular frequency. The "effective susceptibility" $\kappa_{11_{eff}}$ is the susceptibility a rigid bar would need to have in order to present the same capacity as the vibrating bar.

From a curve of $\kappa_{11_{eff}}$ *vs.* the frequency we can determine the following three values: $s_{44}+s_{22}+2s_{23}+s_{33}$, κ_{11}, d_{14}. An example is given in Fig. 3. The circles are measured points. The curve has been computed from Eq. (15) with that combination of constants which would give the best fit.

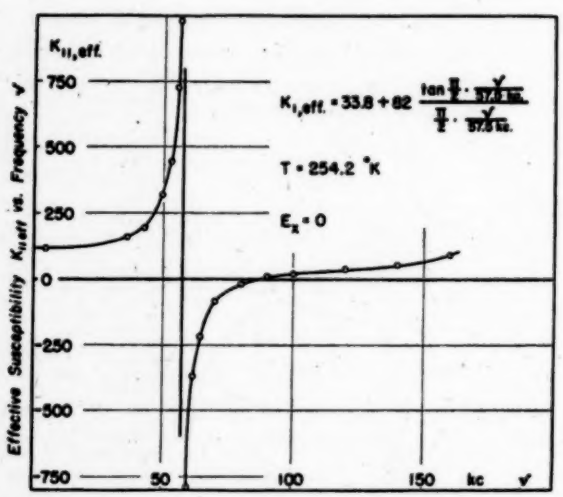

FIG. 3. Variation of $\kappa_{11_{eff}}$ as a function of frequency computed from Eq. (15).

The experimental results can tell us whether we were justified in using (1) as the thermodynamic potential. In particular we should find out whether c_{44} and f_{14} are constants. The following two curves furnish that test. (1) We plot

$$s_{44_0}+(s_{22}+2s_{23}+s_{33})-d_{14_0}^2/\kappa_{11_0}$$
$$=1/c_{44}+(s_{22}+2s_{23}+s_{33})$$

vs. the temperature T (Fig. 4). (2) We plot $d_{14_0}/\kappa_{11_0}=f_{14}/c_{44}$ *vs.* the temperature T (Fig. 5).

Both graphs show horizontal lines, if one disregards the scatter of the points. This scatter is not significant for the following two reasons: 1. The points were obtained by measuring the characteristics of several samples. 2. The points were calculated from quantities which vary by a factor of 20 over the investigated temperature range, as shown by Figs. 6 and 7, where $1/\kappa_{11_0}$ and $1/d_{14_0}$ are plotted as functions of the temperature. (Points below the T axis still represent positive values. Note that the scales above and below the T axis differ. The change of scale has been made to eliminate the kink, predicted by the factor $\frac{1}{2}$ which occurs in Eqs. (9), but is absent in Eq. (8).)

For the sake of completeness $(s_{44}-1/c_{44})^{-1}$ has also been plotted as a function of the temperature in Fig. 8. Figures 6, 7, and 8 differ only in the scale as predicted by Eqs. (8) and (9). From the slope of the curve of Fig. 6 the constant C of Eq. (1) can be determined.

Thus we have shown that

$$1/c_{44}+(s_{22}+2s_{23}+s_{33})$$

and f_{14}/c_{44} are constants. Since it is generally assumed that s_{22}, s_{23}, and s_{33} are constants, we may state that both c_{44} and f_{14} are constants.

The constant B which occurs in the expression (1) for the thermodynamic potential can be determined from the last of Eqs. (13). To this end we apply a d.c. field E_x to the crystal, upon which the a.c. used to energize the Wien bridge is superimposed. We leave the crystal stress-free. Then a plot of $(1/\kappa_{11})^{\frac{1}{2}}$ *vs.* E_x should give a straight line from whose slope we can determine B. The diagram is drawn (Fig. 9) so that for

positive values of E_x the points $(1/\kappa_{11})^{\frac{1}{2}}$ themselves were plotted, whereas for negative values of E_x the values $-(1/\kappa_{11})^{\frac{1}{2}}$ were plotted. In this way we should get an uninterrupted straight line through the origin of the coordinate system. The experiment fulfills the predictions except for two defects. The first is that for small values of $(1/\kappa_{11})^{\frac{1}{2}}$, that is, for large values of κ_{11}, the experimental points no longer lie on the straight line. But this we must expect, since specimens never will exhibit infinitely large susceptibilities. The largest susceptibility recorded was 247, which corresponds to a dielectric constant of 3100. The other defect is that the straight line misses the origin. This is probably caused by some residual stresses in the crystal.

The interesting effect of cross-wise elastic saturation predicted by Mueller may be illustrated in the following way: The first resonance frequency of an X cut 45° bar, i.e., the lowest frequency for which the effective susceptibility $\kappa_{11_{eff}}$ becomes infinite, is given by (see Eq. (15))

$$\nu_1 = 1/l[\rho(s_{44}+s_{22}+2s_{23}+s_{33})]^{\frac{1}{2}}. \qquad (16)$$

This may be rewritten in the following form

$$\nu_1 = 1/l[\rho\{(s_{44}-1/c_{44})+(1/c_{44}+s_{22}+2s_{23}+s_{33})\}]^{\frac{1}{2}}.$$

Thus (see Eqs. (7))

$$\nu_1 = 1/l[\rho\{(f_{14}/c_{44})^2\kappa_{11} + (1/c_{44}+s_{22}+2s_{23}+s_{33})\}]^{\frac{1}{2}}. \qquad (16a)$$

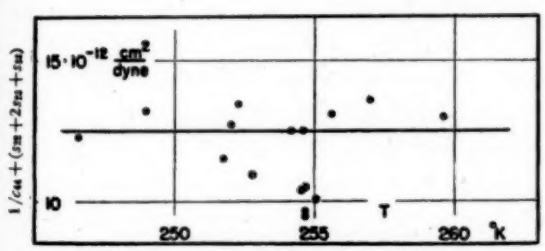

FIG. 4.

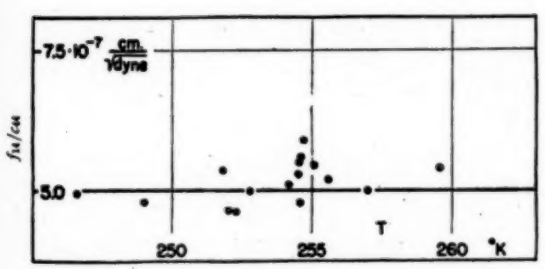

FIG. 5.

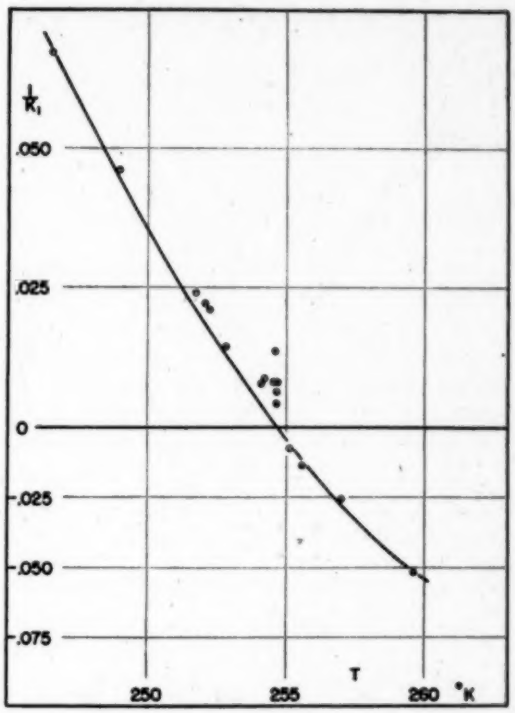

FIG. 6.

Since we have already determined the constants f_{14}/c_{44} and $1/c_{44}+(s_{22}+2s_{23}+s_{33})$, we can compute the resonance frequency ν_1 as soon as we know the susceptibility κ_{11}. As an example, the resonance frequencies were computed for those values of the susceptibility which were plotted in Fig. 9. In Fig. 10 these computed values are compared with the measured values. The agreement is good.

Table I shows the constants determined from our experiments at the lower Curie point compared with Mueller's values, which were obtained from measurements near the upper Curie point. The agreement is remarkable. The significance of this agreement will be discussed below.

At any Curie point a plot of the specific heat *vs.* temperature should show a discontinuity. Thermodynamic arguments show that this discontinuity is given by

$$\begin{aligned} \Delta c &= T_L/2BC^2 \text{ for } T=T_L; \\ \Delta c &= T_U/2BC^2 \text{ for } T=T_U. \end{aligned} \qquad (17)$$

The numerical values are

$$\begin{aligned} \Delta c &= 0.0077 \text{ joule}\cdot\text{cm}^{-3}\cdot{}^\circ\text{K}^{-1} \text{ for } T=T_L; \\ \Delta c &= 0.0090 \text{ joule}\cdot\text{cm}^{-3}\cdot{}^\circ\text{K}^{-1} \text{ for } T=T_U, \end{aligned}$$

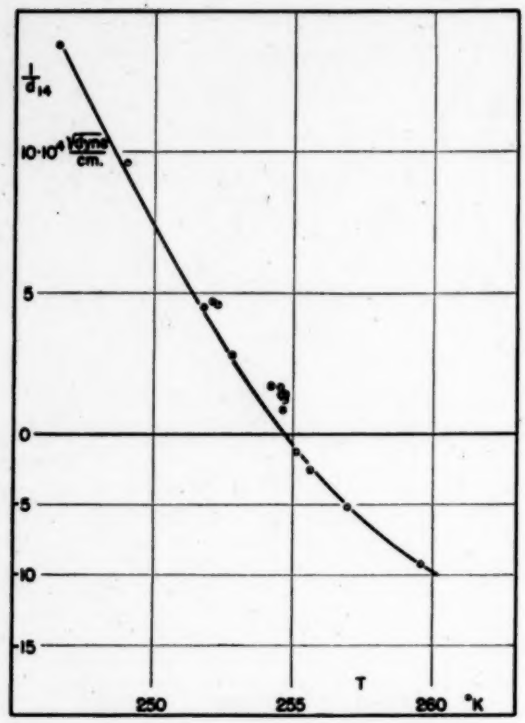

FIG. 7.

for 1 cubic centimeter of rochelle salt. These discontinuities are so small that they were completely masked by the experimental errors of specific heat measurements (cf. Mueller[5]). Thermodynamic considerations also show that due to the smallness of Δc (as compared to the specific heat itself) one can neglect the difference between the isothermal and adiabatic values of the electromechanical response coefficients.

EXPERIMENTAL DETAILS

The crystal samples were X cut 45° bars 2 cm long, 0.2 cm wide, 0.1 cm thick (from foil to foil). The electrodes consisted of gold foils. The crystal samples were thermostated at any desired temperature within 0.1°K (or within 0.01°K for careful measurements) by means of a dry ice-alcohol thermostat. The Wien bridge was energized with only 1 millivolt. If the voltage had been higher, the crystals would no longer have behaved as linear circuit elements. The bridge detector responded to a threshold voltage of 1 microvolt.

The mounting of the crystals deserves some discussion. The expressions (14) and (15) for the

TABLE I. Constants determined at lower Curie point compared with Mueller's values near upper Curie point.

	Values* determined at lower Curie point	Values determined at upper Curie point
$1/c_{44}+(s_{22}+2s_{23}+s_{33})$	$(12.5\pm1.0)\cdot10^{-12}$ cm² dyne⁻¹	$12.6\cdot10^{-12}$ cm² dyne⁻¹
f_{14}/c_{44}	$(5.0\pm0.7)\cdot10^{-7}$ cm dyne$^{-\frac{1}{2}}$	$5.7\cdots6.3\cdot10^{-7}$ cm dyne$^{-\frac{1}{2}}$
C	154°K	178°K
B	$7.0\cdot10^{-8}$ cm² dyne⁻¹	$4.3\cdots7.4\cdot10^{-8}$ cm² dyne⁻¹
T_L	254.7°K	—
T_U	—	296.9°K

* All values are given in electrostatic c.g.s. units.

capacity of the X cut 45° bars were derived under the assumption that the crystals could vibrate freely. The mounting must, therefore, be of such a nature as not to impose restricting boundary conditions. One way of achieving this end is to clamp the bar at its exact center between two knife edges. However we did not succeed in building a secure mounting of this type which would also have fitted into the limited space of the thermostat. A larger thermostat could not be built because of the wartime shortage of equipment.

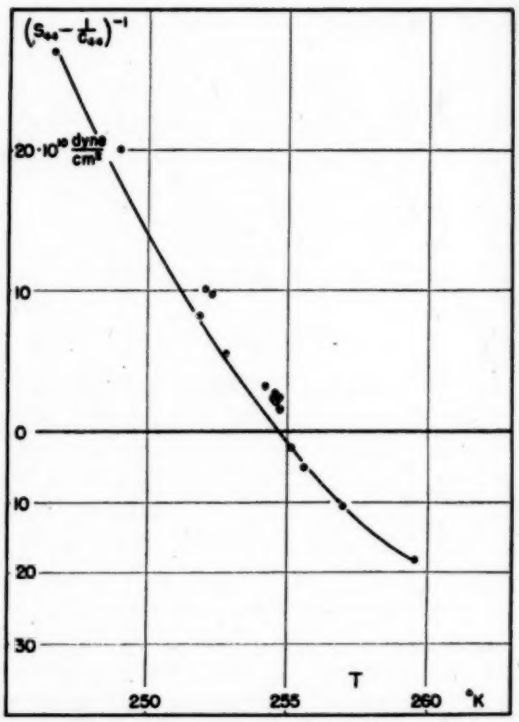

FIG. 8.

The mounting we used is shown in Fig. 11. The bar hangs in two loops, L_1 and L_2, made of thin platinum wire. These loops not only support the crystal but also act as current leads to the lower surface. Over the center portion of the crystal there hangs another such loop, which acts as a current lead to the upper surface. Both the upper and the lower surface, which are perpendicular to the crystallographic x axis, are coated with gold foil. Although platinum and gold are noble metals, it is still necessary to supply a certain amount of contact pressure, which is supplied by a 2-gram weight attached to the center wire.

When the crystal vibrates, waves are set up in the wires. The resulting dynamical disturbance is negligible if the wires are thin enough. We estimated that when their diameter is 0.004 in. the change in impedance of the crystal will be no more than that produced by a one-half percent change in its length.

The weight which is attached to the center loop of the suspension produces bending stresses in the crystal. The Y_x-component of these stresses becomes as large as 10^7 dyne cm^{-2}. One may object that such large stresses produce saturation. However, electric fields also arise which largely compensate these stresses as far as their saturation effects are concerned. This compensation is so complete that the residual saturation of the loop mounting is less than that of other mountings. This is shown by the fact that in our measurements the maximum of the susceptibility at the lower Curie point is twice as high as that reported by Mueller,[5] who used a knife-edge mounting. Thus we may conclude that the loop mounting is as good as others.

PHYSICAL INTERPRETATION

Let us consider a crystal ground into spherical shape and placed in a plate condenser with large plate separation. The thermodynamic potential for small polarization P_x and strain y_x will be of the form

$$A=\tfrac{1}{2}\{\alpha y_x^2+2\beta y_x P_x+\gamma P_x^2\}+f(T),$$

where the coefficients α, β, γ are slowly varying positive functions of the temperature T. For stability reasons the expression $\gamma-\beta^2/\alpha$ will also

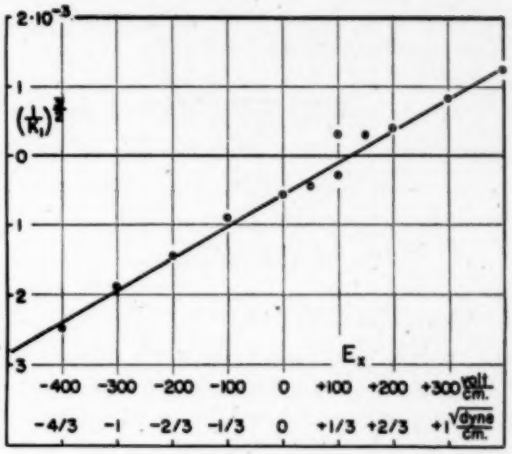

FIG. 9.

be positive. Differentiating A we have

$$-Y_x\equiv+\partial A/\partial y_x=\alpha y_x+\beta P_x;$$

$$E_x\equiv+\partial A/\partial P_x=\beta y_x+\gamma P_x;$$

(E_x is the field at large distances from the sphere). For a stress-free crystal we have

$$y_x=-\beta P_x/\alpha,$$

and thus

$$E_x=(\gamma-\beta^2/\alpha)P_x.$$

We see that the expression $\gamma-\beta^2/\alpha$ is the reciprocal of the susceptibility of a spherical stress-free sample.

If this same crystal is ground into a slab and covered with snugly fitting electrodes, the thermodynamic potential becomes

$$A=\tfrac{1}{2}\{\alpha y_x^2+2\beta y_x P_x+\gamma P_x^2-4\pi P_x^2/3\}+f(T).$$

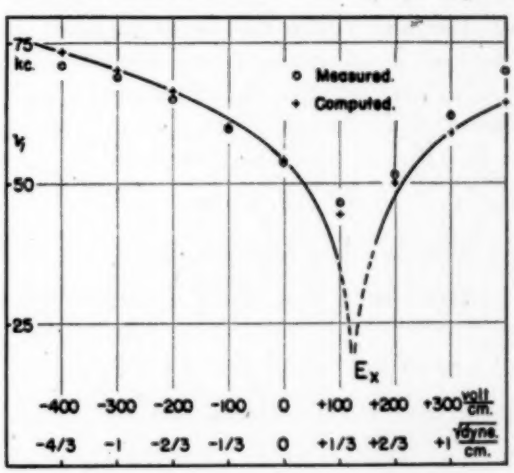

FIG. 10.

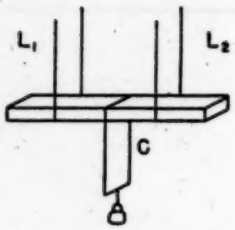

FIG. 11. Crystal suspension.

The additional term $-4\pi P_z^2/3$ takes care of the electrostatic interaction between distant parts of the crystal. For geometric reasons this interaction happens to be absent in the spherically-shaped sample. Of higher order terms only the term $\frac{1}{4}bP_z^4$ may be of importance in some crystals. If we include this term, the thermodynamic potential becomes

$$A=\tfrac{1}{4}bP_z^4+\tfrac{1}{2}\{\alpha y_z^2+2\beta y_z P_z + (\gamma-4\pi/3)P_z^2\}+f(T)$$
$$=\tfrac{1}{4}bP_z^4+\tfrac{1}{2}(\gamma-\beta^2/\alpha-4\pi/3)P_z^2 + \tfrac{1}{2}(\beta^2/\alpha)(P_z+\alpha y_z/\beta)^2+f(T).$$

Except for the notation this agrees with Eq. (1). The reciprocal of the susceptibility of a stress-free slab-shaped sample is now seen to be equal to $\gamma-\beta^2/\alpha-4\pi/3$. The important point is that, whereas $\gamma-\beta^2/\alpha$ was (in percentage) a slowly varying function of the temperature, $(\gamma-\beta^2/\alpha-4\pi/3)$ may be (in percentage) a rapidly varying function. This is the case whenever $(\gamma-\beta^2/\alpha)^{-1}$ happens to be approximately equal to $3/4\pi$. This is not outside the range of possibilities. The quantity $(\gamma-\beta^2/\alpha)^{-1}$ equals 0.18 in the case of flint glass, and 0.20 in the case of diamond. Thus if the lattices of these substances were loosened up somewhat, so that the interatomic "spring" forces were weakened by 25 percent, the quantity $(\gamma-\beta^2/\alpha)^{-1}$ would become equal to

$$3/4\pi=0.24.$$

In rochelle salt it happens that

$$\gamma-\beta^2/\alpha>4\pi/3 \quad \text{for} \quad T<T_L \quad \text{and} \quad T>T_U,$$

and

$$\gamma-\beta^2/\alpha<4\pi/3 \quad \text{for} \quad T_L<T<T_U,$$

so that we can write approximately:

$$\gamma-\beta^2/\alpha-4\pi/3=(T-T_L)(T-T_U)/C(T_U-T_L).$$

Why $\gamma-\beta^2/\alpha$ varies in just this fashion is not known, but it is not surprising, since $\gamma-\beta^2/\alpha$ changes by no more than 5 percent over a temperature range extending from 234°K to 318°K; i.e., in this temperature range of more than 80°K the interatomic "spring" forces change by no more than 5 percent.

In our opinion then, the electromechanical behavior of rochelle salt has its origin in the fact that $(\gamma-\beta^2/\alpha)^{-1}$, the susceptibility of a stress-free spherical sample, happens to be approximately equal to $3/4\pi$. At the two Curie points $(\gamma-\beta^2/\alpha)^{-1}$ is exactly equal to $3/4\pi$. This opinion is based on the experimental fact that the pertinent coefficients in the expression for the thermodynamic potential have the same values at both Curie points. It is no longer necessary to postulate the existence of rotating dipoles. All that occurs is that the lattice deforms as a whole.

Any rhombic hemihedral crystal for which $(\gamma-\beta^2/\alpha)^{-1}$ is approximately equal to $3/4\pi$ would exhibit electromechanical characteristics as violent as those of rochelle salt. Crystals in which $(\gamma-\beta^2/\alpha)^{-1}$ is smaller than $3/4\pi$ by more than perhaps 10 percent will behave in a more or less normal manner. Crystals in which $(\gamma-\beta^2/\alpha)^{-1}$ exceeds $3/4\pi$ by more than about 10 percent will always be permanently polarized, i.e., they will no longer remain rhombic hemihedral, but will become monoclinic hemimorphic. And then they will behave in a more or less normal manner.

APPENDIX

In conclusion we show the design of a mechanical model which is a complete analogy of rochelle salt (Fig. 12).

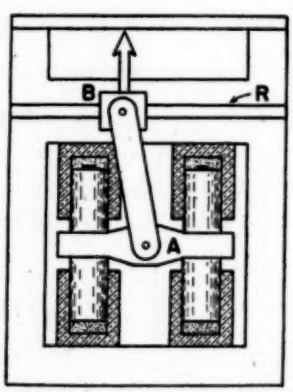

FIG. 12. Model illustrating permanent polarization between two given temperatures.

Four pistons move tightly but smoothly in dashpots. The lower two dashpots contain air, the other two a small amount of liquid. The pistons support a yoke A, which by means of a rod is connected to a shoe B. This shoe can slide along a horizontal rail R.

At low temperatures, when the gas pressure in the dashpots is very small, the yoke will assume its lowermost position; thus the shoe will be in the center of the rail. At moderate temperatures, when the air pressure in the lower dashpots overcomes the weight of the yoke but the liquid has not yet evaporated, the yoke will move up, and thus the shoe will move away from the center. Which side the shoe moves to is a matter of chance, lack of constructional symmetry, or willful interference. The model has become "polarized." At still higher temperatures the liquid in the upper dashpots will evaporate, so that the yoke is driven back to its lower-most position. The shoe is then located at the center again. This model, therefore, has a lower Curie point T_L and an upper Curie point T_U. Between these two temperatures the model is "permanently polarized."

Let ξ represent the distance of the shoe from the center. With the significant terms the thermodynamic potential is then of the form

$$A=(b/4)\xi^4+\tfrac{1}{2}[(T-T_L)(T-T_U)/c(T_U-T_L)]\xi^2+f(T).$$

Let the arrow which is attached to the shoe be made of a thin but broad strip of metal, so that it can be bent forward or backward. Let the plane of this strip be vertical and make an angle φ with the direction of the rail. Introduce two horizontal coordinate axes, x and y, such that the y axis is perpendicular to the plane of the strip and the x axis is perpendicular to the y axis. By moving the shoe along the rail and by bending the arrow, one can place the tip of the latter, within limits, at any position (x,y). The thermodynamic potential belonging to x,y and the temperature T as independent variables is then with the significant terms

$$A=b/4(x/\cos\varphi)^4+\tfrac{1}{2}[(T-T_L)(T-T_U)/c(T_U-T_L)]\times(x/\cos\varphi)^2+\tfrac{1}{2}K(y+x\tan\varphi)^2+f(T),$$

where K is the spring constant of the metal strip. If we introduce new constants B, C, c_{44}, f_{14} defined by

$$B=b/\cos^4\varphi;\quad C=c\cdot\cos^2\varphi;\quad c_{44}=K;\quad f_{14}=K\cdot\tan\varphi,$$

the thermodynamic potential assumes the form

$$A=(B/4)x^4+\tfrac{1}{2}[(T-T_L)(T-T_U)/C(T_U-T_L)]x^2+\tfrac{1}{2}(f_{14}^2/c_{44})[x+(c_{44}/f_{14})y]^2+f(T). \quad (18)$$

If we let x and y correspond to P_x and y_x, respectively, (18) becomes identical with (1). Thus the analogy between the behavior of the model and that of rochelle salt is complete. Let X and Y be the x and y components of the force which is necessary to hold the tip of the arrow at some desired position (x,y). Then X corresponds to the field E_x, and Y corresponds to the shearing stress component $-Y_x$.

We presented this analogy to demonstrate that the behavior of rochelle salt need not be considered mysterious. On the one hand, the peculiar mechanical characteristics of the model result from the fact that, though the pressure in the upper dashpots and the pressure in the lower dashpots are (in percentage) slowly varying functions of the temperature, their difference is (in percentage) a rapidly varying function. Similarly in rochelle salt the quantity $\gamma-\beta^2/\alpha$, which is a lattice property, is (in percentage) a slowly varying function of the temperature, whereas the quantity $\gamma-\beta^2/\alpha-4\pi/3$, which determines the peculiar characteristics, is (in percentage) a rapidly varying function.

ACKNOWLEDGMENT

The author expresses his gratitude to Professor Hans Mueller who suggested the topic of this investigation and helped with encouragement and advice.

A New Method of Separation of the Isotopes He^3 and He^4*

J. G. DAUNT, R. E. PROBST, AND H. L. JOHNSTON
The Cryogenic Laboratory, Department of Chemistry and Department of Physics, The Ohio State University, Columbus, Ohio

AND

L. T. ALDRICH AND ALFRED O. NIER
Department of Physics, University of Minnesota, Minneapolis, Minnesota

(Received July 24, 1947)

IN the course of experiments on the mechanocaloric effect in liquid helium II, first observed by one of us and Mendelssohn,[1] a new method of separation of the isotopes He^3 and He^4 has been developed. These experiments involved the transport of liquid helium II by super-fluid flow through a supra-surface film from one reservoir to another, in a manner similar to that used previously.[1,2] It was possible to confine the transport entirely to the surface film and so avoid the disturbing effects of flow of bulk liquid, such as may occur in flow through sub-surface channels.[3] The flow, therefore, could be employed as a decisive method of ascertaining whether the atoms of the isotope[4] He^3 do not partake in super-flow, a suggestion which has been put forward by Franck.[5]

The experimental arrangement is illustrated in Fig. 1. The vessel B represents the main liquid helium bath maintained at constant temperature below the λ-point. In the bath, B, was situated a glass vessel, A, which was partially filled with liquid helium condensed from a supply of atmospheric helium gas.[6] The vessel, A, was connected to a closed system at room temperature by means of the tube, a, and samples of the gas in this system could be withdrawn with balloons. Inside vessel A a small Dewar vessel, D, was placed, so constructed that the top was closed off by an evacuated glass plug which was ground to fit the Dewar. Leads (1 and 2) to a phosphor-bronze resistance thermometer, T_1, inside the Dewar were sealed through the plug.

The course of a typical experiment was as follows. Initially the small Dewar, D, was empty, although liquid helium II in A surrounded it. On supplying heat electrically by T_1, liquid was transferred from A into the Dewar, D, by super-fluid flow through the supra-surface film. Owing to the fact that the connecting channel was above the liquid levels, no flow of "bulk" liquid took place and the return flow of vapor through the

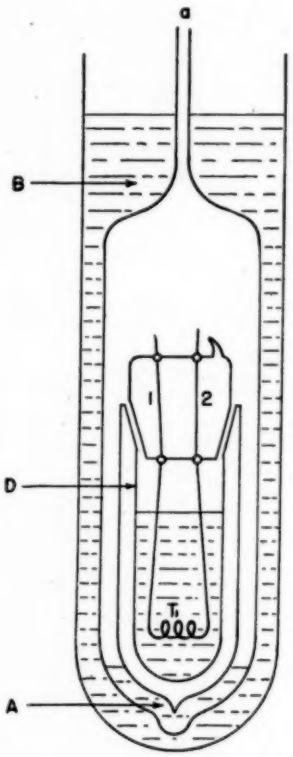

FIG. 1. Arrangement of the cryostat.

* The work at Ohio State University was assisted by Navy Contract No. N6onr-225. T.O.III between the Office of Naval Research and The Ohio State University Research Foundation; that at the University of Minnesota by grants from the Research Corporation and the Graduate School.

[1] J. G. Daunt and K. Mendelssohn, Nature **143**, 719 (1939).

[2] J. G. Daunt, Report to The Physical Society's Conference on Low Temperature Physics, July 1946 (unpublished).

[3] P. L. Kapitza, J. Phys. U.S.S.R. **5**, 59 (1941). Meyer and Mellinck: Manuscripts kindly loaned to us before publication.

[4] L. W. Alvarez and R. Cornog, Phys. Rev. **56**, 613 (1939); Phys. Rev. **56**, 379 (1939).

[5] J. Franck, Phys. Rev. **70**, 561 (1946).

[6] We are indebted to the generosity of Linde Air Products for providing large quantities of atmospheric helium gas.

ground joint was found to be negligible. The liquid in D was therefore completely isolated and the level could be increased above that in A to any desired amount. (This was generally 5 to 10 cm.)

Using the mass spectrometer previously described,[7] the abundance ratio of the isotope He^3 in He^4 for the gas used for condensation into A was found to be 1.20×10^{-6}, in excellent agreement with previous measurements[7,8] on atmospheric helium. Measurements were made on the abundance ratio of the helium collected in the Dewar, D. To collect this helium for measurement, first the liquid both in B and A was evaporated and the space A pumped out; then on waiting, the liquid in D slowly evaporated. Samples of this evaporated gas were taken until all the liquid in D vanished. The first sample taken off showed a ratio of $He^3/He^4\cong1.1\times10^{-7}$. Subsequent samples showed no measurable quantity of He^3, the limit for two of such samples being estimated as $He^3/He^4<5\times10^{-8}$, and for one other $<2\times10^{-8}$. For the whole volume of liquid evaporated from D the ratio He^3/He^4 was less than 5×10^{-8}.

Before concluding that this method of helium transfer acted as a filter for the rarer isotope, it was necessary to investigate the isotopic content of the helium in A. This was performed by connecting A via the tube, a, to a large balloon during the period in which D was filling. This process made at 1.5°K lasted for 90 minutes, allowing ample time for equilibrium to be reached between liquid and vapor. The measured abundance ratio for the vapor was 4×10^{-7}. This low value indicated (a) that a He^3 enrichment rather than a loss occurred in the liquid in A and (b) that the He^3/He^4 liquid-vapor equilibrium below the λ-point is a complicated effect.

One can therefore conclude that within the limits of measurement He^3 does not partake in super-flow. Whether or not this is an indication, as suggested by Franck,[5] that the super-flow of He^4 is essentially connected with the Bose-Einstein condensation phenomenon[9] is not yet clear. There remains the possibility that He^3 has a lower boiling point and a lower λ-point than He^4 and, consequently, super-flow might not be expected to occur until still lower temperatures are employed. This can only be decided by low temperature investigation of pure He^3.

This result also indicates that by using large volumes of liquid in A and transferring it by super-flow into large vessels, such as D, until only a very small quantity of liquid remains, strong concentrations of He^3 in these remainders can be obtained. Work on this is being carried out.

A number of determinations have been made of the relative abundance of He^3 in the vapor phase below the λ-point, using well helium in addition to the measurement reported above on atmospheric helium. These have been briefly reported elsewhere[10] and yield results strikingly different from the measurements above the λ-point carried out by an identical method by Fairbank and Lane.[8] The results indicate that for the vapor the abundance ratio is equal to or less than that for the unrefrigerated gas. This can be explained by our present results, since the tube leading from the liquid sample (e.g., tube A, of Fig. 1) to high temperatures must allow the supra-surface film to climb up and evaporate at a point high up inside the tube.[11] This will cause an excess of He^4 vapor at this point and forbid any but a small diffusion of He^3 from the liquid surface to the room temperature above.

Finally, it may be of interest to add that the mechano-caloric effect observed in these experiments shows that temperature differences of the order 10^{-2} degree can be obtained by mechanically altering the relative height of the liquids in A and D by a few centimeters, and that an exact measurement of the entropy of super-fluid helium II can thereby be obtained. A full description of the quantitative results will be given elsewhere.

---

[7] L. T. Aldrich and A. O. Nier, Phys. Rev. **70**, 983 (1946).
[8] H. A. Fairbank, C. T. Lane, L. T. Aldrich, and A. O. Nier, Phys. Rev. **71**, 911 (1947).
[9] F. London, Nature **141**, 643 (1938); J. Phys. Chem. **43**, 1 (1939).
[10] J. G. Daunt and H. L. Johnston, Ohio State University, Research Foundation Reports to U. S. Navy Office of Research. Report No. 3, April 1, 1947. Letter No. 1, June 1, 1947. Report No. 4, July 1, 1947.
[11] B. V. Rollin and F. Simon, Physica **2**, 219 (1939); J. G. Daunt and K. Mendelssohn, Proc. Roy. Soc. **A170**, 423 (1939).

Second-Order Magnetic Perturbations in Nuclear Quadrupole Spectra and the "Pseudo-Quadrupole" Effect in Diatomic Molecules

H. M. FOLEY
Columbia University, New York, New York
(Received July 28, 1947)

IN the evaluation of nuclear quadrupole interactions from the observed molecular beam or microwave spectra, it is essential to determine whether the interaction between the nuclear magnetic moment and the fields of the orbital electrons may perturb the energy levels in the same manner as does a nuclear quadrupole moment. Van Vleck[1] has pointed out that such a perturbation may exist in the second-order magnetic interaction. It is the purpose of this note to estimate the importance of this and of several other closely related magnetic effects.

The interaction of the nuclear spin angular momentum and magnetic moment with the orbital electrons and the molecular rotation is properly treated in a representation which is the nuclear analog of Hund's "case *b*." Van Vleck[2] and Hebb[3] have treated the analogous case of the magnetic and rotational interactions of the electron spin in a diatomic molecule, starting from a "case *a*" representation. In the case of the nuclear moment interactions in a $^1\Sigma$ molecule with large rotational quantum numbers, it is simpler to proceed directly from "case *b*." In this representation the nuclear spin precesses about the axis of total angular momentum, and the orbital angular momentum vector precesses rapidly about the inter-nuclear axis. The quadrupole-like energy term, which is independent of rotational effects for large rotational quantum numbers, arises from the interaction of the nuclear magnetic moment and the moments of the rapidly precessing components of orbital angular momentum perpendicular to the molecular (Z) axis. This interaction, of the form $A(i_xl_x+i_yl_y)$ yields in second order (case *b*) an energy term

$$W'=\sum_{\Lambda} A_\Lambda{}^2\langle l^2\rangle_{Av}i^2/4\Delta E_{\Sigma\Lambda}, \qquad (1)$$

for a molecule in a $^1\Sigma$ state. The quantity $i\hbar$ gives the component of nuclear spin angular momentum in the direction of the molecular angular momentum, while $\langle l^2\rangle_{Av}\hbar^2$ is the average square of the electronic angular momentum. This energy term has the same dependence on the nuclear spin angular momentum as does the electric quadrupole interaction and contributes additively with the latter term in the total energy expression. The exact evaluation of the coefficient in a particular case requires a knowledge of the molecular wave function. If Van Vleck's "hypothesis of pure precession" is assumed for the precessing orbital momentum, Eq. (1) becomes

$$W'=[(e^2\hbar^2/2m_eM_pc^2)g_N]^2 \times\langle 1/r_e{}^3\rangle_{Av}{}^2i^2L(L+1)/4\Delta E_{\Sigma\tau}, \qquad (2)$$

in which g_N is the nuclear "g factor" and r_e is the distance from the nucleus to a point in the charge distribution of the electrons producing the magnetic interaction. In the cases of H_2 and the alkali molecules, such as Na_2, the combining atoms are in S-states, so that the pure precession hypothesis can hardly be made and the perpendicular components of angular momentum are expected to be small. (Evidence for this fact is given below in the case of H_2.) Insofar as the alkali halides are considered to be composed of S-state ions, the expected perpendicular momentum components will be small. It is well known,[4,5] however, that the ground states of this class of molecules must include a contribution from a state formed from neutral atoms. The bonding P electron of the halogen atom may be considered to be precessing perpendicular to the molecular axis in these Σ-state molecules. When these considerations, together with the usual expression for $\langle 1/r_e{}^3\rangle_{Av}$ involving the observed atomic fine-

[1] Private communication to I. I. Rabi.
[2] J. H. Van Vleck, Phys. Rev. **33**, 467 (1929).
[3] M. H. Hebb, Phys. Rev. **49**, 610 (1936).
[4] L. Pauling, *Nature of the Chemical Bond* (Cornell University Press, Ithaca, New York, 1940).
[5] R. W. Mulliken, Phys. Rev. **51**, 310 (1937).

structure separation, are used to evaluate Eq. (2), the values for the F and Br nuclei in fluoride and bromide molecules are $0.045(\Gamma/d)$ mc and $0.008(\Gamma/d)$ mc, respectively. Γ is the fraction of atomic wave function in the ground state and d is the $\Sigma-\Pi$ energy separation in electron volts. From the ratio of the observed electric dipole moments to the product of the electronic charge and the inter-nuclear separation, it may be concluded that the fraction lies between one-tenth and one-half. The energy level difference d is about four volts. Thus the 'pseudo-quadrupole' effect in these molecules is about 0.001 mc. The effect on the alkali nucleus in these molecules is presumably very much smaller because of the $\langle 1/r_e^3\rangle_{Av}$ factor. In the use of the 'pure precession hypothesis' and in the evaluation of the $\langle 1/r_e^3\rangle_{Av}$ factor from atomic properties it is probable that the interaction energy has been overestimated.

The interaction with electron spin would lead to energy terms similar to Eq. (1) and those given below. This effect, however, in singlet molecules involves the partial decoupling of the total spin by the nuclear moment and will be very much smaller than the interaction with a precessing p-electron described in this note.

In the second-order treatment of the magnetic interactions there occurs a "cross term" between the magnetic interaction given above and the rotational perturbation which produces "Λ-doubling." This term is of the form

$$W''=\sum_{\Lambda} 2AB\langle I^2\rangle_{Av} iJ/\Delta E_{\Sigma\Lambda}, \qquad (3)$$

in which $B=\hbar^2/2I$. To explain the anomalously wide fluorine resonance line in the spectrum of LiF, Nierenberg and Ramsey[6] introduced a term 13.1×10^{-23} $(\mathbf{I}\cdot\mathbf{J})$ ergs into the molecular Hamiltonian. With an estimated inter-nuclear separation 1.7A and with a value of 0.1 for Γ for LiF, Eq. (3) yields for the coefficient 3.8×10^{-22} ergs when evaluated as described above. The overestimate of the effective coupling by only a factor of three is considered a reasonable support for the foregoing theory. In the case of NaBr a coupling coefficient of 5.5×10^{-23} ergs is estimated.

The "cross term" of the "Λ-doubling" matrix element and the interaction with an external magnetic field yields the expression for the electronic contribution to the magnetic moment produced by rotation.

$$\mu_R=\sum_{\Lambda} 2B\langle l^2\rangle_{Av}\mu_e J/\Delta E_{\Sigma\Lambda}, \qquad (4)$$

in which μ_e is the Bohr magneton. The previous methods of evaluation give $0.008J$ and $0.023J$ for the moments, in nuclear magnetons, of NaBr and LiF, respectively. Thus an average moment of not more than one nuclear magneton is to be expected in a molecular beam experiment with alkali halide molecules.

In the case of H_2 the electronic part of the molecular moment per unit angular momentum is accurately known[7] to be 0.12 nuclear magnetons. From Eq. (4) we may evaluate $\langle l^2\rangle_{Av}=0.0044/ev$ which is approximately one-tenth to one-thirtieth the values estimated for the alkali halides. From this evaluation and the observed value of 2.5×10^{-22} ergs for the electronic contribution to the $c\mathbf{I}\cdot\mathbf{J}$ term, the value of the magnetic coefficient A is 3.7×10^{-18} ergs. The pseudo-quadrupole effect in HD and D_2 is consequently entirely negligible ($\sim$1 c.p.s.).

The large values of the perpendicular component of angular momentum which seem to be present in alkali halide molecules lead to a large paramagnetic contribution to the temperature-independent part of the magnetic susceptibility. It is even possible that for this class of molecules this term would be weakly paramagnetic.

[6] W. Nierenberg and N. F. Ramsey (to be published).

[7] N. F. Ramsey, Phys. Rev. **58**, 226 (1940).

On the Two-Meson Hypothesis*

R. E. MARSHAK, *University of Rochester, Rochester, New York*

AND

H. A. BETHE, *Cornell University, Ithaca, New York*

(Received July 29, 1947)

1. INTRODUCTION

WEISSKOPF[1] has underlined the difficulty of reconciling the high rate of production of mesons with their subsequent weak interaction with matter. He has also suggested one possible way of overcoming the apparent lack of reversibility, namely, by postulating that the primary cosmic-ray proton converts a normal nucleon in an "air" nucleus into an "excited" nucleon, capable of emitting mesons. The lifetime of the "meson-pregnant" state can be chosen sufficiently long to account for the weak interaction between mesons and nucleons. An alternative solution of the difficulty was suggested by one of the present authors (R.E.M.) at the Shelter Island Conference. The hypothesis was that two kinds of mesons exist in nature, possessing different masses: the heavy meson was supposed to be produced with large cross section in the upper atmosphere and to be responsible for nuclear forces, whereas the light meson was regarded as a decay product of the heavy meson, and as the normal meson was observed at sea level to interact weakly with matter.[2] In this note we examine briefly some of the consequences of the two-meson hypothesis.

If we postulate the existence of a heavy meson in addition to the normal (light) meson, what properties must we assign to the heavy meson on the basis of cosmic-ray evidence and of our present-day notions of nuclear forces? In particular, what can we say about its mass, its spin, and its lifetime for disintegration into a light meson? Moreover, what are the connections between various processes involving the heavy meson?

2. MASS OF THE HEAVY MESON

It is clear that if we wish to relate the mass of the heavy meson to the range of nuclear forces (in the usual field-theoretic sense), we must assume that its mass is not greater than about 350 electron masses.[3] An experimental determination of the mass and direct evidence for the existence of the heavy meson may be provided by two excellent photographs taken by Lattes, Muirhead, Occhialini, and Powell.[4] Each of these photographs (taken at 10,000 feet) shows a meson stopping in the emulsion, and a secondary meson starting with a kinetic energy of about 2 Mev. The authors suggest the very interesting interpretation that each secondary-meson track is due to the spontaneous decay of a heavy meson into a light one. On this interpretation, the difference in mass between the two mesons is about 25 Mev, provided there is only one recoil particle, i.e., one light quantum or one neutrino (see below). The implication would then be that the heavy meson has a mass of about 125 Mev and the light meson a mass[5] of 100 Mev.

It is tempting to identify the heavy and light mesons of Lattes and co-workers with the two mesons of our theory. That the two kinds of mesons cannot be identified with the components

---

* This note owes its origin to the Conference on the Foundations of Quantum Mechanics held at Shelter Island, New York on June 2–4, 1947. The conference was sponsored by the National Academy of Sciences and was arranged through the kindness of Dr. D. A. MacInnes.

[1] V. F. Weisskopf, Phys. Rev. **72**, 510 (1947).

[2] This hypothesis is not to be confused with previous two-meson theories, such as the one proposed by Schwinger, in which both mesons are assumed to interact strongly with nucleons.

[3] L. E. Hoisington, S. S. Share, and G. Breit, Phys. Rev. **56**, 884 (1939).

[4] C. M. Lattes, H. Muirhead, G. P. S. Occhialini, and C. F. Powell, Nature **159**, 694 (1947). This paper arrived in the United States shortly after the two-meson hypothesis was presented at the Shelter Island Conference. Even more recently, a Russian paper (A. Alichanian, A. Alichanow, and A. Weissenberg, J. Phys. (USSR) **11**, 97 (1947)) has arrived, summarizing some cosmic-ray evidence for the existence of a particle of mass intermediate between that of the meson and the proton; however, this evidence appears less convincing than that of the British, and will not be used in our discussion.

[5] W. B. Fretter, Phys. Rev. **70**, 625 (1946), presumably measures the mass of the light meson (cf. below).

of Schwinger's mixed-meson theory, follows from the extremely short lifetime for the decay of the heavy meson into the light one predicted by the Schwinger theory.[6] Of course, many more experiments must be performed before the existence of the heavy meson and, in particular, the proposed identification can be accepted.

3. LIFETIME OF THE HEAVY MESON

An important feature of the two-meson hypothesis is the requirement that the heavy meson should have a lifetime which is sufficiently long to account for the frequency of heavy meson decays observed by Lattes and co-workers, and sufficiently short to explain the fact that at sea level and underground most mesons fail to interact strongly with nucleons (and must therefore be light mesons). We obtain an upper limit on the lifetime for the decay of a heavy meson into a light one on the basis of the meson capture, scattering, and underground-absorption experiments. A lower limit is arrived at by examining the British data in greater detail.

(a) Upper Limit

One upper limit for the heavy meson lifetime can be derived from the experiment on the capture of slow negative mesons by light atomic nuclei.[7] The negative result of this experiment implies that most of the mesons hitting the apparatus must be light mesons. If this were not the case and heavy mesons had a long enough life to survive in the atmosphere, they would suffer nuclear capture (after being stopped in the apparatus) before they could decay into light mesons. If we take 10 percent as a reasonable upper limit on the fraction of heavy mesons entering the apparatus of Conversi and coworkers, then we find $\tau_H \leqslant 1.5\cdot 10^{-6}$ sec., where τ_H is the lifetime for the heavy meson at rest. This upper limit for τ_H is already shorter than the lifetime for the electron decay of the normal (light) meson.

A closer upper limit on the heavy meson lifetime can be obtained from the experiments on the nuclear scattering of mesons.[8] All investigators of this phenomenon have found that mesons are almost never scattered through large angles ($>20°$ or so). The cross section turns out to be less than 1 percent of the nuclear cross section. Since the primary proton has a nuclear cross section for the production of heavy mesons, the heavy meson should be scattered by nuclei with a similar cross section.[9] Hence, at sea level, at most one meson in a hundred can be heavy. Let us assume that heavy mesons with an energy greater than E survive; therefore, the fraction of heavy mesons with an energy greater than E must be less than 0.01. Now, at sea level, the fraction of mesons with an energy greater than E is $(B/B+E)^{1.8}$ ($B=2$ Bev = energy loss in atmosphere). In other words, a heavy meson must possess an energy 25 Bev before it will penetrate to sea level. If we take 20 km for the height of the meson-producing layer, we get (μ_H is the heavy meson mass)

$$(20\text{ km}/c\tau_H)\cdot(\mu_H c^2/25\text{ Bev}) \geqslant 1, \qquad (1)$$

or

$$\tau_H \leqslant 3\cdot 10^{-7}\text{ sec.}$$

The closest, but not quite so certain, upper limit for the heavy meson lifetime comes from the presence of mesons deep underground. It is found[10] that mesons penetrate the equivalent of 1000 meters of water. Such mesons must possess an energy of at least $2\cdot 10^{11}$ ev, and must be light mesons when hitting the earth. From the smoothness of the number *versus* energy curve underground[11] it follows that heavy mesons of energy up to $2\cdot 10^{11}$ ev (and possibly more) must in general transform into light mesons before they make a nuclear collision. Since the mean free path for a nuclear collision is 1 meter of water (which is equivalent to about 10 km of air at the production level), we find:

$$(10\text{ km}/c\tau_H)\cdot(\mu_H c^2/200\text{ Bev}) \geqslant 1, \qquad (2)$$

or

$$\tau_H \leqslant 2\cdot 10^{-8}\text{ sec.}$$

[6] R. J. Finkelstein (Bull. Am. Phys. Soc., Stanford Meeting, 1947) finds a lifetime of $4\cdot 10^{-18}$ sec.

[7] M. Conversi, E. Pancini, and O. Piccioni, Phys. Rev. **71**, 209 (1947).

[8] R. P. Shutt, Phys. Rev. **69**, 261 (1946). Additional references are given in this paper.

[9] J. R. Oppenheimer (Shelter Island Conference) has pointed out that the reduction of the scattering cross section by the strong coupling theory becomes invalid at high energies (>1 Bev or so).

[10] V. C. Wilson, Phys. Rev. **55**, 6 (1939).

[11] There is a break in this curve at about 250 meters, but this is explained by the onset of radiation loss.

(b) Lower Limit

The two British tracks showing the transformation of a heavy into a light meson must be attributed to positively charged particles since a negative heavy meson must be presumed to be easily captured by a nucleus. The total number of mesons observed to stop in the plates is 65; thus the heavy mesons should be about $2\times 2/65$, i.e., 6 percent of all mesons. From the upper limit on τ_H we can say that all the heavy mesons observed must have been produced in the vicinity of the photographic plate; the slow mesons incident from the air will almost all be light mesons. If τ_H is greater than about $5\cdot 10^{-9}$ sec., then the heavy mesons may have been produced, for example, in the nearby ground (assumed 5 feet away); if $\tau_H < 5\cdot 10^{-9}$ sec., only the matter in the immediate neighborhood of the photographic plate (e.g., the support of the plate) will be effective. Again, the thickness of this neighboring matter, T, must be compared with $v\tau_H$ where v is the meson velocity; the heavy mesons observable in the plate must have originated in a thickness of matter of amount T or $v\tau_H$, whichever is the smaller.

Since we are interested in the smallest value of τ_H which can account for the observed ratio of heavy to light mesons, we note that every meson when produced is heavy, but that those produced in air transform into light ones. The production rate does not change rapidly with elevation (a factor of e for 1-meter water equivalent) so that we may take it to be the same for the light and the heavy mesons which reach the plate. The ratio of observable heavy to light mesons will then depend on the energy distribution of the mesons when produced. Let us assume, for example, that this energy distribution is uniform. Then, if the light mesons stopped in the plate had kinetic energies up to E_0 at the time of their production, the heavy mesons must be able to survive whenever their kinetic energy at production is $\leqslant 0.06E_0$. The energy E_0 is about 200 Mev because for higher energies the beta-decay of the light mesons would greatly reduce their probability of reaching the photographic plate through a considerable thickness of air. Thus the heavy mesons should survive if their initial kinetic energy is less than 12 Mev. The range of such a meson would be about 1 g/cm^2; if the material were Al, this would mean 0.4 cm, and with a velocity $v\sim 10^{10}$ cm/sec., we would get $\tau_H \geqslant 4\cdot 10^{-11}$ sec. However, it is perhaps more probable that the energy distribution is given by the volume element in momentum space up to some high energy; this would increase the relative probability of faster mesons and also increase the estimated lower limit of the lifetime.

4. SPIN OF THE HEAVY MESON

No definite predictions can be made about the spin of the hypothetical heavy meson. The best qualitative theory of nuclear forces so far worked out is based on a pseudoscalar meson field with pseudovector coupling; this would indicate spin 0 for the heavy meson. For spin $\frac{1}{2}$ mesons, a theory giving the correct qualitative features of nuclear forces, and based on a meson-neutrino pair field with tensor coupling,[12] is also possible. Spin 1 mesons by themselves seem excluded.[13] However, predictions of the heavy meson spin of the basis of nuclear forces are untrustworthy in view of the essentially unsatisfactory state of all meson-field theories.

A better indication of the spin of the heavy meson can be secured from an empirical study of its decay into a light meson. If the energy of the light meson is always the same, the heavy meson decay must take place with the emission of a single recoil particle, i.e., a γ-ray or a neutrino. Neutrino or γ-ray emission could be distinguished by the absence or presence of showers associated with the decay process. If the energy of the light meson is not constant, it would follow that the decay involves the emission of at least two γ-rays or two neutrinos and that zero spin characterizes both light and heavy mesons.[14]

5. CONNECTIONS BETWEEN VARIOUS PROCESSES

According to our theory, the light meson is involved in two different processes of small prob-

[12] R. E. Marshak, Phys. Rev. **57**, 1101 (1940).

[13] See G. Wentzel, Rev. Mod. Phys. **19**, 1 (1947). Of course, it is possible that three kinds of mesons exist: two heavy mesons and one light meson (in the sense of our theory).

[14] The spin of the light meson must be 0 or $\frac{1}{2}$ from the measurements on burst production [see R. E. Lapp, Phys. Rev. **69**, 321 (1946)]. The observed bursts are produced by light mesons since energies of less than 10^{11} ev are involved and heavy mesons of this energy would decay into light mesons in the atmosphere (see Section 2(a) of this paper).

ability, *viz.* its capture by nuclei and its birth by the decay of the heavy meson. It is attractive to regard both of these processes as originating from the same fundamental interaction, and in this way[15] to explain the experiment of Conversi *et al.*[7] For the sake of a model, let us assume that the heavy meson possesses spin $\frac{1}{2}$, the light meson spin 0. Let us further assume the following direct interaction:

$$\text{Neutron}\rightarrow\text{proton}+\text{heavy meson}+\text{neutrino}, \quad (3)$$

$$\text{Heavy meson}\rightarrow\text{light meson}+\text{neutrino}. \quad (4)$$

Then the probability for the capture of a light negative meson by a nucleon can be calculated through an intermediate state, thus:

$$\text{Light meson}+\text{proton}\rightarrow\text{heavy meson}+\text{neutrino}+\text{proton}\rightarrow\text{neutron}. \quad (5)$$

Actually, the capture of a light meson can only take place in the presence of two nucleons in order to conserve momentum between the initial and final states. This is achieved in the calculation by adding another intermediate process, namely, the transfer of momentum between the two nucleons by means of the nuclear potential between them. Hence, if we calculate nuclear forces on the basis of (3), and the probability for the decay of the heavy meson on the basis of (4), we can *derive* the probability for capture of the light meson from (5).

Let us denote the strength of the coupling (3) by g. Then, if we neglect the spin and isotopic-spin dependence of nuclear forces, the interaction U between nucleons (calculated from second-order perturbation theory) is roughly:

$$U\sim(g^2/\hbar c)(E_{\max}/\mu_H c^2)^5\mu_H c^2, \quad (6)$$

over a range $(\hbar c/E_{\max})$, where $E_{\max}$ is the energy at which the intermediate states are cut off and supposedly lies somewhere between $\mu_H c^2$ and Mc^2 (M is the mass of the nucleon). The ground state of the deuteron requires the approximate constancy of the potential times the square of the range, so that:

$$(g^2/\hbar c)(E_{\max}/\mu_H c^2)^3\sim\text{const. (of order 1)}. \quad (7)$$

If we denote the strength of the coupling (4) by G, we get:

$$1/\tau_H\sim(G^2/\hbar c)(\Delta\mu/\mu_H)^2(\mu_H c^2/\hbar), \quad (8)$$

where $\Delta\mu$ is the difference in mass between the heavy and light mesons. The calculation for the meson capture leads to the formula:

$$1/\tau_c\sim 1/\tau_H(E_{\max}/Mc^2)(M/\Delta\mu)^2\times(\bar{U}/\mu_H c^2)^2(v/c), \quad (9)$$

where τ_c is the lifetime for capture (per proton) of a light negative meson inside the nucleus, $v(\sim\frac{1}{3}c)$ is the final velocity of the nucleon, $\bar{U}$ (~ 5 Mev) is the effective matrix element of the interaction potential between the two nucleons corresponding to the momentum transfer between them, and where we have already taken account of (7) and (8). It is seen that (9) is not too sensitive to $E_{\max}$; we put $E_{\max}\sim\mu_H c^2$.

The capture lifetime can be deduced from the the experimental result that at about[16] $Z=10$, the capture of slow negative mesons and their disintegration into electrons are about equally likely; from this $\tau_c\sim 10^{-7}$ sec. Inserting numbers into (9), we obtain: $\tau_H\sim 10^{-8}$ sec. This value can easily be in error by a factor 10 or more in view of the crudeness of the calculation (apart from the divergences which have to be cut off) and the choice of a special model. However, the fact that it falls within the range required by the cosmic-ray data at least leaves open the possibility of relating the heavy meson decay to the nuclear capture of light mesons.

Unfortunately, the present theory does not permit us to relate the normal beta-decay of nuclei to the beta-decay of the light meson. This follows from the fact that the light meson interacts so weakly with nucleons that normal beta-decay would be much too slow. Instead, it is necessary to assume that the heavy meson not only decays into a light meson, but is also capable of undergoing electron disintegration.[17] However, the lifetime of the heavy meson for electron disintegration ought to be longer than the lifetime for light meson disintegration in order to insure compatibility with the observed numbers of electrons in the cosmic radiation.[18]

[15] The possibility of such a connection was suggested independently by Lattes *et al*, reference 4.

[16] J. A. Wheeler, Phys. Rev. **71**, 320 (1947); see also E. Fermi, E. Teller, and V. Weisskopf, Phys. Rev. **71**, 314 (1947).

[17] This may be the explanation of the meson track in Fig. 3 of the paper by Lattes *et al* (reference 4) which presumably shows a heavy meson dying in the emulsion with no observable secondary track.

[18] H. A. Bethe and R. P. Feynman, Shelter Island Conference.

Letters to the Editor

PUBLICATION of brief reports of important discoveries in physics may be secured by addressing them to this department. The closing date for this department is five weeks prior to the date of issue. No proof will be sent to the authors. The Board of Editors does not hold itself responsible for the opinions expressed by the correspondents. Communications should not exceed 600 words in length.

On the Production Process of Mesons

VICTOR F. WEISSKOPF
Massachusetts Institute of Technology, Cambridge, Massachusetts
July 28, 1947

ACCORDING to present cosmic-ray evidence, it seems that mesons are produced in the upper atmosphere by the primary cosmic radiation, which consists presumably of protons. The cross section for this production is of the order of nuclear dimensions since the primary radiation is absorbed in about 1-m water equivalent of air. The mesons are presumably produced in showers of several particles. Very much smaller cross sections, however, are found for any interaction of the mesons themselves with matter. After being produced in the first 100 g/cm² of the atmosphere, a considerable fraction of the mesons are able to penetrate through the total atmosphere and even deep underground. The only interaction with matter seems to be the one which is caused by its charge. Scattering by interactions other than electric is small and perhaps nonexistent.[1] Recent experiments have shown that even the absorption of slow mesons by nuclei takes place with a probability far below the expected one.

Nordheim and Hebb have shown that these facts are in contradiction with any simple theoretical description of meson production.[1] One should expect a similar cross section for processes induced by mesons as for processes in which mesons are created. This result follows immediately from any "interaction term" which is introduced into the Hamiltonian in order to describe the meson creation, if one applies the well-known principle of detailed balancing. This difficulty has been repeatedly emphasized by Oppenheimer.[2]

The striking lack of reversibility suggests the possibility that the process of meson creation is not elementary, but consists of a succession of several elementary processes. The total process will not be reversible if one of the successive steps is much slower than the initial one. The following analogy may perhaps clarify the picture: The cross section for the production of fission in uranium by a nuclear particle is of the same order as the cross section for the fission fragments to collide with another fragment, in accordance with the reversibility of the fission process. Let us imagine, for the sake of argument, however, that the fission fragments were not observable and that the only known effect would be the absorption of a nuclear particle by uranium with the subsequent emission of several electrons due to the beta-disintegrations of the fragments. We would then be faced with an analogous lack of reversibility, since the absorption of electrons by nuclei is extremely weak.

A number of possible combinations of processes suggest themselves for the mechanism of meson production. One could assume that the primary cosmic radiation transforms the nucleons into an "excited" state which, after a time long compared to the excitation process, decays with the emission of several mesons. The relatively long life-time of the "meson-pregnant" state would give rise to the small interaction between mesons and nucleons. Another alternative assumption, which was proposed by R. E. Marshak, would be that the primary radiation produces a number of particles which are mesons of a different kind than the ones observed. They have a limited lifetime after which they decay into the actual mesons observed. The lifetime could be long enough to preclude a strong interaction between the observed mesons and the nuclei.

These examples are meant only to exemplify the type of concepts which one may be forced to introduce into our description of meson production to understand the apparent lack of reversibility. The ideas expressed in this note were suggested by the discussions at the Theoretical Physics Conference on Shelter Island, June 2 to 4, 1947, sponsored by the National Academy of Sciences.

[1] L. Nordheim and M. Hebb, Phys. Rev. **56**, 494 (1939).
[2] Lecture delivered at the New York meeting of the American Physical Society, Shelter Island Conference, 1947.

The Thermal Diffusion Constant of Helium and the Separation of He^3 by Thermal Diffusion

B. B. MCINTEER, L. T. ALDRICH, AND ALFRED O. NIER
Department of Physics, University of Minnesota Minneapolis, Minnesota
July 31, 1947

WE have been investigating the possibility of separating He^3 by thermal diffusion, and as part of the preliminary work we have constructed a hot wire column using a platinum wire 0.018 cm in radius. The radius of the water-cooled outer wall was 0.436 cm and the length 305 cm. The power consumption for a wire temperature of 780°C was 1520 watts and the operating pressure 10 atmospheres. Well helium flowed continuously past the lower end of the column at a sufficient rate so that the concentration here could be considered to have its normal value,[1] 1.6×10^{-7}. As the relaxation time for the above conditions would be of the order of 10^4 years, a linear increase in concentration is observed with time and with a negligible draw-off of gas it was possible to produce an enrichment in He^3 of 860 times in a period of 8 days.

During the course of our experiments it was possible to accumulate 52 cm³ at N-P of well helium in which a He^3 enrichment of 300 times had been achieved. The He^3 concentration was sufficient to permit accurate mass-spectrometer analyses and hence a determination of α, the thermal diffusion constant, by the two-bulb method employed in this laboratory[2] for other gases. With the hot and cold bulbs at temperatures of 340° and 0°C, respectively, α was found to have a value of 0.059 ± 0.005. This value is considerably lower than 0.076 tentatively assumed by Jones

and Furry[3] in their design of a separating plant for He^3. Employing our value of α and using Jones' and Furry's theory for column performance, one would predict a 125-fold concentration rise per day as compared with the 108 actually observed. In view of the difficulty of the measurements this may be considered as satisfactory agreement.

From the work of Atkins, Bastick, and Ibbs[4] on thermal diffusion in binary mixtures of rare gases, one would predict a higher value of α in helium than we have found. With the same apparatus as was used for the helium α-determination, we have made a rough determination of the thermal diffusion effect in a helium-neon mixture and found a lower value than that given by the above investigators and in excellent agreement with the new work on binary gas mixtures by Grew.[5]

This work was assisted by Navy Contract N5ori-147, T.O. III, between the Office of Naval Research and the University of Minnesota.

[1] L. T. Aldrich and A. O. Nier, Phys. Rev. **70**, 983 (1946); H. A. Fairbank, C. T. Lane, L. T. Aldrich, and A. O. Nier, Phys. Rev. **71**, 911 (1947).
[2] A. O. Nier, Phys. Rev. **56**, 1009 (1939); **57**, 338 (1940); L. G. Stier, Phys. Rev. **62**, 548 (1942).
[3] R. C. Jones and W. H. Furry, Rev. Mod. Phys. **18**, 151 (1946).
[4] B. E. Atkins, R. E. Bastick, and T. L. Ibbs, Proc. Roy. Soc. **A172**, 142 (1939).
[5] K. E. Grew, Proc. Roy. Soc. **A189**, 403 (1947).

A Random-Absorption Effect in Diffraction of X-Rays from Coarse Powders

ZIGMOND W. WILCHINSKY
Esso Laboratories, Standard Oil Company of New Jersey, Baton Rouge, Louisiana
July 28, 1947

CONSIDERING the statistical distribution and sizes of the grains and voids in a powder sample, the x-ray absorption factor for a given path length in the sample will have a statistical distribution. The average absorption factor obtained in this manner is in general different from the absorption factor obtained by using the average absorption coefficient. The resulting modification of the diffracted x-ray intensities will be referred to as the random absorption effect.

Although it is quite simple to set up the differential equation for the intensity of diffracted radiation, an exact solution of the equation is, in general, not possible. An approximation can be readily obtained, however, as will be demonstrated presently.

Consider a powder of a single substance. This case, besides being simple to handle, is of special interest because the "micro-absorption" effect discussed in a paper by Brindley[1] is zero for this case. The path of a ray penetrating a portion of the sample will be made up of a succession of elementary lengths occurring alternately in the solid material and voids. Let the representative path length between discontinuities be designated by D. Considering diffraction from an opaque powder block as used conventionally in the Geiger-counter x-ray spectrometer, let the sample be divided up into elementary slabs of thickness $D\sin\theta$ as indicated in Fig. 1, θ being the Bragg angle. The contribution to the integrated intensity from the nth slab is given by:

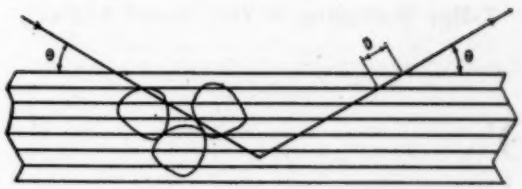

FIG. 1. Relationship of x-ray beam to sample. Several particles are sketched in to illustrate the approximate relationship of particle diameter to D and the thickness of an elementary slab.

TABLE I. Measurements on random absorption effect of x-rays.

Powder size (10^{-4} cm)	μD	(P/P_0)exp	(P/P_0)theo
10 to 20	0.43	0.94	0.91
20 to 44	0.92	0.81	0.82

P_n = (Integrated intensity due to a single slab)
× (Absorption of the beam in the preceding slabs)

$$= \frac{JAv}{\sin\theta}\left\{\int^{D\sin\theta} \exp\left(\frac{-2\mu x}{\sin\theta}\right)dx\right\} \times [v\exp(-\mu D)+v_0]^{2(n-1)}, \quad (1)$$

where J = integrated intensity per unit volume of the solid material on basis of no absorption, A = cross section area of the x-ray beam at the sample, μ = linear absorption coefficient of the solid material, v = fraction of the volume occupied by solid material, $v_0 = 1-v$ = fraction of the volume occupied by voids.

For a solid block, the integrated intensity is $P_0 = JA/2\mu$. The value of P for the powder block is $\sum_{n=1}^{n=\infty} P_n$. Hence, one obtains

$$P/P_0 = [1+\exp(-\mu D)]/[2-v\{1-\exp(-\mu D)\}]. \quad (2)$$

An analogous expression for any number of crystalline components can be obtained in a similar manner. It is interesting to note that Eq. (2) gives the correct value of unity for $D=0$ (very fine powder) and for $v=1$ (solid block).

An experimental check was made on the random absorption effect. Three samples of iron were used: (a) solid block, (b) particles ranging from 10 to 20 microns in diameter, (c) particles ranging from 20 to 44 microns in diameter. In the theoretical evaluation of P/P_0 by Eq. (2), approximate values of D for samples (b) and (c) were taken to be 7.5 and 16 microns, respectively, and a value of 0.5 was assumed[2] for v. Radiation from an iron target was employed in a Geiger-counter x-ray spectrometer. The results are given in Table I:

These results indicate that a random absorption effect is present, and its order of magnitude is given by Eq. (2).

A more complete and detailed discussion of theoretical and experimental results is being prepared for publication.

[1] G. W. Brindley, Phil. Mag. **36**, 347 (1945).
[2] This value is quite reasonable according to experiments on compaction of powders. See for instance, M. Muskat, *Flow of Homogeneous Fluids Through Porous Media* (McGraw-Hill Book Company, Inc., New York, 1937), p. 13.

X-Ray Scattering at Very Small Angles*

W. W. Beeman and Paul Kaesberg
Department of Physics, University of Wisconsin, Madison, Wisconsin
July 21, 1947

DUMOND[1] has recently proposed a method of using the double crystal spectrometer for the measurement of x-ray scattering at very small angles. The scattering material is to be placed between the two crystals. The second crystal is then rotated, scanning a small angular region near the parallel position. Because the parallel position rocking curves with good crystals are only a few seconds of arc wide one hopes to detect scattered x-rays within a few seconds of the forward direction.

DuMond suggests in his letter[1] that the method may have occurred to others independently. This is indeed the case. At this laboratory some preliminary work was done over a year ago. Intense scattering from fibrous materials at right angles to the fiber axis was observed. A survey of the literature revealed that I. Fankuchen (whose interest in the problem was mentioned by DuMond) and M. H. Jellinek[2] had tried the method in 1944. They used the second or analyzing crystal in both the anti-parallel and parallel positions. No experimental results are given in the abstract. These authors attribute the suggestion of the parallel crystal arrangement to H. Friedman. In 1926 Slack[3] observed a considerable broadening of the parallel-position rocking curve when graphite was placed between the two crystals. He suggested that a multiple refraction of the wavefront by the graphite grains was responsible for the broadening. Von Nardroff[4] discussed the idea of multiple refraction quantitatively, and successfully explained Slack's results.

In view of the current speculation, a few comments on the double crystal method may be in order. Figure 1 is typical of the rocking curves which we have obtained with fibrous materials. Close to the central maximum (the region pictured) it is similar to the curves obtained by Slack with granular materials. We were able to continue the curve to several minutes of arc and still detect an increase of intensity with the specimen in place. With ground crystals, measurements might be extended to a degree or two. One can conveniently correct for absorption by running a rocking curve with the specimen before the first crystal.

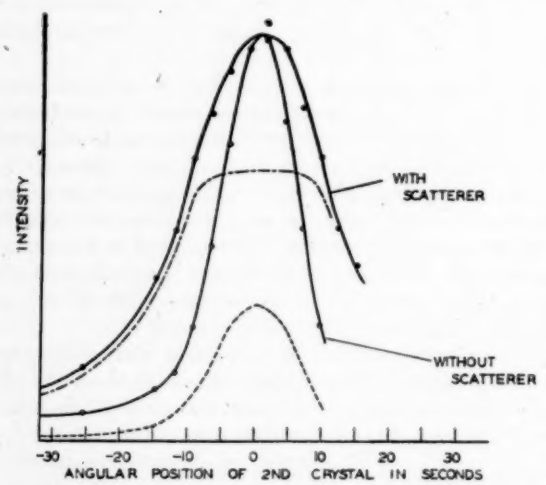

FIG. 1. Parallel-position rocking curves, wood scatterer 0.16 cm thick, tungsten L second order. The two curves are plotted to the same vertical scale.

The refraction effects obscure scattering at very small angles and may somewhat limit the usefulness of the method. Both refraction and scattering from randomly arranged particles[5] (the diffuse small angle scattering that has been so extensively investigated photographically) give an intensity *versus* angle distribution of the form

$$I(\theta) = Ce^{-\theta^2/k^2}.$$

In the case of scattering k is proportional to the x-ray wave-length divided by the particle size, and in the case of refraction to the unit decrement of the refractive index multiplied by the square root of the number of particles traversed. Thus refraction effects may be minimized by using a thin specimen and ignored if one is more than three or four half-widths away from the central maximum. In most cases we found more intensity at two or three minutes of arc than could be accounted for by refraction. The broadening of the central maxima of our curves is apparently due to refraction. The broadening increases with increasing specimen thickness, as predicted by the theory. This was first observed by Slack. Multiple scattering might, of course, cause such an effect.

It will also be noticed that the wave-length dependence of scattering differs from that of refraction. k is proportional to the wave-length for scattering, but to the wave-length squared for refraction.

* This research was supported in part by the Research Committee of the Graduate School from funds supplied by the Wisconsin Alumni Research Foundation.

[1] Jesse W. M. DuMond, Phys. Rev. **72**, 83 (1947).
[2] I. Fankuchen and M. H. Jellinek, Phys. Rev. **67**, 201 (1945).
[3] C. M. Slack, Phys. Rev. **27**, 691 (1926).
[4] R. von Nardroff, Phys. Rev. **28**, 240 (1926).
[5] C. G. Shull and L. C. Roess, J. App. Phys. **18**, 295 (1947).

Compatibility of Primary Protons with the Atom-Annihilation Hypothesis

H. Turner
University of Western Australia, Nedlands, Western Australia
July 31, 1947

THE main objection to Millikan's theory for the origin of cosmic radiation appears to be his belief[1] that electrons are the principal components of the primary rays. This belief is based on his interpretation of the Lemaitre-Vallarta curves[2,3] when used for particles possessing the energy due to a helium atom-annihilation process. According to this interpretation, helium-produced electrons with an energy of 1.87×10^9 ev would first penetrate to the earth at about 54 degrees geomagnetic north, while helium-produced portions with an energy of 0.93×10^9 ev would be first detected somewhere north of 60 degrees geomagnetic north. This utilizes the same scale for protons as for electrons. The fact that there is an increase in total intensity

at about 56 degrees caused Millikan to assume that the incoming radiation must consist of electrons.

However, proton energies cannot be directly read off an electron energy scale. This may be verified by using the formula employed by Lemaitre and Vallarta[4] to calculate, in stormers, the particle energy, x, necessary to penetrate the field of a magnetic dipole of moment M to a distance, r, equal to the radius of the earth (6370 km).

$$x=r(mv/eM)^{\frac{1}{2}},$$

where e, v, and m are, respectively, the charge, velocity, and relativistic mass of the particle.

Assuming that any atom of mass M_A emits a pair of oppositely directed particles each of mass m', with an energy due to the complete annihilation of the remainder of the atom, then

$$\tfrac{1}{2}(M_A-2m')c^2=m'c^2[(1-\beta^2)^{-\frac{1}{2}}-1].$$

From this, it may readily be seen that the relativistic mass $m'/(1-\beta^2)^{\frac{1}{2}}=\frac{1}{2}M_A$. Thus the relativistic mass, m, is constant for any particle emitted by a given atom-annihilation process. In particular, electrons or protons emitted in a helium-annihilation process have a relativistic mass of 3.32×10^{-24} g.

Accepting the values of $M=8.04\times10^{23}$ e.m.u. and $e=1.6\times10^{-20}$ e.m.u., then $x=0.177\sqrt{\beta}$, where β has been written for v/c, and may be calculated from the relativistic and rest mass values. For an electron of 1.87×10^{9} ev, $\beta=0.999$, whence $x=0.177$ stormers. For a proton of 0.93×10^{9} ev, $\beta=0.864$, whence $x=0.165$ stormers, which corresponds to an electron energy of 1.61×10^{9} ev.

On referring to the Lemaitre-Vallarta curves, it is seen that the difference in these particle energies, for vertical incidence, corresponds to a latitude difference of about $1\frac{1}{2}$ degrees, which is within the uncertainty limits of existing data on the latitude of the helium incoming radiation. Thus there is no experimental evidence to suggest that protons could not form the majority of the incoming radiation, thereby removing the principal objection to Millikan's atom-annihilation hypothesis.

[1] R. A. Millikan, Neher, and Pickering, Phys. Rev. **63**, 234 (1943).
[2] Millikan, Neher, and Pickering, Phys. Rev. **61**, 397 (1942).
[3] G. Lemaitre and M. S. Vallarta, Phys. Rev. **50**, 503 (1936).
[4] G. Lemaitre and M. S. Vallarta, Phys. Rev. **43**, 809 (1933).

Primary Cosmic-Ray Protons and the Atom-Annihilation Hypothesis

R. A. Millikan, H. V. Neher, and W. H. Pickering
California Institute of Technology, Pasadena, California
August 8, 1947

In a paper which appeared in the Physical Review [**61**, 397 (1942)] we stated in discussing the atom-annihilation hypothesis (see reference 4, page 398): "It would make no difference so far as all the results considered in this paper are concerned whether the charged particles are electrons, mesotrons, or protons, for at the very large energies here involved the effect of a magnetic field is essentially the same upon them all."

But in a paper in the Physical Review [**63**, 234 (1943)] we incorrectly stated (see page 245): "If, then, the transformation of rest mass energy in the case of the helium atom gave rise to a pair of protons rather than a pair of electrons, then the latitude of first entrance of these helium annihilation rays would be considerably north of Saskatoon instead of at mag. lat. 54 N computed from the Lemaitre-Vallarta curves as the first latitude of entrance of helium annihilation rays on the assumption that the whole rest mass of the helium is transferred into an *electron* pair."

In a subsequent article found in the same journal [Phys. Rev. **66**, 295, reference 1 (1944)] this last statement was corrected, as follows: "The only choice is between an electron pair and a proton pair, but the difference between the latitude of entrance of electrons and protons entering the earth's magnetic field from this mode of origin is in no case, not even in the case of He annihilation rays, large enough to be detected with the resolving power of the experimental techniques we have so far used."

In other words, we here corrected the contradiction between the two statements made in the 1942 and 1943 articles, reaffirming the validity of the 1942 statement and admitting our slip in the 1943 statement after recomputing the latitude of entrance of protons and finding it, within the limits of our observational uncertainty, the same as the latitude of entrance of electrons.

Further, Dr. Dana T. Warren in an article in Phys. Rev. **66**, 252 (1944) also called attention to the contradictory character of our two statements and made essentially the same computations which Mr. Turner has herein made and reached a conclusion identical with his. Therefore it is probably desirable now to emphasize the fact that there is no disagreement by anybody on the point here involved.

Microwave Spectra of Linear Molecules

C. H. Townes, A. N. Holden, and F. R. Merritt
Bell Telephone Laboratories, Murray Hill, New Jersey
July 24, 1947

Work on the spectra of certain linear molecules near 1.25-cm wave-length has continued in these laboratories. Some results not previously reported are described below.

The $O^{16}C^{12}S^{33}$ transition $J=1\rightarrow2$ has been found at 24020.3±0.1 Mc. The interval between this line and the $O^{16}C^{12}S^{32}$ line is 305.75±0.05 Mc. Combining this result with the value 594.59±0.04 obtained by others[1,2] for the interval between the $O^{16}C^{12}S^{32}$ and $O^{16}C^{12}S^{34}$ lines, one can compute the ratio of the mass differences $(S^{33}-S^{32})/(S^{34}-S^{32})$ to be 0.49985±0.0001. The result is only in fair agreement with the value 0.50038±0.0002 obtained from Mattauch.[3] This calculation assumes the quadrupole couplings for S^{33} and S^{34} (to be discussed below) are zero.

It should be pointed out that the inter-nuclear distances for the OCS molecule given by other workers[1,2] have not included the effects of zero-point vibrations, and that the actual errors for the inter-nuclear distance determinations

can be considerably greater than the quoted errors of about 0.005A. Because of the zero-point vibrations, the average bond distances in isotopic molecules may not be the same, and this shift in bond length due to difference in isotopic mass must be known and accounted for before microwave data on moments of inertia can give very accurate values for inter-nuclear distances. The effect of the zero bending-mode vibration on average moment of inertia has been obtained in this laboratory by measurement of the rotation transition $J=1\rightarrow 2$ for OCS molecules excited to the first bending mode ($v_2=1$). In standard notation, this effect may be expressed in terms of a parameter α_2, which has been found to be 10.6 Mc, and its presence produces a correction of about 0.03A in the inter-nuclear distances. Corrections for the other modes of vibration are of the opposite sign, and hence may largely compensate the effect of the bending mode, but until these corrections are known they result in considerable uncertainty in determination of inter-nuclear distance from microwave data. On the other hand, for the intervals between the lines of OCS^{32}, OCS^{33}, and OCS^{34}, the corrections are to a good approximation proportional to the change in mass of the sulphur atom, so that with accurate measurements of the intervals, the ratio of mass differences $(S^{33}-S^{32})/(S^{34}-S^{32})$ may be obtained to an accuracy of about one part in ten thousand without an exact knowledge of the corrections for zero-point vibrations.

Quadrupole splittings of the OCS^{34} and OCS^{33} lines were looked for, but no splitting was found. This means that the S^{34} quadrupole coupling cannot be greater than 1 Mc, or estimating the derivative of the electric field at the nucleus, $\partial^2 V/\partial z^2$, by the method previously described,[4] the S^{34} quadrupole moment must be less than 0.001×10^{-24}. Since this is extremely small (sixty times smaller than the moments of the nuclei of similar size Cl^{35} and Cl^{37}) it seems likely that the spin of S^{34} is zero which necessitates a quadrupole moment equal exactly to zero. Although the OCS^{33} line is very weak because of the low abundance (0.78 percent) of S^{33}, it was probably observed sufficiently well to rule out the possibility of a quadrupole coupling greater than 5 Mc for S^{33}. By reasoning similar to that applied to S^{34}, it seems likely that the S^{33} spin is $\frac{1}{2}$, making the quadrupole moment zero of necessity.

Quadrupole effects due to C^{13} were also looked for in the $O^{16}C^{13}S^{32}$ line found at 24,248.1±0.3 Mc, and in the $Cl^{35}C^{13}N^{14}$ transition $J=1\rightarrow 2$. No quadrupole effect was found; the quadrupole coupling in these cases must be less than 0.5 Mc. This is, as in the case of the sulphurs, a good indication that the C^{13} spin is $\frac{1}{2}$, and agrees with the C^{13} spin determination from band spectra announced by Jenkins[5] shortly after these measurements were made.

A set of eleven lines due to $Cl^{35}C^{12}N^{14}$ molecules in the excited bending mode of vibration were found. They are fitted nicely by assuming the same spin and quadrupole coupling for Cl^{35} as previously given. The energy levels follow the formula for symmetric top molecules with $K=1$, since an angular momentum along the molecular axis is present in these excited molecules.

The excited state ClCN lines of course show l-type doubling as did those for BrCN. Table I lists frequency difference between the two sets of lines produced by l-type doubling in the 1.25-cm region for these molecules and for OCS. It may be noted that the experimental splitting is consistently larger by 40 percent than the theoretical values. Dr. J. Bardeen has pointed out to us that the theory of Nielsen and Shaffer[6] needs to be corrected by dividing by a factor of two, and the theoretical values are given after making this correction.

TABLE I. l-type doubling values.

Molecule	Measurement	Theory
OCS	25.6 Mc	18.7 Mc
ClCN	34.8 Mc	24.0 Mc
BrCN	24.6 Mc	18.2 Mc

[1] T. W. Dakin, W. E. Good, and D. K. Coles, Phys. Rev. 71, 640 (1947).
[2] R. E. Hillger, Washington meeting Am. Phys. Soc., paper B6 (1947). These authors pointed out the zero-vibration errors in oral presentation of their paper.
[3] J. Mattauch, *Nuclear Physics Tables* (Interscience Publishers, Inc., New York, 1946), p. 128.
[4] C. H. Townes, Phys. Rev. 71, 909 (1947).
[5] F. A. Jenkins, Washington meeting Am. Phys. Soc., paper L12 (1947).
[6] H. H. Nielsen and W. H. Shaffer, J. Chem. Phys. 11, 140 (1943).

Calculation of the Shear Elastic Constants of the Alkali Halides

W. J. PRICE
Rensselaer Polytechnic Institute, Troy, New York
July 31, 1947

THE shear elastic constants for copper and certain of the alkali metals have been calculated by Fuchs[1] from theoretical considerations. We report here the results of a similar calculation of these constants for several alkali halides. The shear elastic constants are determined primarily by changes in the Coulomb energy and in the non-Coulomb ion-ion exchange interaction energy.

The two shear elastic constants for cubic crystals are $C_{11}-C_{12}$ and C_{44}. For a NaCl type of lattice the electrostatic contributions to these constants arise (1) from the interaction of each ion with the face-centered cubic lattice of ions of the same sign and (2) from the interaction of each ion with the lattice of ions of opposite sign. These contributions have been evaluated in Table I in units of e^2/δ per molecule, where e is the electronic charge and δ is the lattice constant. Column 1 shows the contribution from the ions of like sign as calculated by Fuchs,[1] column 2 shows the contribution of the unlike ions which we have calculated, and column 3 shows the total electrostatic contribution. The calculations are based on the Ewald method[2] of treating electrostatic energy of the lattice.

For the ion-ion interaction the nearest neighbors and the next nearest neighbors have been considered, using a

TABLE I. Electrostatic contribution to the shear elastic constants of the alkali halides in units of e^2/δ per molecule.

	Like ions[3]	Unlike ions	Sum
$C_{11}-C_{12}$	0.2115	−5.525	−5.31
C_{44}	0.9479	1.60	2.55

repulsive term of the Born-Mayer type. The contribution of the more remote ions is negligible. The ionic radii determined by Huggins and Mayer[3] have been used. A van der Waal attractive term has also been included.

The calculated and the observed shear elastic constants of four alkali halides are shown in Table II. The agreement

TABLE II. Shear elastic constants in units of 10^{11} dyne cm^{-2}.

	Elastic constants	Ion core interaction: Coulomb contribution	Repulsive term	Van der Waal term	Sum	Observed room temperature
NaCl[6]	$C_{11}-C_{12}$	−4.80	7.05	−0.21	2.04	3.62
	C_{44}	2.31	−0.49	−0.008	1.81	1.26
KBr[6]	$C_{11}-C_{12}$	−2.55	5.38	−0.24	2.59	2.91
	C_{44}	1.24	−0.49	0.021	0.77	0.508
KI[7]	$C_{11}-C_{12}$	−1.95	4.32	−0.18	2.19	2.25
	C_{44}	0.94	−0.34	0.011	0.61	0.426
KCl[7]	$C_{11}-C_{12}$	−3.10	6.01	−0.29	2.62	2.89
	C_{44}	1.49	−0.60	0.026	0.92	0.787

is not as good as obtained by Fuchs for the alkali metals. It is significant that the contribution of the repulsive term is large here, while in the alkali metals it is in no case greater than and is often much less than ten percent of the total. In LiFl where, because of the relatively small lattice constant of the material, the repulsive term is quite large, the calculated constants were quite unsatisfactory, even resulting in a negative value for $C_{11}-C_{12}$.

The results are very sensitive to the type of the repulsive energy term chosen. If the Born-Mayer type repulsive term is replaced by the results of Landshoff's quantum-mechanical calculation[4,5] of the ionic exchange forces in NaCl, the shear elastic constants in column 2, of Table III

TABLE III. Shear elastic constants of NaCl in units of 10^{11} dyne cm^{-2}.

Elastic constant	Calculated: Using Born-Mayer repulsive term	Using Landshoff repulsive term	Using Landshoff repulsive and Coulomb correction	Observed: Room temperature	0°K Extrapolated
$C_{11}-C_{12}$	2.04	3.59	4.93	3.62[6]	5.0[8]
C_{44}	1.81	1.15	1.12	1.26[6]	1.3[8]

result. If also the term calculated by Landshoff for a correction of the Madelung form of the Coulomb energy is used, the constants in column 3 result. These results are in much better agreement with the observed values extrapolated to 0°K than are the values calculated by use of the Born-Mayer repulsive term. However, this agreement may be to some extent fortuitous, since Landshoff considered only nearest neighbors.

The writer wishes to express his appreciation to Dr. H. B. Huntington, who suggested the calculation, for his continued interest and helpful discussions.

[1] K. Fuchs, Proc. Roy. Soc. **A153**, 622 (1936); **A157**, 444 (1936).
[2] P. P. Ewald, Ann. d. Physik **64**, 253 (1921).
[3] M. L. Huggins and J. E. Mayer, J. Chem. Phys. **1**, 643 (1933).
[4] R. Landshoff, Zeits f. Physik **102**, 201 (1936).
[5] F. Seitz, *Modern Theory of Solids*, (McGraw-Hill Book Company, Inc., New York, 1940), p. 389.
[6] H. B. Huntington, Phys. Rev. **72**, 321 (1947).
[7] P. W. Bridgman, Proc. Am. Acad. **64**, 19 (1929).
[8] F. C. Rose, Phys. Rev. **49**, 50 (1936).

Nuclear Isomerism in Dysprosium 165*

M. G. INGHRAM, A. E. SHAW, D. C. HESS, JR., AND R. J. HAYDEN
Argonne National Laboratory, Chicago, Illinois
August 7, 1947

THE 1.25 min. *K*-converted gamma-dysprosium activity, produced by slow neutron irradiation of dysprosium, was first reported by Flammersfeld.[1] He concluded that this activity was probably due to an excited state of dysprosium 163. In order to obtain a direct mass assignment of this activity, we irradiated dysprosium isotopes which had been separated with a Dempster-type[2] mass spectrograph employing a high intensity thermal—ion source. The usual photographic plate was replaced by a thin beryllium sheet upon which the isotopes were collected. The separate isotopes showed as visible deposits on the beryllium sheet which was then cut into strips, each of which contained only one isotope. The strips were then individually irradiated for two minutes with slow neutrons in the Argonne heavy-water pile after which the induced activities were followed with a thin-window Geiger-Müller counter. Only the Dy^{164} strip showed appreciable activity above that due to impurities in the beryllium. The activity in other cases is due to the beryllium backing of the deposits. The results are shown in Fig. 1. The upper solid curve shows the decay of the Dy^{164} activity. The lower solid curve is representative of the decay at all other mass positions. In the case of Dy^{164}, the induced activity was larger by a factor of 15 than that induced in any other isotope. As is shown by the dashed lines in Fig. 1, this activity can be resolved into 1.25-minute and 2.6-hour

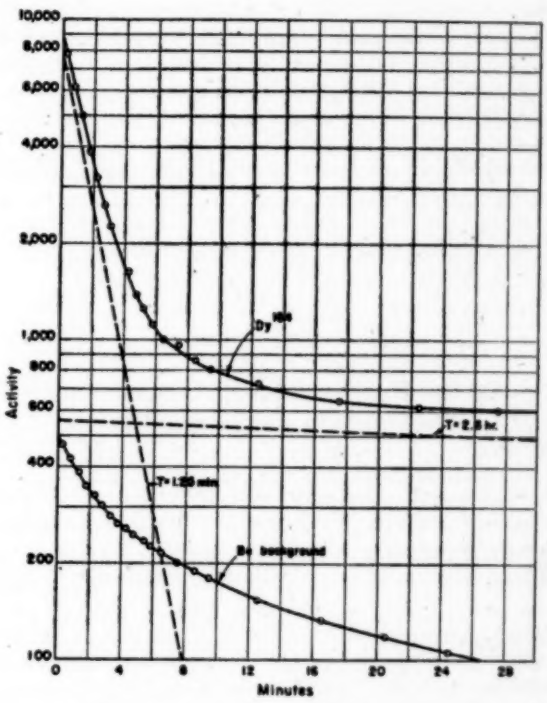

FIG. 1. Decay curves showing (n, γ) induced activity on separated dysprosium samples.

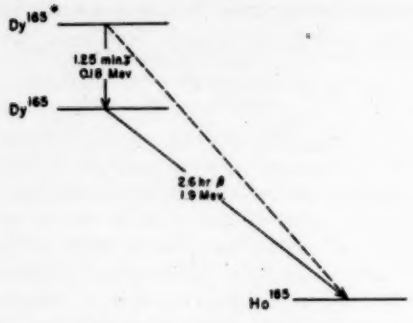

FIG. 2. Energy-level diagram for Dy^{165}.

components. The 2.6-hour activity was previously shown by a different technique[3] to be due to Dy^{165}. The present result shows that both the 1.25-minute and the 2.6-hour activities are produced by neutron irradiation of Dy^{164}, and since the ratio of 1.25-minute to 2.6-hour activities was the same with and without cadmium shielding, the short-lived activity must also have been induced by the slow neutrons in the pile. Thus the 1.25-minute activity must have been formed by an (n, γ) reaction on Dy^{164}, and thus be isomeric with the 2.6-hour activity.

The energy-level diagram for these activities is shown in Fig. 2. Decay curves of activated dysprosium, corrected for the variation of counter efficiency with energy, show that the cross sections for formation of the 1.25-minute and 2.6-hour activities are approximately equal. Thus it appears probable that only the higher excited state of Dy^{165} is formed directly in the (n, γ) reaction on Dy^{164}. If this is the case, the growth of the 2.6-hour activity after a very short bombardment should be observed. Flammersfeld looked for but did not observe this growth. A possible explanation for his negative result is that the higher excited Dy^{164} nucleus emits a beta-particle and transforms directly to Ho^{165}. The emission of one of these betas to every 100 gammas would explain Flammersfeld's results.

* This document is based on work performed under Contract No. W-31-109-eng-38 for the Atomic Energy Project at the Argonne National Laboratory.

[1] A. Flammersfeld, Zeits. f. Naturforschung 1, 190 (1946).
[2] A. J. Dempster, Proc. Am. Phil. Soc. 75, 755 (1935).
[3] Inghram, Hayden, and Hess, Phys. Rev. 71, 270 (1947).

On the Normalization of Characteristic Differentials in Continuous Spectra

AUREL WINTNER
Department of Mathematics, The Johns Hopkins University, Baltimore, Maryland

July 24, 1947

FROM the point of view of explicit determinations, the normalization of characteristic differentials in continuous spectra is one of the most delicate analytical questions in wave mechanics. In many cases, the asymptotic rule to be deduced below can be applied with little effort. What are actually needed are the spectral *densities*, but it will become clear at the end of the deduction that the asymptotic *differentiation* in question is legitimate.

The rule to be obtained is of the Stokes-Kelvin type, but is more explicit in nature. Its proof involves neither the complex machinery of the "steepest descent" nor the principle of stationary phases (Kramers). Correspondingly, nothing like the solution of the wave equation in terms of a definite integral is assumed.

If the energy level is fixed within the "elliptic," or "stable," range of the potential, both the one-dimensional and the radial Schrödinger equations are of the form

$$\psi''+f^2\psi=0, \tag{1}$$

where the primes denote differentiations with respect to the independent variable, say r, and $f=f(r)$ is a given positive function of r. Suppose that f has first and second derivatives which, as $r\to\infty$, satisfy the following restriction:

$$\int^\infty |(f'/f^{\frac{1}{2}})'/f^{\frac{1}{2}}|dr<\infty. \quad (f>0). \tag{2}$$

For instance, if $(f'/f^{\frac{1}{2}})'$ does not change its sign from a certain r onward (which is certain to be the case if f is composed of a finite number of exponentials and powers of r), and if

$$|f'|/f^2<\text{const.} \quad \text{and} \quad \int^\infty f'^2/f^3dr<\infty, \tag{3}$$

then a partial integration shows that (2) must be satisfied. Clearly, (3) is fulfilled by $f=e^r$ and, if $\alpha>-1$, by $f=r^\alpha$. Thus, if f is regular enough, the "frequency" of (1) can be arbitrarily high (as $r\to\infty$), and it can be quite low (with $f(r)\to 0$), though not arbitrarily low.

In any case, the general solution of (1) is supplied by the real and imaginary parts of a constant multiple of a particular solution having the asymptotic form

$$\psi(r)\sim\{f(r)\}^{-\frac{1}{2}}\exp\left\{i\int^r f(q)dq\right\}, \tag{4}$$

where $r\to\infty$. In fact, this holds if only condition (2) is stipulated. In (4), the choice of the lower limit of integration is immaterial, for, if the lower limit is changed, the solution ψ is replaced by a constant multiple of ψ.

Since the real and imaginary parts of (4) represent two linearly independent solutions of (1), it is clear that all solutions of (1) remain bounded if and only if $f(r)$ keeps away from 0, as $r\to\infty$; and that *all* solutions of (1) are capable of the quantum-mechanical normalization $\int|\psi(r)|^2dr=1$ if and only if

$$\int^\infty \{f(r)\}^{-1}dr<\infty$$

holds (the latter contingency represents the physically *degenerate* phenomenon of a "limiting circle"). In the example of Bessel's functions, which belong to $f=r^\alpha$ in (1), these two cases are seen to be characterized by $\alpha\geqq 0$ and $\alpha>1$, respectively, whereas the requirement of (2) was just $\alpha>-1$.

In order to prove that (1) possess a solution $\psi=\psi(r)$ satisfying (4), it is sufficient to apply the method of variation of constants, by placing $\psi=\phi/f^{\frac{1}{2}}$. An easy calculation shows that this substitution transforms (1) into

$$d^2\phi/ds^2+(1+F)\phi=0, \tag{5}$$

where the new independent variable is

$$s=s(r)=\int^{r} f(q)dq, \quad (f>0), \tag{6}$$

and the coefficient $F=F(s)$ in (5) is the function[1]

$$F=\tfrac{5}{16}f'^2/f^4-\tfrac{1}{4}f''/f^3. \tag{7}$$

It is understood that $f=f(r)$ and its derivatives with respect to r must, in (7), be expressed as functions of s by means of the inverse of the substitution (6).

Suppose that $r=\infty$ corresponds to $s=\infty$, i.e., that the integral defined by (6) is divergent (otherwise the situation is quite trivial). Then (6) shows that

$$\int^{\infty} |F|ds<\infty \tag{8}$$

holds if and only if

$$\int^{\infty} |F|fdr<\infty \tag{9}$$

does. On the other hand, it is readily verified from (7) that (9) is equivalent to (2). Hence, (2) means that (8) is satisfied.

It is known[2] that, if F is any continuous function satisfying (8), then $\phi(s)-\phi_0(s)\to 0$ and $d(\phi-\phi_0)/ds\to 0$, as $s\to\infty$, is a pair of asymptotic requirements which establishes a one-to-one correspondence between the solutions, $\phi=\phi(s)$, of (5) and the solutions, $\phi_0=\phi_0(s)$, of the trivial approximation, $(d^2\phi_0/ds^2)+\phi_0=0$, to (5). Since this trivial differential equation admits of the solution $\phi_0(s)=e^{is}$, it follows that (5) has a solution satisfying the limit relation $\phi(s)/e^{is}\to 1$, where $s\to\infty$. Finally, it is seen from (6) that this limit relation is equivalent to (4) by virtue of the definition, $\psi=\phi/f^{\frac{1}{4}}$, of ϕ.

[1] The transformations applied to (1) can be interpreted as an adaptation of Liouville's substitution (as to the latter, see, e.g., E. L. Ince, *Ordinary Differential Equations* (Longmans Green, and Company, London, 1927), pp. 270–271).

[2] The result quoted is due to M. Bôcher, Trans. Am. Math. Soc. 1, 40 (1900). Today it has more than one proof very primitive in nature (see, for example, H. Weyl, *The Theory of Groups and Quantum Mechanics* (Methuen and Company, Ltd., London, 1931), pp. 71–73).

The Isotopic Composition of Normal Krypton and Xenon

M. Lounsbury, S. Epstein, and H. G. Thode
Department of Chemistry, McMaster University, Hamilton, Ontario, Canada
June 3, 1947

RECENTLY a mass-spectrometer investigation of the isotopes of krypton and xenon resulting from the fission of uranium-235 by thermal neutrons was reported.[1] This investigation was carried out with a 180°-deflection Nier-type mass spectrometer.[2] In the course of a parallel investigation with a 90°-deflection sector-type instrument,[3] it was discovered that the measured abundance of krypton 80 in normal krypton was 10 percent greater than the value previously reported by Nier.[4] Because of this discrepancy, it was decided to make a careful investigation of the isotopic composition of normal krypton and xenon. An automatic ion-current recording unit,[5] which increases the precision of isotopic-abundance measurements, was used in this work.

Various possible systematic errors which might arise from resolution difficulties, mass discrimination, ion-current discrimination, or secondary electron emission from the collector plate were investigated. These errors in the isotopic abundances were found to be less than one percent under our operating conditions. The purified gas samples were free from contamination, and there was no evidence of isotopic fractionation either during the course of sample preparation or during the passage of the gas through the capillary leak into the mass spectrometer tube.

Results for Krypton

Abundance data obtained from twenty recorded mass spectrograms of normal krypton using the 90° mass spectrometer and from ten such spectrograms using the 180° instrument are presented in Table I, along with the earlier data of Nier.[4]

TABLE I. Isotopic composition of normal krypton.

	90° M.S.		180° M.S.		Nier*
Mass unit	Abundance (percent)	Mean deviation	Abundance (percent)	Mean deviation	Abundance (percent)
78	0.343	±0.003	0.341	±0.0003	0.35
80	2.223	±0.009	2.223	±0.002	2.01
82	11.510	±0.040	11.490	±0.010	11.53
83	11.490	±0.030	11.470	±0.020	11.53
84	57.000	±0.090	57.040	±0.040	57.10
86	17.420	±0.030	17.440	±0.030	17.47

* See reference 4.

From this table it may be seen that the abundance data for krypton 80 from the present investigation is greater by ten percent than the value reported by Nier. Considering the good agreement between our 90° and 180° data, it would appear that Nier's value must have been in error. This fact was brought to the attention of Professor Nier, who found, on returning to his original records of 1937, that he had used the wrong shunt factor in computing the background correction for krypton 80.[6] In Table II is presented the average of our 90° and 180° mass spectrometer abundance data for normal krypton, along with the corrected data of Nier.[6] Table II gives the final results on the isotopic abundance of normal krypton.

TABLE II. Isotopic composition of normal krypton.

Mass unit	Present data (average) abundance (percent)	Nier's corrected data** abundance (percent)
78	0.342	0.346
80	2.228	2.261
82	11.500	11.500
83	11.480	11.500
84	57.020	56.950
86	17.430	17.430

** See reference 6.

From this table, the good agreement between Nier's corrected values and our abundance data for krypton 82, 83, 84, and 86 is evident. However, in the case of krypton 78 and 80, a discrepancy of about one percent is noted.

Results for Xenon

Abundance data from six complete recorded mass spectrograms of normal xenon using the 180° mass spectrometer are presented in Table III, in which Nier's earlier data are also included.[4]

TABLE III. Isotopic composition of normal xenon.

Mass unit	Present data (180° M.S.) Abundance (percent)	Mean deviation	Nier's data*** abundance (percent)
124	0.095	±0.001	0.094
126	0.088	±0.001	0.088
128	1.917	±0.006	1.900
129	26.240	±0.080	26.230
130	4.053	±0.005	4.070
131	21.240	±0.030	21.170
132	26.930	±0.020	26.960
134	10.520	±0.020	10.540
136	8.930	±0.030	8.950

*** See reference 4.

The agreement between our results for xenon and those previously obtained by Nier is quite within the limits of accuracy claimed.

The authors are indebted to Dr. F. P. Lossing and Mr. R. B. Shields for assistance with the electronic units of the recorder and the mass spectrometers. The financial assistance of the National Research Council of Canada is gratefully acknowledged.

[1] Thode and Graham, Can. J. Research **A25**, 1 (1947).
[2] Thode, Graham, and Ziegler, Can. J. Research **B23**, 40 (1945).
[3] Graham, Harkness, and Thode, J. Sci. Inst. **24**, 119 (1947).
[4] Nier, Phys. Rev. **52**, 933 (1937).
[5] Lossing, Shields, and Thode, Can. J. Research, in press.
[6] Private communication from A. O. C. Nier, April 2, 1947.

Note on the Barometric Coefficient of Cosmic-Ray Intensity

M. KIDNAPILLAI
Department of Mathematics, Ceylon Technical College, Colombo, Ceylon
August 7, 1947

AN analysis of the observations on cosmic-ray intensity was made by Duperier[1] in London to find the connection between surface pressure and cosmic-ray intensity. The high correlation coefficient of -0.87 was obtained between the hourly numbers of cosmic particles, averaged in groups of 24 hours, and the barograph readings at the station averaged over the same time intervals. It was also found that the barometric coefficient β, represented by the slope of the corresponding regression line, was 3.45 percent per cm mercury. The effects of absorption and decay have been separated by expressing the relation between the number of cosmic particles at ground level (N), the barograph reading at the station (B), and the height of the pressure level at which mesons are generated, (H), in the form

$$N-N_m=\mu(B-B_m)+\mu'(H-H_m),$$

where the subscript m refers to mean values μ represents the true absorption coefficient in air, and μ' the mean rate of decay of mesons. The true absorption coefficient in air was found to be 2.28 percent per cm mercury and the mean rate of decay of mesons 5.4 percent per km.

The purpose of the present note is to show that it is possible to find the value of the barometric coefficient by another method. We consider the effects of absorption and decay separately and shall first investigate the variation due to decay. Penner has analyzed the variations of pressure at different levels over Sault Ste. Marie, Michigan, and a diagram showing the variations is reproduced in Haurwitz's book.[2] The conditions over Europe and North America are similar, and Penner's diagram may be regarded as representative for the north temperature latitudes in general. We take the meson-producing layer to be at a height of 16 km corresponding to 75-mm pressure. It is seen from Penner's diagram that the pressure at 16 km rises by 1 mb when the pressure at the ground level rises by 4 mb. The isobar corresponding to 75-mm pressure rises through a height $\delta p/g\rho$, where δp is the rise in pressure at 16 km and ρ is the density of air at that height. Hence when the pressure at 16 km rises by 1 mb, the isobar corresponding to 75-mm pressure rises through 52 meters.

The mean free path (decay) of mesons (L) is related to the lifetime of mesons at rest, τ_0, by the well-known equation $L=E\tau_0/cM$, where M is the rest mass and E the energy of the mesons. If we assume that the mesons have a mean energy of 3×10^9 ev and take M equal to 200 times the mass of an electron and τ_0 equal to 2×10^{-6} sec. (Wilson),[3] we have $L=18$ km. If N_0 is the number of cosmic particles at 16 km, we see that $N_m=N_0e^{-16/18}$. When the pressure level at which mesons are produced rises through 52 meters, $N=N_0e^{-16.05/18}$, and the percentage variation is $(N-N_m)/N_m\times100$, or neglecting the negative sign, 0.28 percent. Hence, we infer that the percentage variation per cm of mercury is 0.92. The variation of cosmic-ray intensity due to true absorption can be deduced from the measurements by Ehmert[4] of the absorption curve in water, and is estimated by Duperier to be 1.65×10^{-3} cm^2/g or 2.24 percent per cm of mercury. Therefore, the barometric coefficient is 3.16 percent per cm of mercury which is in good agreement with the value of 3.45 percent per cm of mercury obtained by Duperier.

[1] A. Duperier, Nature **153**, 529 (1944).
[2] B. Haurwitz, *Dynamic Meteorology* (1941).
[3] J. G. Wilson, Science Progress **35**, 137 (1947).
[4] Ehmert, Zeits. f. Physik **106**, 751 (1937).

H^3 and the Mass of the Neutrino

EMIL J. KONOPINSKI
Indiana University, Bloomington, Indiana
July 28, 1947

THE maximum energy of the β-particles from H^3 has most recently[1] been reported as 11 ± 2 kev. The unusually low energy of this β-spectrum makes it extremely sensitive as an indicator of a non-vanishing rest mass for the neutrino. Coupled with measurements of the H^3 half-life, it shows that the neutrino cannot have a mass greater than 2 to 3 percent of the electron's rest mass. Moreover, the H^3 decay rate as presently known seems 6 to 10 times too rapid in comparison with that of heavier elements unless the neutrino is attributed a finite mass of the magnitude mentioned.

The relation[2] between the half-life t and the maximum energy E_0 (in units of mc^2; here $E_0=0.021_5$) is such that the product $[|M|^2f(E_0)]$ should be the same for all allowed β-transitions. $|M|^2$ is the so-called "nuclear matrix element" which measures the overlapping of the states

connected by the transition. The function $f(E_0)$ is essentially the integral over the well-known statistical distribution of the energy between the electron and the neutrino:

$$f(E_0)=\int_0^{E_0} dE(1+E)(2E+E^2)^{\frac{1}{2}} \times(E_0+\mu-E)(E_0-E)^2(2\mu+E_0-E)^{\frac{1}{2}}.$$

Here μ is the ratio of the neutrino rest mass to that of the electron.

We compare H^3 with He^6, which may be regarded for our purposes as a fair representative of the allowed β-emitters. It has a half-life $t(He^6)=0.8$ sec. and an energy $E_0(He^6)=7.25$. The large energy makes μ negligible in the evaluation[2] of $f(He^6)=1200$. $|M|^2$ is expected[2] to have the value 6 for He^6, so that we have for the resulting product:

$$|M|^2ft=5760 \text{ sec.} \quad (He^6).$$

One gets[2] about this value for most of the allowed transitions.

The published[3] half-life of H^3 is about 30 years. Taking into account experimental uncertainties, it may easily be as low as 20 years. We calculate for both these values. $|M|^2=3$ is expected[2] for H^3. If the neutrino is assumed to have no rest mass, $f(H^3)\approx 0.216E_0^{7/2}=3.2\times10^{-7}$. This yields:

$$|M|^2ft\approx 600 \text{ sec.} \quad (H^3;\ \mu=0;\ t=20 \text{ y.}),$$
$$|M|^2ft\approx 900 \text{ sec.} \quad (H^3;\ \mu=0;\ t=30 \text{ y.}).$$

Either result is far too small; with its low energy, H^3 should have a half-life of $\sim$200 y. on the basis of a neutrino without rest mass.

We now determine a neutrino rest mass μm so that H^3 will also yield $|M|^2ft\approx 5700$. If

$$E_0<\mu<1, \quad f\approx(\pi/4)\mu^2E_0^2[1+(5E_0/8\mu)+\cdots].$$

We obtain $\mu\approx 1/30$ for $t=20$ y. and $\mu\approx 1/45$ for $t=30$ y. Thus a neutrino mass can account for a discrepancy of a factor 10 in the H^3 half-life.

Attention should be directed to the simplicity of the theory on which this determination of the neutrino rest mass is based. Aside from the relatively unimportant factor of 2 arising from the comparison of $|M|^2$, the only theoretical assumption needed was that the electron and neutrino share their energy according to the simple statistical formula which yields the function f.

[1] R. J. Watts and D. Williams, Phys. Rev. **70**, 640 (1946).
[2] E. J. Konopinski, Rev. Mod. Phys. **15**, 209 (1943).
[3] R. D. O'Neal and M. Goldhaber, Phys. Rev. **58**, 574 (1940).

On the Magnetic Field of the Milky Way and Its Effect on Cosmic Radiation

MANUEL S. VALLARTA
Instituto de Física, Universidad de México, México
July 29, 1947

IT was discovered by H. W. Babcock[1] that early-type stars possess very high magnetic fields, corresponding to magnetic moments of the order of 10^{37} gauss-cm^3, and that for stars of approximately the same mass the magnetic field is proportional to the angular momentum. On the assumption that this relation is applicable to a galaxy, he calculates a dipole moment of 10^{39} gauss-cm^3 for the Andromeda nebula (Messier 31) and concludes that "this should apply almost as readily to our galaxy as to the Andromeda nebula."

The purpose of this note is to point out that, so long as the condition of weak magnetic coupling among the stars of a galaxy still obtains, stellar dipole moments are still oriented at random and the resultant field of the galaxy almost vanishes. Under these conditions the considerations developed by Vallarta and Feynman[2] still hold and no effect on an isotropic distribution of charged cosmic rays entering the galaxy from the outside can be expected. Taking into account the order of magnitude of interstellar distances within the galaxy, it can be readily shown that even with stellar dipole moments as high as 10^{38} gauss-cm^3 the condition of weak coupling still prevails.

If high enough stellar magnetic fields are found within our galaxy to insure strong coupling among them, and a resultant galactic field, then observable effects on the intensity of cosmic radiation might well result. Some of the difficulties connected with the explanation of the diurnal and seasonal variations of intensity through the agency of the solar magnetic field alone might then disappear.[3] No galactic magnetic effect can be expected, however, as long as the condition of weak coupling among the stars of a galaxy still holds.

[1] H. D. Babcock, Astrophys. J. **105**, 105 (1947); Phys. Rev. **72**, 83 (1947).
[2] M. S. Vallarta and R. P. Feynman, Phys. Rev. **55**, 506 (1939).
[3] M. S. Vallarta and O. Godart, Rev. Mod. Phys. **11**, 180 (1939); B. Rossi, Cosmic Ray Conference, New York, April 1947.

Calculation of the Interaction between Two Particles from the Asymptotic Phase

CARL-ERIK FRÖBERG
Institute for Mechanics and Mathematical Physics, University of Lund, Lund, Sweden
July 30, 1947

AS is well known, the asymptotic phase of a wave function can be calculated from the potential function. It seems to be of some interest to examine whether the reverse is also true, i.e., whether the potential can be calculated from the asymptotic phase. We shall show that this is possible, at least formally. Questions of convergence will not be taken into consideration.

In the case of elastic scattering the following reduced form of the Schrödinger equation is valid, ψ, being the radial part of the eigenfunction and $u=r\cdot\psi$,

$$\frac{d^2u}{dr^2}+k^2u-\frac{l(l+1)}{r^2}u=-V(r)u. \tag{1}$$

If $V(r)\to 0$ sufficiently rapidly, e.g., as r^{-2} or stronger, as $r\to\infty$, we have the asymptotic solution $u\sim\sin(kr-\frac{1}{2}l\pi+\delta)$, where δ is the phase. Then we get

$$k\sin\delta(k)=\int_0^\infty u_0V(r)u\,dr, \tag{2}$$

where u_0 is the solution for $V=0$ which is regular in the origin, thus

$$u_0=(\tfrac{1}{2}\pi kr)^{\frac{1}{2}}J_{l+\frac{1}{2}}(kr). \tag{3}$$

Now u can be expanded in a series the first term of which is u_0, as follows

$$u=u_0+\sum_{n=1}^{\infty}k^{-n}\cdot\int_0^r dr_n\cdot\int_0^{r_n}dr_{n-1}\cdots\int_0^{r_2}dr_1 \cdot V(r_1)\cdot V(r_2)\cdots V(r_n) \cdot K(r_n,r)K(r_{n-1},r_n)\cdots K(r_1,r_2)u_0(kr_1), \quad (4)$$

where $K(r,s)=u_0(kr)\cdot v_0(ks)-u_0(ks)\cdot v_0(kr)$ and v_0 is defined by

$$v_0(z)=(-)^l\cdot(\tfrac{1}{2}\pi z)^{\frac{1}{2}}J_{-l-\frac{1}{2}}(z). \quad (5)$$

If all terms but u_0 are omitted in the first approximation and we put $f_0(k)=(d/dk)[k\sin\delta(k)]$, we obtain

$$f_0(k)=2\int_0^{\infty}u_0u_0'\cdot r\cdot V(r)\cdot dr. \quad (6)$$

The solution of this equation can be written in the form

$$V(r)=(8/\pi\cdot l!)\int_0^{\infty}k\cdot f_0(k)dk\cdot\int_0^1(ktr)^l \cdot(1-t^2)^l\cdot v_l(2ktr)\cdot dt. \quad (7)$$

Here v_l is identical with v_0 defined in (5).

In the case $l=0$ we have $v_l(z)=\cos z$ and thus

$$V(r)=8/\pi\int_0^{\infty}kf_0(k)dk\cdot\int_0^1\cos 2ktr\,dt =4/\pi\cdot\int_0^{\infty}f_0(k)(\sin 2kr/r)dk, \quad (8)$$

as can be obtained directly from the theory of Fourier integrals.

Formally it will be possible to continue to higher approximations. In doing so we do not change the form of the integral equation, only the function $f_0(k)$ will be modified.

A fuller account of the investigation will be presented in the Arkiv f. Mat., Astr. o. Fys., Stockholm.

I wish to express my gratitude to Professor W. Pauli, Zürich, for suggesting this investigation and for valuable discussions.

A Coincidence Study of Ga^{72}*

C. E. Mandeville and Morris Scherb
Bartol Research Foundation of the Franklin Institute, Swarthmore, Pennsylvania

July 31, 1947

BETA-GAMMA and gamma-gamma coincidences in the disintegration of radioactive Ga^{72} prepared in the Clinton pile have been reinvestigated[1] with the aid of two thin-walled Geiger counters, a coincidence circuit, and a scale of sixty-four. The details of the technique have been described in several publications.[2]

In the case of beta-gamma coincidences, measurements were extended to a beta-ray energy of 1.93 Mev, and all data were corrected for gamma-gamma coincidences, gamma-ray singles in the beta-ray counter, and accidental coincidences. The accidentals were determined by the expression

$$A=N_1N_2(K\tau),$$

where $K\tau$ was four microseconds. The coincidence arrangement was investigated with a strong beta-ray source to ascertain that no genuine coincidences were lost at the resolving time employed. The beta-gamma coincidences per beta-particle recorded in the beta-ray counter are plotted in Fig. 1 as a function of the thickness of aluminum absorber (wall thickness of the beta-ray counter included) between the thin source and the beta-ray counter. The genuine beta-gamma coincidences per beta-particle were observed to decrease from an extrapolated value of 1.63×10^{-3} at zero absorber thickness to 0.58×10^{-3} at a beta-ray energy of 0.72 Mev as determined by Sargent's equation.[3] The soft beta-ray spectrum of Ga^{72}, therefore, has a maximum energy of 0.72 Mev.

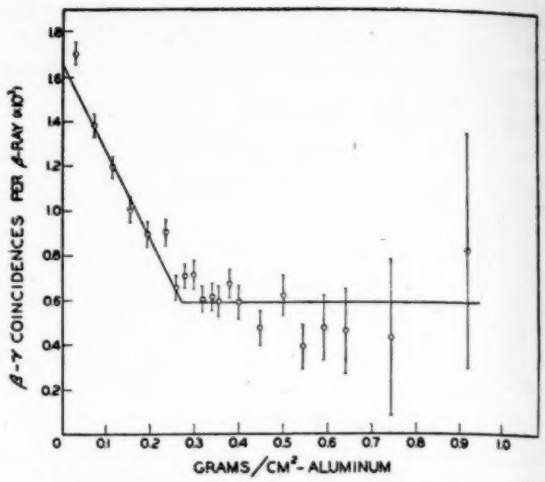

FIG. 1. Beta-gamma coincidences in the disintegration of radioactive gallium.

Gamma-gamma coincidences were observed to be $(0.84\pm0.10)\times10^{-3}$ per quantum recorded in the gamma-ray counter.

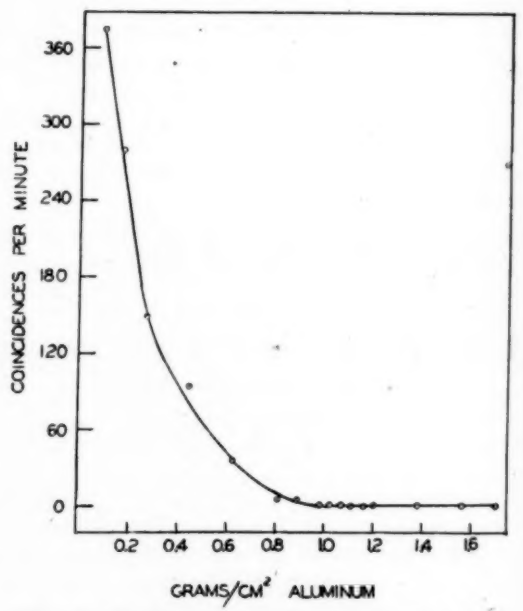

FIG. 2. Coincidence absorption of the Compton recoils of the gamma-rays from Ga^{72}.

The energy of the hard quanta emitted by Ga^{72} has been measured by semicircular focusing of Compton recoils,[4] photoelectric lines in a magnetic lens spectrometer,[5] photoneutron scattering cross section,[6] and coincidence absorption.[1] The values obtained were 2.65, 2.25, 2.50, and 2.4 Mev. The data for coincidence absorption of Compton recoils of the gamma-rays from radioactive gallium are given in Fig. 2. The end point taken from the curve is 1.00 g/cm². This corresponds to a quantum energy of 2.29 Mev.

* Supported by the Office of Naval Research.

[1] A. C. G. Mitchell, E. T. Jurney, and Margaret Ramsey, Phys. Rev. **71**, 324 (1947).
[3] L. M. Langer, A. C. G. Mitchell, and P. W. McDaniel, Phys. Rev. **56**, 422 (1939); J. V. Dunworth, Rev. Sci. Inst. **11**, 167 (1940); F. Norling, Arkiv. f. Mat. Astr. och Fysik **B27(3)**, 9 (1941).
[4] B. W. Sargent, Can. J. Research **17A**, 82 (1939).
[4] C. E. Mandeville, Phys. Rev. **64**, 147 (1943).
[5] L. C. Miller and L. F. Curtiss, Phys. Rev. **70**, 983 (1946).
[6] A. Wattenberg, Phys. Rev. **71**, 497 (1947).

PHYSICAL REVIEW VOLUME 72, NUMBER 6 SEPTEMBER 15, 1947

Proceedings of the American Physical Society

Minutes of the Meeting of the New England Section at Amherst, Massachusetts

May 31, 1947

THE twenty-eighth meeting of the New England Section of the American Physical Society was held at Fayerweather Laboratory of Physics of Amherst College in Amherst, Massachusetts, on Saturday, May 31, 1947. Ninety-seven members of the Section registered. The programme included a symposium of five invited papers on the subject of nuclear physics. There follow the titles of the invited papers and the abstracts of the ten-minute papers relating to research. Abstracts of ten-minute papers relating to the teaching of physics will appear in the American Journal of Physics.

GORDON F. HULL, JR.
Secretary-Treasurer

Symposium on Nuclear Physics

Invited Papers

Plans for Brookhaven National Laboratory, P. M. MORSE, *Brookhaven National Laboratory.*

Recent Results in Nuclear Magnetic Resonance Absorption, E. M. PURCELL, *Harvard University.*

Inelastic Scattering of Protons, C. B. COLLINS, *University of Rochester.*

Beta- and Gamma-Ray Level Schemes, M. D. DEUTSCH, *Massachusetts Institute of Technology.*

Proton Groups in Transmutations, E. POLLARD, *Yale University.*

Contributed Papers

1. The Calculation of Thermodynamic First Derivatives by use of Jacobians. F. H. CRAWFORD, *Williams College.*—Starting with the generalized Clausius equation for dU for a system of n degrees of freedom, it is possible to determine any desired first derivative directly in terms of a standard set of first derivatives. The procedure is essentially a generalization of results obtainable from a treatment given by Shaw[1] for the case of $n=2$. Maxwell's equations, $n(n-1)/2$ in number, are written in a concise Jacobian form. Then the desired derivative is expressed directly as a ratio of two nth-order Jacobians which involve partial derivatives of the dependent variables concerned with respect to a selected set of independent variables. Provided this set contains no conjugate pairs (i.e., such as T and S or p and V, etc.) the Jacobians involve only symmetric or anti-symmetric terms and are particularly simple to handle. It is shown that the number of independent first derivatives in the standard set for the general case is always $n(n+1)/2$. Thus for $n=2$ we have the well-known result that 3 first derivatives must be measured while for a single crystal of the least symmetric type under homogeneous strain, with $n=7$, the set contains 28 first derivatives.

[1] Shaw, Phil. Proc. Roy. Soc. (London) **A234** (1935).

2. Binding Energy of the Quadrielectron. AADNE ORE, *Yale University.*—An attempt has been made to determine the energy of a compound consisting of two electrons and two positrons with greater accuracy than in previous calculations. For this purpose a variational function has been used which is similar to the linear combination of "atomic" and "ionic" functions with adjustable screening constants taken by Weinbaum[1] to approximate the hydrogen molecule. Our function may be written $\Psi=\Psi_\beta+c\Psi_\alpha$ where Ψ_β is the generalized "atomic" function used previously,[2] whereas

$$2\Psi_\alpha=\exp-\tfrac{1}{2}[(1+\alpha)(r_{1a}+r_{2a})+(1-\alpha)(r_{1b}+r_{2b})]+\exp-\tfrac{1}{2}[(1-\alpha)(r_{1a}+r_{2a})+(1+\alpha)(r_{1b}+r_{2b})]+\exp-\tfrac{1}{2}[(1+\alpha)(r_{1a}+r_{1b})+(1-\alpha)(r_{2a}+r_{2b})]+\exp-\tfrac{1}{2}[(1-\alpha)(r_{1a}+r_{1b})+(1+\alpha)(r_{2a}+r_{2b})].$$

While Ψ_β alone yielded the value 0.11 ev for the binding

energy,[2] Ψ gives roughly 0.135 ev when $\alpha=\beta=(0.5)^{\frac{1}{2}}$ and $c=0.052$. In previous calculations considerable improvement in the energy of the quadrielectron could be obtained by slight improvement in the functions. Since this is no longer true we may be near the convergence limit.

[1] S. Weinbaum, J. Chem. Phys. 1, 593 (1933).
[2] E. A. Hylleraas and A. Ore, Phys. Rev. 71, 493 (1947).

3. Microwave Spectra of Several Polyatomic Molecules, B. P. DAILEY AND E. B. WILSON, JR.,[1] *Harvard University.*—The microwave spectrograph using Stark-effect modulation, recently described,[2] has been employed to study the absorption spectra in the region from 20,000 to 30,000 megacycles of a number of polyatomic molecules. For SO_2, lines were found at 20,421, 22,064, 22,225, 22,475, 22,735, 22,904, 22,934, 23,033, 23,419, 23,738, 24,037, 24,083, 24,342, 25,047, 25,170, 25,392, 26,550, 29,000. For nitromethane lines were found at 20,385, 23,250, 24,047, 24,320, 24,603, 25,400. A complex methanol spectrum was observed with lines at 20,898, 20,989, 21,551, 22,095, 23,033, 25,385, 24,040, 24,081, 24,317, 25,050, 24,928.8, 24,954.6, 25,017.8, 25,132.0, 25,300.3, 25,546, 25,796, 25,898, 26,310, 26,562, 23,121, 23,415, 23,450, 23,861, 26,854, 27,450, 28,550, 28,500, 29,950. Mr. R. H. Hughes and Mr. R. Karplus have aided greatly in the course of this investigation.

[1] The research reported in this document was made possible through support extended Harvard University jointly by the Navy Department (Office of Naval Research) and the Signal Corps, U. S. Army under Office of Naval Research, Contract N5ori-76.
[2] R. H. Hughes and E. B. Wilson, Jr., Phys. Rev. 71, 562 (1947).

4. New Techniques in the Measurement of the Capacity of the Electrical Double Layer, D. C. GRAHAME, *Amherst College.*—A minimum in the amplitude of a sinusoidal signal, whose intensity varies only slowly with time, can be timed with good precision by the use of a long-persistence oscilloscope screen punctuated by markers from a high speed electric clock. This fact has been used to improve the accuracy of a technique previously described for the measurement of the capacity of the electrical double layer between mercury and various electrolytic solutions. Circuits have been devised which permit measurement of this quantity with a consistency of 0.1 percent although the absolute accuracy may be a little less good and is limited by mechanical and chemical considerations rather than by the accuracy of the electrical circuits. The relatively high precision now obtainable makes it possible to measure with adequate accuracy the small changes of capacity accompanying changes of concentration, which in turn lead to thermodynamic information concerning the concentration of ions in the electrical double layer. It is found that in most cases positive ions accumulate in the double layer regardless of whether the metal is positively or negatively charged. Applications of this type of information to problems in several fields of science will be discussed.

5. Apparatus for the Study of Bridges and Arcs Between Metallic Contacts. G. F. HULL, JR., W. BAER, AND H. SALTZMAN, *Dartmouth College.**—When metallic contacts carrying a current are separated, the contact may be bridged by a very small globule of metal or an arc may be formed. The metallic bridges under observation vary from 10^{-4} to 10^{-3} cm in length. For investigating bridges in air a cantilever bar[1] is used for producing the required contact separations, while for studying their properties in vacuum, the contact electrodes are mounted inside a cylinder, part of which is a sylphon bellows. One end of the cylinder can be moved with a micrometer screw coupled to a 10 to 1 reduction gear. Contact separations of 10^{-4} cm can be produced. To study transient arcs in air between separating contacts, a lever is used. This lever can be displaced by means of a micrometer screw producing contact separations of 3×10^{-4} cm, or by means of a motor-driven cam, which gives constant velocity of separation of the contact. A commutator with adjustable brushes is attached to the cam to synchronize the transient arc currents and voltages with the sweep of an oscillograph.

* Assisted by the Office of Naval Research under Contract N6ori-219.
[1] G. F. Hull, Jr., Rev. Sci. Inst. 15, 340 (1944).

6. The Vacuum Properties of Some Synthetic Dielectrics. BENJAMIN G. HOGG, *Wesleyan University.*—An investigation has been carried out to determine the vacuum properties of some of the more recently developed dielectrics. Among these dielectrics are a number of plastics. An ionization-gauge method was used similar to that described by Zabel.[1] The research was initiated to determine the suitability of these new materials for use in the vacuum system of a mass spectrograph now under construction at Wesleyan University. The result should prove useful as a guide in the selection of materials when high vacuum is desired.

[1] R. M. Zabel, Rev. Sci. Inst. 4, 233 (1933).

7. Use of Magnetic Amplifiers in Computing Circuits.* ROBERT T. BEYER, *Brown University.*—Magnetic amplifiers have been designed with matched pairs of Permalloy-core transformers as the basic elements. These transformers are driven into the region of saturation by an audiofrequency voltage on the primary winding. The addition of a d.c. bias to one or more of several secondary windings produces a second harmonic signal. This signal is then amplified and phase-detected, and the resultant d.c. is used as negative feedback on one of the secondaries. Circuits embodying these magnetic amplifiers have been used for the algebraic addition of several direct currents ranging from 100 μa to 5 ma, with an accuracy of ±0.1 percent of the maximum sum. These circuits have low input impedance, high stability, and also have the advantage that the input levels of the various currents can be independent of each other and of the output level. By using appropriate feed-back methods, the result of a computation may be expressed as a direct current, a d.c. potential, or a mechanical shaft rotation. Application of these magnetic amplifiers has also been made to the differentiation of slowly varying voltages, using a condenser as the differentiating element.

* This paper is based on a Ph.D. thesis done at Cornell University as part of Contract OEMsr-768 with the Office of Scientific Research and Development. A full report of this research will appear in a forthcoming issue of the Proc. I.R.E.

Proceedings of the American Physical Society

Minutes of the Meeting at Montreal, June 19–21, 1947

THE 279th meeting of the American Physical Society was celebrated at Montreal, in the buildings and on the lawns of McGill University, on Thursday, Friday, and Saturday, June 19th, 20th, and 21st, 1947. This was our second meeting in Montreal: now we know from two experiences that the city and the University have a grand tradition of hospitality. The University entertained us with a garden party which was well attended and greatly enjoyed, and with a tea in the new Radiation Laboratory which was thrown open to our members and guests. The members of the local Committee were constantly busy in our interest, and in particular they even went so far as to intercede with the overcrowded hotels for those of our members who had sought reservations after the passing of the deadline: such a courtesy must not be taken as a precedent. This Committee was headed by Professor A. Norman Shaw, and included Professors J. S. Foster and E. R. Pounder and presumably others: to all of them our gratitude is due. The scientific sessions were well housed in the Moyse Lecture Theatre, in the MacDonald Physics Laboratory, and in the MacDonald Chemistry Laboratory. About three-hundred and fifty people registered for this meeting.

The Division of Solid-State Physics may date its official existence from this meeting, its by-laws having been approved by the Council: its organizers (T. A. Read, F. Seitz, W. Shockley, S. Siegel, R. Smoluchowski, and C. Zener replacing S. Dushman) had arranged a Symposium on the solid state which was held on Saturday. Six invited papers on a variety of subjects figured on the general programme. Seventy-two contributed papers appeared in the Bulletin, though not all were given: the abstracts are appended.

The dinner of the Society was held on Friday evening in the Windsor Hotel: again a word of gratitude must be said, this time to the management of the hotel for consenting to provide a dinner with a very small guarantee—fewer than half of the registrants came to the dinner, the rest missed a very pleasant evening. Among the speakers at the dinner was Dean David L. Thomson of McGill University, who had also welcomed the Society at its opening session. Other speakers were Messrs. A. Norman Shaw and J. S. Foster of McGill University, D. A. Keys of the National Research Council, M. Rouault of the Université de Montréal, and the Secretary. Dean Pegram presided in the enforced absence of the President and the Vice President.

The Council met on Friday afternoon, and elected two candidates to Fellowship and one-hundred and fifty-two candidates to Membership: their names are appended. In addition to accepting the proposed by-laws of the Division of Solid-State Physics, the Council granted a petition for the revision of two articles of the by-laws of the Division of Electron and Ion Optics—its name now becomes Division of Electron Physics, and its scope is broadened—and a petition for the establishment of a Division of Fluid Dynamics in the American Physical Society.

The Society has lost through death G. E. M. Jauncey (Washington University), Henry Shore (Federal Machine and Welder Company), and A. C. Stecher (Chicago).

Elected to Fellowship: Richard Courant, E. P. Ney.

Elected to Membership: (List appended).

Paul Algrain, John Caldwell Allred, Ralph W. Armstrong, Kenneth Francis Bishop, N. F. Bolling, Hendrik de Wet Botha, William W. Bradshaw, Stanley W. Burriss, Herbert J. Carlin, Sultan Ali Chowdary, Robert Leon Chuoke, Harold E. Clark, Eleanor M. Clinton, Billy Frank Cogswell, John Howard Coleman, L. F. Connell, Randolph W. Cornes, Stanley Walter Cousins, Samuel Davidson, William Howard Davis, William E. Deal, Jr., Marius Louis de Angelis, Leticia del Rosario, Bernice Dritz, Edward J. Duckett, Morris J. Ehrlich, Paul H. Egli, Lloyd Espenschied, Richard S. Fallows, Louis Fein, Sidney Fischler, Phyllis Jane Fleming, James C. Fletcher, Erik Forslind, H. K. Forster, Mary Gowen Foulks, Charles E. Francis, Leonard Friedman, Sam B. Garfinkel, Samarendro Nath Ghoshal, Anthony B. Giordano, Henry

Jacob Gomberg, Lloyd E. Gourley, Jr., Robert Lockhart Graham, Ronald A. Gulley, G. O. Haglund, Leonard H. Hall, Henry Harrison, Miles Van Valzah Hayes, Carl Wilhelm Helstrom, Jr., F. A. Heyn, Everett A. Hodges, Paul Frederick Hultquist, Richard W. Johnston, Herman Kohn, Eleanor Karasak, Keaton Keller, Casper T. Keogh, O. S. B., G. Ross Kilgore, Nathan L. Krisberg, Lester E. Kuentzel, James W. Laist, John William Landis, R. J. Lew, Daniel S. Ling, Jr., William Ronald Loosemore, Raymond Douglas Lowde, Perry James Luke, William George Mahlman, Parnell Marc, Don S. Martin, Bernd T. Matthias, Gregg H. McClurg, George J. Mills, David Mintzer, Fred John Morris, George R. Mott, Peter Murden, Robert Mushabac, Morris Newman, Clarence Jonathan Newton, Ralph William Nicholls, Ralph A. Nobles, Amos Norman, Rodney Nudenberg, Donald Hill Perkins, Thomas Gerald Pickavance, H. Polak, Michael L. Polanyi, C. F. Powell, Richard Freeman Post, Henry Clay Price, Ralph Alexis Raimi, Harry Lyman Raub III, James H. Ray, James Reekie, Donald Robert Rhodes, Charles J. Rife, William Woodrow Robertson, Earl S. Rosenblum, Albert William Saenz, Bernard Salzberg, H. Wesley Savage, David Saxon, James H. Schulman, Franklin Robert Scott, Mary Lurline Scott, Jay Seidman, John W. Sheldon, Dora Frantz Sherman, Albert Simon, Charlotte Moore Sitterly, Weldon Rexer Sittner, Alexander Goudy Smith, E. C. Smith, L. Speirs, Maurice D. Stahl, Harry Verdon Stopes-Roe, Haldun A. K. Taskin, Gerold H. Tenney, Sir George Thomspon, George B. Thurston, Pierre Marie Gabriel Toulon, Oscar Alwynne Towler, Jr., Frank E. Towsley, Lansing F. Tryon, Arthur T. Tuma, Lawrence Francois Vassamillet, Salvador Velayos, Roderick Quentin Vogel, Guy Fredrik von Dardel, George Peter Wachtell, Shou-Wu Wang, Alan H. Ward, Harold D. Webb, F. Joachim Weyl, W. J. Whitehouse, Robert H. Whitford, Clyde E. Wiegand, Hanns H. Wolff, Peter Adalbert Wolff, Ta-You Wu.

Karl K. Darrow, *Secretary*
American Physical Society
Columbia University
New York 27, New York

Invited Papers

The Interaction between Electrons and Radiation. F. J. BELINFANTE, *University of British Columbia.*

Methods in Raman Spectroscopy. H. L. WELSH AND M. F. CRAWFORD, *University of Toronto.*

Review of the Topic of Cosmic-Ray Bursts. H. CARMICHAEL, *Chalk River Laboratory, National Research Council of Canada.*

Diffusion of Neutrons. G. PLACZEK, *General Electric Company.*

Ion Sources. A. G. WARD, *Chalk River Laboratory, National Research Council of Canada.*

Progress Report and Plans for the McGill University Cyclotron. J. S. FOSTER, *McGill University.*

Committee on Solid-State Physics

Symposium on the Solid State

Diffraction of Neutrons in Crystals. F. SEITZ, *Carnegie Institute of Technology.*

Theory of Crystal Rectifiers with Application to Copper Oxide. J. BARDEEN, *Bell Telephone Laboratories.*

The Relaxation Spectrum of Metals. CLARENCE ZENER, *University of Chicago.*

Nuclear Magnetic Resonance Absorption in Solids and Liquids. E. M. PURCELL, *Harvard University.*

Conductivity Pulses Induced in Diamond by Alpha-Particles. A. J. AHEARN, J. A. BURTON, AND K. G. MCKAY, *Bell Telephone Laboratories.*

Contributed Papers

A1. "Fragmentation" Bursts at Sea Level. H. CARMICHAEL, *National Research Council of Canada, Chalk River, Ontario.*—Recordings of cosmic-ray ionization made at Cambridge, England, prior to 1936 in a large (175 liter) ion-chamber filled with A, N_2 and H_2, at pressures not much above atmospheric, showed a very sudden large increase in the rate of occurrence of bursts smaller than about 10^6 ion-pairs. It was shown at that time that these small bursts were produced by particles of range short compared with the size of the ion-chamber and they were ascribed to contamination alpha-particles (i.e., 8, 7, 6, etc., particles occurring within a time interval of 0.5 second). This explanation of these bursts never appeared to be completely satisfactory but confirmation of their cosmic-ray origin was not forthcoming until they were compared with the recent data of Kingshill and Lewis. It is now evident that these bursts must be caused mainly by heavily ionizing nuclear fragments of local origin (variously called vaporizations, explosions, or stars). These small bursts connected with the steeper branches of curves published in 1939 which were formerly thought to be due to showers of thinly ionizing particles. Measurements of the original recordings have now been extended to much smaller burst sizes and an attempt is made to correlate all the measurements of both types of bursts with the results of other authors.

A2. Further Investigation of Frequency of Occurrence of Small Cosmic-Ray Bursts. JAMES W. BROXON, *University of Colorado.*—Using Chree's method of superposed epochs, the writer[1] recently found secondary pulses in the frequency of small bursts in a heavily shielded chamber occurring about 27 days before and after primary pulses. As in the case of average ionization currents,[2] the analysis has been extended to investigate correlation with other variables. The method does not indicate clearly a dependence of burst frequency upon magnetic character, nor even a very close relation to the mean ionization current. It does strongly indicate a relation to sunspot areas; fairly regular pulses extending to nearly 10 percent of the mean frequency of the small bursts occur in approximate phase opposition to the primary pulses in sunspot area.

[1] J. W. Broxon, Phys. Rev. **70**, 494 (1946).
[2] J. W. Broxon, Phys. Rev. **62**, 508 (1942).

A3. Cosmic-Ray Induced Fission. DAROL FROMAN, LOUIS ROSEN, AND BRUNO ROSSI, *Los Alamos.**—Eastman special fission plates in contact with 1 mg/cm² metallic foils of U-235 (bare and surrounded with 2" of paraffin), U-238, Pb, and Bi were exposed to cosmic-ray neutrons during five-hour flights at 25,000 and 30,000 ft. The plates are insensitive to alpha and other radiations but record all fission-fragment tracks. At the time of writing this abstract, examination of the plates is incomplete. However, the following results are clear already. The flux of neutrons of energy above the fission threshold of U-238 is small since no tracks have been found in 0.4 cm² of plate examined to date. Cursory examination has given no indication of fission in Pb or Bi. The fission rates of the bare and paraffin-covered U-235 foils are about those which would result on exposure of the bare foils to thermal neutron fluxes of 20 and 130 neutrons/cm² min, respectively, calculated on the basis that the thermal fission cross section for natural uranium is 3 barns. The precision of these values is low but will be improved greatly on further examination of the plates before the meeting.

* Based on work done under contract with the Atomic Energy Commission. The last-named author is now at M.I.T.

A4. Delayed Neutrons from Pu^{239}. F. DE HOFFMAN AND B. T. FELD,* *Los Alamos.*—The delayed neutrons emitted from Pu^{239} have been investigated both with regard to the fraction of all neutrons emitted as delayed neutrons and the delay periods.[1] The ratio of the relative number of delayed neutrons in Pu^{239} to that in U^{235} was found to be 0.47 for neutrons delayed over 2 seconds and 0.40 for neutrons delayed over 5 seconds. Because of the experimental uncertainties these two numbers are probably not significantly different. The shape of the delay curve is found to be very closely the same as that of U^{235}.[2] The delayed neutron decay curve for long irradiation can be represented by the following expression:

$$I=0.301e^{-t/1.6}+0.371e^{-t/7.5}+0.288e^{-t/22.6}+0.040e^{-t/79.6}$$

where t is in seconds and $I(t=0)$ is arbitrarily taken equal to one. This work was carried out under contract with the War Department.

* Now at Massachusetts Institute of Technology.
[1] This work was completed February 1945. Previous work was done by R. R. Wilson, Phys. Rev. and C. Redman and D. Saxon (to be published).
[2] See, for instance, A. H. Snell, Phys. Rev. **70**, 111 (1946).

A5. On the Asymptotic Distribution of Diffusing Monoenergetic Neutrons. P. R. WALLACE,* *National Research Council of Canada, Chalk River.*—It is shown that, in general, the neutron distribution in a finite homogeneous medium R may be treated as due to appropriately chosen sources in an *infinite* homogeneous medium, these sources being distributed over the region *outside* R. Such considerations lead in general to an integral equation for the distribution rather different from the usual Wiener-Hopf integro-differential equation. In particular, this method enables one to obtain perfectly general relations between the angular moments of the asymptotic distribution, independently of the nature of the artificial "sources" referred to above. Thus, for instance, the relation expressing the proportionality of current and gradient of density in the asymptotic region is obtained quite generally and rigorously, without any assumptions about the relative magnitudes of capture and scattering cross sections. The higher moments of the angular distribution are obtained similarly in terms of the higher derivatives of the density. These considerations have been applied, by way of illustration, to obtain information about the angular distribution in a number of simple cases.

* Now at McGill University.

A6. Fluctuations of Neutron Intensity in a Chain-Reacting Pile. E. D. COURANT* AND P. R. WALLACE,** *National Research Council of Canada, Chalk River.*—The method of probability generating functions has been used to study the fluctuations of integrated neutron intensity in chain-reacting piles. A general partial differential equation is obtained for this function, from which are obtained equations for the moments (the first moments are mean values of intensities of neutrons and of neutron-emitting excited fission product nuclei; the second moments are related to their mean-square fluctuations and correlations). The case of a steady power level (constant mean values) has been considered in detail. It is found that the fluctuations do not in general go as $N^{\frac{1}{2}}$ (N being the integrated neutron intensity), but for moderate or high power vary directly with N; in other words the *relative* mean square fluctuations approach a constant magnitude. This fact is related to the wide range of variation in the lengths of the multiplication chains initiated by the production of a neutron. The frequency spectrum of the fluctuations has been determined, and it has been used to study the effect on *observed* fluctuations of the resolving time of the measuring instrument and of the finite time of observation.

* Now at Cornell University, Ithaca, New York.
** Now at McGill University, Montreal, Canada.

A7. The Polarization of the Neutron in an Electrostatic Field. K. M. WATSON, *Iowa State University.*—According to the meson theory of nuclear forces, there is a meson charge cloud enveloping a neutron (or proton). An external electric field will polarize this cloud, causing the neutron to have an electric dipole moment. The results for scalar, pseudoscalar, and vector mesons are the same except for numerical factors. The neutron dipole moment in a field E is approximately (here $\hbar=c=1$)

$$\alpha \simeq 0.1 \frac{\epsilon^2 g^2}{\mu^3} E$$

where ϵ, g, and μ are the electronic charge, dimensionless coupling constant, and meson rest-mass. This will give rise to an elastic scattering cross section for γ-rays scattered by neutrons and to an electrostatic attraction between neutrons and protons or electrons.

A8. The Radial Dependence of the Tensor Force in the Deuteron. WILLIAM G. GUINDON, S. J., *Massachusetts Institute of Technology.*—The deuteron ground-state equations are solved using an $n-p$ interaction: $V=-[J_1(r)+\gamma S_{12}J_2(r)]$. In contrast to previous work,[1] first, the small spin-exchange interaction has been omitted and, second, in the square-well model employed the ranges of ordinary and tensor forces may be different. In place of a single well of depth V_0 and radius r_0, two wells of common depth V_0 (determined from the $n-p$ singlet scattering cross section) and radii r_0 and σr_0 represent $J_1(r)$ and $J_2(r)$ respectively. For a given choice of r_0 and ϵ, the potential V_0 and the binding energy E_0 determine γ and the quadrupole moment Q. By appropriate choice of ϵ, Q may be made equal to the experimental value, for any r_0. For radii in the range $r_0=(2.8\pm0.2)\times10^{-13}$ cm, preliminary results indicate that (1), the correct ratio covers the range $\epsilon=0.95\mp0.10$, and (2), the D-state probability at all these ranges is constant at 4.4 percent. Hence, in this model, (1) the quadrupole moment is rather sensitive to the ratio of the ranges, and (2) no preferred radius r_0 is indicated by comparison of the D-state probabilities with experimental magnetic moments.

[1] W. Rarita and J. Schwinger, Phys. Rev. **59**, 436 (1941).

A9. The Range of Nuclear Forces. H. C. CORBEN AND MULAIKA CORBEN, *Carnegie Institute of Technology.*—Experimentally it has not yet been established that the ranges r_{np} and r_{pp} of neutron-proton and proton-proton forces are identical. On the assumption that charged and neutral mesons possess different masses μ_c, μ_n but the same coupling constant with nucleons, we therefore investigated the pseudoscalar and vector meson theories of nuclear forces in the weak coupling approximation. The potential energies $V_{pp}{}^{1S}$, $V_{np}{}^{1S}$ and (apart from the tensor force) $V_{np}{}^{3S}$ of a two nucleon system then exhibit different r-dependence, but as they may be replaced approximately by square wells of identical "volume" V_0a^3 the corresponding energy levels are practically independent of the ratio μ_c/μ_n. The range r_{np} is then determined by the smaller of μ_c, μ_n so that $r_{pp}\leq r_{np}$ and $\mu_c\geq\hbar(cr_{np})^{-1}$. Violation of the first of these conditions would be difficult to understand on any theory; violation of the second would be a sufficient, though not necessary, condition for eliminating the symmetrical meson theory.

A10. The High Energy Limit of the C^{14} Beta-Ray Spectrum. W. E. STEPHENS AND MARGARET N. LEWIS, *University of Pennsylvania.*—The beta-ray spectrum of C^{14} is being investigated by means of a permanent magnet spectrograph.[1] The preliminary value of the apparent end point is 0.15 ± 0.02 Mev, which agrees with Ruben and Kamen's[2] value of 0.145 Mev. Further efforts to reduce scattering and increase the C^{14} density in the surface of the source are being made.

[1] E. H. Plesset, G. P. Harnwell, and F. G. P. Seidl, Rev. Sci. Inst. **13**, 351 (1942).
[2] Ruben and Kamen, Phys. Rev. **59**, 349 (1941).

A11. The 40-kev transition of ThC″. B. B. KINSEY, *National Research Council of Canada, Chalk River.*—It is well known that the disintegration of ThC with the emission of α-particles gives rise to an excited state of ThC″ at 40 kev. In 1934, Lewis and Bowden, in studying the fine structure of these particles, found that the state is excited in 70 percent of the disintegrations. This transition is of some interest in that the number of conversion electrons due to it is known to be less than one half of the number of excited states which are formed, while the γ-radiation has so far eluded detection. Noting an observation due to Ellis which indicates that the lifetime of the state is less than 10^{-8} sec., an attempt has been made to detect this radiation by a coincidence method using a counter with a xenon filling. A small effect was obtained amounting to about 4 quanta per 100 disintegrations. The emission of γ- and L-radiation is now being studied intensively by absorption and by diffraction methods.

C1. The Decay Scheme of Sc^{46}. ARTHUR E. MILLER AND MARTIN DEUTSCH, *Massachusetts Institute of Technology.*—Sc^{46} produced by slow neutron exposure of scandium in the Clinton pile is shown to emit negative beta-particles of maximum energy 0.36±0.01 Mev. Each beta-particle is followed by the emission of two gamma-rays of 1.12±0.02 Mev and 0.90±0.02 Mev energy, making the disintegration energy 2.38±0.03 Mev. Absorption measurements using a window-less counter gave identical results for He and A filling of the counter indicating the absence of K capture. This work was supported in part under contract N5ori-78 with the Office of Naval Research.

C2. The Decay of Ag^{110} (200 Day). MARTIN DEUTSCH, *Massachusetts Institute of Technology.*—Ag^{110} produced by slow neutron exposure of silver in the Clinton pile emits no detectable K x-rays. K-electron capture cannot constitute more than three percent of the disintegrations. The beta-ray spectrum is complex. More than half of the beta-particles are absorbed by 2 mg/cm² of aluminum. This explains the large ratio of gamma-ray to beta-ray count obtained with the usual counters. The γ-ray spectrum is more complex than previously reported.[1] The 0.9-Mev line[1] is resolved into two components separated by about 0.06 Mev. There is some evidence that the 1.5-Mev line[1] also is complex. This work was supported in part under contract N5ori-78 with the Office of Naval Research.

[1] Deutsch, Roberts and Elliott, Phys. Rev. **61**, 389(A) (1942). Rall and Wilkinson, Phys. Rev. **71**, 321(L) (1947).

C3. The Indium Isotopes Produced by Bombardment of Silver with 20-Mev Alpha-Particles.* D. J. TENDAM AND H. L. BRADT, *Purdue University.*—The assignments of mass numbers 110 and 112, respectively, to the 66-minute and 23-minute In activities are confirmed by their practically identical excitation curves which show clearly that these activities are produced by $Ag(\alpha, n)$ reactions. The decay scheme of the 23-minute In^{112} will be discussed. Whereas the excitation curves for these short periods are almost flat at 20 Mev, that for the 2.7-day In activity still rises steeply. This 2.7-day activity, also produced by $Cd(d, n)$ and $Cd(p, n)$ reactions, obviously is the result of a $Ag(\alpha, 2n)$ reaction, the threshold being (15±0.5) Mev. The 2.7-day period hence must definitely be assigned to mass number 111. We have produced by α-bombardment of Ag a new 6.5-hour In activity which decays chiefly by K-capture to an excited state of the product Cd nucleus, only a few percent of the decay processes leading to the ground state by emission of a forbidden 2-Mev positron spectrum. Because of the shape of its excitation curve, with a threshold ~13 Mev, the 6.5-hour activity is tentatively assigned to In^{109}, as the product of the $(\alpha, 2n)$ reaction with Ag^{107}. However, we have thus far been unable to detect the 330-day Cd^{109} activity which should grow out of In^{109}.

* Assisted by the Office of Naval Research.

C4. The Relative Yields of (α, n) and $(\alpha, 2n)$ Reactions with 15–20 Mev Alpha-Particles.* H. L. BRADT AND D. J. TENDAM, *Purdue University.*—Excitation curves for (α, n) and $(\alpha, 2n)$ reactions have been measured for several elements. As has been shown by R. N. Smith in this laboratory (thesis, unpublished), the relative yield of the $(\alpha, 2n)$ reaction is negligible with α-energies below 15 Mev for a large number of elements investigated. The yield of the $(\alpha, 2n)$ reaction may even, in some of these cases, be quite small at higher energies: for Co^{59} for example, where both reactions lead to definitely assigned periods—the (α, n) reaction to the 9.92-minute Cu^{62} and the $(\alpha, 2n)$ to the 3.4-hour Cu^{61}—the ratio of the $(\alpha, 2n)/(\alpha, n)$ thick target yield, as measured by the saturation intensity ratio of the annihilation radiation of the product β^+-emitters, is only 2 percent at 19 Mev. For Ag^{109}, where the $(\alpha, 2n)$ reaction whose threshold is at 15 Mev (see previous note), leads to the 2.7-day In^{111}, the $(\alpha, 2n)/(\alpha, n)$ thick target yield ratio at 20 Mev is much larger, the $(\alpha, 2n)$ and (α, n) cross sections being nearly equal for this α-energy. If the 6.5-hr. In period is to be assigned to In^{109}, as seems probable, the latter result holds also for the other silver isotope Ag^{107}.

* Assisted by the Office of Naval Research.

C5. A Radiofrequency Spectrometer for the Detection of Resonance Absorption by Nuclear Moments.[1] R. V. POUND, *Harvard University.*—An apparatus for searching in frequency for nuclear moment absorption lines has been constructed. It uses an oscillator with a circuit for automatically maintaining a given low level of oscillation, while its frequency is slowly altered by a clock motor. The sample is placed in the oscillator tank coil and this is put in a modulated magnetic field. A phase mixer that measures the modulation-frequency component in the rectified oscillator voltage registers absorption lines on a recording milliammeter. The resulting apparatus is completely automatic and is of utility for searching for unknown gyromagnetic ratios and for investigating line shape. For these purposes a permanent magnet or an electromagnet regulated to maintain the proton line at a fixed frequency would be useful. Full advantage may thus be taken of the sensitivity of a device of small noise band width by using a sufficiently slow scanning rate. The recorded line is due only to absorption and is not influenced by dispersion. Measurements show it is possible to obtain a noise figure of less than 10, if the level of oscillation is kept low.

[1] E. M. Purcell, H. C. Torrey, and R. V. Pound, Phys. Rev. **69**, 37 (1946).

C6. Design and Performance of Two of the Chalk River Ion-Chambers. B. S. SMITH, H. CARMICHAEL, J. F. STELJES, C. O. PEABODY, AND D. S. CRAIG, *National Research Council of Canada, Chalk River.—Type TPA* is a cylindrical, gas-tight ion-chamber with a $\frac{1}{16}$ inch thick welded steel case, pressure tested to 30 atmospheres and having aluminum electrodes with quartz insulation. The collecting volume is 4.7 liters. Only metals and quartz are used in the construction and the chamber is usually baked out under vacuum before filling. The ion current in commercial argon at 20 atmospheres is 90 percent saturated at a voltage $V=10^4(I)^{\frac{1}{2}}$. In BF_3 at 20 cm Hg the current (2.5×10^{-13} amp for a flux of one slow neutron per sq. cm per second) is 90 percent saturated at a voltage $V=4.5$

$\times 10^8(I)^{\frac{1}{2}}$. *Type TQT* is a 3½-inch diameter, gas-tight, aluminum ion-chamber, of similar construction, with one of its electrodes made of steel and coated with boron. The gas is argon at 50 cm Hg. This ion-chamber is for use in a high flux of slow neutrons and would be capable of passing a saturated ion current of one ma.

C7. The Photo-Multiplier Radiation Detector. FITZ-HUGH MARSHALL AND J. W. COLTMAN, *Westinghouse Research Laboratories.*—The photo-multiplier x-ray detector, consisting of a multiplier photo-tube to measure the light emitted by a fluorescent screen, has been extended in its use to the measurement of alpha-, beta-, and gamma-rays, high energy electrons and protons, and neutrons. Improved light-gathering methods and high frequency circuits have resulted in registration of individual quanta of all these radiations as pulses rising above the noise level of the photo-multiplier's input-stage dark current of 10^8 electrons per second, permitting use of a discriminator-counter circuit. This removes the sensitivity limitation inherent when the instrument is used only for current measurement. At high intensities the detector can be switched from pulse counting to current measurement, with a wide range of overlap for calibration. Employing commercial photo-tubes and screens, this detector is simple, rugged, compact, and spectacularly fast. It competes favorably in sensitivity with all other detectors, including the Geiger counter, and it can cover a tremendous range of intensities. It is most suitable for use with narrow beams of radiation. Thin-window technique is unnecessary for beta-rays, since the phosphor is exposed. Dr. Kuan-Han Sun is responsible for extending the detector to neutron measurement, using boron impregnated phosphors to convert neutrons to alpha-particles.

C8. Some Characteristics of the Photo-Multiplier Radiation Detector. J. W. COLTMAN AND FITZ-HUGH MARSHALL, *Westinghouse Research Laboratories.*—A photo-multiplier tube with a fluorescent material can be used as a detector of single radiation quanta or particles provided that the initiating event releases a number of photoelectrons appreciably greater than the number of dark-current electrons emitted during the phosphorescent response time of the fluorescent material. With fast, efficient phosphors and with mirrors to gather the light, single pulses from x-ray quanta 25 kv and higher can be distinguished above background noise, as well as all types of ionizing nuclear radiations. 5-Mev alpha-particles have been observed to release about 10^4 photoelectrons each and to give pulse heights 50 times background. 1.7-Mev beta-particles give pulse heights 10 times background. The pulse height is proportional to the energy released in the phosphor, and therefore roughly to the energy of the initiating event. For protons, alpha-particles, and beta-particles the counting efficiency approaches 100 percent; for high energy x-rays and gamma-rays, reduced absorption lowers the efficiency. A phosphor layer can be made with sufficient boron content to give a high efficiency for slow neutrons. The upper limit of the counting rate is set largely by the decay time of the phosphor, which is roughly 10^{-6} second.

C9. A Speed Gauge for HV-Ion Beams. WILLIAM ALTAR, M. GARBUNY, AND J. W. COLTMAN, *Westinghouse Research Laboratories.*—Increasingly accurate measurements of nuclear energy levels necessitate an accurate absolute voltage calibration. This is accomplished by a new method based on the original suggestions (R. O. Haxby, W. E. Shoupp, and W. E. Stephens) of timing transit of the beam between two r-f gaps, or transit through a resonant cavity. We obtain the required high accuracy (0.1 percent in voltage) and sensitivity (beam-current 10^{-6} A) by modulating the beam at the source with 70 mc, and after acceleration passing it through two accurately spaced gaps separated by a field-free drift space. The gaps are tightly coupled through a high Q cavity which resonates at the modulation frequency. Generally a particle contributes energy at each gap toward exciting the cavity mode. The resulting oscillation is fed to an indicator. Only when transit time between gaps is exactly an odd number (9) of half-cycles, will the two contributions from a particle cancel each other, giving null at the indicator. A cavity ($Q=6000$) has been built and tested, and should give adequate performance on the basis of computed signal and noise levels. Final runs will employ protons up to 4 Mev from the Westinghouse electrostatic generator.

C10. The Maxwell Bridge at Low Frequencies. V. A. BROWN AND B. P. RAMSAY, *Naval Ordnance Laboratory.*—The Maxwell bridge has been found useful for measuring inductance L and a.c. resistance R_{ac} at periods from 1 sec. to 200 sec. In some of the applications, the inductors had solid ferromagnetic cores and inductances of several hundred henries. The effect upon the bridge circuit of induced currents in the ferromagnetic material is expressed in terms of the equivalent mutual inductance M. The a.c. balance is imperfect unless M is zero. Compensation for mutual inductance by means of an inverse network[1] of capacitors and resistors in the arm opposite M is ineffective in the presence of ferromagnetic core material because the capacitors do not compensate for the effects of magnetic hysteresis. Hence the conventional Maxwell bridge has been selected; it yields approximate value of L and R_{ac}. Factors determining the choice of bridge resistors and of balance indicator are discussed, and typical graphs of L and R_{ac} as functions of frequency are presented.

[1] A. T. Starr, Phil. Mag. 12, 265 (1931).

C11. The Fluxmeter in the Fluxbridge Circuit. H. E. WOLF, H. E. CLEARMAN,[1] AND W. C. WINELAND, *Naval Ordnance Laboratory.*—The fluxbridge is a modification of the Rowland Ring Circuit in which a fluxmeter is used as a null indicator. The advantage of the fluxbridge for accurate work is that the fluxmeter, whether shunted or unshunted, is calibrated in the circuit in which it is used. The theory of the D'Arsonval galvanometer as a fluxmeter is examined, and the merits of using the fluxmeter as a null indicator are analyzed. The fluxbridge has been employed chiefly for measuring the detecting power of induction coils with ferromagnetic cores. Because transients in the fluxbridge have the effect of changing the state of

magnetization of these cores, measurements of detecting power are reproducible only when transient currents are small. Resistance is used in series with the inductors to reduce the magnetizing effects of transients. In order to reduce the sensitivity of the fluxmeter, it is frequently desirable to operate it with a shunt. The time-constants and sensitivity of the fluxbridge are discussed.

[1] Now at Applied Physics Laboratory, Johns Hopkins University.

C12. An Inductively Coupled Degenerative High Voltage Stabilizer.* R. PEPINSKY AND P. JARMOTZ, *Alabama Polytechnic Institute.*—Conventional degenerative d.c. voltage stabilizers have a d.c. connection between the input error voltage and the series-tube grid circuit. This imposes inconvenient insulation problems for stabilized output voltages above a few kilovolts. To overcome these difficulties, a stabilizer has been constructed in which the series tube is inductively coupled to a feed-back amplifier, insulation between high and low voltage circuits having been provided in a transformer. The d.c. feed-back amplifier amplitude modulates a 2-megacycle oscillator. The resulting signal is transmitted through an r-f transformer with 150 kilovolts Bakelite insulation between windings. The output signal is rectified and filtered, and application of the resulting d.c. signal to the series-tube grid controls the voltage drop across that tube. The stabilizer has been used for voltages between 20 kv and 50 kv, at currents from 0 to 50 ma. It operates from a 60-cycle line. An input variation of 1500 volts at the series-tube plate causes an output fluctuation of one volt; a 3500-volt input variation causes a 3-volt output change. The output ripple at 30 kb and 20 ma is 0.05-volt r.m.s.

* Development supported by U. S. Army Signal Corps.

E1. Directions of Magnetization in Powder Patterns. H. J. WILLIAMS, *Bell Telephone Laboratories.*—Some of the simpler powder patterns previously observed[1] on single crystals of silicon iron have been interpreted, so that one knows the direction of magnetization in each portion of the surface. On surfaces almost parallel to (100) the numerous lines, inclined about 45° to a direction of easy magnetization, are boundaries between domains magnetized at 90° to each other. When the lines are just 45°, the normal component of magnetization is constant across the boundary, and there are no free poles; when they deviate from 45° some poles occur and are spread sparsely along the lines. Such lines, slightly curved and joined to form spearheads, are observed when the plane of observation is slightly inclined to (100). They form domains of closure for the magnetization parallel to that direction of easy magnetization which intersects the surface at a small angle, and some flux escapes through the surface. They disappear when the surface is made accurately parallel to (100); the pattern then consists largely of lines parallel to one of the crystal axes, separating antiparallel domains.

[1] Phys. Rev. 70, 106 (1946).

E2. Ferromagnetic Resonance at Microwave Frequencies. W. A. YAGER AND R. M. BOZORTH, *Bell Telephone Laboratories.*—Griffiths[1] has recently described a new resonance phenomenon in ferromagnetic materials at microwave frequencies, and Kittel[2] has given a theory which shows good agreement with the experiments already reported. Electrons having gyromagnetic ratio γ are regarded as precessing about the applied field, H, at a microwave frequency given by $\omega=\gamma(BH)^{\frac{1}{2}}$ instead of the Larmor frequency $\omega=\gamma H$. In the experiments here described, we have used an easily saturable material and reduced the demagnetizing field to a low value. The standing wave ratio was determined in a resonant cavity for various values of the field which was varied from 200 to 10,000 oersteds, and this ratio was converted to apparent permeability with respect to the microwave field. A sharp resonance, about 100 oersteds wide at half-maximum, occurs at a field of 4920 and corresponds to a g of 2.17. This value is substantially above the value 2 for electron spin and is in disagreement with the more direct determinations of Barnett.

[1] J. H. E. Griffiths, Nature 158, 670 (1946).
[2] C. Kittel, Phys. Rev. 71, 270 (1947).

E3. Relaxation Effects in Paramagnetic and Ferromagnetic Resonance. CHARLES KITTEL,* *Massachusetts Institute of Technology.*—A discussion will be given of some theoretical[1,2] aspects of the paramagnetic[3] and ferromagnetic[4] resonance experiments. The resonance condition between frequency and d.c. magnetic field may depend on the line width, and the form of the dependence will vary according to the manner in which the relaxation frequency is introduced into the equations of motion. The *ferromagnetic* resonance experiments of Bozorth and Yager support the classical damping term as introduced by Frenkel. A discussion will be given of the effects of anisotropy and exchange interactions on the condition $\omega=\gamma(BH)^{\frac{1}{2}}$ for ferromagnetic resonance. There is a possibility of obtaining resonance in the anisotropy field of ferromagnetic single crystals. Exchange interaction effects enter when the penetration skin depth is small.

* Fellow of the John Simon Guggenheim Memorial Foundation.
[1] J. Frenkel, J. Phys. U.S.S.R. 9, 299 (1945).
[2] C. Kittel, Phys. Rev. 71, 270 (1947).
[3] E. Zavoisky, J. Phys. U.S.S.R. 10, 197 (1946).
[4] J. H. E. Griffiths, Nature 158, 670 (1946).

E4. Magneto-striction of Annealed and Cold Worked Nickel Rods. J. E. GOLDMAN, *Westinghouse Research Laboratories.*—Resistance strain gauges have been adapted to the measurement of the magneto-striction of polycrystalline rods and strips. Conventional advance wire gauges were used in a balanced d.c. Wheatstone bridge with a Rubicon photoelectric galvanometer as a detector, measurements being made by deflection. Isoelastic gauges have a greater strain coefficient of resistance but are not desirable in this case because of the pronounced magneto-resistance effect in isoelastic wire. The method permits the investigation of magneto-striction in the range from 5×10^{-8} to 10^{-4} with considerable accuracy. Measurements have been carried out on annealed and cold-worked nickel rods of a high grade of purity. The measured saturation

magneto-striction of the annealed nickel rod was -34×10^{-6} ±2 percent in excellent agreement with the value calculated by Becker for polycrystalline nickel with random initial domain distribution. For the cold-worked rod a value of -41×10^{-6} was obtained. The difference between the values for the two states is explained on the basis of the residual stresses resulting from the cold reduction which produces a preferred domain orientation transverse to the direction of work. For such an initial state, the magneto-striction is greater. Quantitative estimates of both the domain anisotropy and stress anisotropy are possible.

E5. A Permeameter for Magnetic Measurements on High Permeability Material. W. J. CARR, JR., *Westinghouse Research Laboratories.*—A new type of permeameter is described for making magnetic measurements on soft magnetic materials. The novel feature of the method is in the measurement of magnetizing force. This is accomplished by placing a small measuring element, consisting of a high permeability core with a winding on it, very close to the surface of the test specimen. The core is energized with a.c. above the knee of its magnetization curve, and the second harmonic in the voltage is a measure of the H-field in the specimen. Values of H from 10^{-2} to 10^{+2} oersteds can be measured on high permeability samples with geometries which heretofore prevented accurate measurements. Errors in the measurement are discussed, and the proper design for the measuring element is given.

E6. The Electrical Behavior of Vacuum Evaporated Tellurium. WAYNE SCANLON AND K. LARK-HOROVITZ,* *Purdue University.*—Tellurium shows certain anomalies in its electric behavior (Hall effect, thermoelectric power). The Hall effect is positive at low temperatures, becomes negative, and then again shows a reversal at high temperatures, remaining positive up to the melting point. X-ray investigation in vacuum from liquid air temperature to the melting point have show that there is no change in crystal structure of tellurium evaporated in vacuum. However, Dowell and Lark-Horovitz have found that tellurium heated in air does show new x-ray diffraction lines around 360°. Experiments with layers of tellurium evaporated in a high vacuum onto a mica strip with suitable electrodes for carrying current and probes for measuring resistivity and Hall effects show, that tellurium investigated from liquid air temperature up to about 300° in vacuum does not exhibit any of anomalies observed before. These samples behave similarly to other elementary semiconductors (Ge, Si). Throughout the whole range of temperature the Hall effect of tellurium remains positive. The resistivity curves show an activation energy of the order of 0.039 ev at low temperature, and go through a maximum followed by a rapid decrease of resistance indicating the intrinsic range of the semi-conductor (activation energy about 0.36 ev). Layers of this type heated in air remain essentially unchanged but show increased resistivity and Hall effect. It seems, therefore, that the anomaly in electrical behavior usually observed in tellurium is not due to a complexity of levels of the semi-conductor itself, but rather to admixtures of foreign layers produced in the preparation of the material in the atmosphere.

* This work has been carried out with the aid of the Signal Corps.

E7. Resistivity and Hall Constant of Germanium Samples at Low Temperatures.* I. ESTERMANN, A. FONER AND J. A. RANDALL, *Carnegie Institute of Technology.*—The Hall Effect was measured on the same germanium samples for which resistivity measurements were reported earlier.[1] In the case of a strongly degenerate sample (0.04 at. percent Al added) in which the resistivity was nearly independent of temperature, the Hall constant remained also independent of temperature between 20° and 300°K, and was also independent of the field strength for fields between 1000 and 7500 gausses. Samples with smaller impurity content, for which the resistivity increases with decreasing temperature, show an increase in Hall constant on cooling from room temperature to liquid nitrogen temperature, apparently followed by a slight decrease on cooling to 20°K. Additional resistivity measurements were carried out with samples containing antimony and tin, prepared and selected like the others at Purdue University. The samples, with 0.04 at. percent Sb added, show essentially the same behavior as those containing small amounts of P or Al. The samples containing tin show a monotonic decrease of resistivity with decreasing temperature. The previously observed increase in resistivity[1] of some samples produced by repeated heating and cooling was found to be due to changes in contact resistance.

* Work done under contract with the Office of Naval Research.
[1] I. Estermann, A. Foner, and J. A. Randall, Phys. Rev. 71, 484, 1947.

E8. Spreading Resistance Discrepancies and Field Effects in Germanium.* RALPH BRAY, K. LARK-HOROVITZ, AND R. N. SMITH,† *Purdue University.*—Contact and spreading resistance determine the forward resistance of metal-Ge point-contact rectifiers. Theoretically the spreading resistance is $\rho/2d$; ρ-semiconductor resistivity, d-contact diameter. Above one volt the contact resistance contribution is negligible and the spreading resistance is then given by the slope of the current-voltage characteristic. However, the spreading resistance so determined on high resistivity ($\rho\sim1$ ohm-cm) n-type Ge decreases with increasing voltage and is lower by factor ten or more than the value predicted from bulk resistivity.[1] The high current densities through the contact (~10 ma through 10^{-6} cm^2) suggest the possibility of field effects. Actually, the bulk resistivity (studied with exponential and constant current pulses) is field dependent and starts to decrease at fields of 100 volts/cm. The time constant of the field effects may be estimated from the progressive increase of spreading resistance with frequency (about 100 Kc).[2] Calculations were made relating at least qualitatively the spreading resistance discrepancies with field dependence measurements of bulk resistivity.

* This work was started under OSRD contract and is continued under Signal Corps contract.
† Now at Boeing Aircraft, Seattle, Washington.
[1] Experiments also show saturation of spreading resistance with increased load and contact area (R. E. Davis).
[2] H. J. Yearian, "Dependence of Forward Conductance and Back Resistance of High Back Voltage Germanium on Voltage and Frequency." NDRC report October, 1945.

E9. Spontaneous Electrical Oscillatons in Germanium Crystals.* S. BENZER, *Purdue University.*—Electrical oscillations in germanium-to-metal point contacts are usually ascribable to negative resistance characteristics or mechanical effects. However, when the metal point is placed at the edges of regions showing the photodiode** effect, strong oscillations of an apparently different nature occur in a circuit containing only a d.c. source and a resistor in series with the crystal. Above a critical voltage (for one polarity only), oscillations begin; the frequency increases from the order of 10^5 c.p.s. at several volts to 10^6 c.p.s. at higher voltages and is insensitive to external circuit reactances. The amplitude may approach the supply voltage and the waveform is usually non-sinusoidal. The frequency and amplitude are strikingly sensitive to illumination and temperature. For a contact at the edge of a photodiode region one would expect to find a thin "sandwich" of N-type germanium between metal and P-type germanium. Such a configuration would have a minimum in the potential of an electron which might lead to oscillations. R. Bray has recently observed similar oscillations with suitably etched P-type germanium crystals.

* Based in part on NDRC report 14-580, October 31, 1945.
** Phys. Rev. 70, 105(A) (1946).

E10. Theory of Low Temperature Semiconductor Resistivity.* V. A. JOHNSON AND K. LARK-HOROVITZ, *Purdue University.*—The resistivity of Ge semiconductors (P and N type) has been calculated for temperatures from 300°K down to about 14°K. Classical statistics have been used for temperatures above the degeneracy temperature T_d, and values for impurity scattering with Fermi statistics below T_d, using the new Hall coefficient values obtained at Carnegie Tech. Residual resistivities[1] calculated from Hall data agree with experimental values. The impurity resistivity ρ_I is given by

$$\rho_I = \frac{3.05\times10^{-15}n}{T^{\frac{3}{2}}} \frac{\ln\left(1+2.88\times10^{7}n^{-\frac{1}{3}}T^{2}x_m^{2}\right)}{J_{\frac{1}{2}}(\mu/kT)}$$

where n = number of electrons/cm³, $J_{\frac{1}{2}}$ = Fermi integral, X_m = energy value maximizing conductivity integral. Graphical and numerical evaluation of the Fermi integral involved gives calculated resistivity curves in close agreement with observations.

* This work was supported by Signal Corps contract.
[1] See V. A. Johnson and K. Lark-Horovitz, Phys. Rev. 71, 374 (1947).

H1. Rectification Characteristics of an Oxide Cathode Interface. W. E. MUTTER, *Research Laboratory of Electronics,** *Massachusetts Institute of Technology.*—Fine wire probes embedded in the coating of an oxide cathode are used to measure the potential drop over the interface and coating under pulsed conditions for both directions of current flow through the cathode. In the case of cathodes prepared on a 5 percent silicon-nickel base and operated at 800°C, the interface voltage is 3 to 5 times greater when the cathode is emitting electrons than when it is receiving the same current density of electrons. With a pure nickel base, there is a relatively small interface voltage which is initially independent of the direction of current flow, but increases during 130 hours of operation and then also exhibits rectification properties. The electrical conductivity of the coating is independent of the current density and the direction of current flow. The use of pure nickel or 5 percent silicon-nickel has no effect on the measured value of the coating conductivity. At temperatures above 800°C the total potential drop over the interface and coating as determined from probe measurements is found to account for deviations from the space charge law observed in experimental diodes.

* This work was supported in part by the Joint Services Contract W-36-039 sc-32037.

H2. Some Electrical Properties of an Oxide Cathode Interface. A. EISENSTEIN, *Research Laboratory of Electronics,** *Massachusetts Institute of Technology.*—When high thermionic emission currents are taken from oxide coated cathodes, voltages appear across the oxide coating and across the interface between the coating and base metal; the latter voltage often exceeds the coating voltage at temperatures below 1100°K. Under pulsed conditions the total voltage drop across the interface and coating, V_{ic}, is not negligible with respect to the applied cathode-anode voltage, V_a. The experimental voltage-current characteristics of a diode should show disagreement with the theoretical Langmuir-Child characteristic by an amount V_{ic}. The emission characteristics of oxide cathodes prepared on a 5 percent Si-Ni base metal (interface of Ba_2SiO_4) show this effect. The actual voltage which appears between the exterior surface of the oxide coating and the anode, $(V_a - V_{ic})$, can be deduced from measurements of the retarding potential required to stop electrons which pass through a small hole in the anode. Values of V_{ic} thus obtained and at temperatures above 1100°K account for the observed deviations from the theoretical Langmuir-Child characteristic. At low temperatures the emission is no longer limited by space charge and the voltage gradient across the interface may reach 10^6 volts/cm. An interesting and unexpected result of this experiment is that a small number of electrons arrive at the anode with energies up to V_a.

* This work was supported in part by the Joint Services Contract W-36-039 sc-32037.

H3. Photoelectric and Optical Properties of Cesium-Antimony Films. J. A. BURTON, *Bell Telephone Laboratories.*—In an attempt to understand the unusually high quantum efficiency of Cs-Sb photoelectric surfaces (1), optical and photoelectric measurements were made in the spectral region from 2255A to 11,000A on a series of semi-transparent films. The optical constants were determined from reflection and transmission measurements. In the ultraviolet the high absorption coefficient (approximately 4.7×10^5 cm^{-1}) must be due to a fundamental absorption band and not to impurity centers. The films appear to be optically homogeneous, and photoelectric measurements with polarized light give the results expected for a volume photoelectric effect. By comparing the photoelectric emission for light incident on the vacuum

side of the films with that for light incident on the quartz side, the mean depth below the surface at which an absorbed quantum produces a photoelectron is estimated to be about 250A. Using this value and the observed optical constants the magnitude of the quantum efficiency and its dependence on film thickness can be explained if the internal quantum efficiency is approximately unity and if the photoelectrons can readily escape into vacuum.

[1] P. Görlich, Zeits. f. Physik **101**, 335 (1936).

H4. Secondary Emission from Conducting Films of Tin Oxide. H. E. MENDENHALL, *Bell Telephone Laboratories.*—In the search for stable secondary emitting surfaces over a wide range of bombarding voltages and operating temperatures, thin stannic oxide films deposited on Vycor, Pyrex and platinum by the Corning Glass Works have been studied. The ratio of secondary to primary electrons from a conducting film of tin oxides on an underlying Vycor (synthetic quartz) was low enough to prevent cumulative charging of the surface bombarded with electrons up to 5000 volts energy. The δ was only slightly above one for primary electrons with more than 300 and less than 1600 volts energy. The maximum value observed was 1.11 at 600 volts primary energy which compares with a δ of value of 2.1 for glass reported by W. Heimann and K. Geyer. This same type of conducting coating on platinum applied to about 3 interference rings in thickness was also used as a target for secondary electron production. An increase in δ ratio to a value 50 percent higher than those reported for clean platinum was observed. The δ was above one between 150 and 6000 volts and reached a maximum of 2.5 when the target was bombarded with 600 volts primary electrons. For a film of 6 interference layers in thickness, δ was above one between 60 and 5000 volts and reached a maximum of 3.25 at 640 volts after being heated to a temperature of 850°C.

H5. Characteristics of Bridges between Metallic Contacts. G. F. HULL, JR., AND W. BAER, *Dartmouth College.**—Bridges between separated platinum and gold contacts have been obtained in air and in vacuum. The bridges observed vary in length from 10^{-4} to 10^{-2} cm. Current-voltage characteristics of platinum and gold bridges show that the product of current and voltage is approximately constant for currents up to about 10 amp. For currents above 10 amp. the electrodes expand changing the bridge dimensions. Photomicrographs of the bridges show that the bridge dimensions remain constant within ± 10 percent over the constant power portion of the bridge characteristic. The platinum and gold bridges melt and disappear at voltages across the bridges of about 0.64 volt for platinum and 0.42 for gold when measurements are made in vacuum. These voltages correspond to the melting temperatures of platinum and gold respectively, which agrees with contact theory.[1] The current-voltage bridge characteristics can be transformed into resistance-voltage characteristics which are then compared with the theory of contact temperature.

* Assisted by the Office of Naval Research.

[1] R. Holm and E. Holm, Wiss. Veröff. Siemens-Werk. **7** [2], 217 (1929).

H6. Single Crystals of Barium Titanate.* B. T. MATTHIAS, R. G. BRECKENRIDGE, AND D. W. BEAUMONT, *Massachusetts Institute of Technology.*—Barium titanate as a ceramic of high permittivity has been known for several years. During the past months it has been possible to synthesize single crystals for investigation of the dielectric properties.[1] As the growth out of the melt encounters considerable difficulties as far as crucible, temperature, and volatility are concerned, barium titanate crystals were grown out of molten barium salts or others. If equimolar parts of barium carbonate and titanium dioxide are dissolved in molten barium chloride, even with a very slow cooling rate extending over a couple of weeks, it is difficult to obtain decent crystals. For aqueous solutions it has been long known[2] that an excess of cations considerably improve crystal growth. For barium titanate it was possible to find an adequate composition with barium carbonate in excess such that with a cooling process of not longer than eight hours perfect crystals up to half a centimeter were obtained. In contradiction of Megaw,[3] these crystals did not have a center of symmetry as they are strongly piezoelectric. The dielectric behavior points towards a new, third kind of ferro-electrics in addition to Rochelle salt and the dihydrogen phosphates.

* The research reported herein was made possible through support of the Navy Department and the Army Signal Corps.

[1] H. Blattner, B. Matthias, W. Merz, and P. Scherrer, Experientia **III**, 4 (April, 1947).

[2] Yamamoto, Sci. Pap. Inst. of Phys. and Chem. Res., Tokyo, **35**, 228 (1939).

[3] H. D. Megaw, Proc. Phys. Soc. **58**, 133 (1946).

H7. On the Classification of Phase Transitions.* L. TISZA, *Massachusetts Institute of Technology.*—A classification of phase transitions is suggested which is more specific than the purely thermodynamical one based on the *order* of the transition. In general, phases correspond to separate regions in phase space. A transition is said to be of the *first kind*, if the separation is realized in ordinary space, and of the *second kind* if it occurs in another subspace of phase space. For transitions of the first kind, the phase rule is valid. Examples are the gas-liquid-solid transitions and those polymorphisms in which the solid phases have unrelated symmetries. These transitions are all of the *first order*. There are, however, transitions of the first *kind* and *second order*, where in the course of thermal expansion a symmetry element appears or disappears ($\alpha-\beta$ transition of quartz, $BaTiO_3$, etc.) In transitions of the second *kind*, the phase rule is not valid and the transition is gradual (λ-anomaly of the specific heat.) The question of physical interest is to establish the nature of the phases which appear mixed. There are a great variety of cases partly not yet understood. These transitions are usually of the *second order*, although cases of *first order* transitions arise too. Examples are ferromagnetism, liquid helium, superconductivity, order-disorder transitions, rotational transitions, etc.

* This research has been supported in part by a joint Army–Navy Contract.

H8. Solubility Gaps in Simple Binary Systems. A. W. LAWSON, *University of Chicago.*—By expanding the second derivative with respect to mole number of the free energy of a two-component phase near its critical point (T_c, x_c) in a Taylor's series of the form $-a(x-x_c)^2+b(x-x_c)(T_c-T)+c(T_c-T)$, one may develop approximate expressions for the various thermodynamic quantities. The constants a, b and c are evaluated by satisfying the critical conditions and the requirement of complete segregation at absolute zero of temperature. Integration yields an expression for the chemical potential of the form,

$$\mu_1=a[(x^2/2)-[2x_c+(1-2x_c)(1-T/T_c)]x+x_c^2(T/T_c)\ln x]+\text{const.}$$

with a similar expression for μ_2 in terms of y. Numerical solution of the two simultaneous equations $\mu_1(x_1)=\mu_1(x_2)$ and $\mu_2(1-x_1)=\mu_2(1-x_2)$ yields the equilibrium values of x_1 and x_2 delineating the solubility gap. This zero-order approximation thus yields a set of universal curves for solubility gaps as a function of the reduced variables T/T_c and x/x_c. The curve $x_c=0.5$ agrees with that computed from Bragg-Williams theory, and fits experimental curves somewhat better than a similar approximation discussed by Hildebrand.

H9. The Wiedemann-Franz-Lorenz Ratio for Copper Alloys. R. RUEDY, *National Research Council of Canada.*—A study of the values obtained for the electrical and thermal conductivities of 10 copper-aluminum, 8 copper-nickel, 8 copper-silicon, 8 copper-manganese, and 50 miscellaneous ternary and quaternary alloys of copper with zinc, tin, lead, manganese, iron, and nickel, measured at different temperatures by C. S. Smith and E. W. Palmer,[1] shows that after subtraction of a constant amount of non-electronic thermal conductivity, the Wiedemann-Franz-Lorenz ratio of all the alloys is in closer agreement with the Lorenz constant given by Sommerfeld's theory of conductivity than with Drude's value for metals. The decrease in the thermal conductivity of copper, caused by a small concentration of another metal in solid solution, is independent of the temperature between at least 40 and 230°C.

[1] Trans. A.I.M.E. 117, 225-243 (1935).

H10. The Structure of Manganese-Rich Alloys of Copper and Manganese.* FRANCIS T. WORRELL, *University of Chicago.*—Manganese-copper alloys containing more than 82 percent manganese have, when appropriately heat treated, a face-centered tetragonal structure[1] with an axial ratio varying from 0.937 for pure manganese to 1.00*(i.e., face-centered cubic) at 82 percent manganese. Alloys in this range often have high internal friction. Zener[2] has suggested that the damping results from the relaxation of stresses across the {101} and {011} interfaces of twins associated with a tetragonal structure. Metallographic examination of the alloy 88 percent manganese, 12 percent copper shows a duplex twin structure, consisting of large twins, such as one finds in face-centered cubic metals, with a fine twin pattern superposed. This structure has been analyzed. The large twins are along the {111} planes, and the fine ones are the postulated tetragonal twins. This analysis has been confirmed by x-ray studies. Possible explanations of this structure will be discussed.

* This research was supported by O.R.I.
[1] Persson, Zeits. f. physik Chemie B9, 25 (1930).
[2] Private communication to the author.

H11. On the Theory of the Use of Isotopes as Tracers. HERMAN BRANSON, *Howard University.*[1]—It is shown that an integral equation can be established which describes some of the important features of chemical and biological systems in which stable and radioactive isotopes are used as tracers. The equation is

$$M(t)=M(0)F(t)+\int_0^t R(\theta)F(t-\theta)d\theta$$

where $M(t)$ is the amount of the substance present at time, t; $R(t)$ is the rate of accumulation, and $F(t)$ is called the "metabolizing" function: that function which multiplies the original amount to give the amount remaining at time, t. Some of the data from experiments with I^{131} and P^{32} are discussed. The experimental procedures for determining properties of biological and chemical systems are shown to yield the functions in the equation. Specific experiments with single and double tracer molecules in progress in our laboratories are mentioned.

[1] Placed on Friday at the author's request.

J1. New Results at Pressures up to 100,000 kg-cm². P. W. BRIDGMAN, *Harvard University.*—A number of improvements have been made in the apparatus for measuring volume decrements up to 100,000 kg/cm². It is now possible to carry seven insulated leads into the external pressure chamber, in which a pressure of 25,000 to 30,000 kg/cm² prevails, to support the piezometer for 100,000. With this increased number of leads it is possible to make measurements of both change of volume and compressive force from the inside of the supporting chamber instead of from the outside, and thus avoid several corrections arising from distortion of the pressure vessels. With this apparatus measurements on thirty new substances have been made to 100,000. The most interesting result is a reversible volume discontinuity in caesium near 50,000 of about 12 percent. The explanation of this is not clear, since already, below 50,000, caesium has assumed the close-packed arrangement. It probably means some deep-seated rearrangement within the atom.

J2. Impingement and Stimulation in Grain Growth. R. SMOLUCHOWSKI, *Carnegie Institute of Technology.*—The usual assumption concerning the process of recrystallization is that new recrystallized grains start growing at random within the deformed metal and grow with a definite rate until all material is recrystallized. It has been variously suggested that there is stimulation, i.e., a growing grain increases the probability of the occurrence of a new center of recrystallization in the proximity of its boundary. In particular Burgers suggested that such stimulated grains have a particular crystallographic relationship to the original grain. By means of an analysis of the shapes of recrystallized grains in aluminum it has been

possible to deduce what was the radius r of the original grain, while the new grain was starting to grow within the distance n from the boundary of the original grain. Also, it was possible to estimate the ratio of the rates of growth of neighboring grains. The results indicate an effect which may be interpreted either as stimulation or as an unstability of small grains relative to large grains. The latter possibility is supported by the presence of grains which have a shape indicating a growth of the larger grain at the expense of the smaller grain.

J3. Studies in Friction II. Maximum Shear Strength of Solids in Relation to the Thermodynamics of Melting. M. EUGENE MERCHANT, *The Cincinnati Milling Machine Company.*—It appears that the *maximum* shear strength of a solid (i.e., its shear strength when behaving as an isotropic material) is related to its melting properties. The process of shear can be crudely treated as stress-activated melting in one degree of freedom. When this is done, the resulting thermodynamic equation relates the maximum shear strength to the density, heat of fusion, and melting point of the solid. The calculated values are useful in cases where the process of shear is restrained from following preferred crystal planes (as in severely cold-worked materials or in thin films on friction surfaces), and where relative rather than absolute values are of most importance. Such calculations have previously been applied to the interpretation of the friction of clean metals.[1] In the present case they have been studied in relation to thin films of solids on friction surfaces, as found, for instance, under conditions of boundary lubrication. Calculated values also are compared with experimental data obtained by Bridgman.[2] A fair degree of correlation exists.

[1] H. Ernst and M. E. Merchant, Proc. Spec. Summer Conf. on Friction and Surface Finish (MIT), 76–101 (1940); *Surface Treatment of Metals* (Am. Soc. for Metals, 1941), pp. 299–337.
[2] P. W. Bridgman, Proc. Am. Acad. 71, 387–460 (1937); Phys. Rev. 48, 825–847 (1935); J. App. Phys. 8, 328–336 (1937).

J4. Speed of Propagation of a Fracture Crack in Metals. EDWARD SAIBEL, *Carnegie Institute of Technology.*—Recently the author has proposed a thermodynamic theory of the fracture of metals[1] which relates fracture to the melting phenomenon. From this point of view and with the use of the Eyring "hole" theory of the liquid state, the rate of formation of the "hole" structure is calculated from chemical reaction rate theory, the reactant being the material before fracture and the product of the reaction being the holes. Since the abolition of cohesive strength is attributed to the formation of the holes, the rate at which they are formed gives directly the rate of propagation of the crack. The effects of temperature and of stress system are also indicated. Using the data of reference 1, it is found that the speed of fracture of a mild steel plate at room temperature, under a tensile stress, is about 75,000 in./sec. Some experimental work[2] done along these lines shows values of the same order of magnitude.

[1] E. Saibel, Metals Technology 14, 1 (February 1947).
[2] M. Greenfield and G. Hudson, Proc. Nat. Acad. Sci. 31, 150 (1945).

J5. Atomic Vacancy and the Viscosity of Grain Boundaries in Metals.* T'ING-SUI KÊ, *The University of Chicago.*—As will be reported in *The Physical Review*, the grain boundary in metals behaves in a viscous manner in the sense that it cannot sustain a shear stress and has a coefficient of viscosity decreasing with an increase of temperature. Recently it has been found by internal friction measurements on 99.991 aluminum specimens of similar grain size that the grain boundary viscosity is lower in a specimen subjected to a heavier plastic deformation prior to recrystallization. It has also been found that the conditions corresponding to a smaller grain boundary viscosity in this metal are conditions that favor grain growth. These and other observed phenomena can be adequately explained by assuming that atomic vacancies or holes are created during plastic deformation and that they "migrate" to the grain boundaries during later heat treatment, as was originally conceived by Hollomon. The accumulation of holes at the grain boundaries should reduce the grain boundary viscosity. According to these assumptions, the heavier the previous deformation, the greater will be the hole density at the grain boundary, and thus the lower the grain boundary viscosity. The larger hole density at the grain boundary favors grain growth because of the associated increase of surface energy.

* This research was supported by ORI.

M1. The Optical Aberrations of the Eye and Night Myopia. M. J. KOOMEN AND R. TOUSEY, *U. S. Naval Research Laboratory.*—It is well known that the human eye becomes somewhat myopic for fields of low brightness. The effect was measured by determining acuity thresholds for the eye with spectacle lenses of different powers placed before the eye, and for white fields ranging from very bright to as low as 0.005 microlambert. From the optimum lens corrections for each brightness level a curve was derived showing diopters of myopia *versus* field brightness. The magnitude of the effect was found to be as much as -2 diopters. Chromatic aberration, foveal and extra-foveal spherical aberration, and pupil diameters were measured for the same observers. It was shown that chromatic aberration along with the Purkinje Effect accounts for only about -0.25 diopter myopia and the remainder is largely caused by extra-foveal spherical aberration and the Stiles-Crawford Effect. The eye aberrations were sufficient to account for the observed myopia and it was not necessary to postulate accommodation at low brightness levels.

M2. Calculation of Index of Refraction of Water Vapor in the Far Infra-Red. F. W. BROWN AND M. A. GREENFIELD, *North American Aviation.*—Optical calculations for instrumentation in the far infra-red are handicapped by lack of experimental data on index of refraction of water vapor beyond 0.7μ. Calculations of the index of refraction were made using the following idealizations of absorption bands: (1) lines in a band are equally spaced and have equal half-widths; (2) all lines in central portion of band have equal intensities. The classical dispersion formula for

index of refraction, n, at the frequency, ν, becomes

$$n-1 \doteq \Sigma \frac{S_i}{\pi d_i} \ln \left[\frac{(\nu_{0i}-\nu+\Delta\nu_{0i})^2+\alpha^2}{(\nu_{0i}-\nu-\Delta\nu_{0i})^2+\alpha^2} \right]^{\frac{1}{2}} \cdot \frac{\nu_{0i}+\nu-\Delta\nu_{0i}}{\nu_{0i}+\nu+\Delta\nu_{0i}}$$

where ν_{0i}, $\Delta\nu_{0i}$ are respectively the average frequency and half-width of i^{th} band, α, d_i are, respectively, the half-line width and average spacing between lines of a band. Values of S_i, the average line intensity, were obtained from known values of the macroscopic coefficient of absorption, using a derived theoretical expression for the absorption of a band. A qualitative estimate was made of the contribution to the index of refraction by the weak absorption lines near the edges of the band.

M3. The Hyperfine Structure of the Ammonia Inversion Spectrum in an Electric Field. J. M. JAUCH, *State University of Iowa.*—The ammonia inversion spectrum shows a hyperfine structure due to the electric quadrupole moment of the nitrogen nucleus.[1] The sensitivity of the microwave absorption measurement can be increased by modulating the frequency of the absorption lines by putting the sample into a variable uniform electric field E.[2] In order to observe any effects due to the nuclear spins it is necessary to stay within a field region for which the spin is not completely decoupled from the angular momentum. The quantum-mechanical treatment of the problem leads to a secular equation of third order which can be factored for all values of J and K, for $M=J$, $J-1$, and 0. For the other cases good approximations are obtained by treating the problem with second-order perturbations for weak and strong fields, respectively, and interpolating numerically for the intermediate region ($E\sim300$ volt/cm). Strong departure from expected displacements proportional to E^2 can occur already at weak fields because of strong perturbations of combining levels. A complete level scheme will be given for the strongest line $J=K=3$.

[1] Dailey, Kyhl, Strandberg, Van Vleck, and Wilson, Phys. Rev. **70**, 984 (1946).
[2] R. H. Hughes and E. B. Wilson Jr. Phys. Rev. **71**, 562 (1947).

M4. The Structure of the *D*-Terms of Li^7. K. W. MEISSNER AND L. G. MUNDIE,* *Purdue University.*—The wave-length material of the arc spectrum of lithium available at the present is rather incomplete and the values not sufficiently accurate for drawing reliable conclusions regarding the fine structure of the D-terms. Therefore, we made new interferometric measurements employing an atomic beam source. The structure of the n^2D-terms ($n=3, 4, 5$) revealed regular term order, the splitting being 0.037 cm^{-1}, 0.020 cm^{-1}, and 0.008 cm^{-1} respectively.

* Now at the Naval Ordnance Laboratory, Washington, D. C.

M5. Infra-Red Spectra of Argon, Krypton, and Xenon between 1.15 and 2.25 Microns.* W. R. SITTNER AND W. S. HUXFORD, *Northwestern University.*—Infra-red spectra emitted by high intensity condenser discharge sources have been recorded. The discharge tubes were designed and constructed in this laboratory. A 1½-inch plane reflection grating, having 15,000 lines per inch, was used. The detector was a lead sulfide photoconductive cell feeding into a broad band amplifier. The amplifier operated a photoelectric paper strip recorder. The probable error in determining wave numbers of lines near 2μ is less than 2 cm^{-1}. Eleven strong and 9 weaker lines were found in the argon spectrum in this region. Of these, seventeen lines were observed for the first time. Thirty-eight lines, consisting of 18 strong and 20 weaker ones, were found in krypton. Twenty-eight of these are new lines. Seventeen lines were found in xenon. Thirteen was strong and four were weak. Sixteen of these were observed for the first time. Most of the spectral lines observed in argon and krypton are due to combinations of terms of the normal atom given by Meggers and Humphreys.[1] The xenon lines are similarly identified, except that the addition of the $2s_4$-term, (12393.9 cm^{-1}, $j=1$) is required.

* This work was supported by the Navy Department, Bureau of Ships.
[1] Bur. Stand. J. Research **10**, 427 (1933); **10**, 139 (1933).

M6. Electrophotography. R. M. SCHAFFERT AND C. D. OUGHTON.—An entirely new photographic process, which does not involve the use of film or chemical solutions, has been developed. The process, known as electrophotography, employs a plate consisting of a thin photoconductive layer on a conductive base. The plate is sensitized by electrostatic charging, and after exposure, the image is developed by dusting the plate with micronized powder. Prints are made by transferring and fixing the powder image to paper or other materials. The plate can be re-used numerous times. The paper describes the fundamental principles of the electrophotographic process, and directs particular attention to its applications.

M7. The Silver Bromide Grain of Special Photographic Emulsions. W. KNOWLES, *McGill University,* AND P. DEMERS, *Chalk River.*—Using an electron microscope, the grains of several undeveloped emulsions useful in nuclear physics, and of a few others, were examined. They appear as regular hexagons of rather uniform size. Here are the approximate diameters: Eastman 548, 0.03μ; our formula II, 0.04 to 0.08μ according to lot examined; Ilford D, 0.12μ, $-C_1$ and C_2, 0.16μ; B_1, 0.21μ: Eastman V-O, 0.25μ; $-\alpha$, 0.28μ; −Microfilm, 0.42μ; −Lantern slide, 0.6μ. The grains ought to be flat, thickness being probably about ⅛ diameter. About half the grains carry a bump and sometimes a horn protruding on one side, which is thought to be the visible image caused by the electrons. A layer of adsorbed gelatine 0.01μ thick is visible around the grains. The closely packed grains in our concentrated emulsions never showed a long protruding ribbon as visible in Lippman emulsion, on development; instead, as seen in one picture obtained of an α-ray track at these high magnifications, each developed grain viewed as a unit in the optical microscope arises from some 30 Ag Br grains developed around the one carrying the impression.

* Now at the University of Montreal.

M8. Regression of the Latent Image of Nuclear Tracks in the Photographic Emulsion. J. LAPALME AND P. DEMERS, *University of Montreal.*—Plates were irradiated with α-rays and protons, kept at room temperature for 0 to 120 days (8 to 14 months in some cases), and developed in D19 at 20C 5 minutes: Eastman α, V–O, Ilford D1, C1, C2, D1, and 15 minutes: Eastman 548, and our own formula II.[1] In every case fading of the track is perceptible after less than a day, it is severe after a month especially for protons. Grain spacing Δ in α-ray tracks follows this approximate equation at first: $1/\Delta \sim \exp-(t/T)^{\frac{1}{2}}$; with $T=5$ to 50 days, according to ionizing power, and to emulsion used, but the general law is not so simple. Fading is much faster at 42C; at −85°C it is too slow to be observed in several months. Sensitivity also is observed to increase with temperature. Fading should be due in part at least to "evaporation" of active specks in Ag Br crystals. These findings are important for interpreting cosmic-ray data concerning number and grain density of tracks. On the other hand, age of tracks can be estimated from their density, sometimes within a few hours.

[1] Demers, Can. J. Research (to be published).

M9. Radioactive Stars Showing Migration of Single Nuclei in the Photographic Emulsion. PIERRE DEMERS, *University of Montreal.*—Some of our plates, kept 5 months between making and developing, showed a splitting of the well-known five-branched thorium stars, for instance the α-ray of Rd Th and that of Th X radiating from one point, and those of Tn, Th A, and Th C′ from another point as far as several microns away from the first. This is interpreted as showing the migration of a Tn nucleus from the point where it was formed to the point where it decayed. Such a conclusion was confirmed by a study of plates containing added Th or Ra developed after a few days, through range and age (see next abstract) determinations. In some instances, one star out of 10 showed on close scrutiny at least the minimum perceptible displacement (0, 1–0, 2μ) between the centers of emission. Displacements have been observed showing the occasional migration of the following nuclei: Rn, Tn, Th A, Th B or C, or C′. The importance of such migrations seem large in view of the short periods and delays involved. They are greater than the recoil ranges. Probably the heterogeneous structure of the emulsion provides in places paths of easier motion.

S1. On the Nuclear Mass Defect. GERTRUDE SCHWARZMANN, *New York City.*—Interpretation of particle waves as alternating currents with direct current components allows for interpreting dematerialization as superposition of, and materialization as decomposition of a light wave into a pair of particle waves, and is based on the following assumptions: The entities of both light and matter exist as corpuscles and as waves. Transitions of corpuscles into waves occur in electromagnetic fields, those of waves into corpuscles in field-free regions. The direct current component of the wave is equal in magnitude and sign to the direct current conveyed by the associated corpuscle. Wave and associated corpuscle have equal velocities, frequencies, and energies. Two particle waves, having equal velocities, frequencies, and direct current components equal in magnitude and opposite in sign, are a pair of particle waves. Interpretation of mass defect of any satellite as the mass equivalent of its negative energy, and of the neutrons as atoms, allows for interpreting the nuclear mass defect as the sum of the mass defects of the intranuclear satellites. Computed from this angle the magnitude of the force of attraction between central body and satellite in the neutrons explains why positrons and negatrons are observed but *in statu nascendi*, even if materialization and dematerialization occur by equal pairs.

S2. Continuous particles. M. HESSABY, *Teheran (now at Institute for Advanced Study).*—A reinterpretation of Maxwell's equations in general relativity leads to the deduction of a metric tensor for the field of an uncharged particle which yields a finite density of energy at every point in space, the integral of the energy being equal to the mass of the particle. The potential obtained is $\gamma=1-(2m/r)+(2m^2/r^2)$. Similarly, the electrostatic potential obtained for the electron is $\log[1-(2ke/r)+(2k^2e^2/r^2)]$ where $k=3.8\times10^{-4}$, which gives charge and energy densities whose integrals are respectively equal to the charge and to the mass of the electron. Two positive charges should attract each other at distances smaller than 3.7×10^{-13} cm, and a positive charge should attract a neutral mass. A certain solution of the wave equation of Maxwell's theory leads to the notion of a harmonic spherical wave surrounding a particle in motion, and to Schrödinger's equation.

S3. Integral and Rational Eigenvalues in the Nuclear Domain and their Significance. ENOS E. WITMER, *University of Pennsylvania.*—The writer[1] has shown that the known nuclear eigenvalues appear to be integral (in the ground state of stable nuclei) or rational multiples of a natural unit for that particular physical quantity. It seems altogether improbable that this result could be obtained from any theory of nuclei in which the constituent particles are held together by forces which are continuous functions of continuously varying space coordinates, *even with quantum-mechanics.* It seems probable that the observed results can be obtained only from some theory in which all the quantities involved are rational or integral numbers. This seems to point to the necessity of "quantizing" the space and time coordinates. We use the word "quantization" here to refer to any theory which by its very nature implies the existence of a minimum measurable distance and/or gives a discrete character to space-time. The number 42, which appears to play an important role in connection with nuclei and elementary particles, possibly derives its importance from the fact that space is three-dimensional. Note also that the Riemann-Christoffel tensor of general relativity has 21 (one-half of 42) *distinct* components.

[1] E. E. Witmer, Proc. Nat. Acad. Sci. **32**, 283 (1946).

S4. On the Recurrence-Time Probability for the Harmonic Oscillator in the Limit of Vanishing Mass. A. J. F. SIEGERT, *Syracuse University.*—The differential equation for the coordinate $y(t)$ of a harmonic oscillator in Brownian motion as a function of time reduces to first order for vanishing mass, so that in this limit $y(t)$ becomes Markoffian in the ordinary sense. The recurrence-time probability $w(a/t)dt$, i.e. the probability that y returns to a value a for the first time after a time between t and $t+dt$, becomes singular at $t=0$, but one can define the probability $q(a/t)dt$ that—for a time instant t_0 chosen at random—the largest time interval, which contains t_0 but no roots of the equation $y(t')=a$, is of duration between t and $t+dt$. If both $w(a/t)$ and $q(a/t)$ exist, we have $q(a/t)=(t/\bar{t})w(a/t)$ where $\bar{t}=\int_0^\infty tw(a/t)dt$. This equation can be used to obtain the recurrence-time probability for the harmonic oscillator when the mass approaches zero at fixed $t>0$, since $\bar{t}$ is known for the general case,[1] and $q(a/t)$ can be obtained from the known first-passage time probability for Markoffian random functions.[2]

[1] S. O. Rice, *Mathematical Analysis of Random Noise*, p. 63.
[2] A. J. F. Siegert, Phys. Rev. 71, 485 (1947).

S5. Theory of the Increase in Rigidity of Rubber During Cure. HUBERT M. JAMES AND EUGENE GUTH, *Purdue University, and University of Notre Dame.*—The rigidity of rubber, considered as a network of flexible molecules with Gaussian configuration functions, can be calculated when certain statistical features of the network are specified. In particular, it is sufficient to know the distribution of lengths and vector-mean extensions of the network segments. The assumption that the vector-mean extensions have Gaussian distributions corresponds to a similar postulate in the theory of Wall, and leads to the same proportionality between rigidity and the number G_a of segments per unit volume in the "active" part of the molecular network. Consideration of the process of cure shows that this assumption cannot be expected to be correct, though it gives results of the right order of magnitude. As an alternative approach to the problem we have studied the increase in rigidity as cure proceeds, using a more realistic picture of the process of cure than those hitherto employed. The final result resembles that given by earlier theories, except that G_a is replaced by B_a, the number of bonds formed within the network during cure. Since B_a is smaller than G_a by a factor of 2 or more, this theory leads to the prediction of lower rigidities per bond formed.

S6. Further Simplifications in the Derivation of Thermodynamical Relations. H. KAUFMAN AND A. NORMAN SHAW, *McGill University.*—A brief review of the usefulness of Jacobians in simplifying thermodynamical analysis, in obtaining new results, and in teaching. An account of a recent application to a system involving electric and magnetic fields.

S7. Minimum Sparking Potentials of Barium, Magnesium and Aluminum in Xenon. HAROLD JACOBS AND ARMAND P. LAROCQUE, *Sylvania Electric Products.**—The minimum sparking potentials of Ba, Mg, and Al in xenon are determined and found to be 82±2V, 120±1V and 151±2 volts, respectively. The regulation voltages are measured in the tubes studied and found to be 67±1V, 111±1V, and 135±3V, respectively. A rough calculation of γ_m, the ratio of electrons liberated per positive ion bombarding the cathode at the minimum sparking potential, is made and a relationship found such that lower work functions for the three metals indicate a higher γ.

* This work was undertaken in association with the Applied Physics Laboratory of the Johns Hopkins University and sponsored by the United States Navy.

S8. Interference Patterns on the Walls of Tubes Carrying High Frequency Discharges. R. W. STEWART, J. I. LODGE, AND J. K. ROBERTSON, *Queen's University.*—Under certain conditions, deposits exhibiting interference patterns are thrown down on the walls of tubes carrying high frequency discharges in air and other gases. The index of refraction of these deposits, as measured by a new method, has the value 1.487±0.003 for tubes of Pyrex glass and quartz, with carrier gases, air, and helium. It is concluded that the deposits are silicon dioxide, in the form of cristobalite. Similar measurements for polystyrene tubes give values of the index which are a function of the thickness of the deposit, and range from 1.25 to 1.35. In this case it is considered that the deposits are polystyrene, the variation in the index being ascribed to changes in density.

S9. Structural Absorption of Sound in Water. LEONARD HALL, *Brown University.*—Structural relaxation is found capable of accounting for the excess ultrasonic absorption in water. It implies a coefficient of bulk viscosity for water several times greater than that of shear-viscosity. Approximate calculation of the ultrasonic absorption coefficient reproduces reasonably well the temperature variation experimentally observed by Fox and Rock in the range 0–30°C and preliminary measurements made in Brown Laboratory by Smith in the range of 30–80°C. During compression of a liquid the molecules are brought uniformly closer together and also rearranged or repacked more closely. The former process is relatively rapid and may be considered instantaneous. The latter structural compression involves the breaking of intermolecular bonds, lags the applied pressure, and leads to absorption. A relaxation treatment may be applied to the structural compression. The acoustic wave perturbs molecular transitions to and from the sites of closer packing through the work performed by or against it in the volume change. The activation energy determining the rate of transition should be close to that for shear viscous flow and the configuration of closer packing, approximately that of closest packing. The structural absorption can be conveniently expressed by a temperature dependent factor times the shear viscosity absorption.

S10. Impedance of Biological Cells at Microwave Frequencies. T. M. SHAW, D. E. JAMISON, AND J. A. GALVIN, *Western Regional Research Laboratory.*—Very little data exist on the dielectric properties of biological materials in the microwave region. In the present work, the loss

factor and dielectric constant of aqueous suspensions of yeast cells (*Saccharomyces cerevisiae*) were measured at 3.3×10^9 c.p.s. The results were correlated with existing data at lower frequencies. The impedance measurements were made according to a scheme used by Knerr and by Cooper, with a modification whereby a resonant section of waveguide was substituted for the parallel wire transmission line used by them. It was thus possible to reduce to less than one-tenth the amount of suspension used in the measurements and to eliminate errors caused by stray fields. The measurements show that the dielectric constant, ϵ', of a suspension of yeast cells at 3.3×10^9 c.p.s. can be expressed by the equation, $\epsilon'=\epsilon_0'-CK$ for yeast concentrations of 0 to 20 percent by volume. Here, ϵ_0' is the dielectric constant of the suspension medium (water or salt solution), C is the concentration of yeast, and K is a constant. The loss factor is practically identical with that of the suspension medium. By the use of the Cole circle diagram, the present results are shown to be consistent with a proposed electrical model of biological cells.

S11. The Measurement of Rainfall by Radar. J. S. MARSHALL, R. C. LANGILLE, W. M. PALMER AND D. W. PERRIE.—The power of radar echoes from rain has been observed to be proportional to ΣD^6, the drop-diameters to the sixth power summed over unit volume. This is in agreement with theory, but the power of the echoes is probably many times greater than theory indicates. Empirically, ΣD^6 is found to be nearly proportional to R^2, where R is the intensity of rainfall.

Supplementary Programme

SP1. Regularities in the Properties of Metallic Elements. R. SMOLUCHOWSKI, *Carnegie Institute of Technology.**—A relation between metallic properties and the atomic structure of the elements is as a rule quite complicated because of the specific character of electronic interactions in metals, and also because of the complex nature of some of the relatively easily measured properties. Among others, the Poisson's ratio, as pointed out by Köster, shows certain regularities in the periodic system. These are considered in a qualitative manner from the point of view of the repulsion between ions due to overlap and electrostatic forces between ions and valence electrons. The anomaly in the ferromagnetic group is discussed. Further, the differences and similarities of properties in the copper, silver, gold group are considered.

* To be called at the end of Session H if time permits.

SP2. New Autoradiographic Method. P. DEMERS AND V. FREDETTE, *Université de Montréal.**—It should be possible to cover or surround a microscopic sample on section containing a radioactive α-emitter, carried on a glass slide, with an emulsion sensitive to α-ray tracks, and after drying, waiting and developing, and eventual staining of the specimen, to see simultaneously under the microscope the detailed structure of the cell, or crystal, etc., and the α-tracks at the same time, coming from the spots where the radioactive substance was present. Identification of the region in the structure which contains or retains certain molecules or nuclei, becomes feasible, with great accuracy. This method has been successfully applied with our new emulsions to microbe cells retaining Ra SO_4. (Clostridium, Staphylococcus, Saccharomyces, etc.) The track may designate its origin in or on the cell within 0.1–0.2μ.

* To be called at the end of Session M if time permits.

To Be Read by Title

T1. Near Infra-red Spectra of the Planets. ARTHUR ADEL, *University of Michigan.*—Kuiper, Wilson, and Cashman have recently recorded low dispersion spectra of several stars and planets, employing a lead sulfide cell in the region 0.75–2.6 mu.[1] Carbon dioxide bands appear in the spectrum of Venus at 2 and 1.6 mu, and the spectra of Jupiter and Saturn are cut up by extremely heavy bands. The authors are aware of the probable origin of these bands in methane and ammonia, but add that, "laboratory intensities are still lacking." It seems worth while, in this connection, to describe some unpublished curves recorded in conjunction with experiments bearing on water cell temperatures and planetary atmospheres.[2] Glass prismatic solar spectra were obtained through large concentrations of carbon dioxide, methane, and ammonia. The principal regions of absorption are: CO_2: 2, 1.6, 1.2 mu;[3] CH_4: 2.5–1.7, 1.4, 1.17, 1.01, 0.88, 0.80;[4] NH_3: 2.5–2.1, 1.98, 1.68, 1.51, 1.30, 1.22, 1.18, 1.02, 0.98, 0.79. The bands have been correlated with their corresponding vibrational transitions.

[1] Kuiper, Wilson, and Cashman, Astronom. J. **52**, 154 (1947).
[2] Arthur Adel and C. O. Lampland, Ap. J. **93**, 391 (1941).
[3] Arthur Adel and D. M. Dennison, Phys. Rev. **43**, 716 (1933).
[4] Arthur Adel and V. M. Slipher, Phys. Rev. **46**, 902 (1934).

Author Index to Abstracts of papers presented at the Montreal Meeting

Adel, Arthur—T1
Ahearn, A. J., J. A. Burton, and K. G. McKay—R3
Altar, William, M. Garbuny, and J. W. Coltman—C9
Bardeen, J.—Q2
Belinfante, F. J.—G1
Benzer, S.—E9
Bradt, H. L. and D. J. Tendam—C4
Branson, Herman—H11
Bray, Ralph, K. Lark-Horovitz, and R. N. Smith—E8
Bridgman, P. W.—J1
Brown, F. W. and M. A. Greenfield—M2
Brown, V. A. and B. P. Ramsay—C10
Broxon, James B.—A2
Burton, J. A.—H3
Carmichael, H.—A1, G3
Carr, W. J., Jr.—E5
Coltman, J. W. and Fitz-Hugh Marshall—C8
Corben, H. C. and Mulaika Corben—A9
Courant, E. D. and P. R. Wallace—A6
Demers, Pierre—M9
—— and V. Fredette—SP2
Deutsch, Martin—C2
Eisenstein, A.—H2
Estermann, I., A. Foner, and J. A. Randall—E7
Foster, J. S.—I3
Froman, Darol, Louis Rosen, and Bruno Rossi—A3
Goldman, J. E.—E4
Guindon, William G.—A8
Hall, Leonard—S9
Hessaby, M.—S2
de Hoffman, F. and B. T. Feld—A4
Hull, G. F., Jr. and W. Baer—H5
Jacobs, Harold and Armand P. LaRocque—S7
James, Hubert M. and Eugene Guth—S5
Jauch, J. M.—M3
Johnson, V. A. and K. Lark-Horovitz—E10
Kaufman, H. and A. Norman Shaw—S6
Kê, T'ing-Sui—J5
Kinsey, B. B.—A11
Kittel, Charles—E3
Knowles, W.—M7
Koomen, M. J. and R. Tousey—M1
LaPalme, J. and P. Demers—M8
Lawson, A. W.—H8
Marshall, Fitz-Hugh and J. W. Coltman—C8
Marshall, J. S., R. C. Langille, W. M. Palmer, and D. W. Perrie—S11
Matthias, B. T., R. G. Brechenridge, and D. W. Beaumont —H6
Meissner, K. W. and L. G. Mundie—M4
Mendenhall, H. E.—H4
Merchant, M. Eugene—J3
Miller, Arthur E. and Martin Deutsch—C1
Mutter, W. E.—H1
Pepinsky, R. and P. Jarmotz—C12
Placzek, G.—I1
Pound, R. V.—C5
Purcell, E. M.—R2
Ruedy, R.—H9
Saibel, Edward—J4
Scanlon, Wayne and K. Lark-Horovitz—E6
Schaffert, R. M. and C. D. Oughton—M6
Schwarzmann, Gertrude—S1
Seitz, F.—Q1
Shaw, T. M., D. E. Jamison, and J. A. Galvin—S10
Siegert, A. J. F.—S4
Sittner, W. R. and W. S. Huxford—M5
Smith, B. S., H. Carmichael, J. F. Steljes, C. O. Peabody, and D. S. Craig—C6
Smoluchowski, R.—J2, SP1
Stephens, W. E. and Margaret N. Lewis—A10
Stewart, R. W., J. I. Lodge, and J. K. Robertson—S8
Tendam, D. J. and H. L. Bradt—C3
Tisza, L.—H7
Wallace, P. R.—A5
Ward, A. G.—I2
Watson, K. M.—A7
Welsh, H. L. and M. F. Crawford—G2
Williams, H. J.—E1
Witmer, Enos E.—S3
Wolf, H. E., H. E. Clearman, and W. C. Wineland—C11
Worrell, Francis T.—H10
Yager, W. A. and R. M. Bozorth—E2
Zener, C.—R1